EARTH PRESSURES AND DEFORMATIONS IN CIVIL INFRASTRUCTURE IN EXPANSIVE SOILS

A Dissertation

by

GYEONG TAEK HONG

Submitted to the Office of Graduate Studies of
Texas A&M University
in partial fulfillment of the requirements for the degree of

DOCTOR OF PHILOSOPHY

May 2008

Major Subject: Civil Engineering

EARTH PRESSURES AND DEFORMATIONS IN CIVIL INFRASTRUCTURE IN EXPANSIVE SOILS

A Dissertation

by

GYEONG TAEK HONG

Submitted to the Office of Graduate Studies of
Texas A&M University
in partial fulfillment of the requirements for the degree of

DOCTOR OF PHILOSOPHY

Approved by:

Co-Chairs of Committee,	Robert L. Lytton
	Charles P. Aubeny
Committee Members,	Giovanna Biscontin
	Christopher C. Mathewson
Head of Department,	David V. Rosowsky

May 2008

Major Subject: Civil Engineering

ABSTRACT

Earth Pressures and Deformations in Civil Infrastructure in Expansive Soils.

(May 2008)

Gyeong Taek Hong, B.Eng., Dongguk University, Seoul, Korea;

M.Eng., Dongguk University, Seoul, Korea

Co-Chairs of Advisory Committee: Dr. Robert L. Lytton
Dr. Charles P. Aubeny

This dissertation includes the three major parts of the study: volume change, and lateral earth pressure due to suction change in expansive clay soils, and design of civil infrastructure drilled pier, retaining wall and pavement in expansive soils.

The volume change model in expansive clay has been refined to reinforce realistic characteristics of swelling and shrinkage behavior of expansive clay soils. Refinements include more realistic design soil suction versus depth profiles and improved characterizations of the effects of soil cracking, overburden stress, and lateral earth pressure. The refined model also includes an algorithm of assigning suction-volumetric water content curves and diffusivity through the soil.

The typical lateral earth pressure distribution during wetting against a stationary wall is proposed. The proposed stationary retaining wall-soil system in expansive soils includes an upper movement active zone and a lower anchor zone. Mohr's circles and failure envelopes are used to define the effective horizontal stress and shear failure in an unsaturated soil. The prediction of the horizontal pressures due to suction change in a soil is compared with the in situ measurement of natural horizontal pressures and the measurements from the large scale tests. It is found that agreement between the measured and predicted horizontal pressures is satisfactory. Case studies of axial and bending of the pier are presented with both uniform and non-uniform wetting. The pier

case study for axial behavior shows a good agreement with a heave at ground surface and uplift forces. Three case studies for bending behavior of the pier and retaining wall are presented based on suction change.

Pavement design program has been refined to extend the design capabilities into both flexible and rigid pavements supported by pavement treatments. The comparative case studies using both current and new methods in pavement design show that the current method criterion of 1-inch is unnecessarily conservative. Furthermore, the current method does not provide a means of anticipating subgrade shrinkage that will result in longitudinal cracking along the edge of the pavement. The design calculations with both methods lead to the conclusion that neither the swelling movement, as in the current method, nor the total movement, as in the new method, is a reliable indicator of likely acceptable pavement performance. Instead, all of these case studies show that it is important to use the predicted history of the present serviceability index and the international roughness index as the proper design guideline for an acceptable treatment of the subgrade of an expansive soil.

ACKNOWLEDGEMENTS

I would like to thank my co-advisors, Dr. Robert L. Lytton and Dr. Charles P. Aubeny, for their professional guidance, invaluable advice, encouragement, patience and support throughout my doctoral studies. I am also thankful for the suggestion and inspiration from my committee members, Dr. Giovanna Biscontin and Dr. Christopher C. Mathewson. I want to express my sincere gratitude to my friends and colleagues for their friendship and assistance throughout my study at the Texas A&M University. In particular, I would like to thank the Korean students in Civil Engineering for their help and kindness. Finally, I would like to extend my appreciation to my family for their encouragement and support throughout the duration of my study.

TABLE OF CONTENTS

CHAPTER Page

CHAPTER Page

Page

LIST OF FIGURES

FIGURE Page

FIGURE Page

FIGURE Page

FIGURE Page

FIGURE Page

FIGURE Page

FIGURE Page

FIGURE Page

LIST OF TABLES

TABLE Page

CHAPTER I
INTRODUCTION

1.1 General

In many parts of the world, severe damages have been reported in pavements and buried structures in expansive clay soils due to swelling and shrinkage phenomena when moisture increase and decrease in the clay, respectively. In recent years, many researchers have been devoting increasing attention to study of these phenomena and developing constitutive and computational models applied to the engineering behavior of expansive soils. The possibilities offered by these models to make successful predictions of the engineering behavior and provide design guideline for civil infrastructure in expansive soils are expected.

1.2 Problem Statement and Research Objectives

The previous version of an one-dimensional swell-shrink model inserted in program PRES (Jayatilaka 1999) is refined to reinforce realistic characteristics of swelling and shrinkage behavior of expansive clay soils. The evaluation of the existing Texas Department of Transportation (TxDOT) procedure Tex-124-E (TxDOT 1999) to predict the swelling and shrinkage of expansive soils is required regarding to the unrealistic assumptions and several disadvantages. The refinement of pavement design model PRES (Jayatilaka 1999) is needed to add remedial methods and environmental conditions and based on the field observation.

Buried structures such as retaining walls and drilled piers in expansive soils, are subjected to uplift forces and friction forces due to swelling of the soil. They are also subjected to horizontal swelling pressures tending to cause horizontal deformations and bending. These foundations require reasonably accurate predictions of the expected movements and pressures of the expansive soils to be made in order for the foundations to be designed successfully (Lytton 1995). The prediction of horizontal pressures exerted by the swelling of the soil is needed to provide an important guideline for the design of buried structures.

This dissertation follows the style and format of the *Journal of Geotechnical and Geoenvironmental Engineering*.

Specific objectives of this research are summarized as follows:

1) Refinement of previous version of one-dimensional swell-shrink model to reinforce realistic characteristics of swell-shrink behavior of expansive soils.

2) Refinement of previous pavement design model with remedial methods and environmental conditions.

3) Evaluation of current pavement design method and comparative case study using both old and new methods.

4) Model development for prediction of horizontal earth pressure against a stationary wall.

5) Development of design model of drilled pier and retaining wall.

1.3 Organization of the Dissertation

Chapter II presents briefly a through literature review of recent study and proposed methods on soil suction, suction versus water content curve, moisture diffusion properties, and shear strength of unsaturated soils. The free energy of the water in soil, and total, osmotic, and matric suctions are described. The soil water characteristic curve and its hystersis are presented. The simplified linear approach for unsaturated moisture flow is reviewed based on seasonal variation of moisture. The shear strength of unsaturated soil is described.

Chapter III illustrated the volume change in expansive clay based on the constitutive equation, soil swell parameters, suction-versus-volumetric water content curves, suction envelopes for wet and dry conditions and diffusivity. An example of calculation of swelling and shrinkage is presented. The volume change model to predict the swelling and shrinkage is described regarding to the initial and final value of the matric suction and mean principal stresses. The method to estimate suction compression index is presented based on Atterberg limits and soil particle size distributions. The estimation of mean principal stress compression index is presented based on the relationship with the suction compression index and the slope of suction- volumetric water content curve. The simplified suction – volumetric water content curves for natural clays, stabilized, and inert soils are illustrated. The exponential suction profiles for the side of extreme dry and wet conditions are described based on the diffusivity in a soil mass. The estimation of moisture diffusion coefficient can be determined by empirical

equation or laboratory measurement with crack correction. One example of calculation of both swelling and shrinkage is presented.

Chapter IV begins with the literature review of numerous studies to estimate the horizontal swelling pressure against retaining walls and piers in expansive soils. Concept of horizontal earth pressure proposed on a stationary wall due to suction change is described. The stress states in the both movement active and anchor zones are illustrated based on Mohr's circle and failure envelopes. The typical pattern of swelling pressures on a stationary wall in the three zones is proposed. The prediction of the horizontal earth pressures due to suction change in a soil is compared with the in situ measurement of natural horizontal pressures and the measurements from the large scale lateral swelling tests.

Chapter V is devoted to describing the axial and lateral behavior of the drilled pier due to uniform or non-uniform wetting around the pier in expansive soils. The literature review of drilled pier study in expansive soils is presented. A numerical model for use in design is presented for prediction of the stresses and axial and bending displacements in a drilled pier in expansive soils. The prediction of horizontal earth pressure and shear stress on the shaft of the pier are described based on the suction profiles around the pier. The transfer curve is proposed for the prediction of shear stress induced on the shaft of the pier. The stress state around the pier and non-linear suction dependent elastic modulus of the unsaturated soils are developed. A numerical model for use in design of the pier is presented including a beam column approach and linear distribution of shear stress around the circumference of the pier. Case studies of axial and bending of piers are presented with both uniform and non-uniform wetting.

Chapter VI presents a case study of lateral behavior of retaining wall in expansive soils.

Chapter VII illustrates the theoretical background of pavement design program which calculates pavement roughness on expansive soil subgrades. A regression model to extrapolate deformations any wheel path of interest from the vertical movements at the edge of pavement is presented. The literature review of pavement roughness and prediction of roughness development with respect to serviceability index (SI) and international roughness index (IRI) are presented. The roughness model with respect to

SI and IRI for the both flexible and concrete pavements is described based on the relationship between serviceability and international roughness index and roughness parameters in this model.

Chapter VIII presents the design analysis for six case study sections for both flexible and rigid pavements with remedial measures vertical moisture barriers, and lime stabilized and inert soil layers. The design parameters for structural properties of pavement and traffic and suggested levels of reliability for various functional classifications are presented. The transverse distribution of vertical movements is discussed.

Chapter IX compares current PVR (potential vertical rise) method with case study results. The existing PVR method is reviewd. The comparative case study using both PVR method and new method are presented. The study of pavement treatments with acceptable predicted performance is presented. The subgrade movements are compared with PVR for the both flexible and rigid pavements with or without pavements treatments.

Chapter X presents the summary and conclusions of this research and recommendations for future study.

CHAPTER II
UNSATURATED SOIL MECHANICS

This chapter reviews briefly soil suction, soil-water characteristic curve, moisture diffusion through unsaturated soils and the shear strength of unsaturated soil.

2.1 Soil Suction

Soil suction is commonly referred to as the free energy state of water (Edlefsen and Anderson 1943). The free energy of the soil water can be measured in terms of the partial vapor pressure of the soil water (Richards 1965). When water enters into unsaturated soils, the water can be absorbed and stored by the soil and the applied energy per unit volume of water is called soil suction or total suction. The thermodynamic relationship between the free energy of the soil water and the partial pressure of the pore-water vapor can be written as follows:

$$-h_t = \frac{RT}{mg}\ln(\frac{P}{P_o}) \qquad (2.1)$$

where h_t = the total suction (kPa)

R = the universal (molar) gas constant (8.31432 J/mole K)

T = the absolute temperature

m = molecular mass of water vapor (18.016 g/mole)

g = gravitational constant

P = the partial pressure of pore water vapor pressure (kPa)

P_o = the saturation pressure of water vapor over a flat surface of pure water at the same temperature (kPa)

The total suction has two components, matric and osmotic suction. Addition of two components is total suction as follow:

$$-h_t = -h_m - h_o \tag{2.2}$$

where h_t = total suction (m)

h_m = matric suction (m)

h_o = osmotic suction (m)

Osmotic suction is the equivalent suction derived from the measurement of the partial pressure of the water vapor in equilibrium with a solution identical in composition with the soil water, relative to the partial pressure of water vapor in equilibrium with free pure water (Aitchison and Woodburn 1969). Osmotic suction is the result of the lowering of the relative humidity of the pore fluid by the presence or concentration of soluble salts in the pore water and can be expressed by using Van't Hoffs' Equation.

$$-h_o = \pi = \frac{vRTC\phi}{g} \tag{2.3}$$

where π = osmotic suction

ν = ionic activity

C = molar concentration (moles/liter)

ϕ = osmotic coefficient

The capillary phenomenon is associated with the matric suction component of total suction. The height of water rise and the radius of curvature have direct implications on the water content versus suction relationship in soil (Fredlund and Rahardjo 1993). In the capillary tube model, the vertical resultant of the surface tension is responsible for holding the weight of the water column, which has a height of *h*:

$$2\pi rT\cos\alpha = \pi r^2 h\rho g \tag{2.4}$$

where r = radius of the capillary tube

T = surface tension of water

α = contact angle

h = capillary height

g = gravitational acceleration

Equation (2.4) can be rearranged to give the maximum height of water in the capillary tube h:

$$h = \frac{2T}{\rho g R} \tag{2.5}$$

where R = radius of curvature of the meniscus

when the air pressure is atmospheric (i.e., u_a=0) and the water pressure is negative (i.e., $u_w = -\rho g h$), the matric suction $u_a - u_w$ can be expressed as follows:

$$\left(u_a - u_w\right) = \frac{2T}{R} \tag{2.6}$$

The magnitudes of soil suction can range from 0 kPa to 1 GPa. Total suction can be measured with the filter paper, transistor or thermocouple of chilled-mirror psychrometers. Matric suction can be measured with filter paper, tensionmetor, thermal or electrical conductivity sensors and null-type axistranslation apparatuses. Osmotic suction can be measured using the pore fluid squeezer technique. The osmotic suction value can be indirectly estimated by measuring the electrical conductivity of the pore-water from the soil.

2.2 Soil-Water Characteristic Curve

The soil water characteristic curve (SWCC), which represents the relationship between matric suction and water content, is of fundamental importance in unsaturated soils. SWCC is influenced by the type of mineral in the soil, the void size distribution, particle

structures, and confining stress on the soil. The soil-water characteristic can be defined as the relationship between soil matric suction and volumetric water content, or gravimetric water content, or the degree of saturation. A typical suction-versus-volumetric water content curve is illustrated with the air entry value and residual suction of unsaturated soils in Fig. 2.1. The air entry value represents the differential pressure between the air and water that is required to cause de-saturation of the largest pores (Vanaplli et al. 1996).

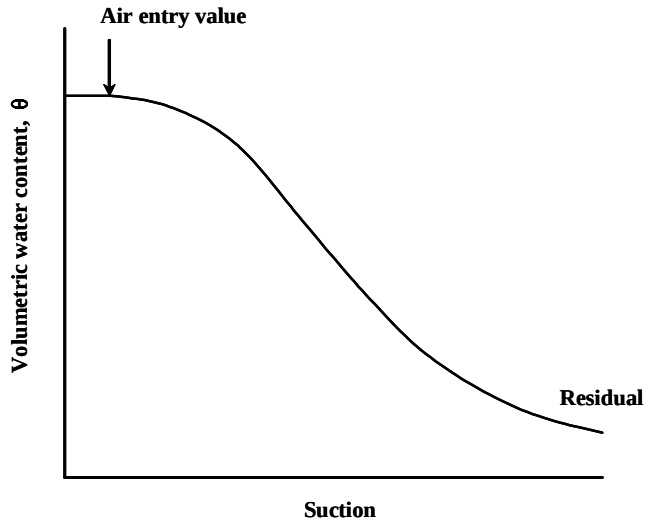

Fig. 2.1. Typical Suction-versus-Volumetric Water Content Curve

The soil-water characteristic curve exhibits hysteresis during drying and wetting cycles as shown in Fig. 2.2. At a particular suction level, the degree of saturation or water content will be different. The non-uniform pore size distribution in a soil, as well as the presence of entrapped air in the pore-water, are considered to be the main causes for hysteresis in the soil-water characteristics curve (Hoyos 1998).

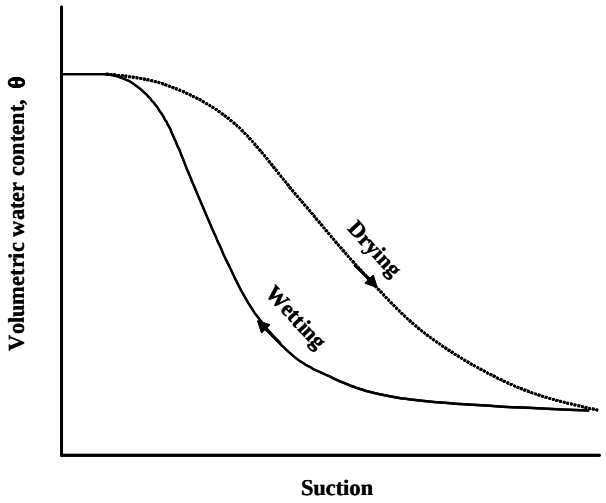

Fig. 2.2. Typical SWCC Hystersis

2.3 Moisture Diffusion in Unsaturated Soil

The moisture diffusivity properties of unsaturated properties of soils exert a critical influence on the depth to which seasonal variations of moisture and suction at the ground surface extend into the soil mass. Depending on the two assumptions: (1) the unsaturated permeability is linearly related to the reciprocal of total suction and (2) the desorption relationship is linear when the matric potential is expressed in terms of pF, moisture flow through unsaturated soil is expressed by (Mitchell 1979):

$$v = -k_0 \frac{h_0}{h} \frac{dh}{dx} \tag{2.7}$$

where

v = velocity of flow (cm/sec)

k_0 = saturated permeability (cm/sec)

h_0 = total suction

h = suction in cm of water

Soil suction is conveniently measured in logarithmic units of pF, thus *du*/*dx* and velocity of flow *v* can be expressed by:

$$\frac{d}{dx}(u) = \frac{0.4343}{h}\frac{dh}{dx} \tag{2.8}$$

where $u(\text{pF}) = \log_{10} h = 0.4343 \log_e h$

$$v = \frac{k_0 h_0}{0.4343}\frac{d}{dx}(u) \tag{2.9}$$

The unsaturated moisture flow for a two-dimensional soil domain is given by:

$$\frac{\partial^2 u}{\partial x^2} + \frac{\partial^2 u}{\partial y^2} + \frac{f(x,y,t)}{p} = \frac{1}{\alpha}\frac{\partial u}{\partial t}$$
$$\alpha = \frac{\gamma_w}{\gamma_d}\frac{p}{c},\ c = \frac{\partial w}{\partial u},\quad p = \frac{k_0 h_0}{0.4343} \tag{2.10}$$

where

α = diffusion coefficient

γ_w = water density

γ_d = soil dry density

c = inverse slope of log suction (pF) vs. gravimetric water content curve (pF^{-1})

$f(x,y,t)$ = a flow quantity which may be used to model a moisture source or sink with respect to space and time

For a sinusoidal suction change by effects of climate at the soil surface, the one-dimensional analytical solution for suction $u(y,t)$ at any depth y is given by:

$$U(y,t) = U_e + U_o \exp\left(-\sqrt{\frac{n\pi}{\alpha}}\, y\right)\cos\left(2\pi n t - \sqrt{\frac{n\pi}{\alpha}}\, y\right) \tag{2.11}$$

where

y = depth

U_e = the equilibrium value of suction expressed as pF

U_o = the amplitude of pF (suction) change at the ground surface

n = the amplitude of suction cycles per second (1 year=31.5×10^6 seconds)

α = the soil diffusion coefficient using Michell's unsaturated permeability (ranges between 10^{-5} and 10^{-3} cm^2/sec)

t = time in seconds

2.4 Shear Strength of Unsaturated Soil

For most saturated soil mechanics problems, it is sufficient to approximate the shear stress on the failure plane as a linear function of the normal stress called Mohr-Coulomb failure criterion as follows:

$$\tau_f = c' + (\sigma - u_w)\tan\phi' \qquad (2.12)$$

where τ_f = shear stress along failure plane

c' = effective cohesion

σ = normal stress on the failure plane

u_w = pore water pressure and

ϕ' = angle of internal friction

Fredlund et al. (1978) suggested an expression for the shear strength of an unsaturated as follows:

$$\tau_f = c' + (\sigma - u_a)\tan\phi' + (u_a - u_w)\tan\phi^b \qquad (2.13)$$

where σ–u_a = net normal stress

u_a–u_w = matric suction and

ϕ^b = friction angle indicating the rate of change of shear strength with suction

The reversible thermodynamic principles are used to describe the stress generated on the soil skeleton due to tension in the pore water (Lamborn 1986). The soil-water characteristics curve is used to predict the shear strength of unsaturated soils. The formulation is as follows:

$$\sigma_{ij} = \theta \frac{\partial F_w}{\partial \left(\varepsilon_{ij}\right)_w} \tag{2.14}$$

where F_w = the Helmholtz free energy in the water,

ε_{ij} = strain in the water,

θ = volumetric water content, and

σ_{ij} = stress on the soil due to the water.

Since matric suction is a derivative of the Helmholtz free energy, the stress due to soil suction can be redefined as follows:

$$\sigma = -f\theta h_m \tag{2.15}$$

where f = the unsaturated shear strength function

h_{m} = matric suction,

θ = volumetric water content, and

σ = stress on the soil due to water

Lytton (1995) proposed the following shear strength using two stress variables and Lamborn's approach as follows:

$$\tau = c' + \left[(\sigma - u_a) + f\theta(u_a - u_w)\right]\tan\phi' \tag{2.16}$$

The above equation includes a term that accounts for the transition zone between the air entry point and the suction at which continuous air void starts. Lytton (1995) also

describes that the $\tan\phi^b$ term is bound by the product of $\theta\tan\phi'$ and the upper and lower bound of values of unsaturated shear strength function in the transition zone as in Fig. 2.3. The upper and lower bound of unsaturated shear strength function f_1 and f_2, respectively, in the transition zone is given in the following equations:

$$f_1 = \left(\frac{\theta_a - \theta}{\theta_a - \theta_u}\right) + \frac{1}{\theta}\left(\frac{\theta - \theta_u}{\theta_a - \theta_u}\right) \tag{2.17}$$

$$f_2 = \frac{1}{\left(\frac{\theta_a - \theta}{\theta_a - \theta_u}\right) + \theta\left(\frac{\theta - \theta_u}{\theta_a - \theta_u}\right)} \tag{2.18}$$

where θ = volumetric water content at current suction

θ_a = volumetric suction at air entry and

θ_u = volumetric water content at unsaturation (continuous air void).

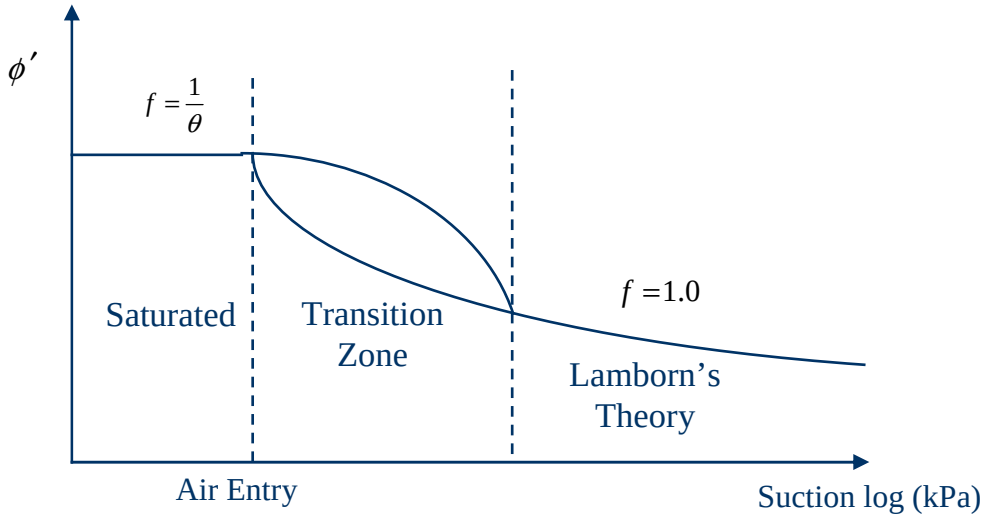

Fig. 2.3. Transition of Friction Angle due to Matric Suction from Saturated to Unsaturated State (after Lytton 1995)

CHAPTER III
VOLUME CHANGE IN EXPANSIVE SOILS

3.1 Introduction

The prediction of movement in expansive soil is important principally for the purpose of designing foundations and other ground supported structural elements such as pavements. In design, the principle interest is in making an accurate estimate of the range of movements that must be sustained by the foundation. It is for this reason that envelopes of maximum heave or shrinkage are important for design purpose.

There are three categories of methods of predicting movements in expansive clays: oedometer, empirical, and suction methods. The oedometer methods basically use the consolidation theory in reverse and are based on determining a swelling property of the soil by one of two tests: the constant volume or swell-pressure test and the consolidation-swell test. Objective studies of these methods (e.g., Osman and Sharief, 1987 and Dhowian et al. 1987) show that the oedometer methods always overpredict the in situ heave except in those rare cases where the capillary moisture conditions are met in the field as in the case where high water tables are present on the site.

The empirical or semi-empirical methods are based on a correlation between laboratory or field measurements and soil indices such as the liquid limit, plasticity index, and clay content. There are large numbers of these empirical relations in the literature, but all are hampered by having been developed locally and, thus, are not applicable except in their locale of origin. McDowell's method (McDowell 1956), which has been incorporated into the Tex-124-E specification (Texas Department of Transportation 1999), is another empirical method and the discussion presented above shows its shortcomings. In general, empirical relations all suffer from the same limitations of being confined to their locale of origin and having to rely upon an assumed final moisture condition. These limitations apply to both laboratory samples and to field measurements.

The methods using soil suction have the distinct advantage of using the moisture energy for predicting the heave and shrinkage of soil. Movements in expansive soils are generated by change of suction that is brought about by entry or loss of moisture. The volume change depends upon the total stress states that surround the soil. The following section details the philosophy behind the method and then outlines the comprehensive framework for predicting the movement of expansive soil based on changes of suction.

3.2 Constitutive Equations for Volume Change in Expansive Soils

The comprehensive framework developed at Texas A&M University for predicting the differential movement of expansive soil based on change of suction finds its roots in the early work carried out by Juarez-Badillo (1986). It may be mentioned that Juarez-Badillo successfully predicted the expansion and settlement characteristics of highly compressible Mexico City clays based on his theory of natural limits.

The natural limits in this process are mean principal stress, suction, and volume (Fig. 3.1). Under conditions of zero mechanical pressure and suction, the soil reaches its maximum volume, Vo; under conditions of zero suction and infinite mechanical mean principal stress, the soil volume compresses to the volume of the solids alone, Vs; and under conditions of zero mean principal stress and infinite suction, the soil volume compresses to the dry volume, Vd, in which the dry soil contains a volume of air-filled voids. For small increments of volume change on the volume–mean principle stress-suction surface (Fig. 3.2), $\Delta V/V$ is linearly related to the logarithms of the mechanical pressure and suction components.

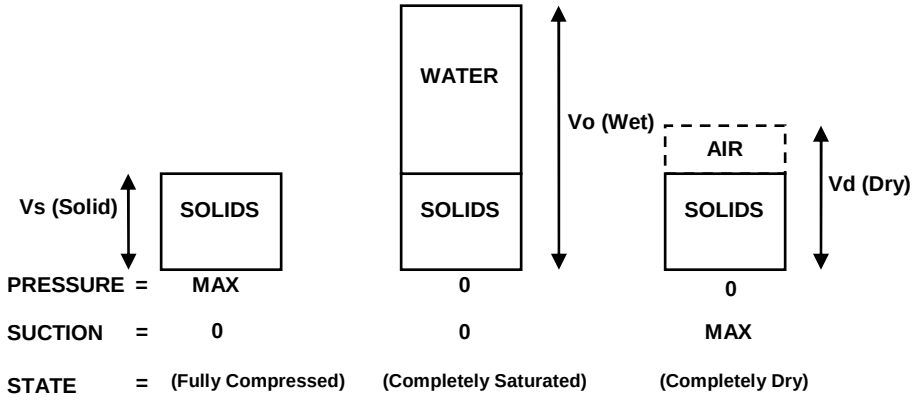

Fig. 3.1. Natural Limits of Volume Change Process in Unsaturated Soils

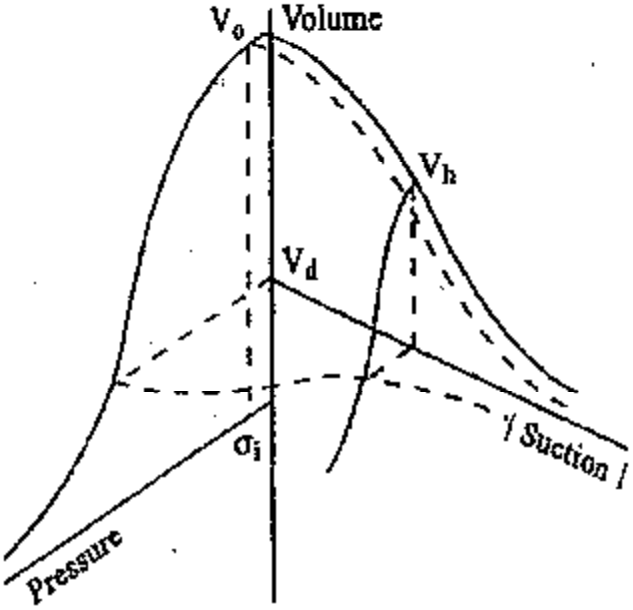

Fig. 3.2. The Volume–Mean Principal Stress-Suction Surface

In general, the relation between these components and a change in osmotic suction, π, is:

$$\frac{\Delta V}{V} = -\gamma_h \log_{10}\left(\frac{h_f}{h_i}\right) - \gamma_\sigma \log_{10}\left(\frac{\sigma_f}{\sigma_i}\right) - \gamma_\pi \log_{10}\left(\frac{\pi_f}{\pi_i}\right) \qquad (3.1)$$

where:

$\frac{\Delta V}{V}$	=	the volume strain
h_i, h_f	=	the initial and the final values of matric suction
σ_i, σ_f	=	the initial and the final values of mean principal stress
π_i, π_f	=	the initial and the final values of osmotic suction
γ_h	=	the matric suction compression index
γ_σ	=	the mean principal stress compression index
γ_π	=	the osmotic suction compression index

The mean principal stress compression index γ_σ is related to the commonly used compression index C_c by:

$$\gamma_\sigma = \frac{C_c}{1+e_o} \left(\text{refer to } \frac{\Delta \text{V}}{\text{V}} = \frac{C_c}{1+e} \log \frac{\sigma_f}{\sigma_i} = \gamma_\sigma \log \frac{\sigma_f}{\sigma_i} \right) \tag{3.2}$$

where e_o = the void ratio

In order to predict the total movement in a soil mass, initial and final values of the matric suction, osmotic suction, and mean principle stress profiles with depth must be known.

It is the change of matric suction that generates the heave and shrinkage, while osmotic suction rarely changes appreciably, and the mean principal stress increases only slightly in the shallow zones where most of the volume change takes place. It is commonly sufficient to compute the final mean principal stress σ_f from the overburden, surcharge, and foundation pressure and treat the initial mean principal stress σ_i as a constant corresponding to the stress-free suction-versus-volume strain line. Because there is no zero on a logarithmic scale, σ_i may be regarded as a material property, i.e., a stress level below which no correction for overburden pressure must be made in order to

estimate the volume strain. It has been found to correspond to the mean principal stress at a depth of 2.6 ft.

The mean principal stress is estimated by:

$$\sigma = \frac{1+2K_o}{3}\sigma_z \tag{3.3}$$

where σ_z = the vertical stress at a point below the surface in the soil mass

K_0 = the lateral earth pressure coefficient

The lateral earth pressure coefficient K_0 is given by:

$$K_0 = e\left(\frac{1-\sin\phi'}{1+\sin\phi'}\right)\left(\frac{1+d\sin\phi'}{1-k\sin\phi'}\right)^n \tag{3.4}$$

Values of the coefficients *e, d, k,* and *n* for different soil conditions are given in Table 3.2. With an active soil, which can crack itself in shrinking and generate large confining pressures in swelling, the lateral earth pressure coefficient K_o can vary between 0.0 and passive earth pressure levels. Typical values that have been back-calculated from field observations of heave and shrinkage are given in Table 3.1.

Table 3.1. Typical Values of Lateral Earth Pressure Coefficient for Several Different Conditions (Lytton et al. 2005)

Conditions	K_o	e	d	k	n
Cracked	0	0	0	0	1
Drying (Active)	1/3	1	0	0	1
Equilibrium (at rest)	1/2	1	1	0	1
Wetting (within movement active zone)	2/3	1	1	0.5	1
Wetting (below movement active zone)	1	1	1	1	1
Swelling near surface (passive earth pressure)	3	1	1	1	2

The regression equation between the angle of internal friction ϕ' and plasticity index, PI, based on the empirical correlation (Fig. 3.3) from the triaxial compression tests is given by:

$$\phi' = 0.0016PI^2 - 0.3021PI + 36.208 \quad (3.5)$$

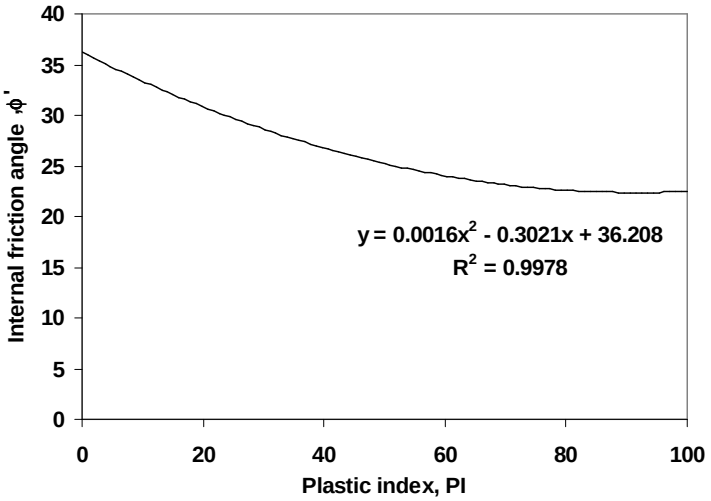

Fig. 3.3. The Regression Equation Based on the Relation on the Empirical Correlation between ϕ' and PI (after Holtz and Kovacs 1981)

The vertical strain is estimated from the volume strain by using a crack fabric factor f_c:

$$\frac{\Delta H}{H} = f_c\left(\frac{\Delta V}{V}\right) \quad (3.6)$$

where $\frac{\Delta H}{H}$ = the vertical strain

f_c = $0.67 - 0.33\Delta pF$ ($\Delta pF =$ the change of suction, $1/3 \le f_c \le 1.0$)

Back-calculated general values of f_c are 0.5 when the soil is drying and 0.8 when the soil is wetting. The level to which the lateral pressure rises is limited by the Gibbs free energy (suction) released by the water; the level to which it drops on shrinking is limited by the ability of the water phase to store released strain energy. The total heave or shrinkage in a soil mass is the sum of the products of the vertical strains and the increment of depth to which they apply, Δz_i:

$$\Delta H = \sum_{i=1}^{n} f_c \left(\frac{\Delta V}{V} \right)_i \Delta z_i \tag{3.7}$$

where:

n = the number of depth increments

Δz_i = the ith depth increment

f_c = the crack fabric factor

$\left(\frac{\Delta \mathrm{V}}{\mathrm{V}} \right)_{i,swelling} = -\gamma_h \log\left(\frac{h_f}{h_i} \right) - \gamma_\sigma \log\left(\frac{\sigma_f}{\sigma_i} \right)$

$\left(\frac{\Delta \mathrm{V}}{\mathrm{V}} \right)_{i,shrinkage} = -\gamma_h \log\left(\frac{h_f}{h_i} \right) + \gamma_\sigma \log\left(\frac{\sigma_f}{\sigma_i} \right)$

3.3 Estimating Soil Swelling Parameters from Index Properties

The principal material property needed to compute the vertical movement is the suction compression index γ_h. Historically, this has been estimated with the chart developed by McKeen (1981), shown in Fig. 3.4. The two axes are given by the activity ratio A_c and the cation exchange activity ratio CEA_c which are defined as follows:

$$A_c = \frac{PI\%}{\frac{\%-2micron}{\%-No.200sieve} \times 100} \tag{3.8}$$

where:

$PI\%$ = the plastic index in percent

$$CEA_c = \frac{CEC \frac{milli\,equivalents}{100\,gm\,of\ dry\,soil}}{\frac{\%-No.2\,micron}{\%-No.200\,sieve} \times 100} \tag{3.9}$$

where:

CEC = the cation exchange capacity in milliequivalents per 100 gm of dry soil

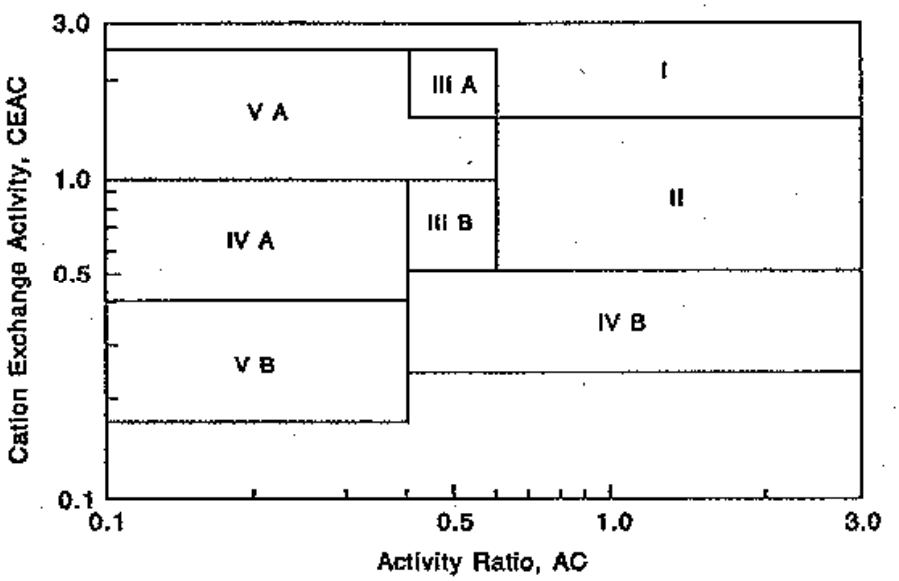

Fig. 3.4. Chart for Prediction of Suction Compression Index Guide Number (McKeen 1981)

The denominator of both activity ratios is known as the "percent fine clay" and represents that percent of the portion of the soil that passes the No. 200 sieve and is finer than 2 microns.

The cation exchange capacity (CEC) may be measured with a spectrophotometer or it may be estimated with sufficient accuracy by the following equation that was developed by Mojeckwu (1979).

$$CEC \cong (PI\%)^{1.17} \tag{3.10}$$

The regions on the chart each have a volume change guide number corresponding to the suction compression index of a soil with 100 percent fine clay. Values of the guide numbers are given in Table 3.2. The actual suction compression index is proportional to the actual percent of fine clay in the soil. Thus, the actual γ_h is given by:

$$\gamma_h = \gamma_o \times \left[\frac{\% - 2\,micron}{\% - No.200\,sieve} \right] \tag{3.11}$$

Table 3.2. Values for a Soil with 100% Fine Clay Content

Region	Volume Change γ_0 Guide Number
I	0.220
II	0.163
IIIA	0.096
IIIB	0.061
IVB	0.061
VA	0.033
VB	0.033

The mean principal stress compression index γ_σ is related to γ_h by the following equation (Lytton 1994):

$$\gamma_\sigma = \gamma_h \frac{1}{1+\frac{h}{\theta\left(\frac{\partial h}{\partial \theta}\right)}} \tag{3.12}$$

where:

θ = the volumetric water content

$\frac{\partial h}{\partial \theta}$ = the slope of the suction-versus-volumetric water content curve (Fig. 3.5)

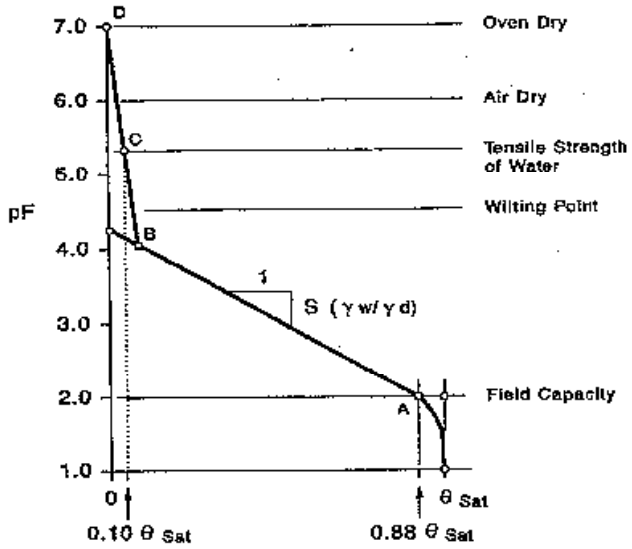

Fig. 3.5. Suction-versus-Volumetric Water Content Curve (Lytton 1994)

The slope of the suction-versus-volumetric water content curve is given by:

$$\left[\frac{\partial h}{\partial \theta}\right] = \frac{1}{0.4343}\frac{S\gamma_w}{\gamma_d}h \tag{3.13}$$

The value of *S* is negative and can be estimated from:

$$S = -20.29 + 0.1555(LL) - 0.117(PI) + 0.0684(-\#200) \tag{3.14}$$

where:

LL = the liquid limit in percent

PI = the plasticity index in percent

$-\#200$ = the percent of soil passing the #200 sieve.

Because both *S* and *h* are negative, the slope is inherently positive. The correction term in the relation between γ_h and γ_σ given in Eq. (3.11) is found by:

$$\frac{h}{\theta\left[\frac{\partial h}{\partial \theta}\right]} = \frac{0.4343}{Sw} \tag{3.15}$$

where w = the gravimetric water content

Because S is negative, so is the correction term. An approximate suction (pF)-versus-volumetric water content curve can be constructed with the empirical relationships given above and the saturated volumetric water contents given in Table 3.3. The construction is illustrated in Fig. 3.5. First, point A is located at the intersection of the field capacity volumetric water content ($=0.88\theta_{sat}$) and a pF of 2.0. Second, a line with a slope of $S\left(\gamma_w / \gamma_d\right)$ is drawn from point A to its intersection with the vertical axis. Third, point C is located at a volumetric water content of $0.10\theta_{sat}$ and the tensile strength of water (pF=5.3 or 200 atmospheres). Fourth, point D is located at zero water content and a pF of 7.0, corresponding to oven dry. Fifth, a straight line is drawn between points C and D to its intersection with the first line.

This construction makes it possible to estimate water contents once the computed suction profiles are known. This allows measured water contents to be compared with the predicted values.

Table 3.3. Range of Saturated Volumetric Water Content by Unified Soil Classification System (Mason et al. 1986)

Unified Class	Ranges of θ_{sat}
GW	0.31-0.42
GP	0.20
GM	0.21-0.38
GM-GC	0.30
SW	0.28-0.40
SP	0.37-0.45
SM	0.28-0.68
SW-SP	0.30
SP-SM	0.37
SM-SC	0.40
ML	0.38-0.68
CL	0.29-0.54
ML-CL	0.39-0.41
ML-OL	0.47-0.63
CH	0.50
$\theta_{sat} = n$ (porosity), where n is porosity	

3.4 Estimating Soil Swelling Parameters Based on LL and PI

The method developed herein represents a refinement of earlier methods. The method builds on these earlier methods in that it is consistent in the use of low cost and easily available testing methods (Atterberg limits and soil particle size distributions) to predict soils properties and behavior (Covar and Lytton 2001).

This method was developed based on the soil data of the Soil Survey Laboratory (SSL) of the National Soil Survey Center. Most of the data in the present database were obtained over the last 40 years with approximately 75 percent of the data being obtained in the last 25 years. The SSL database may be accessed online at http://www.statlab.iastate.edu/soils/ssl. The database is also available on CD-ROM from the SSL.

For this study, the researchers filtered the SSL database to retain only those records that contained non-null results for the following tests:

- liquid limit,
- coefficient of linear extensibility,
- plasticity index,
- percent passing 2 micron,
- plastic limit,
- percent passing No. 200 sieve, and
- cation exchange capacity.

This data filtering produced a subset of the data containing approximately 6500 records (Fig. 3.6). Next, the data records were partitioned based on Casagrande (1948) and the Holtz and Kovacs (1981) mineral classification (Fig. 3.7). This partitioning step resulted in eight separate data groups, each representing a group with some mineralogical similarity.

The method is “stable” in the sense that each mineralogical zone or group is explicitly defined; thus, no arbitrary distinctions can affect the results. Within each group, the practitioner needs only the liquid limit, plasticity index, and the fine clay

fraction (%) to get an estimate of the soil compression index (Figs. 3.8 to 3.15). The soil compression index can then be explicitly entered into Eq.(3.7) to calculate shrink and swell behavior. Small changes in soil index properties result in small changes in the derived soil compression index within each mineralogical based group. The proposed method, therefore, provides a quick and stable prediction of an important soil property using low cost and commonly available soil test procedures.

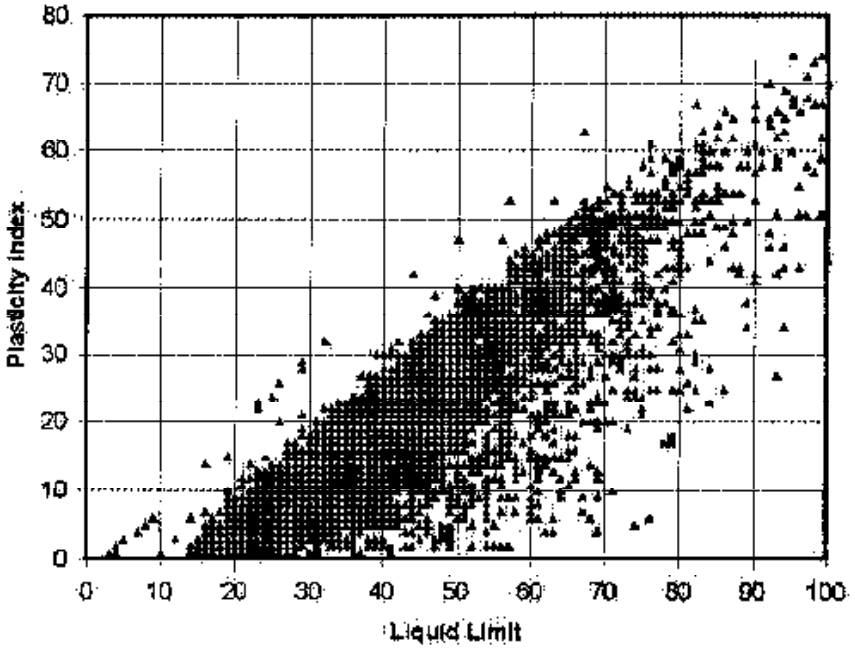

Fig. 3.6. Data Set (6500 records) for Soil Compression Index Calculations (Covar and Lytton 2001)

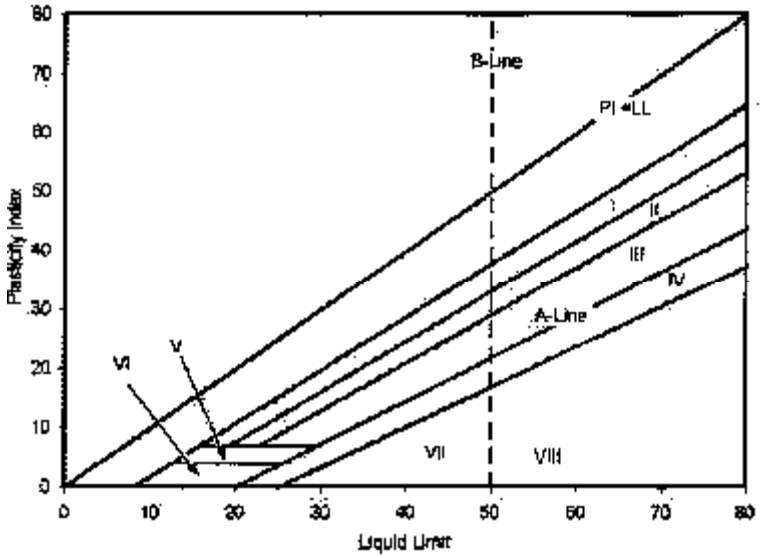

Fig. 3.7. Data Filter for Partitioning Database on Mineralogical Types (after Casagrande 1948; Holtz and Kovacs 1981)

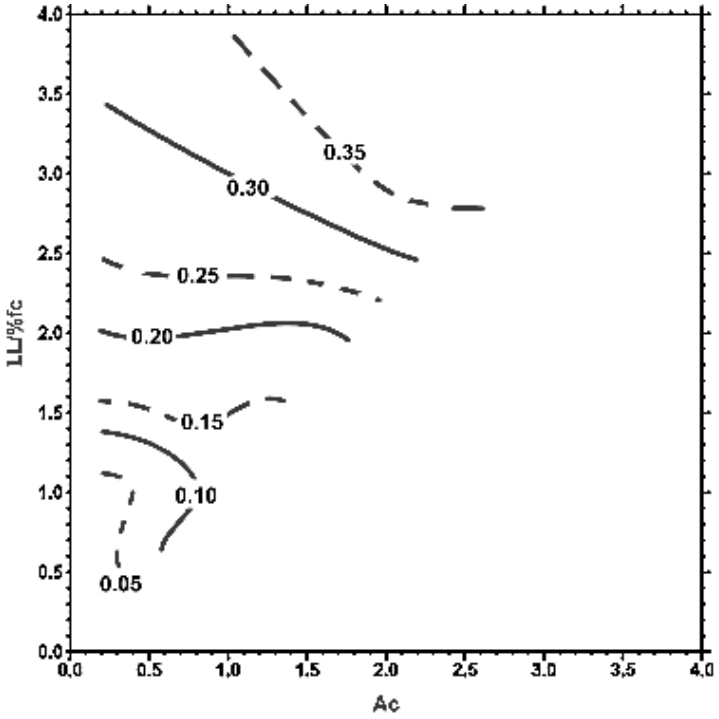

Fig. 3.8. Zone I Chart for Determining γ_o (Covar and Lytton 2001)

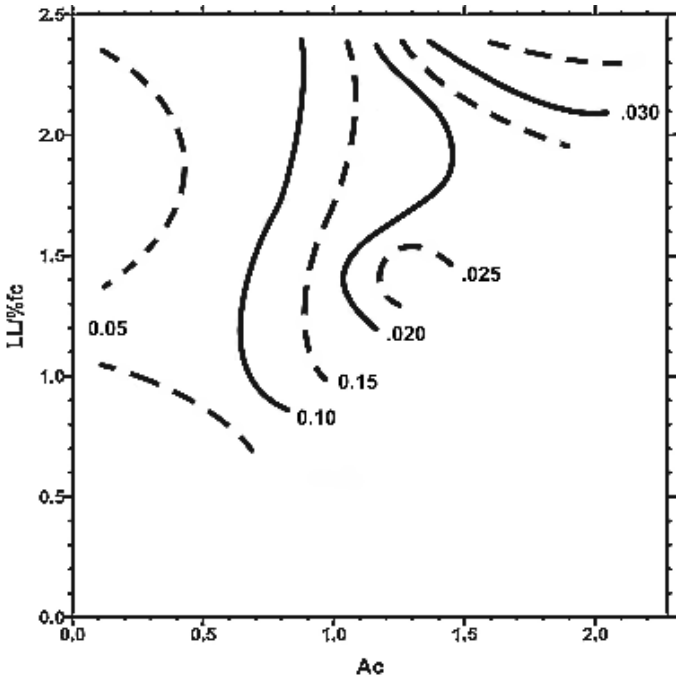

Fig. 3.9. Zone II Chart for Determining γ_o (Covar and Lytton 2001)

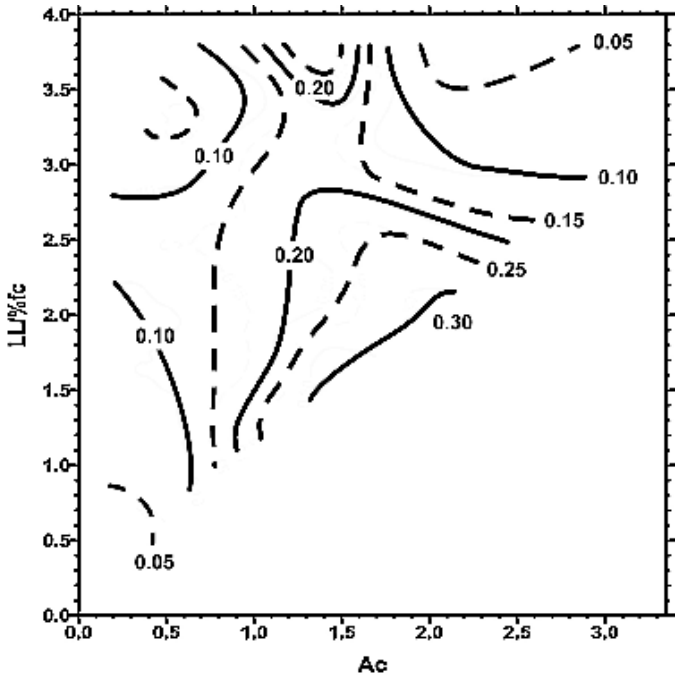

Fig. 3.10. Zone III Chart for Determining γ_o (Covar and Lytton 2001)

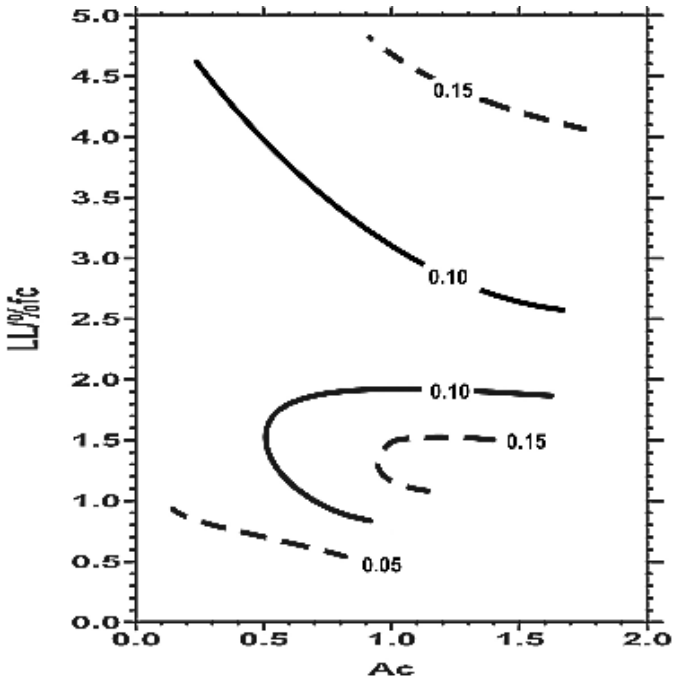

Fig. 3.11. Zone IV Chart for Determining γ_o (Covar and Lytton 2001)

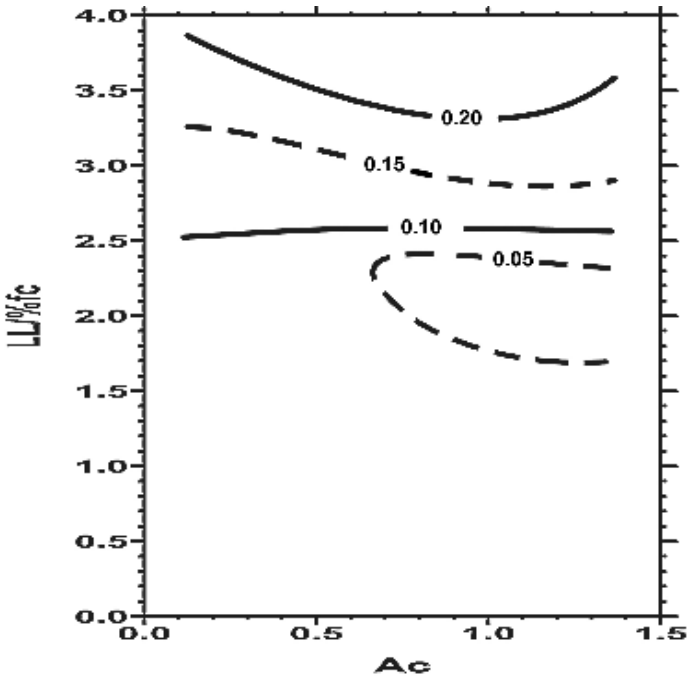

Fig. 3.12. Zone V Chart for Determining γ_o (Covar and Lytton 2001)

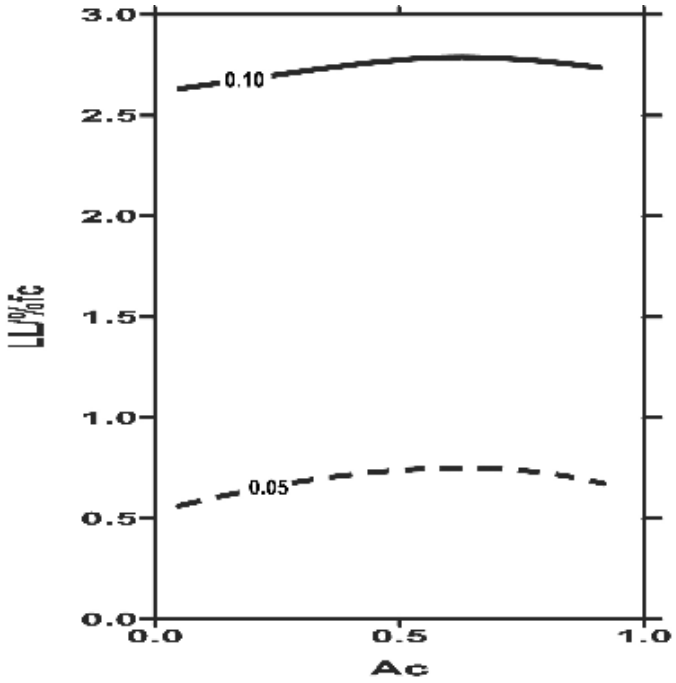

Fig. 3.13. Zone VI Chart for Determining γ_o (Covar and Lytton 2001)

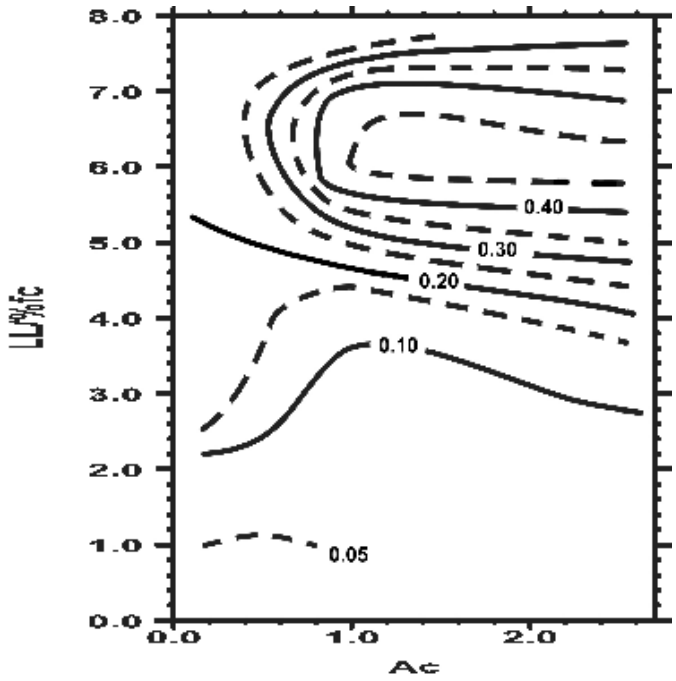

Fig. 3.14. Zone VII Chart for Determining γ_o (Covar and Lytton 2001)

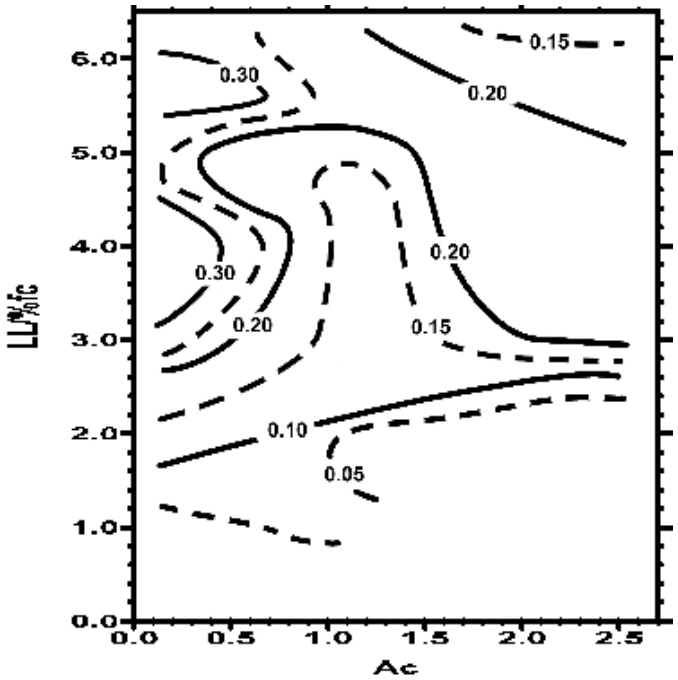

Fig. 3.15. Zone VIII Chart for Determining γ_o (Covar and Lytton 2001)

The suction compression index obtained from Eq. (3.11) is corrected to compensate for the different initial volume of soil mass during a wetting or drying process.

$$\gamma_{h(swelling)} = \gamma_h e^{\gamma_h} \tag{3.16}$$

$$\gamma_{h(shrinkage)} = \gamma_h e^{-\gamma_h} \tag{3.17}$$

A suction compression index for stabilized soil can be estimated using Atterberg limits, soil particle size distribution of the natural soil to be stabilized, and the percent of stabilizing material such as lime or cement.

If lime is used as a stabilizing material,

$$\mathrm{PI}_{\text{stabilized}} = \mathrm{PI}_{\text{unstabilized}} \left(\frac{9 - \%\,\mathrm{lime}}{9} \right) \tag{3.18}$$

$$LL_{stabilized} = \frac{PI_{stabilized}}{a} + b \tag{3.19}$$

If cement is used as a stabilizing material,

$$\mathrm{PI}_{\text{stabilized}} = \mathrm{PI}_{\text{unstabilized}} \left(\frac{8 - \%\,\text{cement}}{8} \right) \tag{3.20}$$

$$LL_{stabilized} = \frac{PI_{stabilized}}{a} + b \tag{3.21}$$

The parameters *a* and *b* can be determined using the mineral classification chart (Fig. 3.7) for untreated soil. Typical values of these parameters are shown in Table 3.4.

Table 3.4. Determination of Parameters *a* and *b* Corresponding to Mineral Classification

Group	*a*	*b*
I	0.85	11
II	0.81	14
III	0.73	20
IV	0.68	25
V	0.68	25
VI	0.68	25

The empirical suction-versus-volumetric water content curve for natural, inert, and stabilized soil can be simplified as in Figs. 3.16, 3.17, and 3.18, respectively.

3.5 Suction-versus-Volumetric Water Content Curves

The suction-versus-volumetric water content curve for natural clay soil is simplified using the following process:

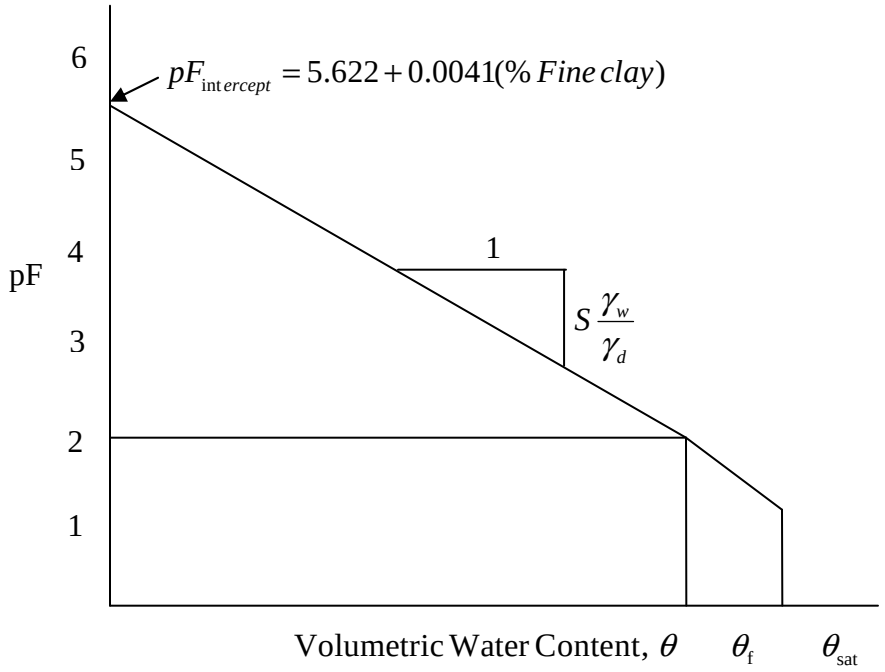

Fig. 3.16. Suction-versus-Volumetric Water Content Curve for Natural Clay Soil

The slope of suction-versus-gravimetric water content S is estimated by:

$$S = -20.29 + 0.1555(LL\%) - 0.117(PI\%) + 0.0684(\% - \#200) \tag{3.22}$$

From the geometric relation in Fig. 3.16, the relation of volumetric water content to the suction (pF) is given by:

$$\frac{\theta}{1.0} = \frac{pF_{\text{intsept}} - pF}{|S|\frac{\gamma_w}{\gamma_d}} \tag{3.23}$$

From rearranging Equation (3.23), the volumetric water content is:

$$\theta = \frac{pF_{\text{intersept}} - pF}{|S|\frac{\gamma_w}{\gamma_d}} \tag{3.24}$$

Gravimetric water content *w* is given by:

$$w = \frac{pF_{\text{intersept}} - pF}{|S|} \tag{3.25}$$

The suction-versus-volumetric water content curve for inert soil is simplified using the following process:

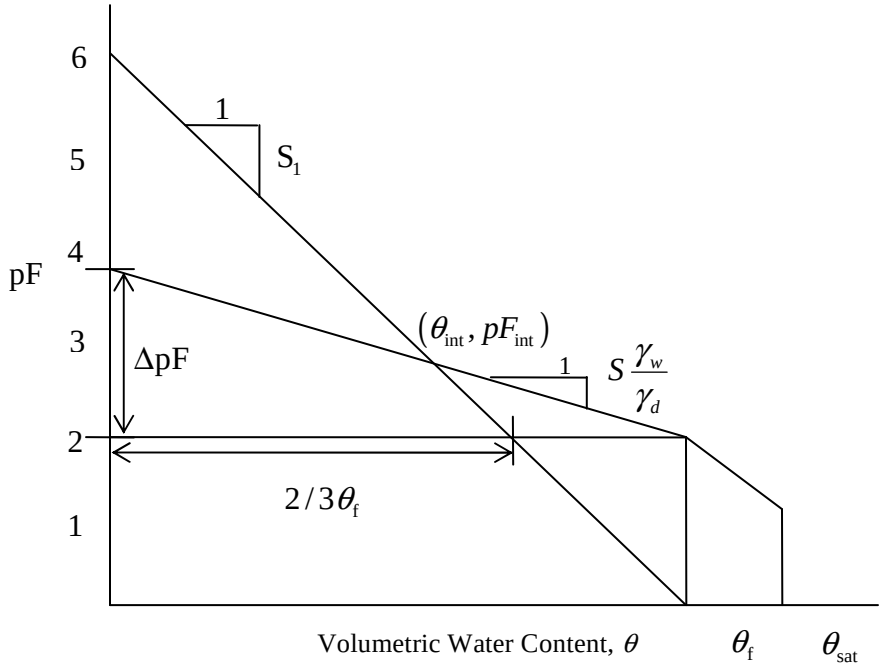

Fig. 3.17. Suction-versus-Volumetric Water Content Curve for Inert Soil

where:

S_1 = the slope from zero to the volumetric water content at the intersection

θ_{int} = the volumetric water content at the intersection

pF_{int} = the suction value at the intersection

The first slope S_1 using the geometric relation in Fig. 3.17 is as follows:

$$\frac{6.0-2.0}{\frac{2}{3}\theta_f}=\frac{|S_1|}{1.0} \tag{3.26}$$

From rearranging Eq. (3.26), S_1 is given by:

$$|S_1| = \frac{6.0}{\theta_f} \tag{3.27}$$

where:

$$\theta_f = 1 - \frac{\gamma_d}{G_s \gamma_w} \text{ (assuming } G_s = 2.70) \tag{3.28}$$

Using the second slope $S\frac{\gamma_w}{\gamma_d}$ ΔpF can be estimated as follows:

$$\frac{\theta_f}{\Delta pF} = \frac{1}{|S|\frac{\gamma_w}{\gamma_d}} \tag{3.29}$$

$$\Delta pF = \theta_f |S| \frac{\gamma_w}{\gamma_d} \tag{3.30}$$

The suction at the intersection pF_{int} can be expressed by:

$$pF_{\text{int}} = (2.0 + \Delta pF) - |S| \frac{\gamma_w}{\gamma_d} \theta_{\text{int}} \tag{3.31}$$

$$pF_{\text{int}} = 6.0 - |S_1| \theta_{\text{int}} \tag{3.32}$$

From Eqs. (3.31) and (3.32):

$$\theta_{\text{int}} = \frac{\Delta pF - 4.0}{|S|\frac{\gamma_w}{\gamma_d} - |S_1|} \tag{3.33}$$

$$pF_{\text{int}} = 6 - |S_1| \theta_{\text{int}} \tag{3.34}$$

Therefore, the volumetric water content on the two lines is given by:

$$\theta = \frac{6.0 - pF}{|S_1|} \qquad (0.0 \le \theta \le \theta_{\text{int}}) \tag{3.35}$$

$$\theta = \frac{pF_{\text{int}} - pF}{|S_1|\frac{\gamma_w}{\gamma_d}} \qquad (\theta_{\text{int}} \le \theta \le \theta_f) \tag{3.36}$$

And the gravimetric water content *w* is given by:

$$w = \frac{6.0 - pF}{|S_1|} \frac{\gamma_w}{\gamma_d} \qquad (0.0 \le \theta \le \theta_{\text{int}}) \tag{3.37}$$

$$w = \frac{pF_{\text{int}} - pF}{|S|} \qquad \left(\theta_{\text{int}} \le \theta \le \theta_f\right) \tag{3.38}$$

The suction-versus-volumetric water content curve for stabilized soil is simplified with the following process:

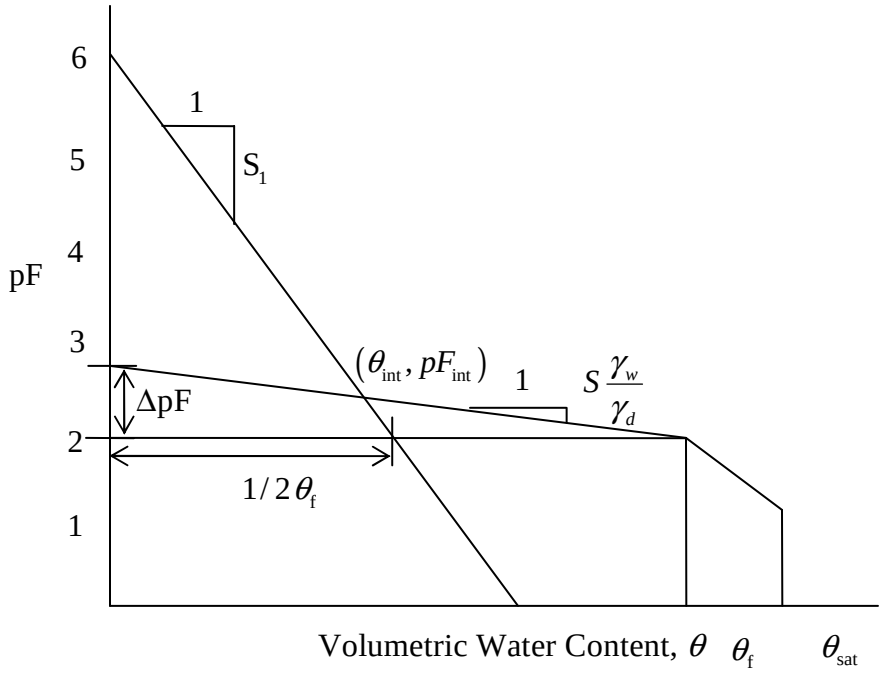

Fig. 3.18. Suction-versus-Volumetric Water Content Curve for Stabilized Soil

where:

S_1 = the slope from zero to the volumetric water content at the intersection

θ_{int} = the volumetric water content at the intersection

pF_{int} = the suction value at the intersection

The first slope S_1 using a geometric relation in Fig. 3.18 follows:

$$\frac{6.0 - 2.0}{\frac{1}{2}\theta_f} = \frac{|S_1|}{1.0} \tag{3.39}$$

From rearranging Equation (3.39):

$$|S_1| = \frac{8.0}{\theta_f} \tag{3.40}$$

where:

$$\theta_f = 1 - \frac{\gamma_d}{G_s \gamma_w} \text{ (assuming } G_s = 2.70) \tag{3.41}$$

Using the second slope $S\frac{\gamma_w}{\gamma_d}$, ΔpF can be estimated as follows:

$$\frac{\theta_f}{\Delta pF} = \frac{1}{\frac{1}{2}|S|\frac{\gamma_w}{\gamma_d}} \tag{3.42}$$

$$\Delta pF = \theta_f \frac{1}{2}|S|\frac{\gamma_w}{\gamma_d} \tag{3.43}$$

The suction at the intersection pF_{int} can be expressed by:

$$pF_{\text{int}} = (2.0 + \Delta pF) - \frac{1}{2}|S|\frac{\gamma_w}{\gamma_d}\theta_{\text{int}} \tag{3.44}$$

$$pF_{\text{int}} = 6.0 - |S_1|\theta_{\text{int}} \tag{3.45}$$

From Eq. (3.44) and (3.45):

$$\theta_{\text{int}} = \frac{\Delta pF - 4.0}{\frac{1}{2}|S|\frac{\gamma_w}{\gamma_d} - |S_1|} \tag{3.46}$$

$$pF_{\text{int}} = 6 - |S_1|\theta_{\text{int}} \tag{3.47}$$

Therefore, the volumetric water content on the two lines is given by:

$$\theta = \frac{6.0 - pF}{|S_1|} \qquad (0.0 \le \theta \le \theta_{\text{int}}) \tag{3.48}$$

$$\theta = \frac{pF_{\text{int}} - pF}{\frac{1}{2}|S|\frac{\gamma_w}{\gamma_d}} \qquad (\theta_{\text{int}} \le \theta \le \theta_f) \tag{3.49}$$

And then the gravimetric water content is given by:

$$w = \frac{6.0 - pF}{|S_1|}\frac{\gamma_w}{\gamma_d} \qquad \left(0.0 \le \theta \le \theta_{\text{int}}\right) \tag{3.50}$$

$$w = \frac{pF_{\text{int}} - pF}{\frac{1}{2}|S|} \qquad \left(\theta_{\text{int}} \le \theta \le \theta_f\right) \tag{3.51}$$

These characteristics of the natural soil, inert soil, and stabilized soil are integrated into the pavement design program WinPRES, which is used to design both flexible and rigid pavements on expansive soils.

3.6 Estimation of Suction Profile

For design purposes, it is desirable to compute the total heave that occurs between two steady state suction profiles, one given by constant velocity of water entering the profile (low suction due to wetting) and the other given by constant velocity of water leaving the profile (high suction level due to drying).

The suction profile for two transient states can be predicted approximately using (Mitchell 1979):

$$U(Z,t) = U_e + U_o \exp\left(-\sqrt{\frac{n\pi}{\alpha}}Z\right)\cos\left(2\pi nt - \sqrt{\frac{n\pi}{\alpha}}Z\right) \tag{3.52}$$

where:

Z = depth

U_e = the equilibrium value of suction expressed as pF

U_o = the amplitude of pF (suction) change at the ground surface

n = the amplitude of suction cycles per second 1/(1 year=31.5×10^6 seconds)

α = the soil diffusion coefficient using Michell's unsaturated permeability (ranges between 10^5 and 10^3 cm^2/sec)

t = time in seconds

Tables of values of U_e and U_o for clay soils with different levels of Mitchell's unsaturated permeability have been found using a trial and error procedure. The dry

suction profile has a U_e value of 4.5 and a U_0 value of 0.0. The wet suction profile has U_e and U_0 values that vary with the soil type and Thornthwaite moisture index (TMI). The exponential suction profile for the side of extreme dry and wet conditions is expressed based on the equation for a transient state (Eq. 3.52):

$$U(Z) = U_e \pm U_0 \exp\left(-\sqrt{\frac{n\pi}{\alpha}}Z\right) \tag{3.53}$$

3.7 Estimation of Moisture Diffusion Coefficient

The moisture diffusion coefficient α is the most critical parameter controlling the depth of the moisture active zone and the suction envelope of the extreme case for wet and dry condition in the field. Laboratory measurements of α on intact clay samples will normally be far less than that representative of field conditions. The moisture diffusion coefficient α can be determined by using empirical equation (Lytton 1994) or laboratory measurement with crack correction.

Estimation of Empirical Diffusivity α

An empirical diffusion coefficient α can be estimated from (Lytton 1994):

$$\alpha = 0.0029 - 0.000162(S) - 0.0122(\gamma_h) \tag{3.54}$$

where γ_h is the suction compression index, and S is the slope of the suction-water content curve in the Eq. (3.22)

However, a site-specific determination is definitely desirable when sufficient data are available. Two approaches for a site-specific determination are discussed below.

Laboratory Measurement with Crack Correction

The unsaturated soil diffusivity test performed in the laboratory represents conditions of an intact soil mass. While intact conditions can occur under certain conditions such as the absence of root penetration or desiccation cracking, more commonly some degree of

cracking can be expected within the soil mass. Such cracking will substantially increase the apparent diffusivity α_{field} of the soil mass to well above that indicated from a laboratory test. In addition, the existence of fractures will generate heterogeneity in the soil mass such that α_{field} depends on sampling location; hence, α_{field} must be expressed in probabilistic terms. Figure 3.19 shows the relationship of the ratio $\alpha_{field}/\alpha_{lab}$ expressed in terms of probability of non-exceedance for crack depths ranging from 1 to 16 ft. This figure shows that for crack depths up to 16 ft, α_{field} can exceed α_{lab} by a multiplier of greater than 100.

Figure 3.20 shows the general nature of desiccation crack patterns in a soil mass. Crack patterns near the ground surface are usually closely spaced. However, the spacing of deep cracks is much wider than the shallower cracks, with crack spacing being approximately equal to crack depth. Estimating crack depth through direct observation is generally difficult. However, there are several indirect indicators of crack depth that are reasonably reliable. The first is the occurrence of any root fiber. Tree roots cannot penetrate an intact clay mass; i.e., root penetration occurs along cracks in clay soils. In addition, the roots induce desiccation within a vicinity of about 2 ft; therefore, cracking will extend to about 2 ft deeper than the deepest root fiber.

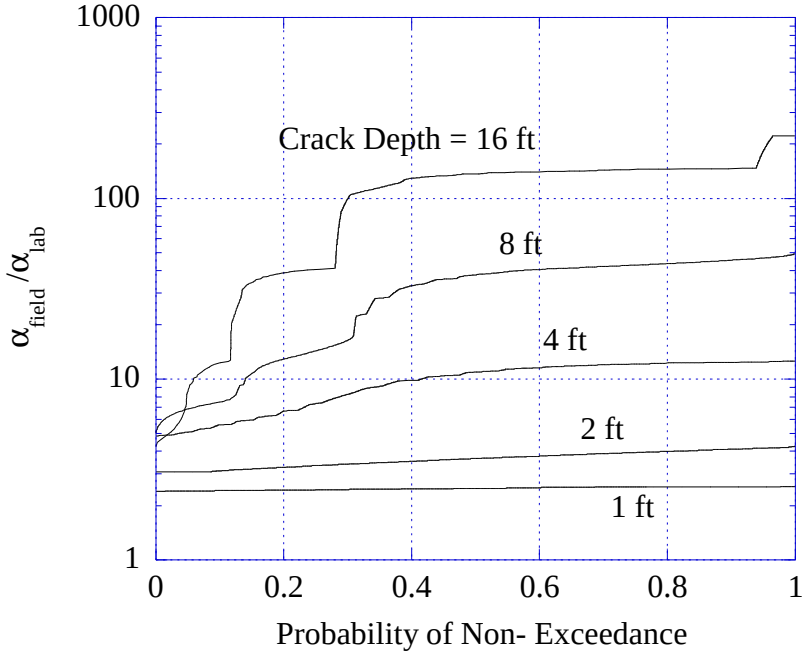

Fig. 3.19. Adjustment of Laboratory Measurements of Diffusivity for Effects of Cracking

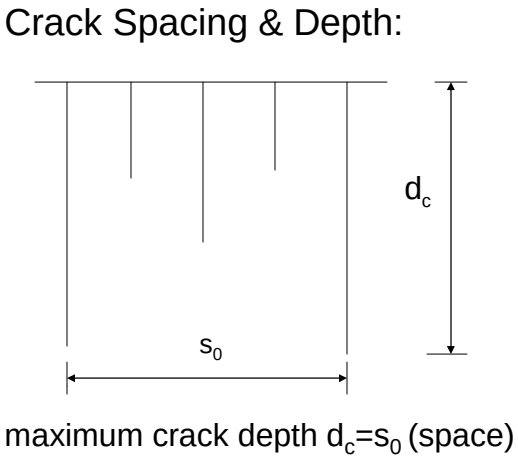

Fig. 3.20. Desiccation Crack Pattern in a Soil Mass

Example 1

A diffusivity measured in a laboratory diffusion test indicates $\alpha_{lab} = 8.0x10^{-5}$ cm^2/sec. Root fibers in the borehole from which the soil sample was taken were observed to a depth of 6 ft. Estimate the field diffusivity α_{field} corresponding to a 50% level of non-exceedance.

Since roots were observed to a depth of 6 ft, a maximum crack depth of 8 ft should be assumed. From Fig. 3.19, for a 50% level of non-exceedance and a crack depth of 8 ft, $\alpha_{field}/\alpha_{field}=40$. Hence:

$$\alpha_{field} = 40 \times 8.0x10^{-5}\ cm^2/sec = 3.2x10^{-3}\ cm^2/sec \qquad (3.55)$$

A second indicator of tree root depth is a suction profile at or near the wilting point of vegetation, about 4.5 pF. Figure 3.21 shows the characteristic suction profile of a deep root zone. Corrections for crack depths estimated through this method are computed in an identical manner as that shown in the above example.

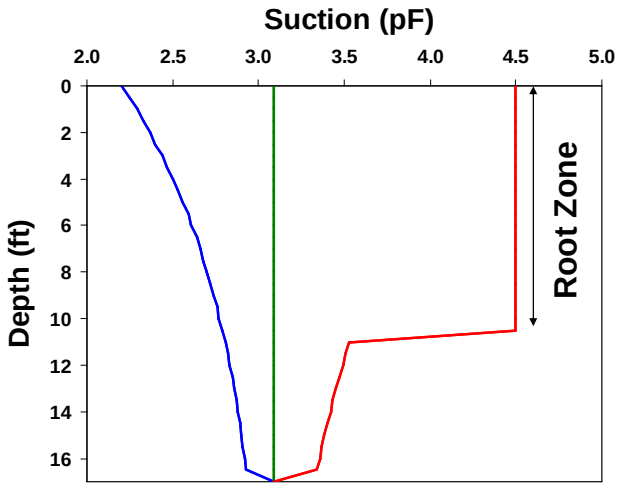

Fig. 3.21. Characteristic Suction Profile for a Deep Root Zone

Diffusivity from the Depth of Moisture Active Zone

Estimates of the depth of the moisture active zone y_{ma} can also provide a basis for estimating field diffusivity α_{field} using the relationship:

$$\alpha_{field} = 0.6\, n\, (y_{ma})^2 \qquad (3.56)$$

where n is the frequency of seasonal suction variation, usually 1cycle/yr.

Example 2

An examination of a suction profile indicates that an equilibrium suction is reached at a depth of 12 ft. Estimate the field diffusivity α_{field}. In this case, the depth of the moisture active zone y_{ma} = 12 ft. Based on the Equation (3.56), assuming a seasonal frequency n = 1 yr leads to:

$$\alpha_{field} = 0.6\ (1\ \text{cycle/yr})\ (12\ \text{ft})^2 = 86.4\ \text{ft}^2/\text{yr}$$

Conversion to units of cm^2/sec leads to $\alpha_{field} = 2.6 \times 10^{-3}\ cm^2/sec$.

3.8 Example of Calculation of Swelling and Shrinkage

One of typical study sections, Fort Worth North Loop IH820 section B, is used to show the input parameters and results using this model. Laboratory test data such as Atterberg limits, particle size distribution, measured suctions, and moisture diffusion test results are used in this analysis. Table 3.5 shows the thickness of soil layers, liquid limit (LL), the plasticity index (PI), the percent of soil particles passing the #200 sieve, the percentage of soil particles finer than 2 microns, corrected suction compression index, and diffusion coefficient in each soil layer.

Table 3.5. Soil Properties and Diffusivity Based on Laboratory Tests

Soil Layer	Thickness (ft)	LL (%)	PI (%)	-#200 (%)	-2μm (%)	$\gamma_{h\_corrected}$	α_{field} (cm^2/sec)
1	3.5	60	36	85	30	0.0706	3.36×10^{-3}
2	1.5	55	30	80	25	0.0469	3.36×10^{-3}
3	4	65	38	85	30	0.0565	3.31×10^{-3}
4	0.5	30	15	35	10	0.0257	3.44×10^{-3}
5	1.5	53	32	80	25	0.0547	3.86×10^{-3}
6	4	45	15	99	37	0.0262	3.04×10^{-3}

The suction envelope defines the depth of the moisture-active zone and the magnitude of seasonal suction variations that occur within this zone. Measured matric suction of 3.45 pF by filter paper test of soil sample at depth of 13 ft to 14 ft is used to represent equilibrium suction as an initial condition, h_i in the Equation (3.1). The suction values of 2.5 pF and 4.5 pF at ground surface are used to define as a field capacity and wilting point, respectively as shown in Fig. 3.22(a). The suction envelope of wet side from ground surface to the depth of moisture active zone, 15 ft, is defined as a final suction condition h_f in the calculation of swelling movements as shown in Fig. 3.22(b). The suction envelope of dry side is defined as a final suction condition h_f in the calculation of shrinkage movements. Vertical swelling and shrinkage are calculated from volume change, crack fabric factor and the increment of soil elements in Eq. (3.7) as shown in Fig. 3.22(b). The results show that the swelling movement of 2.5 inches and the shrinkage movement of 1.3 inches are predicted at ground surface.

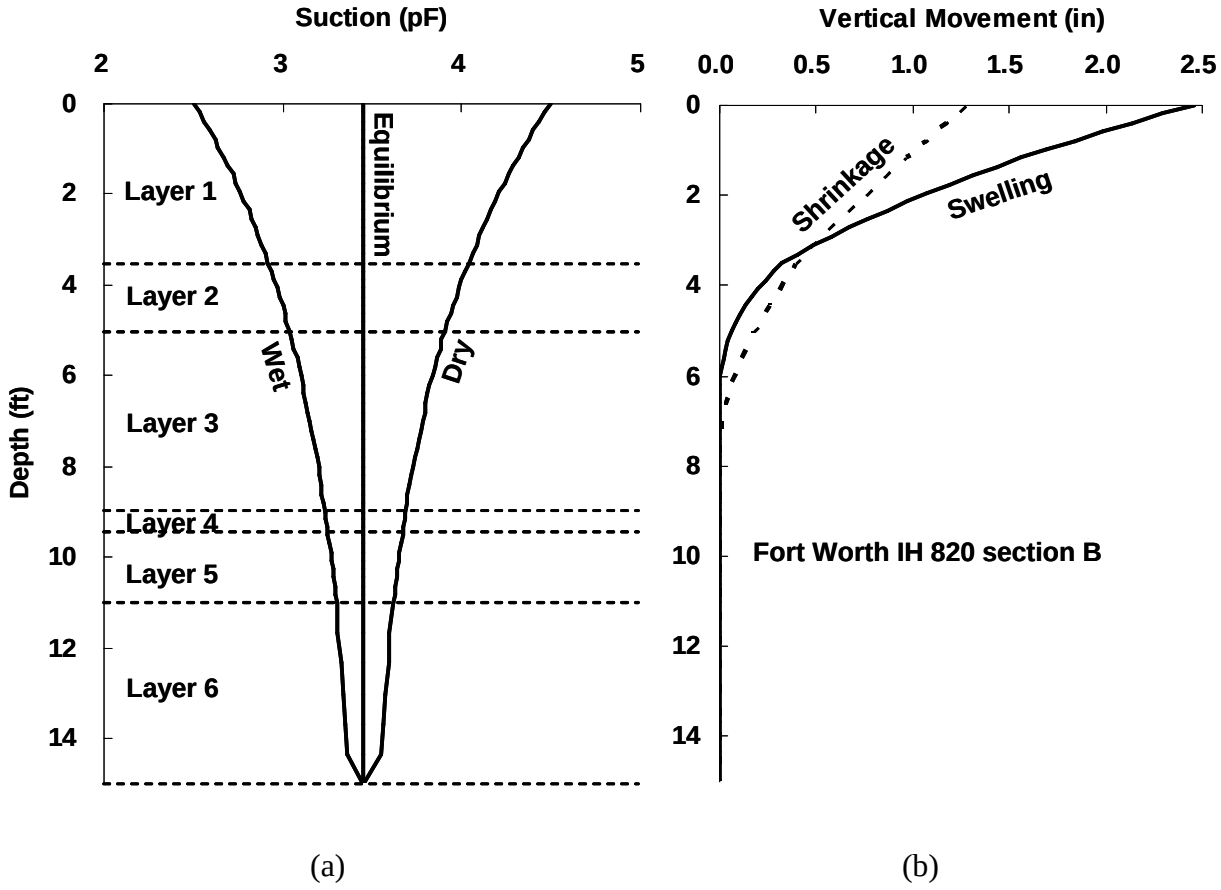

Fig. 3.22. Suction Profiles and Accumulated Vertical Movements versus Depth. (a) Suction Profiles versus Depth, (b) Vertical Movements versus Depth

Using the same methodology above, swelling movements required on the prediction of horizontal pressures on stationary walls in the following chapters IV, V and VI and swelling and shrinkage movements at the edge of the pavements in the following Chapter IX are calculated. Therefore, the same module to estimate the suction profile and swelling and shrinkage movements is used in the three numerical models WinPRES (Windows based Pavement Roughness on Expansive Soils), RWES (Retaining Wall in Expansive Soils), and DRES (Drilled Pier in Expansive Soils) written in the Fortran language and developed in Visual Basic.

CHAPTER IV
HORIZONTAL EARTH PRESSURE IN A STATIONARY WALL DUE TO SUCTION CHANGE

4.1 Introduction

Buried structures such as foundation piles, caissons, pipes, and buried conduits, are subjected to uplift and friction forces due to swelling and shrinking of the soil. They are also subjected to horizontal swelling pressures tending to cause horizontal deformations and bending. It is possible for cracks and fissures in the soil mass to accommodate lateral volume change. However, the large lateral swelling pressure will be developed due to the effect of restrained soil without cracks in a wetting process. In this chapter, the horizontal earth pressure caused by suction change on a stationary wall is presented using Mohr's circles and failure criteria and passive stress state in the movement active zone.

Numerous researches have been performed to estimate the lateral earth pressure against retaining walls and piers in expansive soils. The typical pattern of horizontal swelling pressures on the stationary wall in the three zones is proposed. The volume change equation and the concept of effective stress of unsaturated soil are used to formulate horizontal swelling pressure equations in pressure zones I, II and III. The shear strength of soil can be estimated using the geometry of a Mohr's circle. The prediction of the horizontal pressures due to suction change in a soil is compared with the in situ measurement of natural horizontal pressures observed by Brackley and Sanders (1992) and the measurements from large scale tests (Katti et al. 1979; Komornik 1962). These large horizontal predicted pressures are of great significance in explaining some of the structural failures in expansive soils. Therefore, the prediction of horizontal swelling pressure as a factor in the design of structures is needed.

4.2 Literature Review

Kassiff and Zeitlen (1962) reported the results of a study of the stresses induced in pipes buried in a field of expansive clays and exposed to seasonal changes, as well as irrigation. The measurements showed that high stresses resulted in the pipe through inequalities in the lateral and vertical swelling behavior of the clay, and that these stresses could be greater than those caused by internal pressure. It was found that the swelling forces were strongly influenced by the effect of lateral restraint of the pipe. The bending moments caused by soil pressures were found to be magnified by the rigidity of the pipe connections.

Kurzeme and Richards (1974) monitored earth pressures on the wall and soil suctions in the clay to investigate the behaviour of the retaining wall in expansive clay. A 7.5 m deep basement of the Gouger Street Mail Exchange building in Adelaide, South Australia, required the construction of a reinforced concrete retaining wall, supporting over most of its depth, stiff Hindmarsh clay. It was found that the earth pressures increased at the bottom of the wall, leveling off at a value of 1.3 to 4 times the overburden while the initial earth pressures were negligible. The pressure increase moves progressively up the wall with time. The most likely cause of this pressure increase seems to be the accumulation of water in the initial gap between the wall and the clay, followed by the local swelling of the clay.

Komornik and Zeitlen (1973) performed two model pile tests to evaluate the forces exerted on piles by the swelling of expansive soils leading to the design of piles for adequate resistance and stability. In order to measure the stresses induced in the piles and compare the results to laboratory results, the two model piles were instrumented using electrical resistance and vibrating wire strain gages mounted on the reinforcement of the piles. The expansive soils surrounding the piles were subjected to different wetting conditions, both uniform and non-uniform. It was found that both piles showed about the same values of shear forces, but the pile subjected to non-uniform wetting experienced high moments.

The large scale retaining wall model studies to simulate the filed conditions in black cotton expansive soils were performed by Joshi and Katti (1980). It was found that the lateral pressure variation with depth in expansive black cotton soils was significantly different from that of conventional soils. The lateral pressure at a shallow depth of 3.0 ft was recorded to be 3.0tsf.

The lateral swelling pressure determined using a hydraulic triaxial cell for a clay was found to be approximately twice as large as the vertical swelling pressure determined from a conventional odometer cell (Fourie 1989).

Brackley and Sanders (1992) installed vibrating-wire earth cells in a highly expansive, unsaturated lacustrine clay deposit, to measure the natural in situ horizontal pressure. Four suction profiles were monitored using psychrometers, complemented by laboratory testing with psychrometers and pressure plate apparatus. The horizontal pressures were monitored using earth pressure cells for several years. It was found that the total horizontal earth pressure developed in the lacustrine clay was two to four times the total vertical stress. This indicates a possible condition of passive failure of the soil. Seasonal fluctuation related to rainfall and evapo-transpiration was observed.

4.3 Concept of Lateral Earth Pressure on a Stationary Wall due to Suction Change

Figure 4.1(a) shows that suction change appears at all depths from the initial to final suction profiles which represent the equilibrium and extreme wet conditions, respectively. The lateral earth pressure on a stationary wall due to this suction change tends to increase from the ground surface as shown in Fig. 4.1(a). These lateral earth pressures are predicted based upon the variation of suction, suction compression index, and overburden pressure with depth. The lateral earth pressure increase with depth near the ground surface is limited by the maximum soil strength that can be supported by the overburden pressure as shown in Fig. 4.1(b). At greater depths, the lateral swelling pressure caused by small suction change is less than the classical at rest lateral earth pressure (Fig. 4.1(c)). Thus, the three zones proposed for the typical distribution of lateral earth pressures are shown in Fig. 4.1(d).

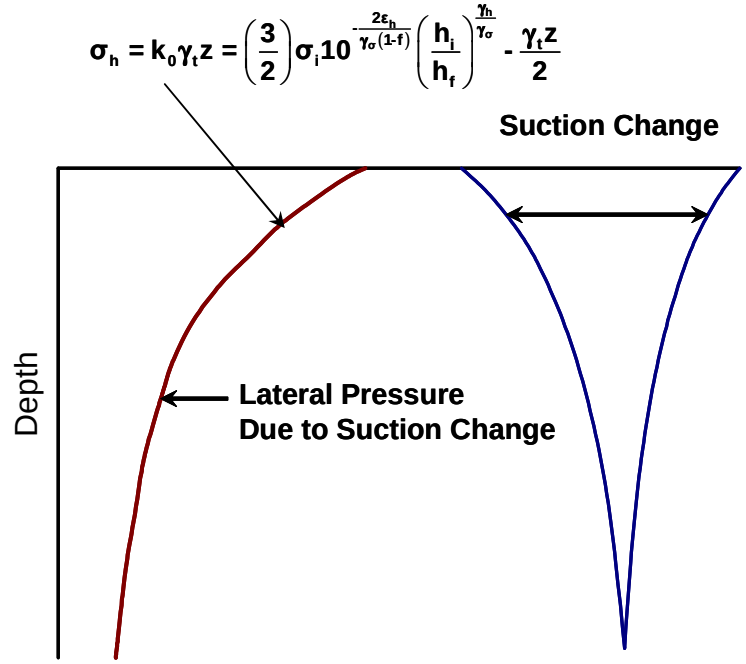

(a)

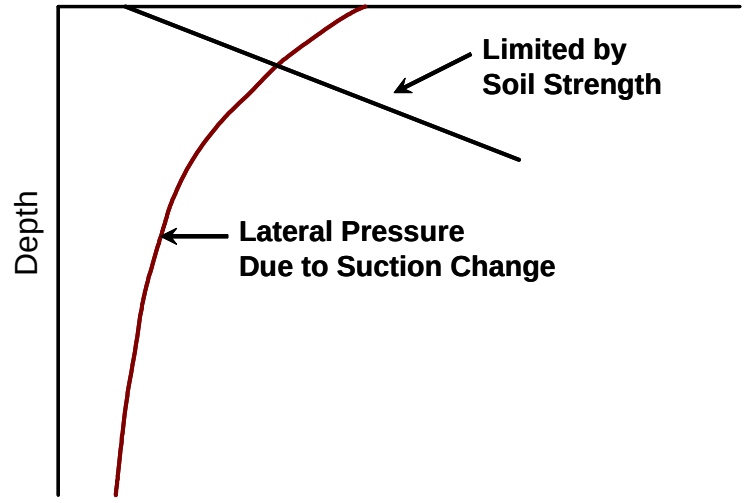

(b)

Fig. 4.1. Concept of the Lateral Earth Pressure on a Stationary Wall due to Suction Change. (a) Lateral Pressure due to Suction Change, (b) Lateral Pressure Limited by Soil Strength near the Ground Surface, (c) Lateral pressures by Small Suction Change, (d) Typical Distribution of Lateral Earth Pressure.

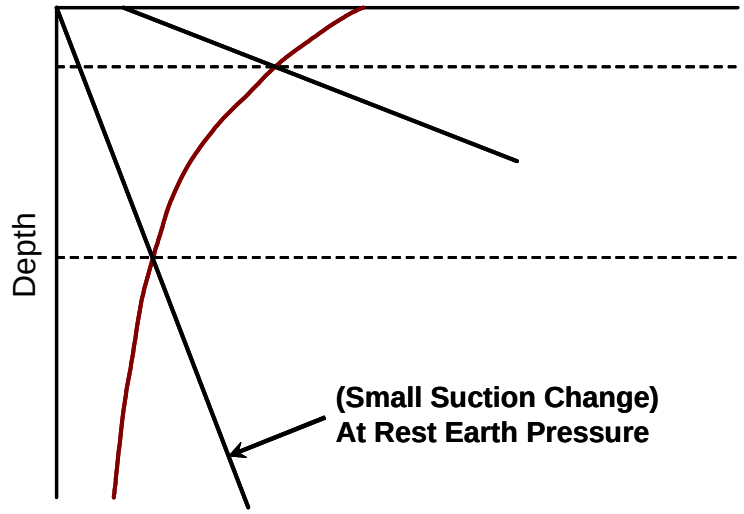

(c)

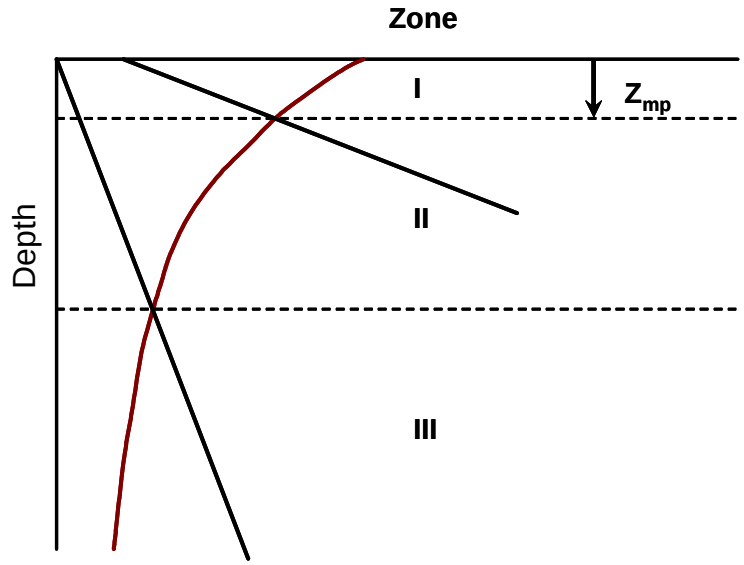

(d)

Fig. 4.1. continued.

4.4 Stress State in the Movement Active Zone

The proposed stationary retaining wall-soil system condition in expansive soils includes an upper movement active zone to the zero swell depth within a moisture active zone and a lower anchor zone (Fig. 4.2(b)). The suction variation from the initial equilibrium U_E to the final wet condition U_{wet} and the cumulated vertical swelling movement ΔH are shown in Fig. 4.2(a).

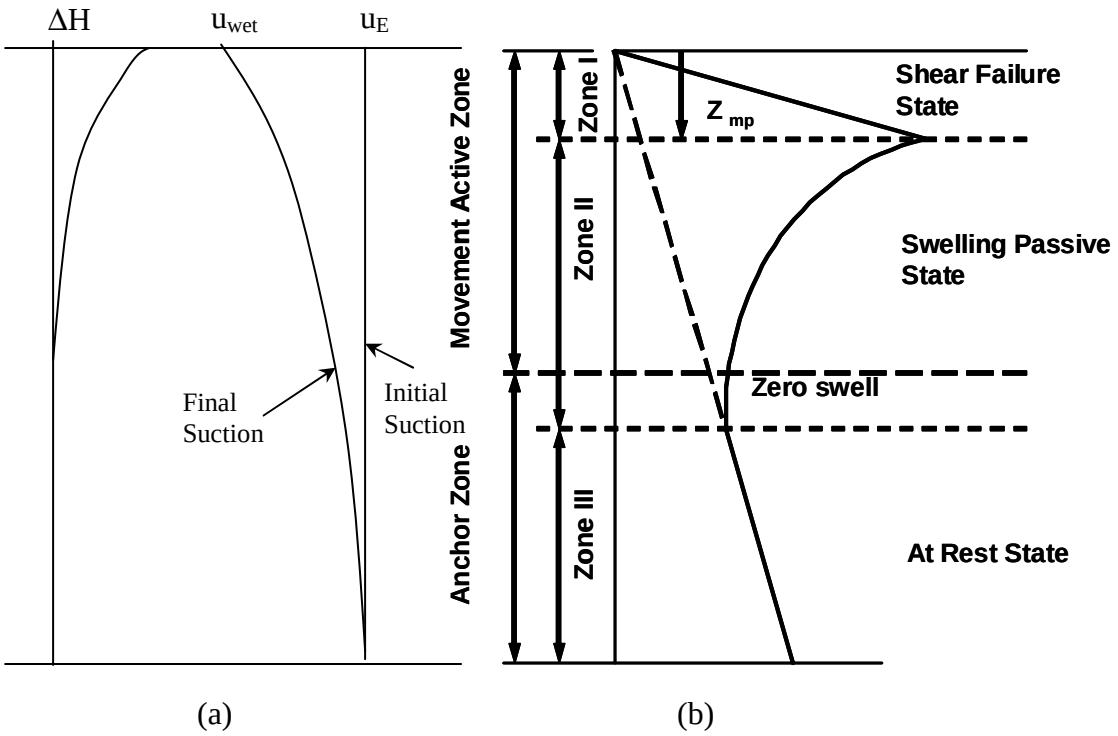

Fig. 4.2. Proposed Stationary Retaining Wall-Soil System in Expansive Soils. (a) Initial and Final Suction Envelopes and Accumulated Vertical Heaves with Depth, (b) Proposed Three Earth Pressure Zones on a Stationary Retaining Wall.

Three typical stress state zones are proposed. Zone I is the upper zone where a passive failure state of stress exists to a depth z_{mp} at which the maximum lateral swelling pressure occurs. Measured maximum lateral pressures near the ground surface are reported within a depth of 2 or 4 ft. Joshi and Katti (1980) found the maximum horizontal pressure near a depth of 3 ft. It was found that the maximum lateral pressure

occurs at the depth of 2.5 ft in a model pile test by Komornik (1962). Symons et al. (1989) reported that their measured lateral pressure over the upper 3.0–4.5 ft was substantially in excess of the calculated limiting passive values in experimental retaining walls. Brackley and Sanders (1992) indicated that a passive failure due to horizontal pressure developed at shallow depths in a field. Zone II represents lateral passive pressure state due to large suction change. The lateral pressure decreases as the suction change decreases (Fig. 4.2(b)). It is appropriated that the zone III within the anchor zone is in the classical at rest condition.

Mohr's circles and failure envelopes are used to define the effective horizontal stress and shear failure in an unsaturated soil. Figure 4.3 represents the state of stress in a soil element which is subjected to the effective vertical and horizontal stress and the shear stress caused by the swelling of soil in the movement active zone at which the horizontal stress is greater than the vertical stress. Since the shear stresses exist on a soil element, the maximum and minimum principal stress planes are not the same as the vertical or horizontal planes of the soil element. The effective horizontal stress and the shear strength of soil are determined on the basis of the geometry of a Mohr's circle as shown in Fig. 4.3.

Based on Eq. (3.6), the vertical and horizontal strains in a soil are given by:

$$\varepsilon_v = f_c \frac{\Delta V}{V} \qquad \text{(vertical swelling strain)} \qquad (4.1)$$

$$\varepsilon_h = \left(\frac{1 - f_c}{2}\right)\frac{\Delta V}{V} \qquad \text{(horizontal swelling strain)} \qquad (4.2)$$

where $\Delta V/V$ = volumetric strain and f_c = crack fabric factor.

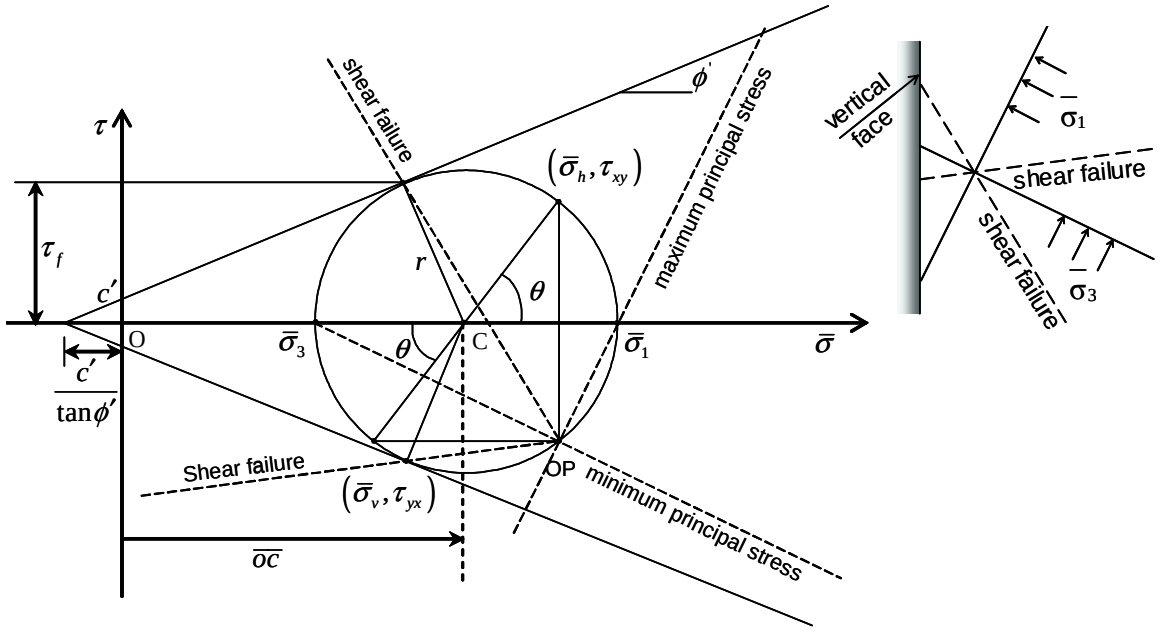

In figure, where:

τ_f = the shear strength of the soil

c' = the cohesion of the soil

ϕ' = the internal friction angle

r = radius of Mohr's Circle

θ = angle between the horizontal plane and point $(\bar{\sigma}_h, \tau_{xy})$

$\bar{\sigma}_1$ = maximum principal stress

$\bar{\sigma}_3$ = minimum principal stress

$\bar{\sigma}_h$ = effective horizontal stress

$\bar{\sigma}_v$ = effective vertical stress

τ_{xy} = shear stress

$\overline{OC}$ = distance from the origin to the center of Mohr's Circle

OP = origin point in Mohr's Circle

Fig. 4.3. Mohr's Circle Representation of the Stresses in the Movement Active Zone

From Equation (3.1), the horizontal strain is given by:

$$\varepsilon_h = \left(\frac{1 - f_c}{2}\right)\left[-\gamma_h \log_{10}\left(\frac{h_f}{h_i}\right) - \gamma_\sigma \log_{10}\left(\frac{\sigma_f}{\sigma_i}\right)\right] \tag{4.3}$$

where the mean final principal stress σ_f can be expressed as follows;

$$\sigma_f = \gamma_t z \frac{(1+2K_o)}{3} = \frac{\gamma_t z}{3} + \frac{2K_o \gamma_t z}{3} = \frac{\gamma_t z}{3} + \frac{2\sigma_h}{3} \tag{4.4}$$

where γ_t is unit weight of the soil, z is the depth of the soil, K_o is the earth pressure coefficient and σ_h is the total horizontal stress.

Considering that the soil is in a passive state due to soil expansion in a laterally restrained soil mass in the zone II, the total horizontal earth pressure σ_h is determined with the volume change Eq. (3.1):

$$\sigma_h = K_o \gamma_t z = \left(\frac{3}{2}\right)\sigma_i 10^{-\frac{2\varepsilon_x}{\gamma_\sigma(1-f)}}\left(\frac{h_i}{h_f}\right)^{\frac{\gamma_h}{\gamma_\sigma}} - \frac{\gamma_t z}{2} \tag{4.5}$$

The effective horizontal and vertical stresses $\bar{\sigma}_h$, $\bar{\sigma}_v$ are expressed as follows;

$$\bar{\sigma}_h = \sigma_h - \theta f h_m \tag{4.6}$$

$$\bar{\sigma}_v = \sigma_v - \theta f h_m \tag{4.7}$$

where h_m = matric suction; θ = volumetric water content; f = factor ranging from 1/θ to 1 depending on degree of saturation. The pore-pressure term $f\theta h_m$ corresponds to the Mohr-Coulomb strength equation with a single internal friction angle ϕ' in an unsaturated soil as follows (Lytton 1995);

$$\tau_f = c' + \left[(\sigma - u_a) + f\theta(u_a - u_w)\right]\tan\phi' \tag{4.8}$$

where τ_f = shear strength of soil; ϕ' = internal friction angle; c'=cohesion; σ = total stress normal to failure plane; u_a = pore-air pressure; u_w = pore-water pressure.

Based on the geometry of a Mohr's circle, the shear strength of soil τ_f and the shear stress τ_{XY} are given by;

$$\tau_{\mathrm{f}} = \left(\frac{\bar{\sigma}_h + \bar{\sigma}_v}{2} \right) \sin\phi' \cos\phi' + c' \left(1 - \sin^2 \phi' \right) \tag{4.9}$$

$$\tau_{\mathrm{xy}} = \left\{ \left[\left(\frac{1 - \sin^2 \phi' \cos\phi'}{\cos\phi'} \right) c' + \left(\frac{\bar{\sigma}_h + \bar{\sigma}_v}{2} \right) \sin\phi' \cos\phi' \right]^2 + \left(\frac{\bar{\sigma}_h - \bar{\sigma}_v}{2} \right)^2 \right\}^{\frac{1}{2}} \tag{4.10}$$

The effective horizontal stress below at a depth at which the vertical stress becomes greater than the horizontal stress in a soil mass is determined in a similar manner. The effective horizontal stress in the passive failure stress state zone I is computed based on the vertical effective stress and the failure criterion of the soil in terms of *r* and θ in the Mohr circle as shown in Fig.4.3;

$$\bar{\sigma}_h = \bar{\sigma}_v + 2r\cos\theta \tag{4.11}$$

The same θ. in soil element through all depths in the zone I is proposed according to the same pattern of shear crack failure near ground surface. The magnitude of *r* and $\overline{oc}$ in the zone I are expressed using the same θ_{zmp} above the z_{mp}:

$$\overline{oc} = -\frac{\bar{\sigma}_v + c'\cos\phi'\cos\theta}{\cos\theta\sin\phi' - 1} \tag{4.12}$$

$$r = c'\cos\phi' + \overline{oc}\sin\phi' \tag{4.13}$$

The shear strength of the soil and shear stress are given by;

$$\tau_f = r \cdot \cos\phi' \tag{4.14}$$

$$\tau_{xy} = r \cdot \sin\theta \tag{4.15}$$

The maximum shear stress τ_{max} at the interface between the soil and the vertical plane of the wall is determined by choosing a minimum value of the shear stresses calculated as follows:

$$\tau_{\max} = \min\left(\tau_f, \left|\tau_{xy}\right|\right) \tag{4.16}$$

The shear factor, α, is given by:

$$\alpha = \frac{\left|\tau_{xy}\right|}{\tau_f} \tag{4.17}$$

4.5 Stress State in the Anchor Zone

The vertical stress must be greater than the horizontal stress in this anchor zone corresponding to an at rest condition using a Ko ($=1-\sin\phi'$) condition as shown in Fig. 4.4. Figure 4.4 shows that the origin point OP the maximum and minimum principal planes, the shear failure plane and the shear strength of soil in a soil mass.

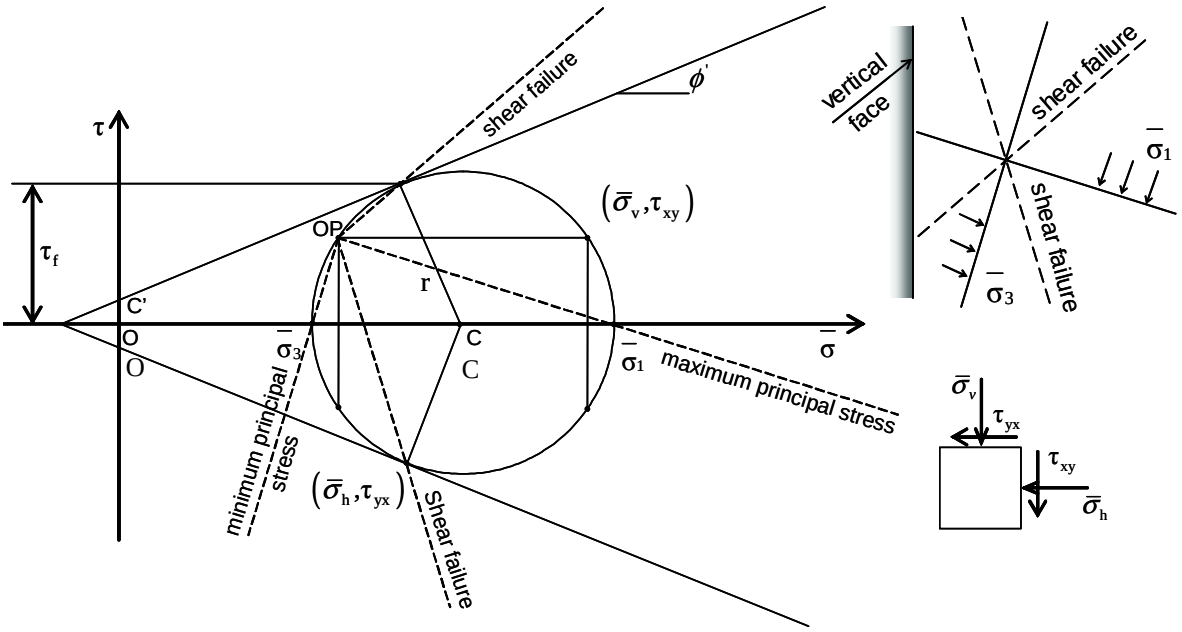

Fig. 4.4. Mohr's Circle Representation of the Stresses in the Anchor Zone

The magnitude of $\overline{oc}$ and r are expressed by;

$$\overline{oc} = \frac{\bar{\sigma}_v + \bar{\sigma}_h}{2} \tag{4.18}$$

$$r = c' \cos\phi' + \overline{oc} \sin\phi' \tag{4.19}$$

The shear strength of the soil and the shear stress are given by;

$$\tau_f = r \cdot \cos\phi' \tag{4.20}$$

$$\tau_{xy} = r \cdot \sin\theta \tag{4.21}$$

The maximum shear stress $\tau_{\max}$ at the interface between the soil and the vertical plane of the wall and the shear factor α are given by;

$$\tau_{\max} = \min\left(\tau_f, \left|\tau_{xy}\right|\right) \tag{4.22}$$

$$\alpha = \frac{\left|\tau_{xy}\right|}{\tau_f} \tag{4.23}$$

4.6 Comparison with Measured Lateral Pressure According to the Suction Change

The prediction of the horizontal pressures based on suction change in a soil was compared with the in situ measurements of natural horizontal pressures observed by Brackley and Sanders (1992).

The Leeuhof site, Vereeniging, South Africa was chosen for the experiment because it was an area where severe problems had been caused by swelling clay, and a great deal of information was available on the properties of the soil (De Bruijn, 1973). An extensive investigation of the properties of fissured clays in the Vereeniging was carried out by Williams & Jennings (1977). It was found that the mean angle of the fissures to the horizontal is 43 degree based on a survey of the dip angle of slickensided fissures in an exposed cutting in Vereeeniging. It was considered that the fissures were caused by a passive failure of the soil resulting from a gradual increase in the horizontal pressure during seasonal swelling of the clay. Figure 4.5 shows the Leeuhof soil profile together with measured moisture content, densities, plasticity indices, soil suctions, undrained shear strength and predicted potential heave.

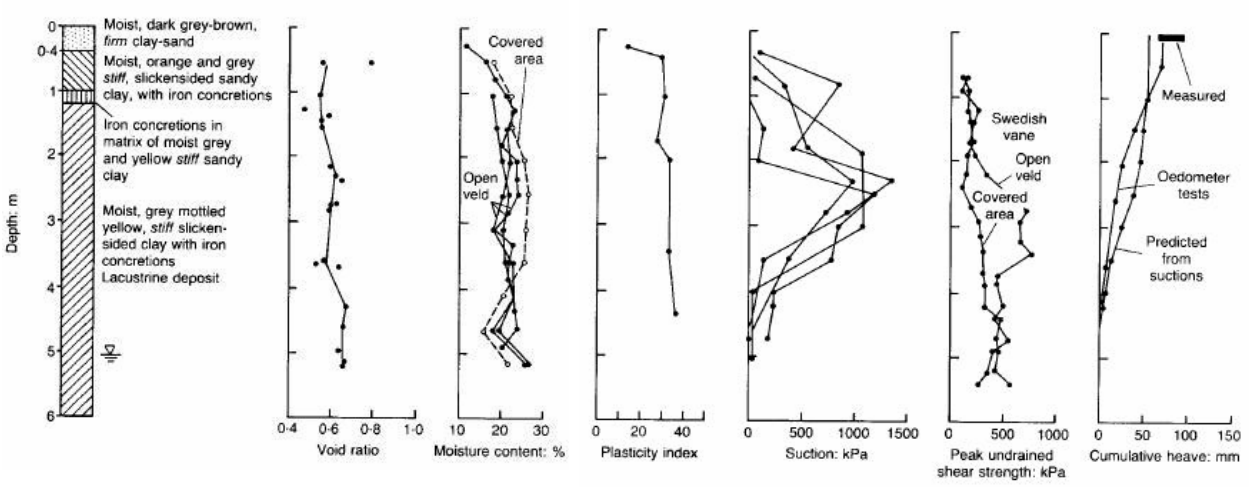

Fig. 4.5. Soil Properties at Leeuhof Test Site (Brackley and Sanders 1992)

The four suction profiles recorded using the in situ psychrometers for more than a year shows the seasonal range of suction. The four suction profiles are examples from many sets of such results. The suctions near the water-table are low and suctions in the upper profile vary considerably (0-1000 kPa). The suction variations observed in a test site over more than one year indicated that the variations were caused by evapo-transpiration and rainfall in the upper soil layer and the large seasonal change of water table in the lower soil layer.

The BRS pressure cell (Thomas and Ward 1969) was installed in a highly expansive unsaturated lacustrine clay deposit for the long-term measurement of in situ natural lateral stresses. Nine cells were installed at four depths 2.8 ft (0.85 m), 3.3 ft (1.0 m), 6.6 ft (2.0 m) and 7.2 ft (2.2 m) below the ground surface at the site. Figure 4.6 shows the measured lateral pressures, the variations in the water-level and the recorded rainfall. It was found that the BRS cells experienced a drift in the zero reading during operation. It was suggested that the readings over the early period after installation are probably more reliable than later readings because the change with time may not have been linear (Brackley and Sanders 1992).

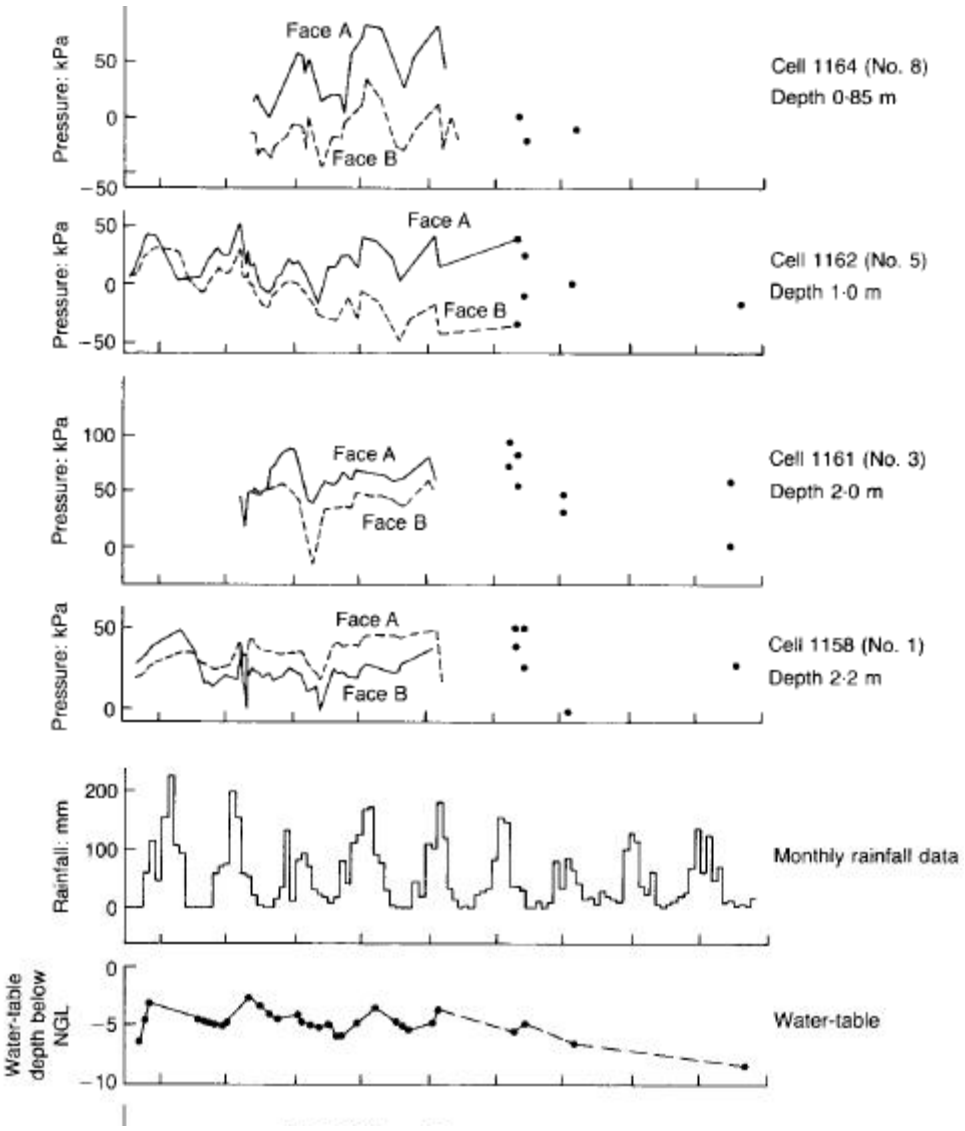

Fig. 4.6. Measured Lateral Pressures and the Variation in the Water-Level and the Recorded Rainfall in Test Site (Brackley and Sanders 1992)

In order to predict the heaves and pressures in a site, the initial and final suction profiles are determined corresponding to the four suction profiles observed by Brackley and Sanders (1992). The suctions in terms of pF in depths 1 ft – 4 ft and 14 ft – 16 ft vary considerably because of rainfall and evapo-transpiration near the ground surface

and the seasonal change of water table, respectively (Fig. 4.7(a)). However, it was found that the suction has remained consistently high at a depth of around 9 ft. The predicted heave of 2.8 inches is in agreement with the measured heaves which ranged between 2.6 and 3.7 inches at the ground surface as shown in Fig. 4.7(b). Figure 4.7(c) represents the prediction of the shear strength of the soil.

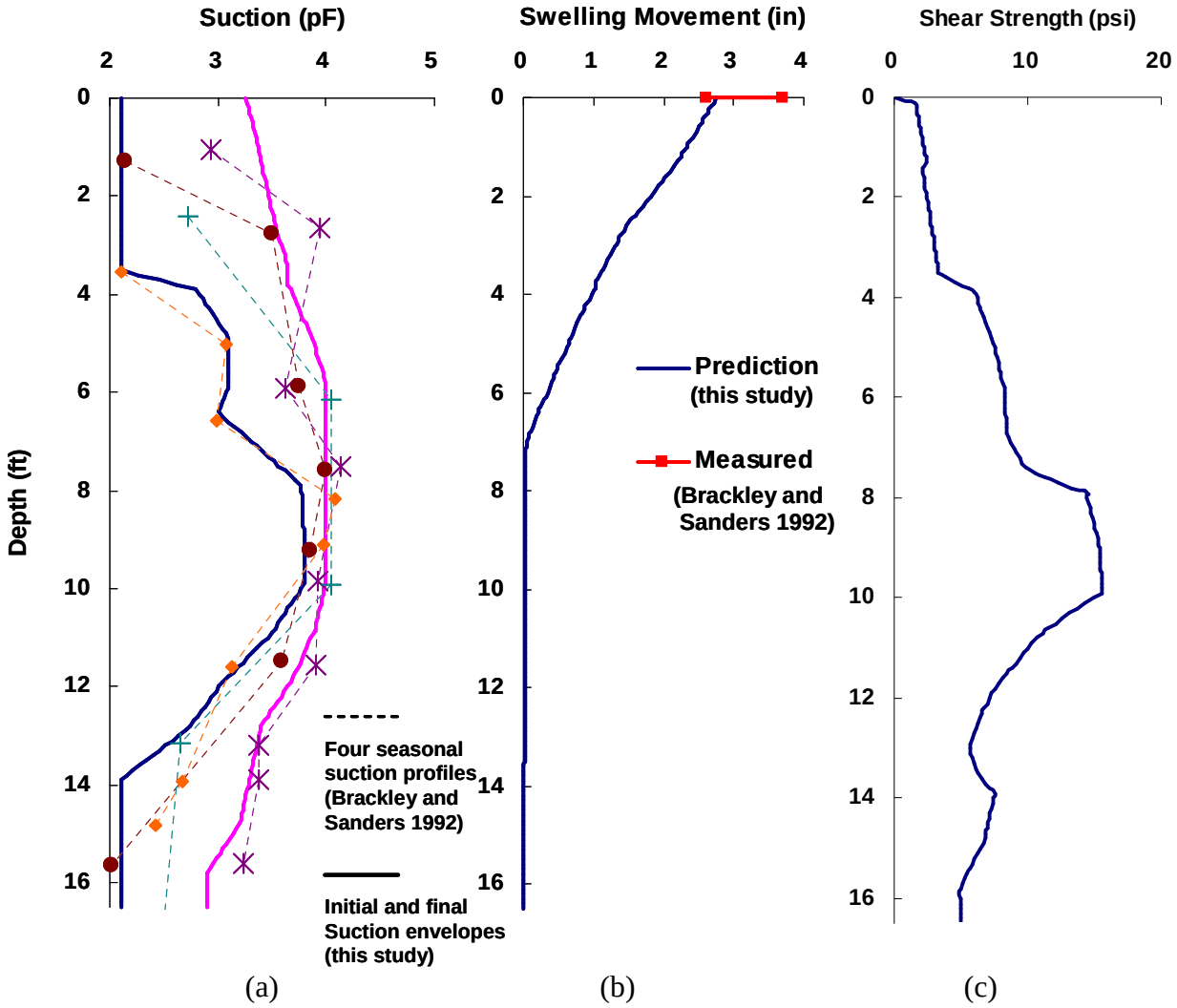

Fig. 4.7. Prediction of Swelling Movement and Shear Strength of the Soil. (a) Four Measured Suction Profiles, (b) Measured and Predicted Heaves, (c) Predicted Shear Strength of the Soil.

The maximum measured values of lateral pressure in the rainy season at the end of the early years 1978, 1979 and 1980 show good agreement with the predicted values at five depths 2.8 ft, 3.3 ft, 6.7 ft, 7.2 ft and 14.4 ft as shown in Fig. 4.8.

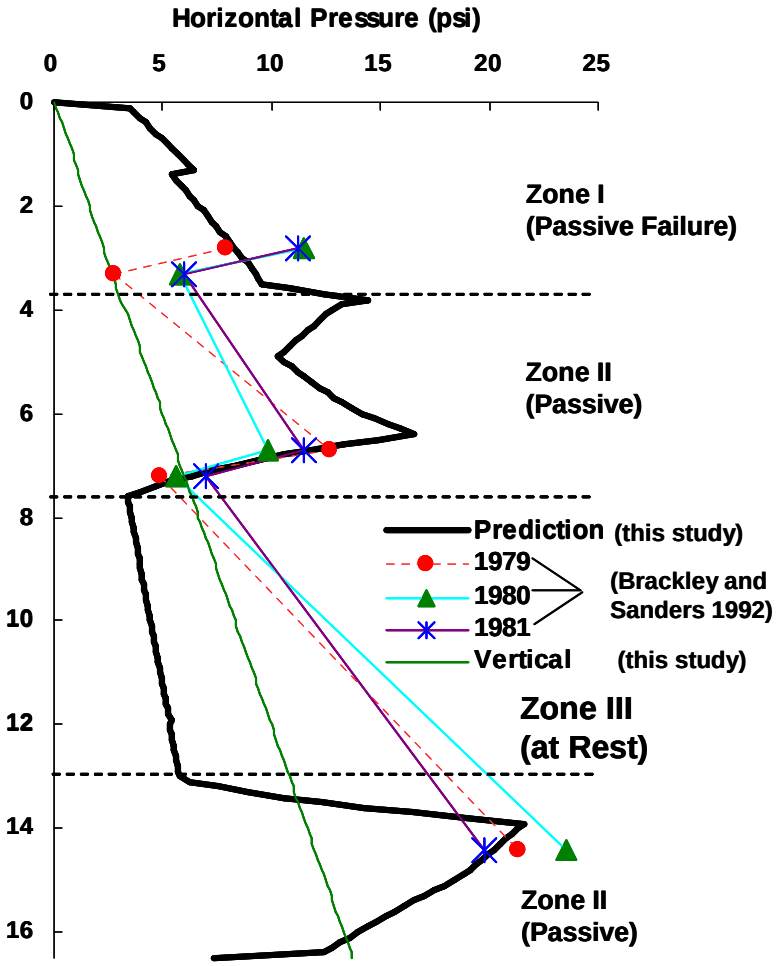

Fig. 4.8. Comparison with Measured Horizontal Stresses at Four Depths

Zone I represents passive failure near the ground surface. In this study, the predicted lateral pressure distribution includes two Zones II both of which represent the passive stress state caused by the swelling of the soil due to large suction changes. The seasonal suction change in the upper Zone II ranged from 0 ft to 5.6 ft and is influenced

by the rainfall and evapo-transpiration and that in the lower Zone II ranged from 13 ft to 15 ft and is influenced by the water table changes. The magnitude of the maximum horizontal pressures measured at five depths is compared with calculated vertical pressures (Table 4.1).

Table 4.1 Comparison between Maximum Measured Horizontal Pressures and Vertical Pressures

Depth (ft)	Year	Measured horizontal pressure (psi)	Vertical pressure (psi)
2.8	1981	11.3	2.3
3.3	1981	6.0	2.7
6.7	1979	12.7	5.6
7.2	1981	7.0	6.0
14.4	1980	23.5	11.9

It was found that the magnitude of the total horizontal pressure that developed in the lacustrine expansive clay, in natural conditions under a grass cover, was two to four times the total vertical pressure (Brackley and Sanders 1992). This indicated that the natural horizontal pressure in expansive clay soils may equal the pressure required to cause passive failure of the soil mass along existing fissures.

Joshi and Katti (1980) carried out large scale retaining wall model studies in black cotton expansive soil deposits in India. The Atterberg limits of the soil were: liquid limit 81.5 % and plasticity index 38.3 %. The grain size distribution of the soil was: 96 % passing No. 200, and 56 % passing the 2 micron size (Kate and Katti 1980). The test tank was made up of stiffened mild steel plates with internal dimensions of 3.0 ft x 4.0 ft in plan and 9.0 ft in depth. After saturation, the lateral swelling pressure measured near the ground surface was negligible, but it increased to 3.0 tsf, which is the swelling pressure of soil within a shallow depth of 3.0 ft. With further depth the lateral pressure appeared to remain the same as shown in Fig. 4.9(c).

Figure 4.9 presents the suction profiles predicted and the comparison between prediction and measurement of swelling movements and lateral pressures. It was necessary that the suction variations be back-calculated based on the measured swelling

movement and lateral pressures, and the saturation conditions. At an initial condition the suction of air dry soil likely might be nearly 3.7 pF and the final suction at all depths seemed to be nearly 2.3 pF as shown in Fig 4.9(a).

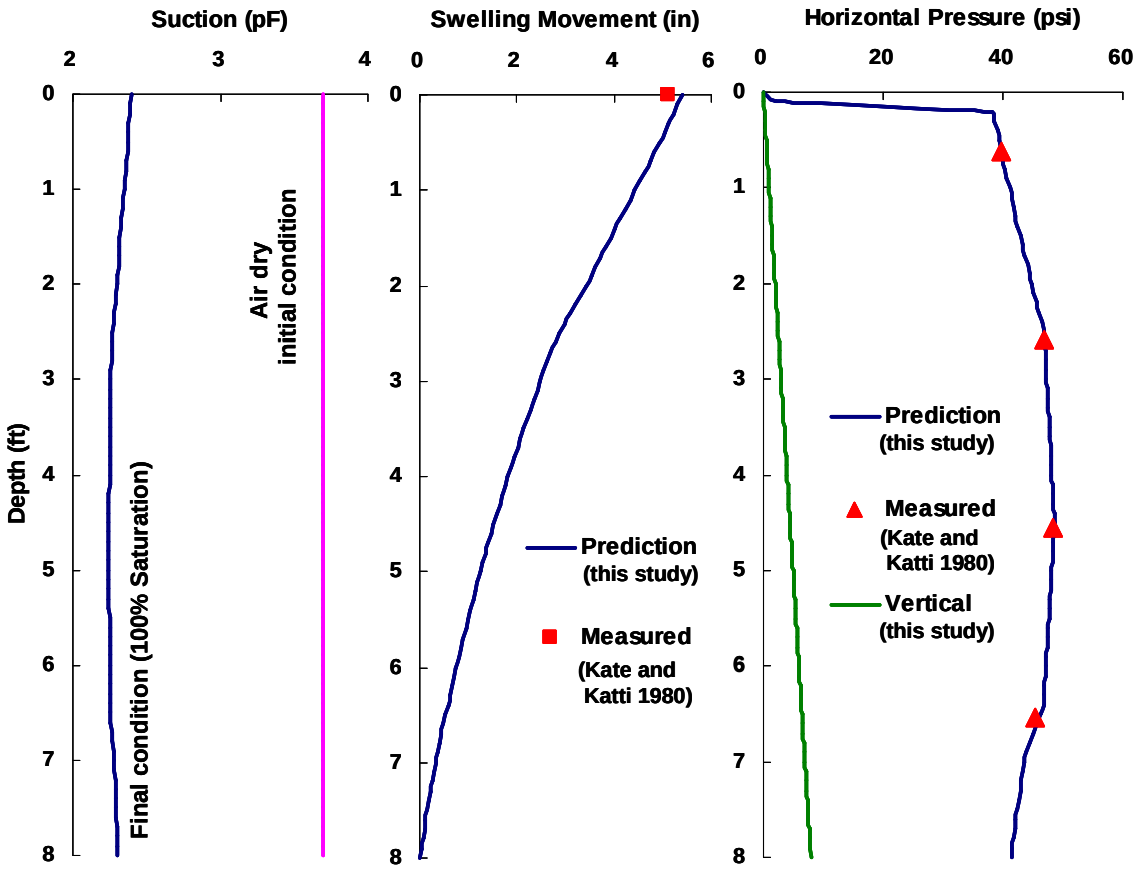

Fig. 4.9. Comparison with Measured Swelling Movements at Ground Surface and Measured Horizontal Swelling Pressures in Large Scale Test. (a) Predicted Initial and Final Suction Envelopes, (b) Measured and Predicted Heaves, (c) Measured and Predicted Lateral Pressures

The predicted vertical movement of 5.4 inch is in good agreement with the measured swelling movement of 5.1 inch at the ground surface (Fig. 4.9(b)). Figure 4.9(c) shows that the prediction of the lateral pressure distribution matches the measured pressures. It is important to note that the lateral pressure characteristics are different as compared to those of the classical retaining wall-soil system and the lateral pressures developed are much higher than the vertical stresses (Joshi and Katti 1980). The high lateral pressure developed is likely caused by the short width of test tank which does not allow the passive failure in a soil.

A model pile was instrumented in a test drum with a diameter of 4.0 ft and 5.0 ft in height to measure the lateral stresses induced in the concrete pile by swelling of expansive soils (LL 76 %; PI 48 %; 90 % passing No. 200; 62% less than 2 micron) on the site of Kibbutz Mizra, Israel (Komornik 1962). The expansive soils surrounding the pile were subjected to even wetting conditions. Based on the swelling movement observed at ground surface and lateral pressure measured in the concrete pile, the calculated suction varies from 3.7 pF to 2.2 pF as shown in Fig. 4.10(a). The mismatch between the measured and predicted heaves likely be caused by the large skin friction developed on the pile and drum wall which is causing resistance against heaving (Fig. 4.10(b)). It was found that the zone of passive failure of soil was expected to be at a depth of 0.5 ft and the large lateral pressure of 55 psi occurs at a depth of 2.7 ft as shown in Fig. 4.10(c).

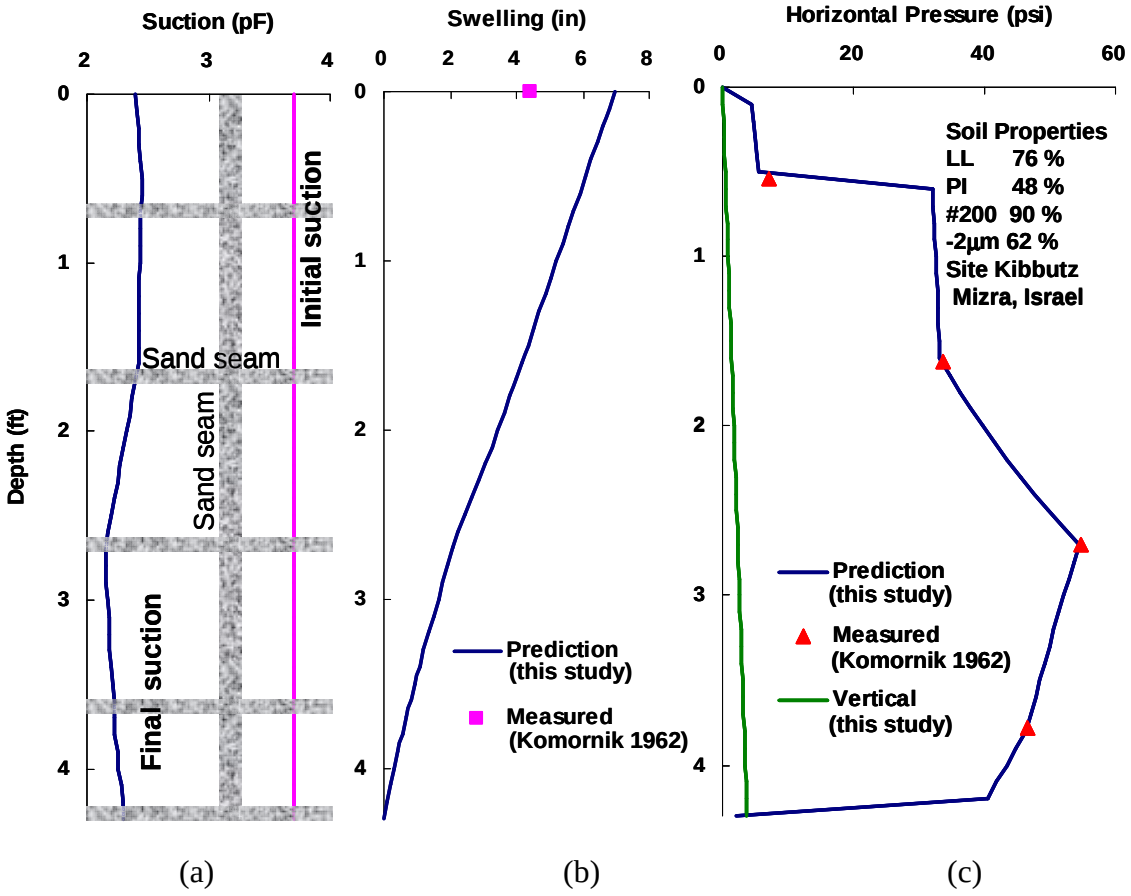

Fig. 4.10. Comparison with Measured Swelling Movements at Ground Surface and Measured Horizontal Swelling Pressures in Large Scale Test. (a) Predicted Initial and Final Suction Envelopes, (b) Measured and Predicted Heaves, (c) Measured and Predicted Lateral Pressures (Komonik 1962).

CHAPTER V
DRILLED PIER IN EXPANSIVE SOILS

5.1 Introduction

In this chapter, a numerical model for use in design is presented for prediction of the stresses and axial and bending displacements in a drilled pier in expansive soils. With suction profiles around the pier, the prediction is based on the horizontal earth pressures caused by the expanding of the soil and shear stresses which act on the shaft of the drilled pier. The prediction of shear stress induced on the surface of a drilled pier is supported by the load transfer curve which represents the relationship of the shear stress corresponding to the relative displacement between the soil and the pier shaft. In the study of the lateral behavior, the load-deflection curves are developed based upon the stress state around the pier and non-linear suction dependent elastic modulus of the unsaturated soils. A numerical model of the bending and stretching of a pier includes a beam column approach and linear distribution of shear stress around the circumference of the pier between the maximum and minimum shear stresses. Case studies of axial and bending of piers are presented with both uniform and non-uniform wetting.

5.2 Literature Review

Donaldson (1967) instrumented a test anchor pile of nine inches in diameter and twenty six feet long in expansive soils to monitor the development of tensile force in the pile with time. The test site was flooded by means of four holes which were drilled to a depth of fifteen feet and then filled with water. Tensile forces of up to 17,000 lbs. were measured in a pile at a depth of fifteen feet during an accelerated heaving test. The results showed that the tensile stresses develop most rapidly where there is preferential wetting of the soil, and, the full uplift force of the pile develops if enough moisture is available (Donaldson 1967). In order to assess the magnitude and distribution of forces generated by expansion of the foundation strata in a site underlain by deep expansive

soil, a test group of tension piles has been installed (Blight 1984). It was found that the tension stresses applied to the concrete piers due to the swelling of the soil, were large enough to crack the concrete. This study indicates that enough steel reinforcement has to be provided in order to avoid failure of the concrete pier due to tensile stresses.

The seven test shafts at Lackland Air Force Base, Texas, were installed to investigate the long term performance of drilled shafts in expansive soil beneath lightly loaded areas (Johnson and Stroman 1985). A vertical load test was performed on an instrumented shaft of 36 inches in diameter and 36 feet long with a 4 foot diameter bell. Results of the vertical load test indicated that the shaft experienced an intermediate plunging failure at 250 tons, after this, the shaft held 130 tons more, which is attributed to the end bearing capacity. The data obtained from these load tests indicated a gap had occurred in the shaft near the base of the shaft and could have been caused by tensile fracture. Authors concluded that the drilled shaft foundations in expansive soils should be loaded near the allowable bearing capacity assuming a minimum factor of safety, and, that the amount of reinforcing steel required to resist uplift thrust caused by swelling of the soil should be based on the maximum shear strength of the adjacent soil.

Bhandari et al. (1987) investigated the behaviour of short uniform diameter, single and double bulb piles in a typical Indian black cotton soil deposit during the stage of swelling. The pile dimensions are following: shaft diameter, 1 ft; underream diameter, 2.5 ft; and 11.5 ft length. The uplift forces induced within the piles were monitored using vibrating wire load cell assemblies placed at appropriate elevations within the piles. The vertical displacements of the piles were also monitored using water level gauges. The single underreamed pile displacements were slightly less than those of uniform diameter piles but the displacements of double underreamed piles were either equal to or more than those of the uniform diameter piles. The results showed that the vertical displacements of the piles were found to be in the order of 25 to 40 percent of the ground surface heave, and, the magnitude of the pile displacements was from 60% to 75% less than the ground surface heave. Authors concluded that the largest tensile force was found to develop in the case of single underreamed pile and the maximum tensile force

regardless of the type of pile was found to occur at about 70% of the length of the pile. In view of the largest uplift load recorded in the single underreamed pile, no reinforcement greater than 0.5% of the cross-sectional area appears to be necessary.

In order to investigate the effects of seasonal moisture changes in the soil on the unit shear stresses imposed on the sides of the drilled shaft, a field study at the site, National Geotechnical Experimentation Site at the University of Houston, Texas, was performed by Kim and O'Neill (1998). A 1 ft diameter and 13.8 ft length instrumented drilled shaft was installed in a moderately expansive clay soil during the dry season and monitored over a period of about 15 months beginning in September, 1994. The maximum tensile force of 55 kN in the shaft was recorded and occurred at a depth of around 6.6 ft.

5.3 Soil-Pier System in Expansive Soils

The pier-soil system in expansive soils is proposed to predict the axial and lateral behavior of the pier during wetting. In uniform wetting process around the pier, it is anticipated that symmetric suction variations and lateral earth pressures occur around the pier, and the shear stresses caused by swelling of the soil tend to lift the pier as shown in Fig. 5.1. Unsymmetrical lateral pressures and the shear stresses induced by the differential non-uniform wetting around the pier result in bending moments and lateral deflection of the pier. The suction profiles and accumulated heaves for the both left and right sides of the pier are shown in Fig. 5.2. It is proposed that the curved surface forming the boundary of the wedge known as the horizontal active zone is parabolic as in Terzaghi, Peck and Mesri (1996). The z_{mp} is used to define the length of the passive failure at ground surface shown in Fig. 5.2. The unsymmetrical shear stress and horizontal pressure distributions for the both left and right sides of the pier are shown in Fig. 5.3.

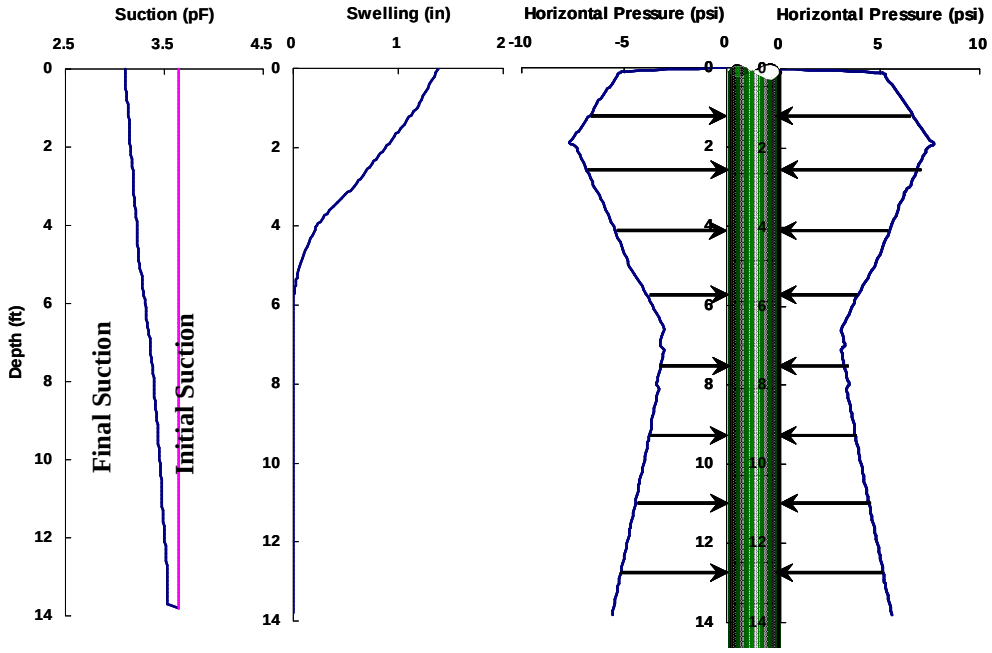

Fig. 5.1. Soil-Pier System in Uniform Wetting

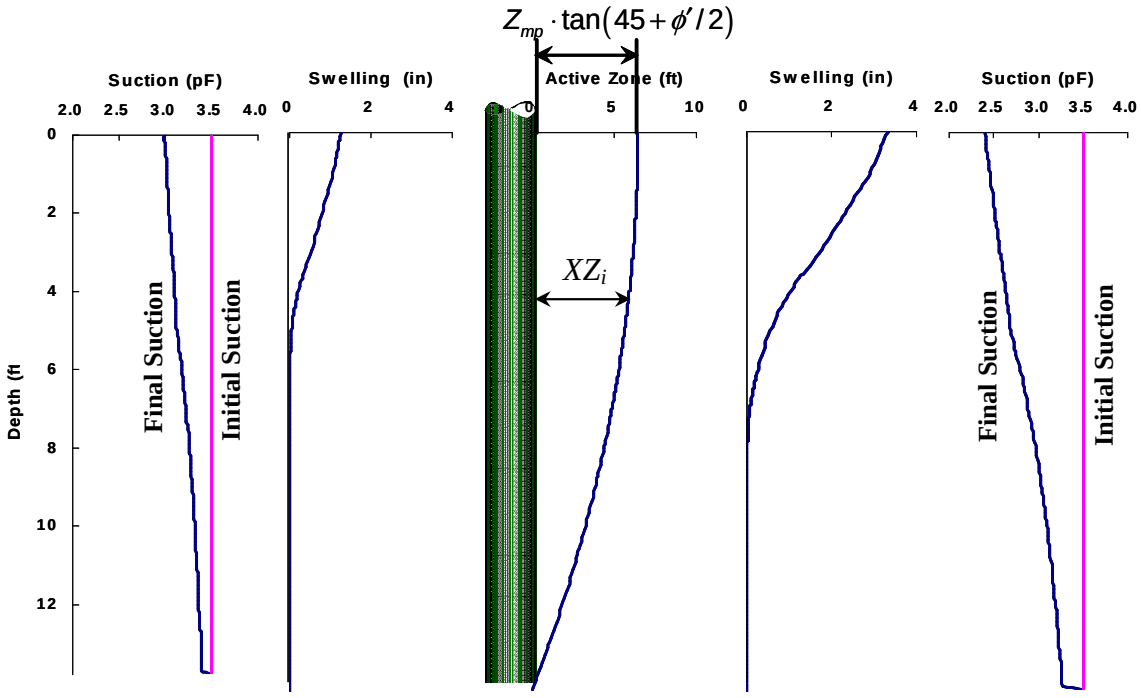

Fig. 5.2. Lateral Behavior of the Pier in Non-Uniform Wetting

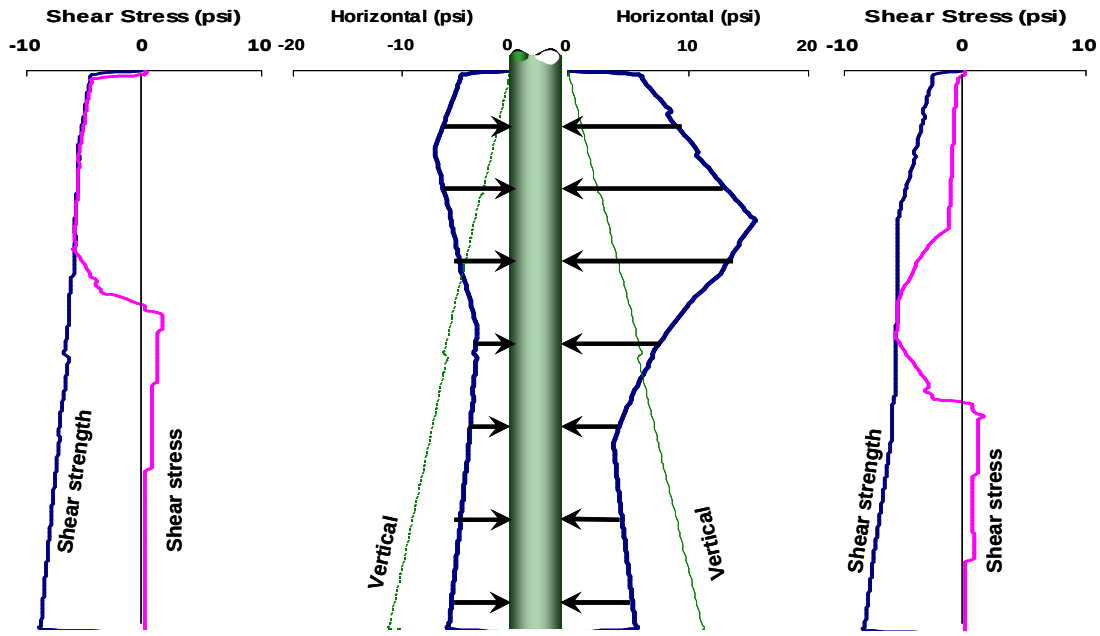

Fig. 5.3. Shear Stress and Horizontal Pressures in Non-Uniform Wetting

5.3.1 Load Transfer Curves

The relative displacement between the soil and the side of pier reaches the ultimate shearing resistance, when the relative displacement is 1.2% (Aurora et al. 1981) of the diameter of the pier shown in Fig. 5.4. The relationship between shear stress and relative displacement is proposed as follows;

$$\tau = \frac{S}{2}\left(\frac{\delta}{0.0015b}\right)^{\frac{1}{3}} \tag{5.1}$$

where τ is the shear stress between soil and the pier; S is the ultimate shearing resistance; δ is the relative displacement; b is the diameter of the pier.

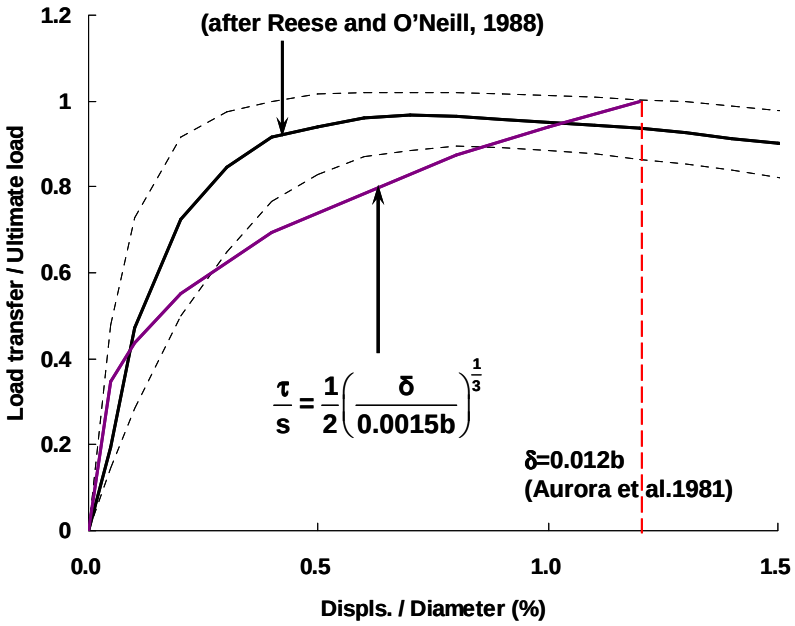

Fig. 5.4. Load Transfer Curve

Figure 5.5 illustrates (a) the accumulated heaves of the soil, (b) upward movement of the pier, (c) relative displacement, and (d) shear stress at the interface between the soil and shaft of the pier in case of uniform wetting process around the pier. The zero relative displacement occurs at the point at which the swelling movement is equal to displacement of the pier. It is above the zero swell line since the uplift force caused by the swelling of the soil in the movement active zone influences the pier in the anchor zone. Figure 5.5(d) shows how the uplift shears are counteracted by the anchorage shears on the pier shaft in the anchor zone. Shaft shear stresses are developed upward and downward with respect to the shaft in the upper and lower portion of the pier, respectively.

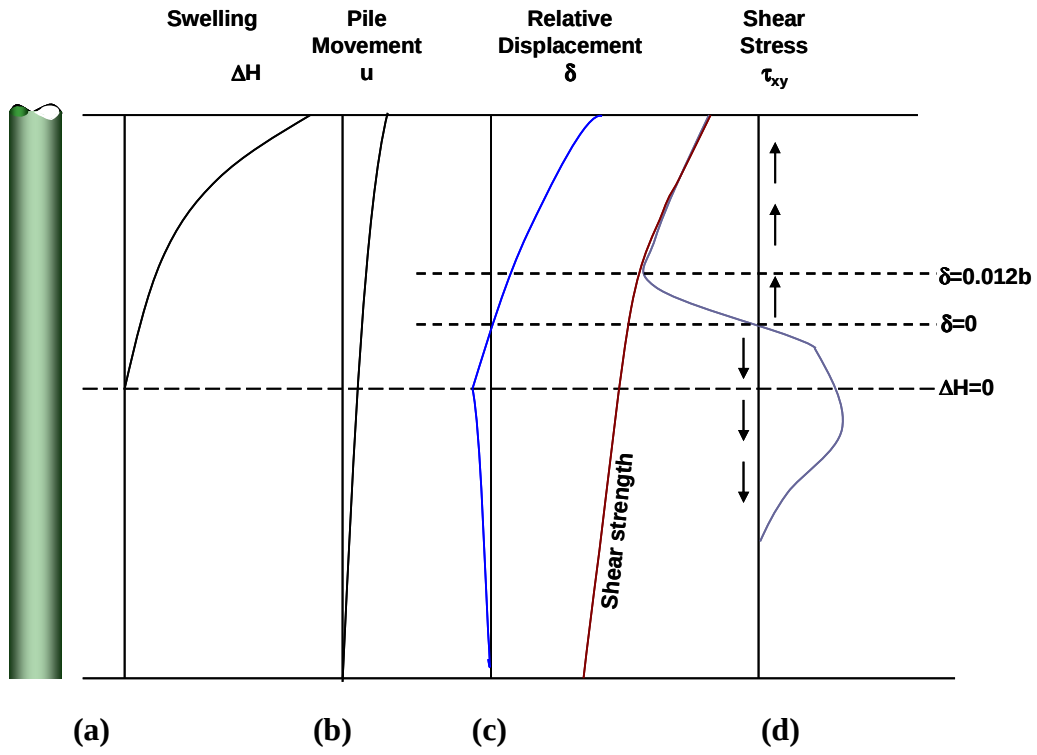

Fig. 5.5. Axial Behavior of the Pier with No Load Applied at Top of the Pier in Uniform Wetting. (a) Accumulated Heave of the Soil, (b) Upward Displacement of the Pier, (c) Relative Displacement between the Soil and the Pier, (d) Shear Strength of the Soil and Shear Stress at a Interface.

5.3.2 Load versus Deflection Curves

It is required to avoid being confused with the classical lateral earth pressure *at-rest*, *active*, and *passive pressures* in this study. The *neutral*, *decrease of lateral stress*, and *increase of lateral stress states* are used to define the stress state in a soil on the shaft of the pier during wetting as follows (Fig. 5.6.);

1) *Neutral stress state*

   The pier is static and the soil mass is also in a state of static equilibrium. In that case, the horizontal effective stress is referred to as the *neutral stress*.

2) *Decrease of lateral stress state*

The wall does not move either to the right or to the left of its initial position. The horizontal effective stress will decrease and be smaller than the vertical effective stress on a Mohr's circle and thus failure of the soil will occur shown in Fig. 5.6. This situation represents *Decrease of lateral stress state*, and the horizontal effective stress is *Decrease of lateral stress*.

3) Increase of lateral stress state

The wall does not move either to the right or to the left of its initial position. The horizontal effective stress will increase and be greater than the vertical effective stress on a Mohr's circle and thus failure of the soil will occur shown in Fig. 5.6. This situation represents an *Increase of lateral stress state*, and the horizontal effective stress is the *Increase of lateral stress*.

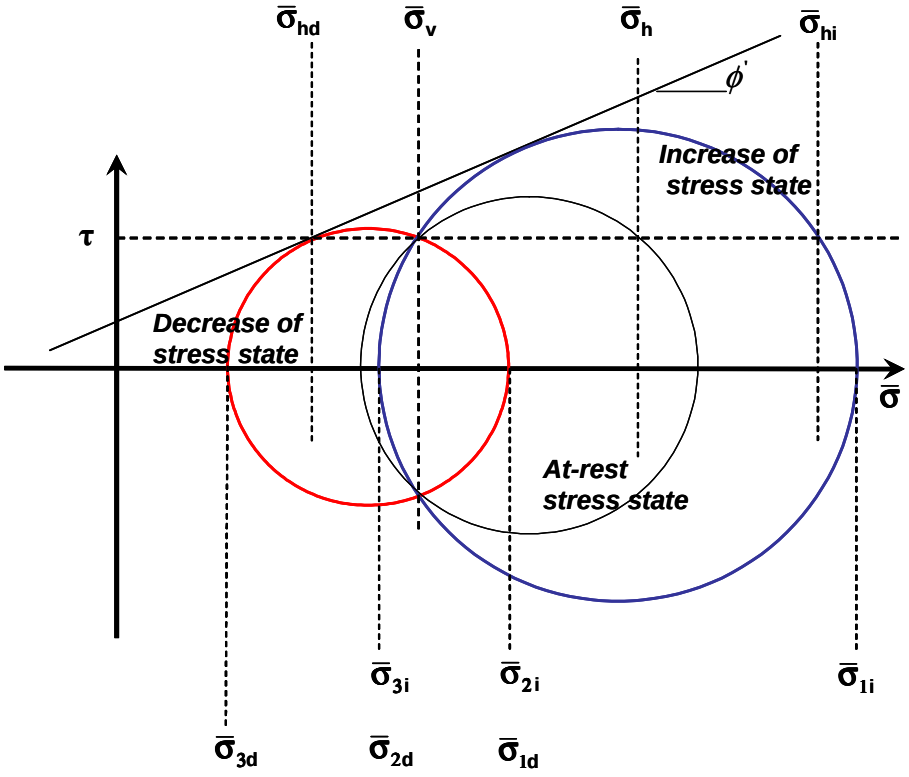

Fig. 5.6. Neutral Stress, Decrease of Lateral Stress, and Increase of Lateral Stress States

In Fig. 5.6, where:

$\bar{\sigma}_v$ = constant effective vertical stress

$\bar{\sigma}_h$ = effective horizontal stress at a Neutral stress state

$\bar{\sigma}_{hd}$ = effective horizontal stress at a Decrease of lateral stress state

$\bar{\sigma}_{hi}$ = effective horizontal stress at an Increase of lateral stress state

$\bar{\sigma}_{1d}$, $\bar{\sigma}_{2d}$, and $\bar{\sigma}_{3d}$ = effective maximum, intermediate, and minimum principal stresses at a Decrease of lateral stress state

$\bar{\sigma}_{1i}$, $\bar{\sigma}_{2i}$, and $\bar{\sigma}_{3i}$ = effective maximum, intermediate, and minimum principal stresses at an Increase of lateral stress state.

The elastic modulus in each soil element is predicted based on the its current mean principal stress, matric suction, Poisson's ratio, and the suction compression index, as follows (Lytton et al. 2005);

$$E_S = \frac{\left(\sigma_m - \theta f h_m\right)\left(1 + \frac{0.4343}{sw}\right)}{0.4343\gamma_h} \frac{(1+\nu)(1-2\nu)}{(1-\nu)} \tag{5.2}$$

where E_s = elastic modulus of unsaturated soil

σ_m = mean principal stresses, σ_{mi} for *Increase of lateral stress state* and σ_{md} for *Decrease of lateral stress state* are given by (refer to Fig. 5.6.);

$$\sigma_{mi} = \left(\sigma_{1i} + \sigma_{2i} + \sigma_{3i}\right)/3$$

$$\sigma_{md} = \left(\sigma_{1d} + \sigma_{2d} + \sigma_{3d}\right)/3$$

h_m = matric suction

ν = Poisson's ratio

θ = volumetric water content

f = factor ranging from $1/\theta$ to 1 depending on degree of saturation

$f \cong 1 + \frac{S-85}{15}\left(\frac{1}{\theta} - 1\right)$, where S = degree of saturation

γ_h = suction compression index

s = the slope of log-suction versus water content curve

w = the gravimetric water content

A case study to determine the P-Y curves for the left and right sides of the pier is performed in the case of the non-uniform wetting around the pier in moderately expansive soils at a site National Geotechnical Experimentation, Houston, Texas (Kim and O'Neill 1998). The elastic modulus in soil elements at the left side of the pier are calculated based on the suction changes and mean principal stresses. Figure 5.7 shows that the magnitude of elastic modulus in case of an *Increase of lateral stress state* is greater than that in case of a *Decrease of lateral stress state*. As overburden pressure increases, the rate of elastic modulus in case of an *Increase of lateral stress state* to those in case of a *Decrease of lateral stress state* increases.

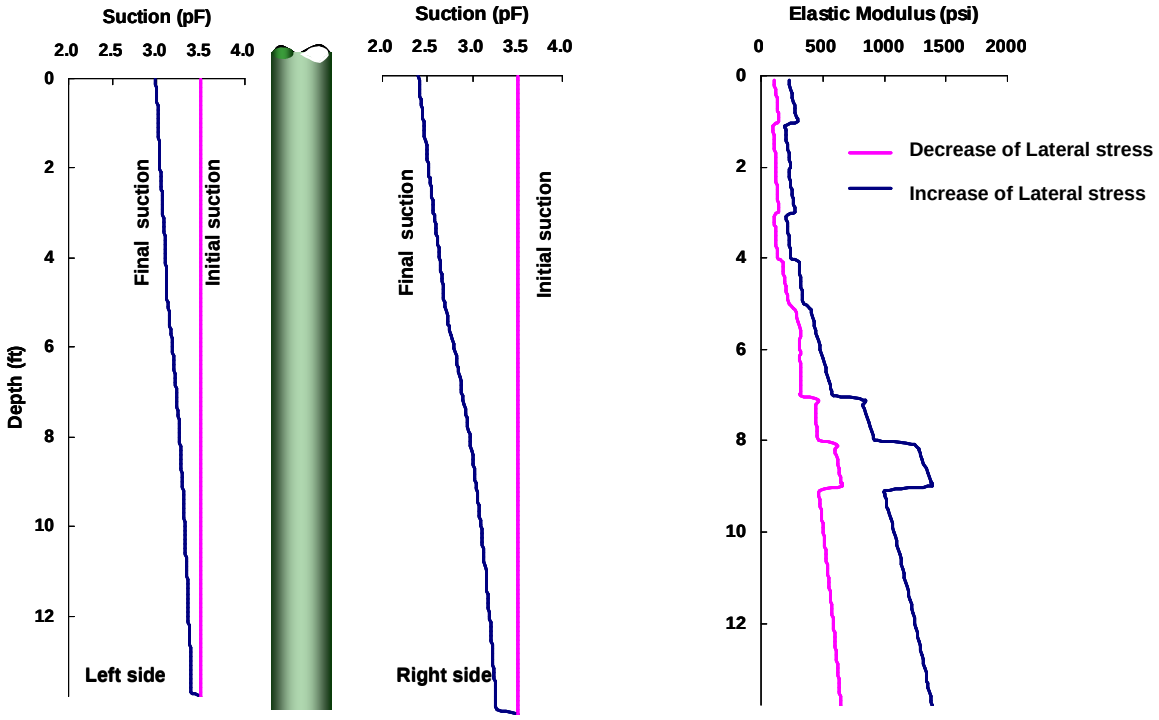

Fig. 5.7. Distribution of Elastic Modulus of Unsaturated Soil Predicted for a Decrease of Lateral Stress State and an Increase of Lateral Stress State

Figure 5.8 shows the theoretical stress strain curves for both the *Increase of lateral stress state* and *Decrease of lateral stress state* based on the predicted elastic modulus of unsaturated soil and the following relationship (Matlock 1970);

$$\frac{\Delta\sigma}{\frac{\Delta\sigma_{ult\_d}}{2}} = \left(\frac{\varepsilon_h}{\varepsilon_{50\_d}}\right)^{\frac{1}{3}} \tag{5.5}$$

$$\frac{\Delta\sigma}{\frac{\Delta\sigma_{ult\_i}}{2}} = \left(\frac{\varepsilon_h}{\varepsilon_{50\_i}}\right)^{\frac{1}{3}} \tag{5.6}$$

where $\Delta\sigma$ = $\sigma_1 - \sigma_3$

$\Delta\sigma_{ult\_d}$ = $\Delta\sigma_{Neutral} - \Delta\sigma_d$

$\Delta\sigma_{ult\_i}$ = $\Delta\sigma_i - \Delta\sigma_{Neutral}$

ε_h = horizontal strain

ε_{50_d} = horizontal strain when $\Delta\sigma$ reaches at the 50 percent of the $\Delta\sigma_{ult\_d}$ in case of a *Decrease of lateral stress state*

ε_{50_i} = horizontal strain when $\Delta\sigma$ reaches at the 50 percent of the $\Delta\sigma_{ult\_i}$ in case of an *Increase of lateral stress state*

With the suction variations and distribution of elastic modulus predicted in a case study in Fig. 5.8, the predicted stress strain curves in a soil element at a depth of 6.5 ft are given in Fig. 5.9.

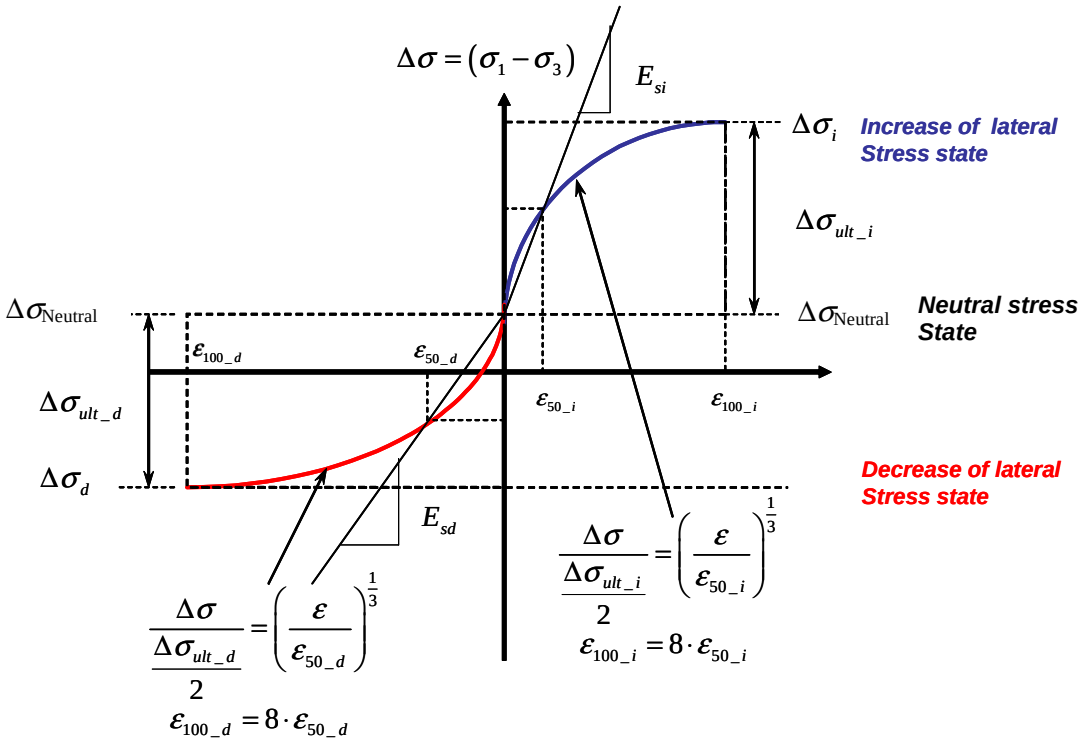

Fig. 5.8. Stress Strain Curves for a Decrease of Lateral Stress State and an Increase of Lateral Stress State

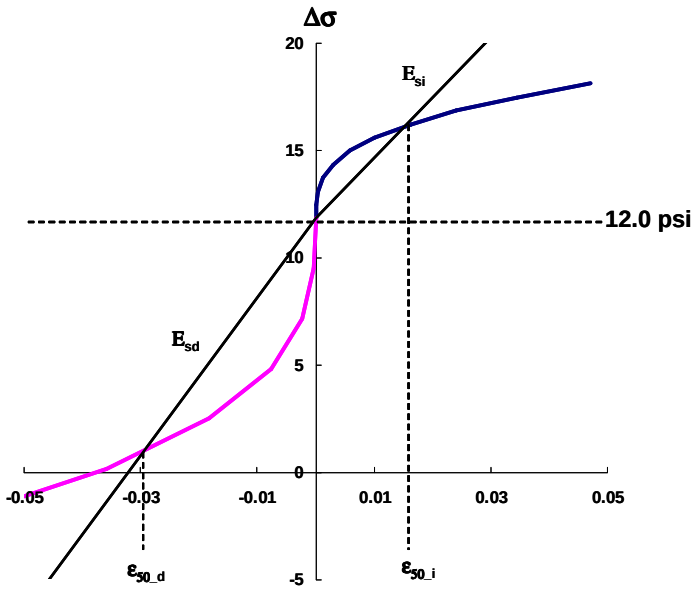

Fig. 5.9. Predicted Stress Strain Curves for a Decrease of Lateral Stress State and an Increase of Lateral Stress State

A numerical model for the axial and lateral behavior of the pier computes P-Y curves for both the left and right sides of the pier and uses the composition of them based on the sign convention of BMCOL76 solution (Matlock et al. 1981) as shown in Fig. 5.10. The deflection X corresponding to the force Q is computed by multiplying the horizontal strain by the length of the horizontal active curve XZ_i (Fig. 5.2) at i^{th} station of the pier model. From a case study in the same site above, the both left and right P-Y curves and the composition curve are shown in Fig. 5.11.

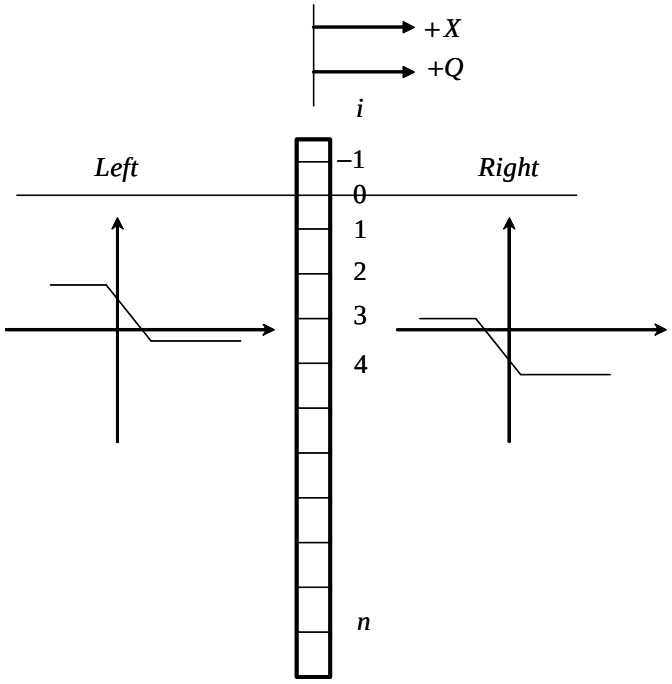

Fig. 5.10. P-Y Curves for Both the Left and Right Sides of the Pier in Case of Non-Uniform Wetting

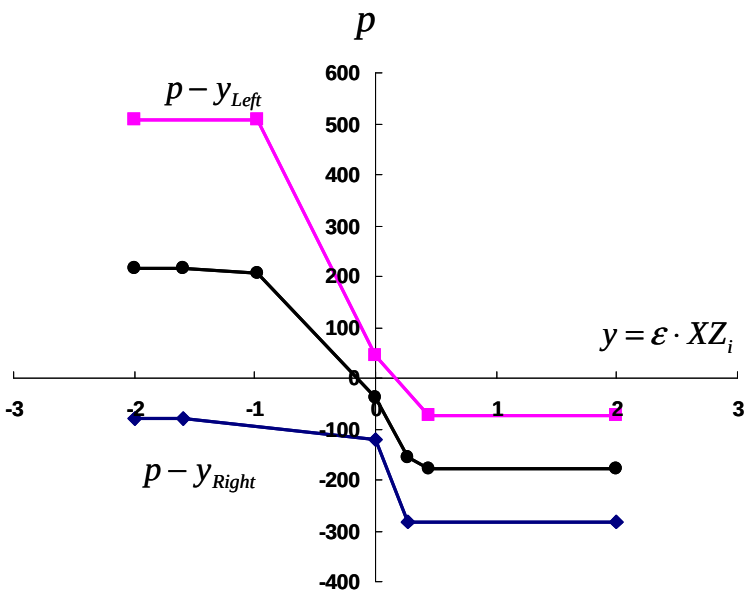

Fig. 5.11. Composition of P-Y Curves for Both the Left and Right Sides of Pier in Case of Non-Uniform Wetting

5.3.3 Distribution of Shear and Lateral Stresses around the Pier

It is appropriate to state that the distribution of shear stress around the circumference of a pier linearly decreases between the maximum and minimum shear stresses shown in Fig. 5.12. The moments $m(z)$ taken around axis of the pier cross-section caused by differential shear stress at a depth z can be expressed:

$$m(z) = -\frac{b^2}{\pi}\left[\tau_{xy}(z)_{\max} - \tau_{xy}(z)_{\min}\right]\Delta z \qquad (5.7)$$

where b=diameter of pier; $\tau_{xy}(z)_{max}$ and $\tau_{xy}(z)_{min}$ = the maximum and minimum shear stress, respectively, at a depth z; Δz = increment of soil element;

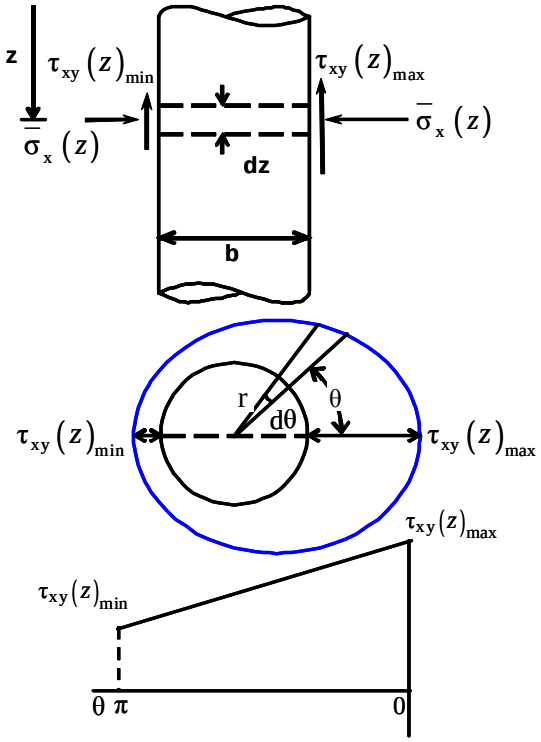

Fig. 5.12. Distribution of Shear Stresses around the Pier

In a similar approach, the horizontal force, $\overline{q_h}(z)$, caused by pressure imbalance at a depth *z* is given by;

$$\overline{q_h}(z) = \frac{2b}{\pi}\left[\overline{\sigma_h}(z)_{\max} - \overline{\sigma_h}(z)_{\min}\right]\Delta z \qquad (5.8)$$

where $\overline{\sigma_h}(z)_{\max}$ and $\overline{\sigma_h}(z)_{\min}$ = the maximum and minimum horizontal pressure; Δz = increment of soil element.

5.4 Numerical Model of Drilled Pier Using Beam Column Approach

A numerical model for the design and analysis of axial and lateral behavior of the pier includes the volume change model, the lateral earth pressure model in expansive soils and the BMCOL76 solution (Matlock et al. 1981). The axial behavior of a cylindrical pier acted upon by an uplift force caused by the swelling of the surrounding soil is

predicted based on the nonlinear load transfer support curves developed at each station element of the pier. A numerical model also calculates the unsymmetrical lateral earth pressures and moments in the pier caused by the differential wetting around the pier. The effects of horizontal imbalance pressures, moments caused by shear stresses on the side of the pier and axial thrust on the behavior of beam-column in bending are included.

Axial Model

The mechanical model of a short segment of a member under axial loading is shown in Fig. 5.13. The member is considered to be composed of a series of deformable springs of equal length h connected at ridge joints at stations denoted by the symbol i. The member stiffness is considered as a linear spring of stiffness AE/h, where A is the cross-sectional area and E the modulus of elasticity. External loads Q and support springs S may be placed at each station i. The internal member force in each spring is termed the thrust and denoted by the symbol T.

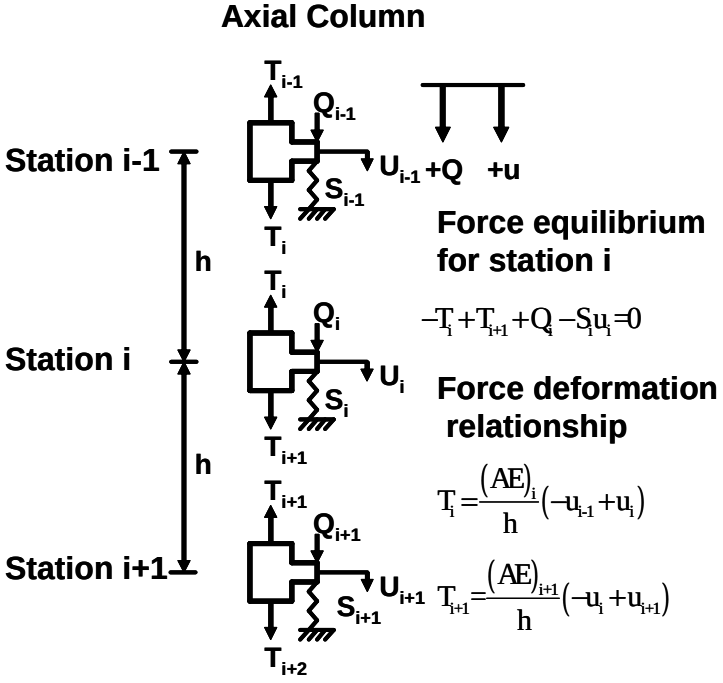

Fig. 5.13. Mechanical Model for Axial Beam-Column (Matlock et al. 1981)

Lateral Model

The mechanical model of a short segment of a beam-column subjected to lateral loads and restraints is shown in Fig. 5.14. The real member is modeled as a series of ridge bars of length h connected by elastic hinges at each joint, or station, i. The bending stiffness of each joint is the bending moment divided by the concentrated angle change $(M_i/Q_i)/h$ or F_i/h where F is the product of the modulus of elasticity E and the moment of inertia of the cross section i. External loads Q and linear springs S may be placed at each station i. Couples and rotational restraints at a station i create forces only at adjacent stations as shown in Fig. 5.14. Axial thrust T in each bar creates an additional couple acting on the bar, of magnitude $T_i(-w_{i-1}+w_i)$, the subscript i denoting the bar number.

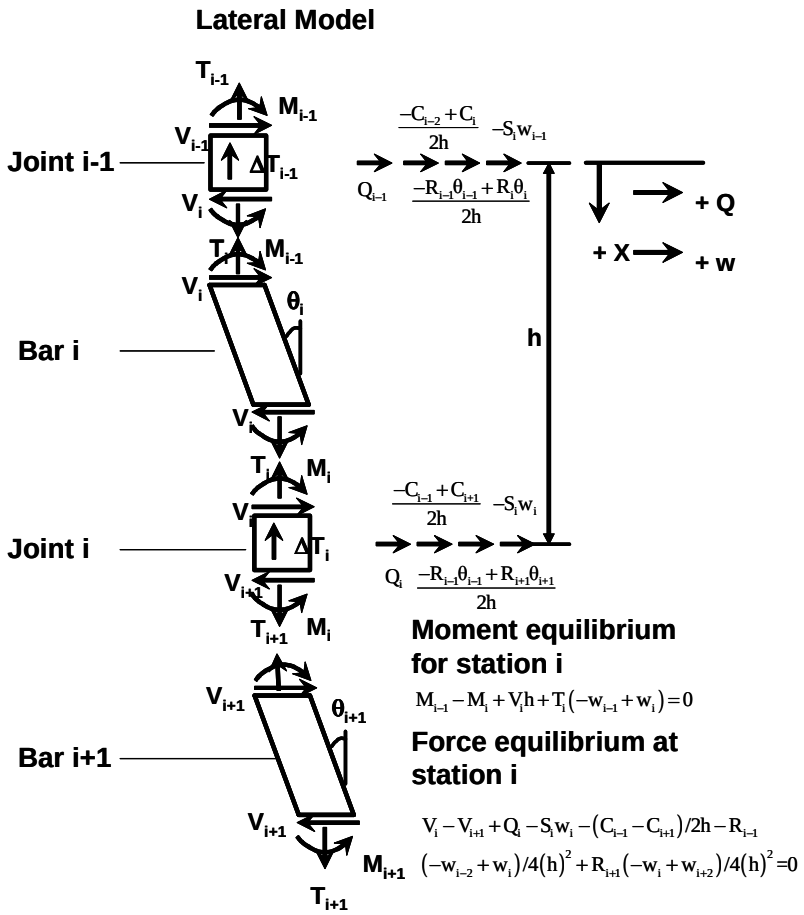

Fig. 5.14. Lateral Beam Model (Matlock et al. 1981)

Nonlinear Support- springs

In soil-supported foundation elements, it is desirable to describe supports which do not develop reactions in direct proportion to the beam-column displacement. Non-linear support curve is illustrated in Fig. 5.15. The symbol Q represents the reaction developed by the nonlinear support. The symbol u represents the axial displacement of the column. To represent a relative displacement between the soil and beam column, the support curve is assumed to be shifted or displaced a distance with respect to the original zero displacement position. The beam-column displacement is denoted as u_i. At the point of intersection of the support curve and the beam-column displacement, the nonlinear curve may be replaced by two temporary elastic constants, the tangent to the curve $–S_0$ and the intercept Q_0 of the tangent at the original zero displacement position. The support reaction from the nonlinear curve is then expressed as $Q_0 – S_0w_i$.

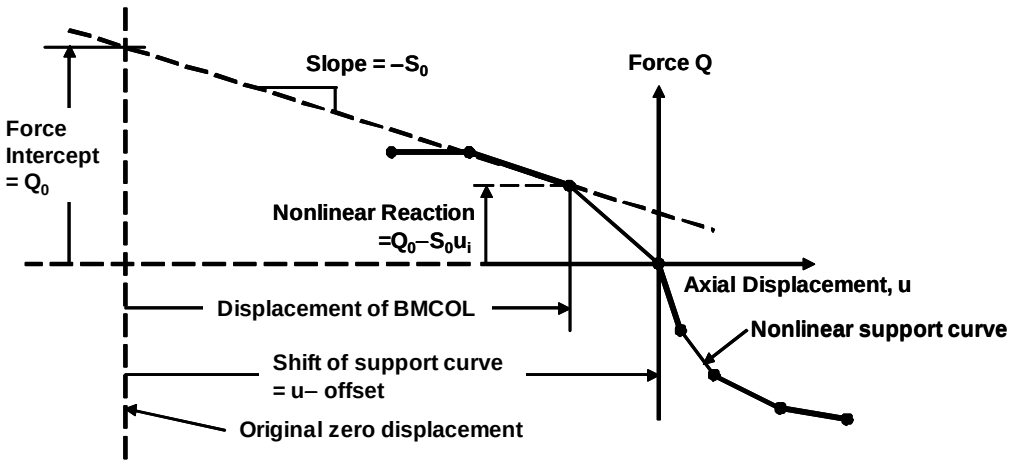

Fig. 5.15. Representation of Shifted Nonlinear Support Curve by Tangent Force Intercept and Stiffness (Matlock et al. 1981)

5.5 The Pier Case Study: Axial Behavior due to Uniform Wetting

The predictions of the axial and bending behavior of the pier corresponding to the field measurements (Kim and O'Neill 1998) are compared with the available measured data. In order to investigate the effects of seasonal moisture changes in the soil on the unit shear stresses imposed on the sides of the drilled shaft, a field study at the site, National Geotechnical Experimentation Site at the University of Houston, Texas, was performed by Kim and O'Neill (1998). The test site stratigraphy and schedules of rebar and concrete in the drilled shaft at a site are shown in Fig. 5.16. A 1.0 ft diameter and 13.8 ft length instrumented drilled shaft was installed in a moderately expansive clay soil during the dry season and monitored over a period of about 15 months beginning in September, 1994. Figure 5.17 represents suction in bars versus time and uplift force versus time at the site. In this case study, the maximum measured surface swelling movement of 1.4 inch in April 1995 was used together with a pile head upward displacement of 0.16 inch and maximum measured uplift forces of 55kN, 34kN and 19kN at the depths 6.6 ft, 3.6 ft and 1.5 ft, respectively (Fig. 5.17). Twelve soil layers based on the borehole logs and the initial suction as an equilibrium suction of 3.7 pF and final suction of 3.1 pF at the ground surface are used for this case study.

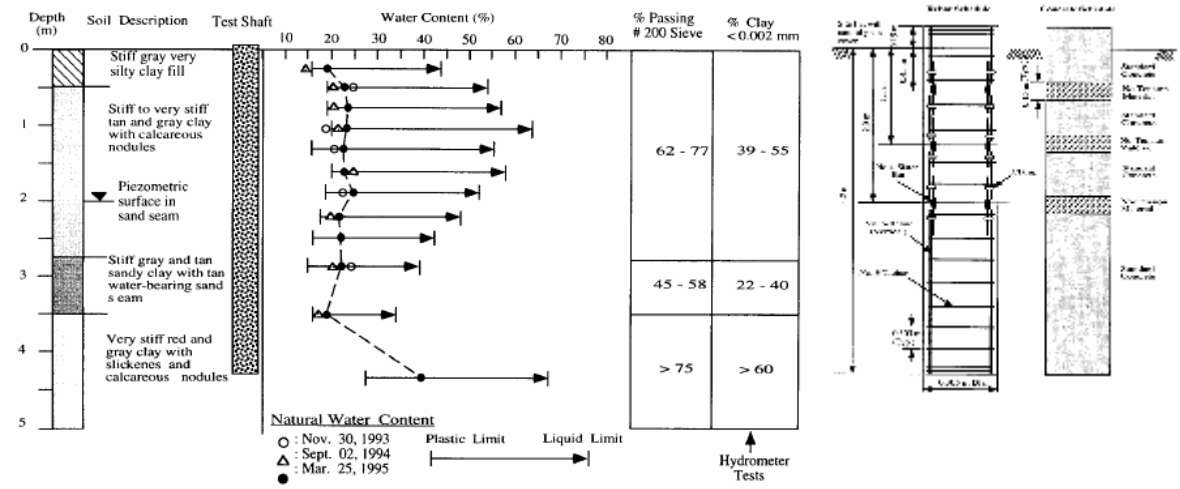

Fig. 5.16. Test Site Stratigraphy and Schedule of Rebar and Concrete in Drilled Shaft at a Site NGES-UH (Kim and O'Neill 1998)

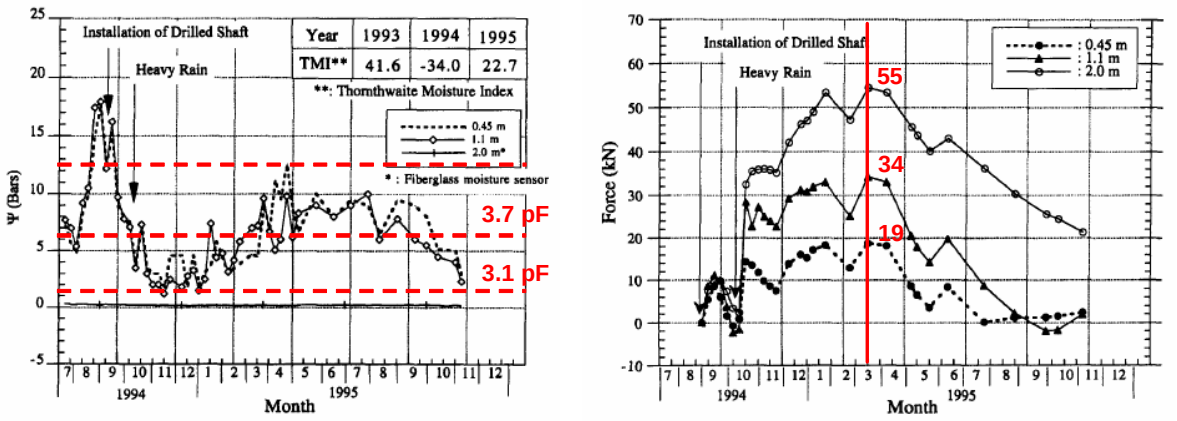

Fig. 5.17. Bar versus Time (1 bar=100 kPa) and Uplift Force versus Time at a Site NGES-UH (Kim and O'Neill 1998)

The initial and final suction profiles at the site and the calculated swelling movements and horizontal earth pressures versus depth are shown in Fig. 5.19(a). The maximum measured heave of 1.4 inch is in agreement with the predicted heave at ground surface. It is found that the maximum horizontal earth pressure of 7.8 psi occurs at a depth of around 2.0 ft which shown in Fig. 5.18(a). Figure 5.18(b) shows the predicted shaft shear stress, shear strength of the soil and axial tensile stress in the pier. The uplift shears transition into by the anchorage shears on the pier shaft. The transition occurs at the depth around 5.5 ft. The results showed that the agreement is good between the measured and predicted axial tensile stresses, but the prediction somewhat overestimates the tensile stress at the depth of 3.5 ft.

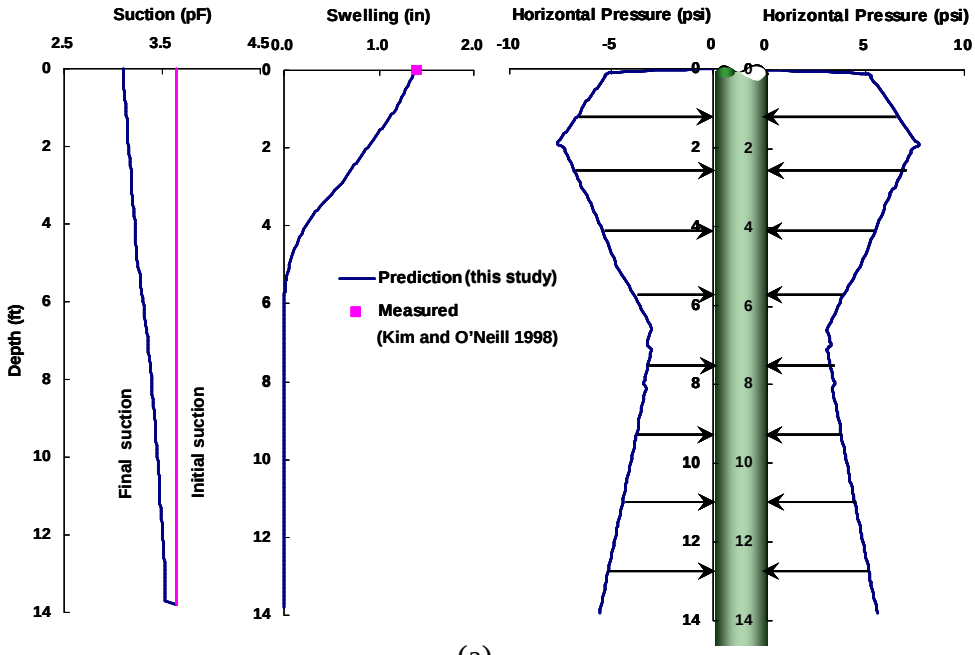

(a)

(b)

Fig. 5.18. The Pier Case Study: Axial Behavior due to Uniform Wetting. (a) Suction Change, Swelling Movement and Horizontal Earth Pressure versus Depth, (b) Shear Stress, Shear Strength of the Soil and Axial Tensile stress versus Depth

5.6 The Pier Case Study: Bending Behavior due to Non-uniform Wetting around the Pier

5.6.1 Pier with Different Final Suction Envelope

In order to evaluate the effects of unsymmetrical lateral pressure caused by non-uniform wetting around the pier, the case study of bending behavior of the pier was performed with the different final suction variation on the left and right sides of the pier. The suction variation from the initial equilibrium suction of 3.5 pF to the final suction of 3.0 pF at a ground surface on the left side of the pier results in a surface swelling movement of 1.3 inch (Fig. 5.19(a)). Figure 5.19(a) also shows that the suction variation from the initial suction of 3.5 pF to the final suction 2.4 pF on the right side of the pier results in a swelling movement of 3.3 inches at the ground surface. A 7.0 ft length of the horizontal active zone at the ground surface was predicted using the zmp-depth of 2.0 ft. The distributions of the shaft shear stress on both the left and right sides of the pier are shown in Fig. 5.19(b). The maximum horizontal pressure of 6.9 psi occurs at a zmp-depth of 2.0 ft, on the left side of the pier and the maximum pressure of 15.6 psi occurs at a zmp-depth of 3.7 ft on the right side of the pier (Fig. 5.19(b)). In Figure 5.19(c), a deflection of 2.7 inches at the ground surface is predicted because of the horizontal stress relief from the neutral stress condition. The lateral displacement of the pier relieves the pressure on one side and increases the pressure on the other side of the pier. This relation between lateral displacement and net lateral pressure must be found by iteration, starting with the horizontal pressure distribution predicted by assuming that the pier does not move laterally. Figure 5.19(c) gives the distribution of lateral loads, bending moments, and shear forces in the pier.

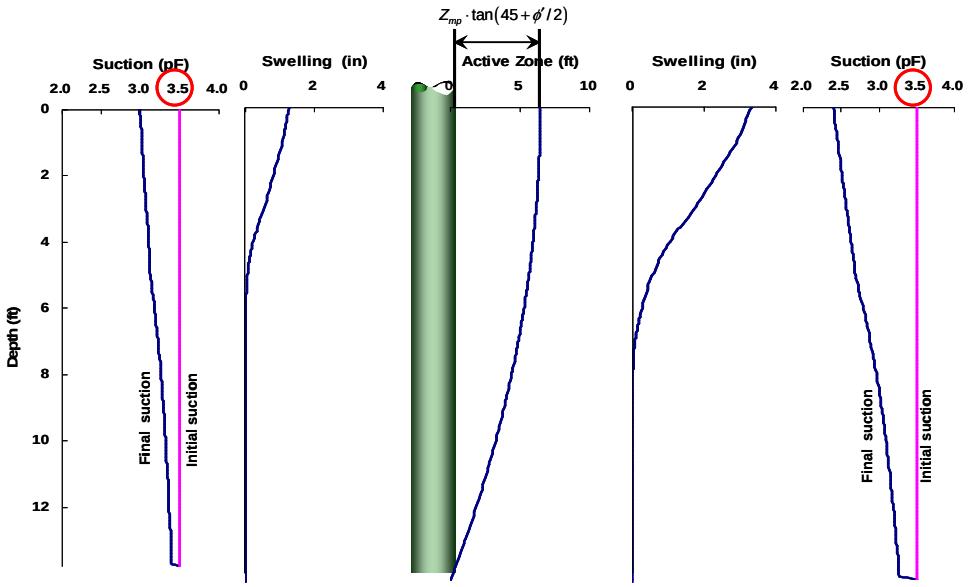

(a)

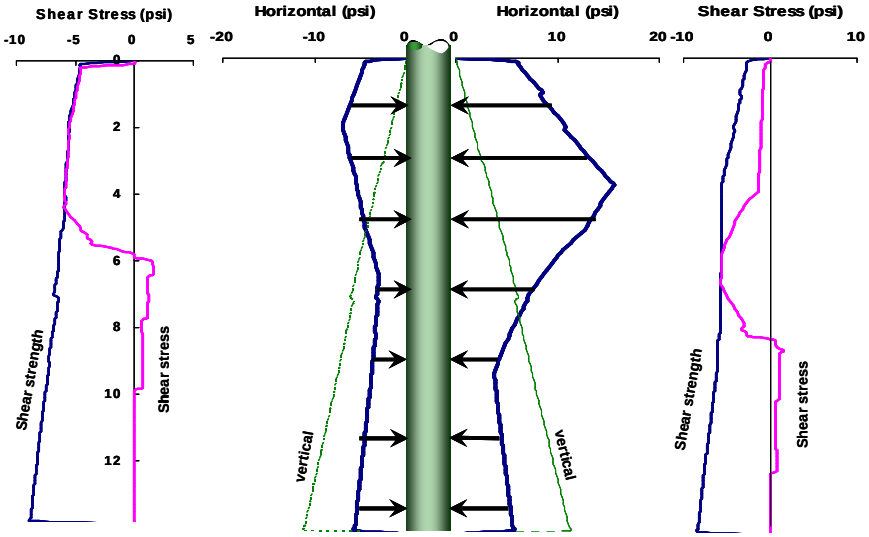

(b)

Fig. 5.19. Distribution of Stresses and Deformations in the Left and Right Sides of the Pier in Non-Uniform Wetting Condition with the Different Final Suction Envelope. (a) Suction Changes, Swelling Movements, and Horizontal Movement Active Zone, (b) Shear Stresses on Pier Shaft and Horizontal Earth Pressures in the Pier, (c) Deflection, Lateral Load, Bending Moments and Shear Force in the Pier

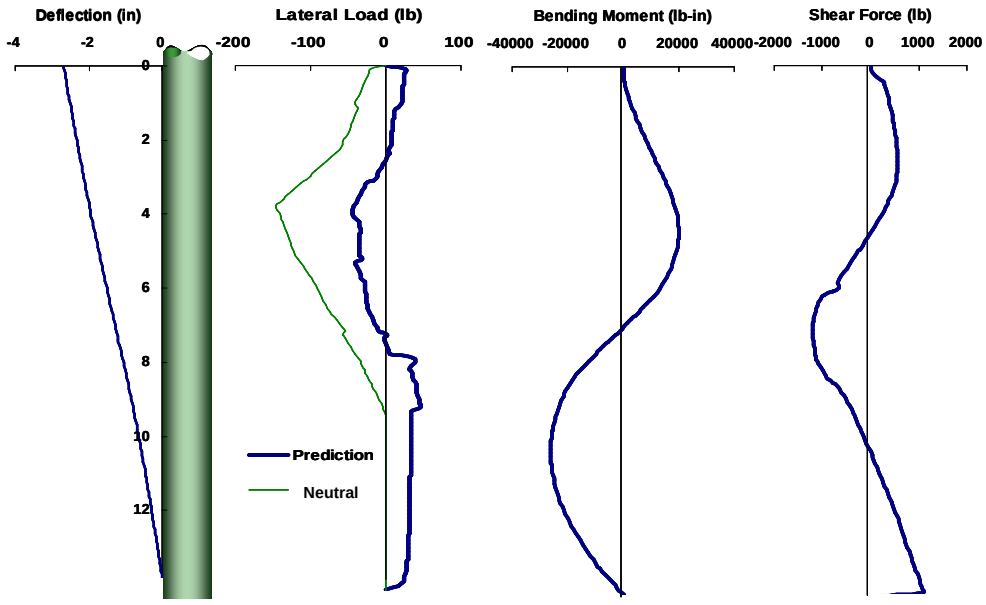

(c)

Fig. 5.19. continued.

5.6.2 Pier with Different Initial Suction Envelope

Another case study was performed for the different initial suction profiles around the pier. With the same final suction of 2.5 pF, non-uniform suction profiles induced by the initial suctions of 3.0 pF and 3.5 pF at the ground surface in the left and right side of the pier, respectively, leads to the horizontal earth pressure imbalance around the pier shown in Fig. 5.20(a). A heave of 3.0 inches on the left side and a heave of 1.2 inches on the right side of the pier are predicted. Maximum horizontal pressures of 15 psi and 7 psi occur at depths of 3.0 ft and 1.4 ft, respectively (Fig. 5.20(a)). As would be expected, a deflection of 4.9 inches at the ground surface is found toward the right side of the pier corresponding to the horizontal stress relief as shown in Fig. 5.20(b). This figure illustrates predicted the shear stress distribution, deflections, the lateral load, bending moment, and shear forces in the pier.

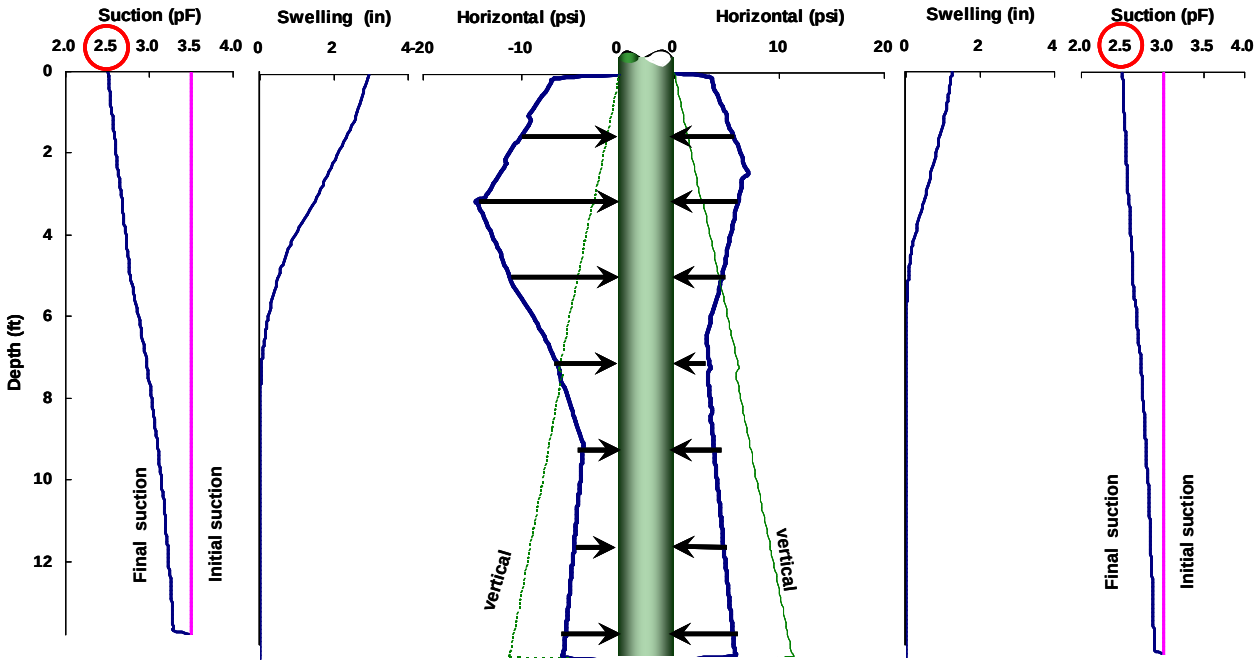

(a)

Fig. 5.20. Distribution of Stresses and Deformations in the Left and Right Side of the Pier in Non-Uniform Wetting Condition with the Different Initial Suction Envelope. (a) Suction Change, Swelling Movements, and Horizontal Earth Pressure, (b) Shear Stresses ,Shear Strength of the Soil, Deflection, Lateral Load, Bending Moment and Shear Force

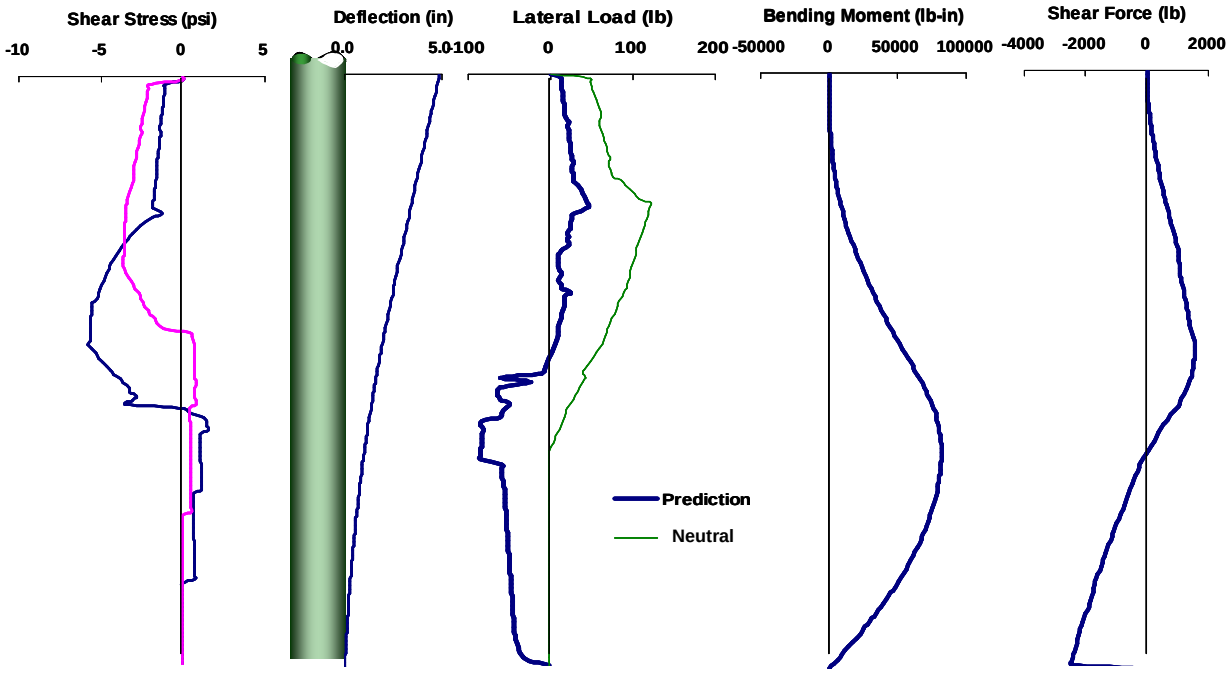

(b)

Fig. 5.20. continued.

CHAPTER VI
RETAINING WALL IN EXPANSIVE SOILS

6.1 Introduction

This chapter presents the soil-retaining wall systems and the prediction of stresses and deformations caused by soil expansion due to suction change against wall. The case study results including predicted heaves, lateral pressures in the both left and right side of the wall and predicted deflections, bending moments and shear forces in the wall are presented. The retaining wall model includes the swell-shrink prediction procedure in Chapter III, horizontal earth pressure prediction in Chapter IV, and the load transfer and load deflection curves developed in Chapter V.

6.2 Retaining Wall-Soil System in Expanding Soils

The typical retaining wall-soil system in expansive soil is illustrated in Fig. 6.1. The large lateral earth pressures could be developed by suction change at near ground surface and at deep depths caused by rainfall and the seasonal change of water table, respectively. Figure 6.1 represents the bulging failure at a shallow depth at which the maximum lateral pressure occurs as discussed in Chapter III.

In this study, the simplified retaining wall-soil model includes the suction envelopes, predicted heaves and the horizontal active length *XZ* in the both left and right side of the wall as shown in Fig. 6.2. The development of lateral earth pressure from the neutral stress state to equilibrium stress state after stress relief in the both sides of the wall is represented in Fig. 6.3.

The *P-Y* curves at each station are computed based on the non-linear suction dependant elastic modulus of unsaturated soil at depth. The composition of P-Y curves from the both left and right sides of the wall is used in analysis procedures. In Fig. 6.3, the lateral stress relieves are illustrated from the neutral stress state to the net lateral pressure.

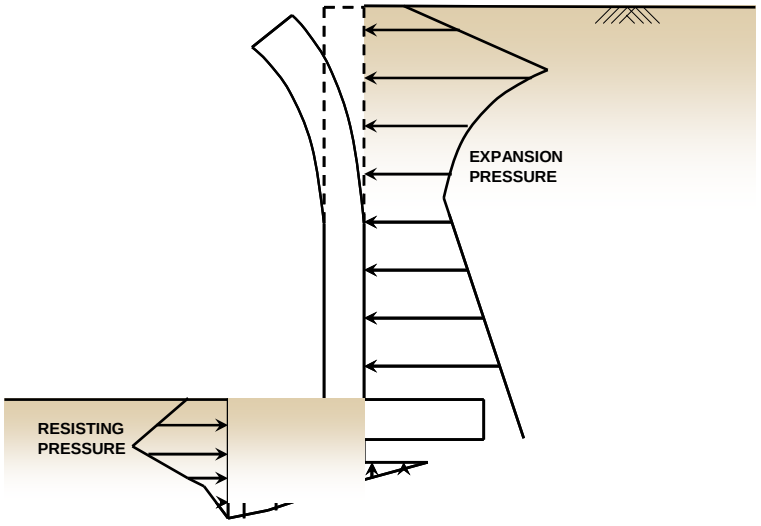

Fig. 6.1. Representation of the Lateral Behavior of Retaining Wall in Expansive Soils

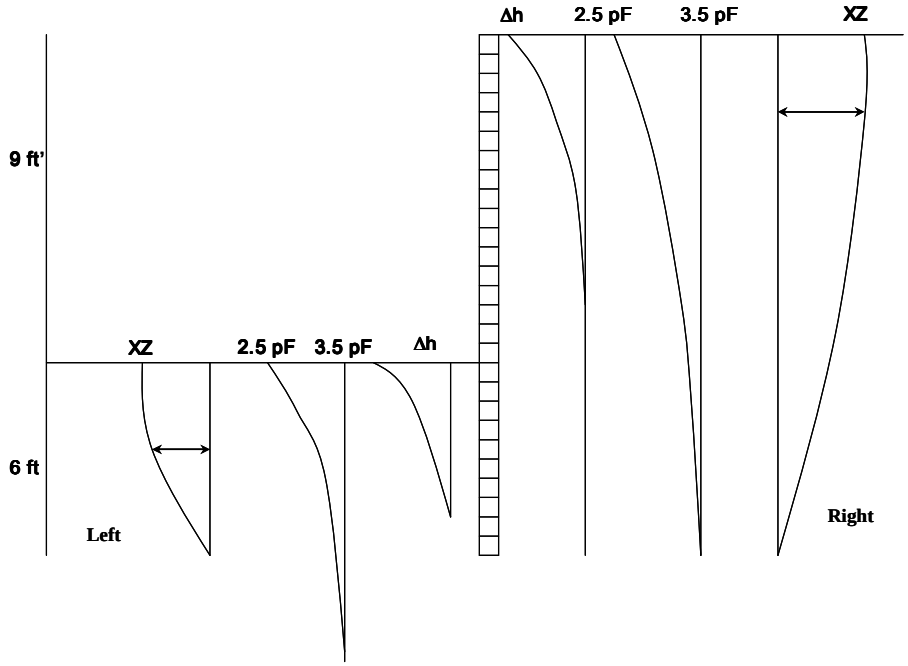

Fig. 6.2. Proposed Retaining Wall System with Suction Envelopes, Heaves and Horizontal Active Zones in the Left and Right of the Wall in Expansive Soils

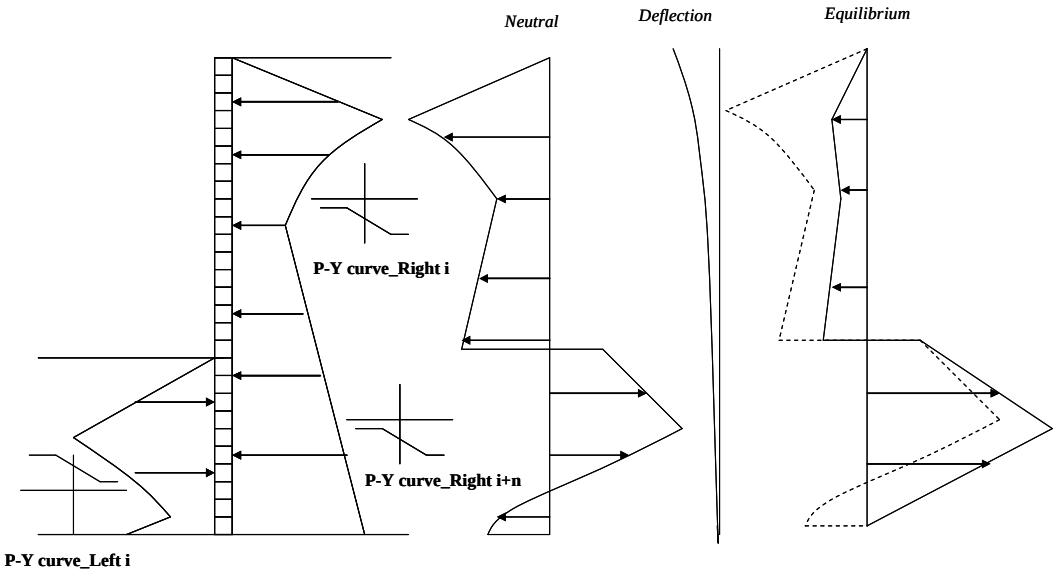

Fig. 6.3. Lateral Pressure Distributions on a Retaining Wall

6.3 Retaining Wall Case Study

A case study is performed to present the retaining wall behavior using a soil properties at site NGES (Kim and O'Neill 1998). The initial suction of 3.5 pF and final suction of 2.5 pF at ground surface are used to assign the suction envelopes in the both left and right side of the wall. Heaves of 0.8 inch and 1.3 inch in the left and right side of the retaining wall are predicted, respectively. The lateral swelling pressure distribution predicted with depth of zmp 2 ft at a stationary wall illustrated in Fig. 6.4(a). The maximum lateral pressures of 6 psi and 8 psi occur at a zmp-depth of 2 ft, respectively, in the left and right side of the retaining wall.

A deflection of 9 inches at ground surface is predicted from the lateral stress relief starting with the neutral pressure distribution predicted by assuming that the retaining wall does not move laterally. In Fig. 6.4(b), the lateral stress relieves are illustrated from the neutral stress state to the net lateral pressure found by iteration. Figure 6.4 gives the distribution of lateral loads, bending moments, and shear forces in the retaining wall.

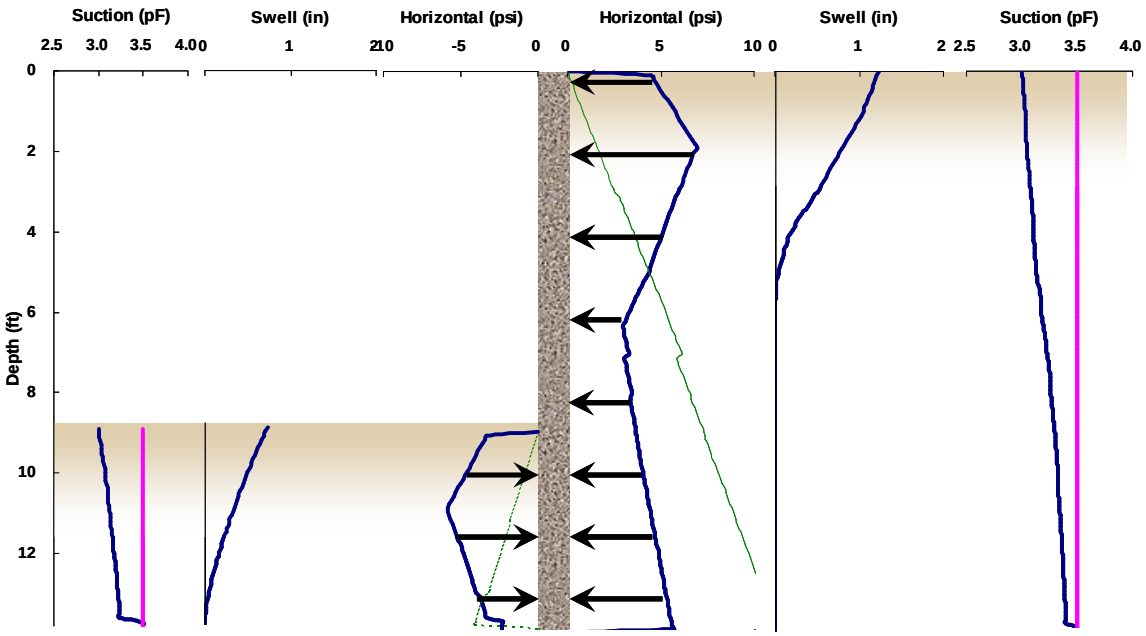

(a)

Fig. 6.4. Retaining Wall Case Study. (a) Suction Changes, Heaves, and Horizontal Pressures, (b) Deflection, Lateral Loads, Bending Moment and Shear Force.

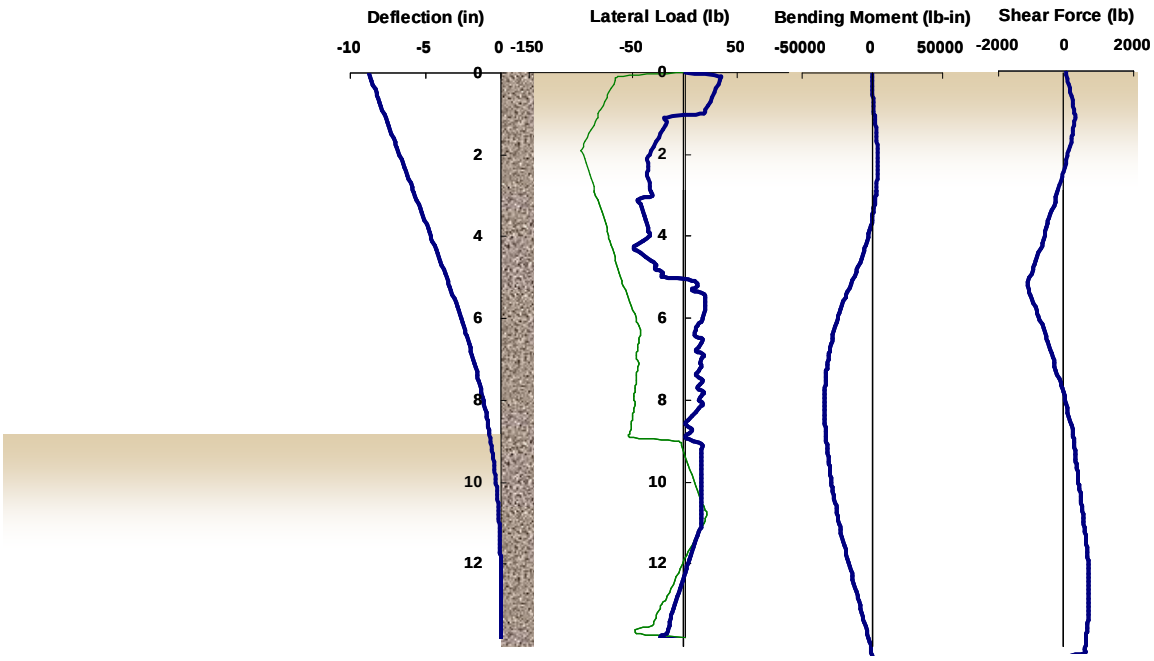

(b)

Fig. 6.4. continued.

CHAPTER VII
THEORETICAL BACKGROUND OF PAVEMENT DESIGN PROGRAM

7.1 Introduction

The pavement design program WinPRES is a model to estimate the development of pavement roughness on expansive soil subgrades, including the effects of the depth of a vertical barrier and thickness of inert and stabilized soil. The program generates graphically a suction envelope at the edge of the pavement, calculates vertical movement at the edge of the pavement and at any wheel path of interest, and then estimates the serviceability index and the international roughness index with time.

This program has been refined and advanced from the previous one, PRES, developed by Jayatilaka (1999). A more realistic suction profile with depth is added. The crack fabric factor f_c, initial mean principal stress σ_i, and the lateral earth coefficient K_0 are refined as noted in Chapter III. The method to determine suction compression index (SCI) γ_h is modified using low cost and easily available testing methods such as Atterberg limits and soil particle size distributions instead of using cation exchange activity (CEAc). The suction-versus-volumetric water content curves as simplified for natural, inert, and stabilized soil are used to estimate the depth of available moisture, d_{am}, and the mean principal stress compression index γ_σ. The effects of the thickness of inert and stabilized soil are added and the program is extended to be used in both rigid and flexible pavement systems.

A volume change model was developed to estimate the vertical movement at any point on a pavement surface in order to correlate the vertical movement to the rate of increase of roughness measurements made in different wheel paths of the pavement sections. This model estimates the total vertical movement including the swelling and shrinkage in a single column soil at the edge of the pavement using the subgrade soil properties and extreme suction envelope for the given locality based on the Thornthwaite

moisture index and drainage conditions. The probable vertical movement (PVM) in any given wheel path is then calculated using a set of regression equations.

The model, which predicts the rate of increase of pavement roughness in terms of serviceability index and international roughness index with time, is based upon the predicted movement of the subgrade soil and the roughness measurements that were observed in the monitoring program conducted by TTI for over 15 years on Texas pavements.

The vertical movement model and the roughness model developed were then assembled in the program PRES written in the Fortran language. The input data are entered to the new program through a Windows graphical user interface developed using a Visual Basic tool.

7.2 Two-Dimensional Vertical Movement

Jayatilaka (1999) suggested a regression model to estimate the relationship between one-dimensional and two-dimensional vertical movement, using the two programs MOPREC and FLODEF developed by Gay (1994):

$$\frac{VM_{2D}}{VM_{1D}} = \xi_1 \exp\left[\left(\xi_2 \frac{d}{D}\right)^{\xi_3}\right] \qquad (7.1)$$

where:

VM_{2D}	=	Two-dimensional vertical movement (extrapolated vertical movement from one-dimensional vertical movement)
VM_{1D}	=	one-dimensional vertical movement
d	=	distance from the center of the pavement to the point where the vertical movement needs to be calculated
D	=	half width of the pavement
ξ_1, ξ_2, ξ_3	=	regression coefficients

The FLODEF program calculates the transient unsaturated moisture flow and deformation in an expansive clay using a sequential analysis of flow and deformation.

The one- dimensional vertical movement program MOPREC was used in the development of regression equations for the estimation of vertical movement in a two-dimensional domain.

The regression equations for the parameters ξ_1, ξ_2, and ξ_3 were developed using a multiple linear regression analysis with the statistical analysis software package developed by SAS Institute, Inc. :

For pavement width less than 18.0 m:

$$\xi_1 = 0.0561 + 1.5872(d_{am}) + 0.1244(S_m) - 0.1936(\log_e D) - 0.0007139(VM_{1D} * S_m) - 0.1443(DB * d_{am}) \quad (7.2a)$$

$n = 240 \qquad R^2 = 0.91$

$$\xi_2 = -0.068 + 0.09134(S_m) - 0.101(DB) - 0.000188(TMI^2) + 0.321(\log_e D) + 0.000153(VM_{1D} * S_m) + 0.000706(VM_{1D} * DB) \quad (7.2b)$$

$n = 240 \qquad R^2 = 0.85$

$$\xi_3 = \exp(1.8061 - 0.4397(S_m) + 0.4711(\log_e D) + 0.08855(DB^2) - 0.000143(VM_{1D} * TMI) + 0.003022(VM_{1D} * DB) - 1.2592(DB * d_{am})) \quad (7.2c)$$

$n = 240 \qquad R^2 = 0.78$

For pavement width less than 22.0 m:

$$\xi_1 = 0.3736 + 0.4141(d_{am}) + 0.04078(S_m) - 0.0924(\log_e D) - 0.000426(VM_{1D} * S_m) - 0.02584(DB * d_{am}) \quad (7.3a)$$

$n = 240 \qquad R^2 = 0.80$

$$\xi_2 = +0.0298 + 0.09345(S_m) - 0.08724(DB) - 0.00001643(TMI^2) + 0.1701(\log_e D) + 0.00049(VM_{1D} * S_m) + 0.000256(VM_{1D} * DB) \quad (7.3b)$$

$n = 240 \qquad R^2 = 0.81$

$$\xi_3 = \exp(3.5562 - 0.8125(S_m) + 0.3707(\log_e D) + 0.05649(DB^2) - 0.000306(VM_{1D} * TMI) - 1.6175(d_{am}) - 0.4207(DB * d_{am}) \quad (7.3c)$$

where:

VM_{1D} = vertical movement from 1-D program (mm)

DB = depth of barrier (m)

d_{am} = depth of available moisture (m)

D = half width of pavement (m)

S_m = mean suction at site (pF)

TMI = Thornthwaite moisture index

For pavement widths between 18 m and 22m, the parameters $\xi_1, \xi_2,$ and ξ_3 are estimated from the following equation:

$$\xi_3 = \frac{\left[\xi_{18}(22 - D) + \xi_{22}(D - 18)\right]}{4} \tag{7.4}$$

where

ξ = parameter $\xi_1, \xi_2,$ or ξ_3 for the pavement width of D,

ξ_{18} = parameter $\xi_1, \xi_2,$ or ξ_3 estimated from the equations for the pavement widths less than 18 m (Equation 7.2(a), 7.2(b), or 7.2(c)), and

ξ_{22} = parameter $\xi_1, \xi_2,$ or ξ_3 estimated from the equations for the pavement widths less than 22 m (Equation 7.3(a), 7.3(b), or 7.3(c)).

The depth of available moisture refers to the quantity of water that the soil is capable of storing for use by plants. It depends on soil properties that affect the retention of water and the depth of the root zone. The depth of available moisture is estimated from the following relationship:

$$d_{am} = \sum_{i=1}^{N} (\theta_{wi} - \theta_{di}) \Delta z_i \tag{7.5}$$

where:

Δz_i = thickness of element in the i^{th} layer

N = number of layers

θ_{wi} = volumetric moisture content in the wetting suction envelope of the i^{th} layer

θ_{di} = volumetric moisture content in the drying suction envelope of the i^{th} layer

7.3 Pavement Roughness

Pavement roughness is an indicator of road condition or riding quality of a pavement. The roughness increases over time with the loss of smoothness in the pavement due to traffic loading and forces exerted by swelling of clay subgrades. A large number of different roughness indices have been developed by many researchers. However, the Serviceability Index (SI) and the International Roughness Index (IRI) may be the most widely used roughness indices at present.

Serviceability Index (SI)

The serviceability performance concept in the design of pavements was emerged from the AASHTO road test (Carey and Irick 1960). In the AASHTO road test, the serviceability of pavements was rated subjectively by a panel made up of men selected to represent many important groups of highway users. The mean of the individual ratings was defined as the Present Serviceability Rating (PSR) and it was a number between zero and five. A predictive model, the Present Serviceability Index (PSI), was developed to reproduce the PSR based on physical characteristics of the pavement surface. The physical measurements in the predictive model for flexible pavements included the percent cracking, percent patching, rut depth, and average slope variance. For rigid pavements, the parameters considered were percent cracking, percent patching, and average slope variance.

International Roughness Index (IRI)

The International Roughness Index (IRI) emerged from the International Road Roughness Experiment (IRRE) held in Brasilia, Brazil in 1982 (Sayers et al. 1986). The World Bank initiated the IRRE in order to find best practices appropriate for the many types of roughness measuring equipment in use. It was conducted by research teams from Brazil, England, France, the United States, and Belgium. Both profilometric methods and Response-Type Road Roughness Measuring System (RTRRMS) were used in the experiment and the IRI was measured from both types of instruments. The IRI is based on the roadmeter measure, called by its technical name of Average Rectified Slope (ARS) and has units of slope such as m/km or in/mile. The IRI is influenced by wavelengths ranging from 1.2 m to 30 m and is linearly proportional to roughness (Sayers and Karamihas 1996). An IRI of zero means the profile is perfectly flat. There is no theoretical upper limit to IRI. Values of IRI for different types of pavements are shown in Fig. 7.1.

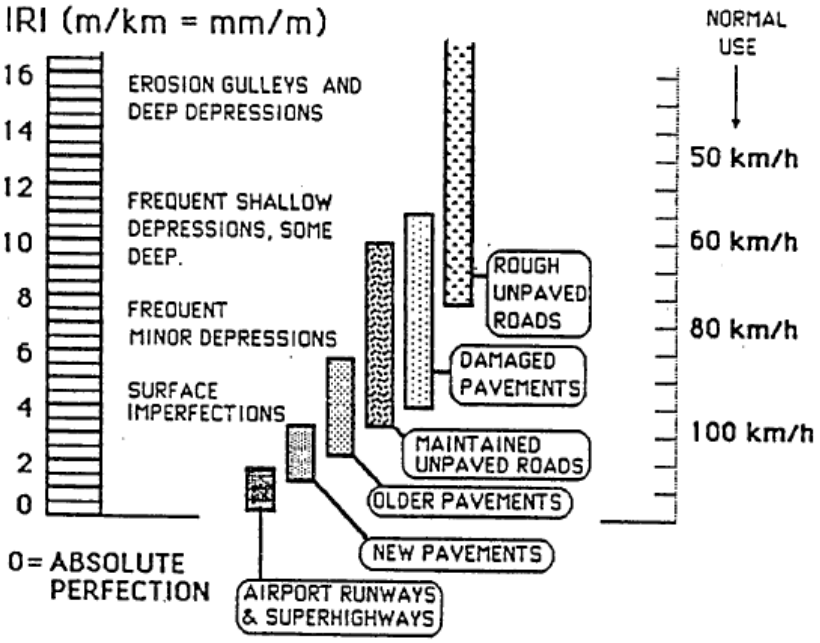

Fig. 7.1 Typical Values of International Roughness Indices (Sayers et al. 1986)

The IRI is defined as a property of a single wheel-track profile and the following points fully defined the IRI concept (Sayers 1995) as follows:

1. The IRI is computed from a single longitudinal profile. The sample interval should be no longer than 300 mm for accurate calculations. The required resolution depends on the roughness level, with the finer resolution being needed for smooth roads. A resolution of 0.5 mm is suitable for all conditions.
2. The profile is assumed to have a constant slope between sample elevation points
3. The profile is smooth with a moving average whose base length is 250 mm.
4. The smoothed profile is filtered using a quarter-car simulation, with specific parameter values, at a simulated speed of 80 km/hr.
5. The simulated suspension motion is linearly accumulated and divided by the length of the profile to yield IRI.

7.4 Prediction of Pavement Roughness in Expansive Soils

The American Association of State Highway and Transportation officials' guide for design of pavement structures (AASHTO 1993) presents a procedure to estimate the serviceability loss due to expansive soils. In this procedure, the serviceability loss is calculated from a plot of serviceability loss versus time which is generated using three estimated parameters. The three parameters are: (1) swell rate constant, (2) potential vertical rise, and (3) swell probability. The swell rate constant estimates the rate at which swelling will take place. This value varies from 0.04 to 0.20 depending on the moisture supply and the soil crack fabric at the site. The potential Vertical Rise (PVR) is estimated from a laboratory test, empirical procedure, or by experience and it represents the amount of swell that can occur due to the presence of expansive clay in the subgrade. The swell probability represents the percentage of the project length that is subject to swell. If the plasticity index of the subgrade soil exceeds 30 and the layer thickness exceeds 600 mm or if the PVR exceed 5 mm, the swell probability is taken as 100 percent. The serviceability loss due to expansive soils (ΔPSI_{sw}) is calculated from the following relationship:

$$\Delta PSI_{sw} = 0.00335 * PVR * P_s * (1 - e^{-\theta t}) \qquad (7.6)$$

where

PVR = potential vertical rise (in)

P_s = swell probability,

θ = swell rate constant, and

t = time (years).

Lytton et al. (1976) studied the development of roughness in two gilgai fields in Texas and found that the cracking patterns in soil determined the roughness pattern and suggested that the roughness could be predicted from the mineralogical and pedologic properties of a clay deposit. Wave analysis using the Fast Fourier Transformation technique was performed on the profilometer data collected from those sites and they

developed the following relationship between Serviceability Index (SI), wave length (λ), and amplitude (a);

$$SI = 5.00 + 0.1774\lambda - a(126.4 - 0.1665\lambda^2) \quad a^2(1684.4 - 21.99\lambda) \tag{7.7}$$

They concluded that the field amplitude-wavelength relations were a practical upper limit of the roughness that would develop on a pavement.

Velasco and Lytton (1981) used a similar procedure to analyze profilometer data collected in 23 pavement sections in Texas and the graphs of half amplitude versus frequency were fitted by the following equation:

$$\frac{a}{2} = cf^n \tag{7.8}$$

where

a = mean amplitude, in inches,

f = frequency, in cycles/foot, and

c, n = regression constants.

The values of two constants, c and n, were found to depend upon the composite flexural stiffness of the pavement, time, climatic measures, and several physicochemical soil properties. They developed two empirical models to predict c and n and then these were correlated to the Serviceability Index reduction (ΔPSI).

The pavement sections in that study contained five rigid pavements. Omitting these rigid pavements and assuming a new regression analysis for the data and proposed the following model to predict the serviceability loss;

$$\Delta PSI = 39396c^{1.544}\left|n\right|^{9.59} \tag{7.9}$$

McKeen (1985) used the procedure proposed by Velasco and Lytton (1981) to analyze the roughness pattern on airport pavements and to develop a thickness design procedure for airport pavements using a mathematical model for an elastic beam on a deformed foundation. The parameters used to model the roughness pattern were the weighted amplitude and characteristic wavelength.

Gay (1994) studied the development of pavement roughness in expansive soils with and without vertical moisture barriers. The following roughness prediction models developed through the regression analysis of the rates of roughness development (*dR/dt*) and the expected value of vertical movement (ΔH) were used for the prediction of roughness measures for the different cases studied in this study.

Serviceability Index (SI)

The change in SI/year *dR/dt* is given by:

$$\frac{dR}{dt} = \beta_1(\Delta H) + \beta_2 \qquad (7.10)$$

where for category

A Moisture barriers with paved medians
β_1 = 0.02176 β_2 = 0.03226

B Moisture barriers with sodded medians
β_1 = 0.03430 β_2 = 0.07269

C Control sections with and without medians
β_1 = 0.04418 β_2 = 0.12461

International Roughness Index (IRI)

The mean rate of change of IRI (in/mile/year) *dR/dt* is given by:

$$\frac{dR}{dt} = \beta_1(\Delta H) + \beta_2 \qquad (7.11)$$

where for category

A Moisture barriers with paved medians

β_1 = 0.61939 β_2 = 1.2954

B Moisture barriers with sodded medians

β_1 = 1.5825 β_2 = 2.0105

C Control sections with and without medians

β_1 = 2.7014 β_2 = 4.0146

Minimum Expected Bump Height (BH)

$$\frac{dR}{dt} = \beta_1 + \beta_2 \exp(\beta_3 \Delta H) \tag{7.12}$$

where for category

A Moisture barriers with paved medians

β_1 = 0.011 β_2 = 0.012 β_3 = 0.216

B Moisture barriers with sodded medians

β_1 = 0.010 β_2 = 0.011 β_3 = 0.305

C Control sections with and without medians

β_1 = 0.000 β_2 = 0.018 β_3 = 0.302

7.5 Development of Pavement Roughness Model

The development of roughness on pavements with time is cased by the combination of traffic loading applied on the pavement and the swelling of subgrade soil where the pavements are built on expansive soils. It was found that the pavement performance can be modeled through a sigmoidal type curve (Jayatilaka 1999). The sigmoidal models with respect to PSI and IRI to estimate the loss of serviceability and increase of roughness with time are given by:

With respect to PSI:

$$PSI = PSI_0 - (PSI_0 - 1.5)\exp\left[-\left(\frac{\rho_s}{t}\right)^{\beta_s}\right] \tag{7.13}$$

With respect to IRI:

$$IRI = IRI_0 + (4.2 - IRI_0)\exp\left[-\left(\frac{\rho_i}{t}\right)^{\beta_i}\right] \quad (7.14)$$

where:

PSI_0 = initial serviceability index of the pavement (usually 4.2)

t = time in months

IRI_0 = initial IRI in m/km or in/mile (usually 1.19 m/km)

$\rho_s, \beta_s, \rho_i, \beta_i$ = roughness parameters

A terminal PSI of 1.5 corresponds to an IRI of 4.2 m/km. In the roughness parameters, the best values for β_s and β_i were found to be 0.66 and 0.56, respectively, using nonlinear regression. Considering the development of roughness caused by both traffic and expansive soil, the parameters ρ_s and ρ_i were suggested by the following forms:

$$\rho_s = A_s - B_s \Delta H \quad (7.15a)$$

$$\rho_i = A_i - B_i \Delta H \quad (7.15b)$$

where:

ΔH = total vertical movement in mm, including both shrinkage and swelling

A_s, A_i = parameters that are functions of traffic, structural number (SN) of the flexible pavement, pavement section, and resilient modulus of subgrade soil (M_r)

B_s, B_i = constants

The values of B_s and B_i were estimated for a site by assigning a reliability and using the following relationships:

$$B_i = 35.817 + 8.158Z \quad (7.16a)$$

$$B_s = 17.960 + 4.195Z \quad (7.16b)$$

where Z = standard normal variable corresponding to the assigned reliability.

Z can be determined from Table 7.1.

Table 7.1. Standard Normal Deviates for Various Levels of Reliability

Reliability (%)	Standard Normal Deviate (Z)	Reliability (%)	Standard Normal Deviate (Z)
50	0.000	93	-1.476
60	-0.253	94	-1.555
70	-0.524	95	-1.645
75	-0.674	96	-1.751
80	-0.841	97	-1.881
85	-1.037	98	-2.054
90	-1.282	99	-2.327
91	-1.340	99.9	-3.090
92	-1.405	99.99	-3.750

The parameters A_s and A_i were estimated using the American Association of State Highway and Transportation Officials (AASHTO) design equation (AASHTO 1993) for flexible pavements.

7.5.1 Relationship between Serviceability Index and International Roughness Index

Jayatilaka (1999) collected subgrade soil properties and surface profile measurements in several pavement sections in the state of Texas where moisture barriers have been installed. The pavement sections included Interstate-410, Interstate-10, U.S. 281, and General McMullen Drive in San Antonio, Interstate-30 in Greenvile, Interstate-10 in Sierra Blanca, Interstate-635 in Dallas, Interstate-10 in Seguin, and FM-1516 in Converse. The 690D Surface Dynamics Profilometer owned by the Texas Department of Transportation was used to obtain relative elevation profiles of the road surface in all of the test sites. The profilometer records relative elevations along the right and left wheel paths of the surface when it traverses on a roadway. The measurements are obtained at 6 inches intervals and saved in a computer file. The relative elevations of right and left wheel paths are recorded in two columns in units of thousandths of an inch.

This computer file is used as the input file for the computer programs that are used to obtain profile statistics. The profile statistics, International Roughness Index

(IRI) and Serviceability Index (SI), are used to develop roughness predicted models in this study. The computer program VERTAC (McKenzie et al. 1986) is used to obtain IRI and SI of all of the pavement sections. The program VERTAC is capable of calculating both IRI and SI. The SI is calculated from the profile measurements using two regression equations between SI and Mays Ridemeter Index (MO), and MO and Root Mean Square Vertical Acceleration (RMSVA) at baselengths of 4.0 ft and 16 ft. The International Roughness Index is calculated from the International Roughness Index algorithm incorporated in this program.

The length of the roadway section that was used in the program depended on the lengths of barrier and control sections. The serviceability Indices and International Roughness Indices obtained from this program were used in the development of roughness prediction models. In addition, these data were used to develop a relationship between the IRI and SI. A regression relationship between SI and IRI was developed using SI and IRI values calculated using the VERTAC program for all the pavement sections studied in this research study. A plot of IRI versus SI and the fitted model is shown in Fig. 7.2.

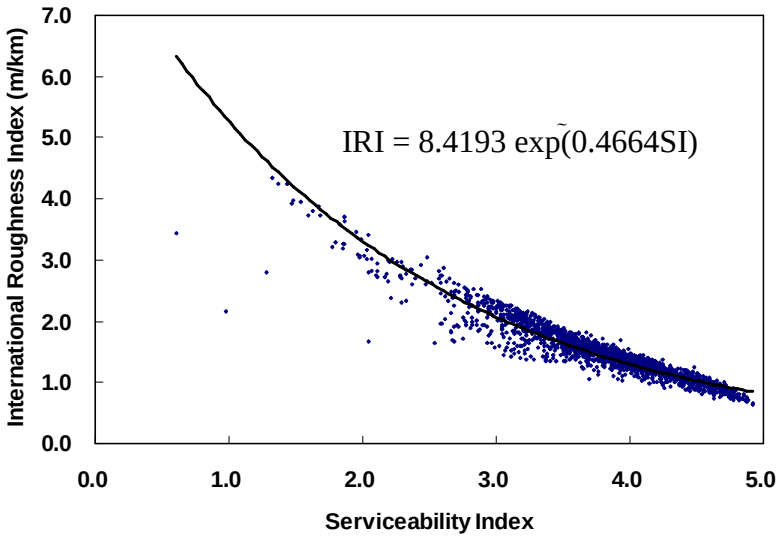

Fig. 7.2. International Roughness Index versus Serviceability Index (Jayatilaka 1999)

7.5.2 Determination of Roughness Parameters

Roughness Parameter A_s in the Flexible Pavement

The AASHTO design based on the results of the AASHTO road test for flexible pavements is as follows:

$$\log_{10} W_{18} = -ZS_0 + 9.36\log_{10}(SN+1) - 0.20 + \frac{\log_{10}\left[\frac{\Delta PSI_w}{PSI_0 - 1.5}\right]}{0.4 + \frac{1094}{(SN+1)^{5.19}}} + 2.32\log_{10} M_r - 8.07 \qquad (7.17)$$

where:

W_{18} = 80 KN (18 kip) single-axle load applications

Z = standard normal deviate

S_0 = combined standard error, 0.44 in flexible pavements (AASHTO)

SN = structural number of pavement, in inches

ΔPSI_w = loss of serviceability due to traffic

PSI_0 = initial serviceability (usually 4.2)

M_r = resilient modulus of subgrade soil, in lbf/in^2

The 80 kN single-axle load applications for a specific time interval in the analysis period can be calculated from the following traffic equation used by the Texas Department of Transportation:

$$W_{18} = \frac{N_c}{C(r_0 + r_c)}\left[2r_0 t_k + \left[\frac{r_c - r_0}{C}\right] t_k^2\right] \qquad (7.18)$$

where:

W_{18} = the total accumulated number of 80 kN (18 kip) ESALs up to the time, t_k

C	=	analysis period
t_k	=	time in years
r_0	=	average daily traffic (ADT) in one direction when t_k =0.0
r_c	=	average daily traffic (ADT) in one direction when $t_k = C$
N_c	=	total 80 kN (18 kip) ESALs over the analysis period, C (provided by TxDOT's TPP Division)

Equation (7.17) is modified to:

$$\log_{10}\left[\frac{\Delta PSI_w}{(PSI_0 - 1.5)}\right] = \lambda \tag{7.19}$$

where λ is given by:

$$\lambda = \left[0.4 + \frac{1094}{(SN+1)^{5.19}}\right] \times \left[\log_{10} W_{18} - 9.36\log_{10}(SN+1) + 8.27 - 2.32\log_{10} M_r + ZS_0\right] \tag{7.20}$$

Equation (7.19) can be expressed as:

$$\Delta PSI_w = (PSI_0 - 1.5)10^{\lambda} \tag{7.21}$$

From Equation (7.13), the total serviceability loss (ΔPSI_t) is given by:

$$\Delta PSI_t = (PSI_0 - 1.5)\exp\left[-\left(\frac{\rho_s}{t}\right)^{0.66}\right] \tag{7.22}$$

When the vertical movement (ΔH) is equal to zero, from Eq. (7.15a), $\rho_s = A_s$. Then, the total loss of serviceability calculated from Eq. (7.22) is equal to the serviceability loss due to traffic (ΔPSI_w) as follows:

$$\Delta PSI_w = (PSI_0 - 1.5)\exp\left[-\left(\frac{A_s}{t}\right)^{0.66}\right] \tag{7.23}$$

Solving Eqs. (7.21) and (7.23), A_s is given by:

$$A_s = t\left[\log_e(10^{-\lambda})\right]^{\left(\frac{1}{0.66}\right)} \tag{7.24}$$

A value of t of 480 months (=40 years) is assumed to be the time required for the roughness due to expansive clays to be complete, and λ is estimated for 40 years. This value of A_s is used in Eq. (7.15) to predict the PSI history of a flexible pavement on expansive clay.

Roughness Parameter A_i in the Flexible Pavement

Since the AASHTO design equation is not available in terms of IRI, the parameter A_i cannot be estimated directly as in the case of A_s. A regression relationship between PSI and IRI was developed using PSI and IRI values calculated in the previous study by Jayatilaka (1999):

$$IRI = 8.4193\exp(-0.4664PSI) \tag{7.25}$$

where IRI is in m/km.

A relationship for A_i is developed using Eq. (7.25) and assuming an initial serviceability index of 4.2. From Eq. (7.21), the PSI at any time is given by:

$$PSI = PSI_0 - (PSI_0 - 1.5)10^{\lambda} \tag{7.26}$$

When $PSI_0 = 4.2$, this equation is simplified to:

$$PSI = 4.2 - 2.7(10^{\lambda}) \tag{7.22}$$

From Eq. (7.25), the corresponding IRI is given by:

$$IRI = 8.4193 \exp\left[-0.4664(4.2 - 2.7(10^{\lambda}))\right] \tag{7.28}$$

From Eq. (7.25), the initial IRI, which corresponds to PSI of 4.2, is estimated to be 1.19 (m/km). Then the change in IRI due to traffic (ΔIRI_w) is given by:

$$\Delta IRI_w = 8.4193 \exp\left[-0.4664(4.2 - 2.7(10^{\lambda}))\right] - 1.19 \tag{7.29}$$

From Eq. (7.14), the total change in IRI (ΔIRI_t) is given by:

$$IRI_t = (4.2 - 1.19) \exp\left[-\left(\frac{\rho_i}{t}\right)^{0.56}\right] \tag{7.30}$$

When the vertical movement (ΔH) is equal to zero, from Eq. (7.15b), $\rho_i = A_i$.

Then, the total change in IRI calculated from Eq. (7.30) is equal to the change in IRI due to traffic (ΔPSI_w) as follows:

$$\Delta IRI_w = 3.01 \exp\left[-\left(\frac{A_i}{t}\right)^{0.56}\right] \tag{7.31}$$

Solving Equations (7.29) and (7.31), A_i is given by:

$$A_i = t\left[\log_e\left(\frac{3.01}{8.4193 \exp\left(-0.4664(4.2 - 2.7\left(10^{\lambda}\right)\right) - 1.19}\right)\right]^{\left(\frac{1}{0.56}\right)} \tag{7.32}$$

As in the case of PSI, t is taken as 480 months and λ is estimated for 40 years.

This equation for A_i is used in Eq. (7.15b) to predict the IRI history of a flexible pavement on expansive soil.

Roughness Parameter A_s in the Concrete Pavement

A similar process is used to find the A and B coefficients to predict the roughness and riding quality development due to both traffic and expansive clays. The process starts with the AASHTO 1993 concrete pavement design program for rigid pavements as follows:

$$\log_{10} W_{18} = -Z_R S_0 + 7.35\log_{10}(D+1) - 0.06 + \frac{\log_{10}\left[\frac{\Delta PSI}{4.5-1.5}\right]}{1+\frac{1.624\times10^7}{(D+1)^{8.46}}} + (4.22-0.32\,p_t)\log_{10}\left[\frac{S_c' C_d\left(D^{0.75}-1.132\right)}{215.63J\left(D^{0.75}-18.42/\left(E_c/k\right)^{0.25}\right)}\right] \tag{7.33}$$

where:

D = thickness of concrete layer (inches)

S_c' = modulus of rupture of concrete (psi)

J = load transfer coefficient

C_d = drainage coefficient

E_c = modulus of elasticity of Portland cement concrete (psi)

k = modulus of subgrade reaction (lb/in^3)

S_0 = combined standard error, 0.34 in rigid pavements (AASHTO 1993)

Z_R = standard normal deviate

p_t = terminal present serviceability index

ΔPSI = loss of serviceability due to traffic

Equation (7.33) is modified to

$$\log_{10}\left[\frac{\Delta PSI_w}{(PSI_0 - 1.5)}\right] = \lambda \tag{7.34}$$

where λ is given by:

$$\lambda = \left[1 + 1.624\times10^7/(D+1)^{8.46}\right]\times\lambda' \tag{7.35}$$

where:

$$\lambda' = \log_{10} W_{18} - 7.35\log_{10}(D+1) + 0.06$$
$$-(4.22 - 0.32\,p_t)\log_{10}\left[\frac{S_c' C_d\left(D^{0.75} - 1.132\right)}{215.63J\left(D^{0.75} - 18.42/\left(E_c/k\right)^{0.25}\right)}\right] + Z_R S_0 \tag{7.36}$$

Equation (7.34) can be expressed as:

$$\Delta PSI_w = (PSI_0 - 1.5)10^{\lambda} \tag{7.37}$$

From Eq. (7.13), the total serviceability loss (ΔPSI_t) is given by:

$$\Delta PSI_t = \left(PSI_0 - 1.5\right)\exp\left[-\left(\frac{\rho_s}{t}\right)^{0.66}\right] \tag{7.38}$$

When the vertical movement (ΔH) is equal to zero, from Eq. (7.15a), $\rho_s = A_s$. Then, the total loss of serviceability calculated from Eq. (7.38) is equal to the serviceability loss due to traffic (ΔPSI_w) as follows:

$$\Delta PSI_w = (PSI_0 - 1.5)\exp\left[-\left(\frac{A_s}{t}\right)^{0.66}\right] \tag{7.39}$$

Solving Equations (7.37) and (7.39), A_s is given by:

$$A_s = t\left[\log_e(10^{-\lambda})\right]^{\left(\frac{1}{0.66}\right)} \tag{7.40}$$

where t = 40 yrs = 480 months is the time at which all of the roughness developed by expansive soils is estimated to be complete.

Roughness Parameter A_s in the Concrete Pavement

A relationship for Ai developed using Eq. (7.25) and assuming an initial serviceability index of 4.5. From the Eq. (7.21), the PSI at any time is given by:

$$PSI_0 - PSI = (PSI_0 - 1.5)10^{\lambda} \tag{7.41}$$

Since $PSI_0 = 4.5$ from the AASHTO Road Test, this is simplified to:

$$PSI = 4.5 - (3.0)10^{\lambda} \tag{7.42}$$

From Eq. (7.25), the corresponding IRI is given by:

$$IRI = 8.4193 \exp\left[-0.4664(4.5 - (3.0)10^{\lambda})\right] \tag{7.43}$$

The initial IRI corresponding to an initial $PSI_0 = 4.5$ is estimated to be 1.032 (m/km). Then the change in IRI due to traffic (ΔIRI_w) is given by:

$$\Delta IRI_w = 8.4193\left[-0.4664(4.5 - 3.0(10)^{\lambda})\right] - 1.032 \tag{7.44}$$

Then, the total change of IRI is:

$$\Delta IRI_t = (4.2 - 1.032)\exp\left[-\frac{\rho_i}{t}\right]^{0.56} \tag{7.45}$$

If $\Delta H = 0.0$ and $\rho_i = A_i$, then the total change in IRI obtained from Eq. (7.15b) is equal to the change in IRI due to traffic alone as follows:

$$\Delta IRI_w = (3.168)\exp\left(-\frac{A_i}{t}\right)^{0.56} \tag{7.46}$$

Solving Eqs. (7.43) and (7.46), A_i is given by:

$$A_i = t\left[-\log_e\left(\frac{3.168}{8.4193\exp\left[-0.4664\left(4.5-3.0(10)^{\lambda}\right]-1.032}\right)\right]^{\left(\frac{1}{0.56}\right)} \tag{7.47}$$

where as before t = 40 years, or 480 months, and λ_r is determined for the 40-year period.

These equations for both flexible and rigid pavements are used to estimate the rate of increase roughness (IRI) and decrease of riding quality (PSI) due to both traffic and expansive clay movements.

CHAPTER VIII
DESIGN OF NEW PAVEMENTS WITH REMEDIAL MEASURES

8.1 Introduction

Based on the pavement design model developed in Chapter VII, the design analysis of six case study sections in the three sites Fort Worth, Atlanta, and Austin includes laboratory test results, climatic and drainage condition, dimension of road, roughness and traffic information. All input and output parameters, and figures of typical sections for the six study sections are presented in Appendix.

The typical soil properties in each analysis section are required as following; Atterberg limits, particle size distribution, values of suction, and climatic and geometric conditions.

The typical cross sections of the road for the six design sections are developed using the number of lanes and the width of shoulder. The pavement sections of both flexible and rigid pavement are estimated with different structural numbers (SN) and concrete thicknesses (D), respectively.

The typical values of the falling weight deflectometer modulus of the subgrade soil of 10,000 psi are used for the flexible pavement. A 28-day compressive strength of the concrete of 4000 psi, mean modulus of rupture of concrete of 650 psi, drainage coefficient of 1.0, modulus of subgrade of 515 pci, and load transfer coefficient of 3.2 for the rigid pavements are used as input parameters.

The average daily traffic in one direction and the total 18 kip single axle loads in the traffic analysis period of 30 years for the three sites are assumed based on traffic information provided by the Fort Worth and Atlanta Districts. The initial serviceability indexes for flexible and rigid pavement are assumed to be 4.2 and 4.5, respectively. Generally, the minimum acceptable serviceability index after 30 years is 2.5. The regression equation between the international roughness index and the serviceability index is used. The design analysis is performed with both flexible and rigid pavements

including treatments vertical moisture barriers, and lime stabilized and inert soil layers. The input parameters used for three case study sites are presented in Table 8.1.

Table 8.1. Design Parameters for Structural Properties of Pavement and Traffic

Design Parameters		Study Sites			
		Fort Worth North Loop Interstate 820	Atlanta U.S. 271	Austin State Route 1	
				Main Lanes	Frontage Road
Number of Lanes		5	1	4	3
Distribution of Traffic (inner to outer)		0.16, 0.16, 0.16, 0.20, and 0.32	1.0	0.19, 0.19, 0.24, and 0.38	0.20, 0.33, and 0.47
Average Daily Traffic of Outer Lane	t=0 yr	13,712	10,000	16,283	4,028
	t=30 yr	21,744	20,000	25,821	6,837
Total W_{18} of Outer Lane (t=30 yr)		8,415,520	2,500,000	9,993,430	2,472,059
Width of Pavement (ft)		83.0	44.0	62.0	50.0
Distance from the Center of Pavement (ft)		27.0	9.0	21.0	15.0
Falling Weight Deflectometer Modulus of subgrade Soil		10,000 psi for Flexible Pavement, Modulus of Subgrade Soil for Rigid Pavement is 300 pci (k =FWD/19.4)			
28-day Compressive Strength of Concrete		4,000 psi			
Mean Modulus of Rupture of Concrete		620 psi			
Drainage Coefficient		1.0			
Load Transfer coefficient		2.9			
Initial Serviceability Index		4.2 for Flexible Pavement and 4.5 for Rigid Pavement			
Initial International Roughness Index		75.2 in/mile for Flexible Pavement and 65.4 in/mile for Rigid Pavement			
Reliability		50% for Prediction and 95% for Design			

The following explanation of reliability was taken from the textbook *Pavement Analysis and Design* by Huang (1993). Reliability is a means of incorporating some degree of certainty into the design process to ensure that the various design alternatives will last the analysis period. The level of reliability to be used for design should increase as the volume of traffic and public expectation of availability increase. Table 8.2 presents recommended levels of reliability for various functional classes.

Table 8.2. Suggested Levels of Reliability for Various Functional Classifications

Functional Classification	Recommended Level of Reliability	
	Traffic	Expansive Soil
For Prediction	50%	50%
For Design		
Interstate and other freeways	85 – 99.9 %	80 – 99.9 %
Principal arterials	80 – 99.0 %	75 – 95.0 %
Collectors	80 – 95.0 %	75 – 95.0 %
Local	50 – 80.0 %	50 – 80.0 %

The 50 percent reliability level is used for prediction, and the reliability levels of 90 percent and 95 percent are used for the design of flexible pavement and rigid pavement, respectively. The 50 percent reliability level that is used for prediction uses Eq. (7.11) with standard normal deviate, Z, set equal to zero in predicting the expected value of the riding quality or roughness, without taking into account the variability of the input data.

The typical results are obtained using the program WinPRES for the six sections (three sections at the Fort Worth site, one section at the Atlanta site, and two sections for main lanes and frontage road lanes at the Austin site). The program output provides the suction profile with depth, total vertical movement swelling plus shrinkage at the edge of the pavement and at the outermost wheel path, serviceability index, and international roughness index with time. The wet and dry suction envelopes in the cases when no moisture control is used and when a stabilized soil layer is present are generated within the program. The design analysis is performed with flexible and rigid pavements with vertical moisture barriers, lime stabilized and inert soil layers, and different thicknesses of asphalt concrete and Portland cement concrete.

8.2 Fort Worth North Loop IH 820 Section A

8.2.1 One-Dimensional Model

Figure 8.1 shows the suction profile developed up to the depth of the moisture active zone, which is shown to be 15 ft. The initial suction for wetting at the surface is estimated using the climatic data, the Thornthwaite moisture index, and the drainage condition at the site. The equilibrium suction of 2.58 pF, which was obtained from lab tests of the soil sample, is attributed to a water table being near the depth of 17 ft and yields only a small amount of heaving. In the stabilized soil layer, the suction envelope for wetting may not exceed the equilibrium suction or 3.5 pF (Rajendran and Lytton, 1997), whichever is smaller (Fig. 8.2).

The total vertical movement at the edge of the pavement and at the outer wheel path is shown in Table 8.3. The result shows that a negligible heave, 0.07 inch, is caused by a low equilibrium suction, which results in little change of suction in the wetting side. By adding a stabilized soil layer, it is found that the reduction of vertical movement in the outer wheel path is about 15 percent.

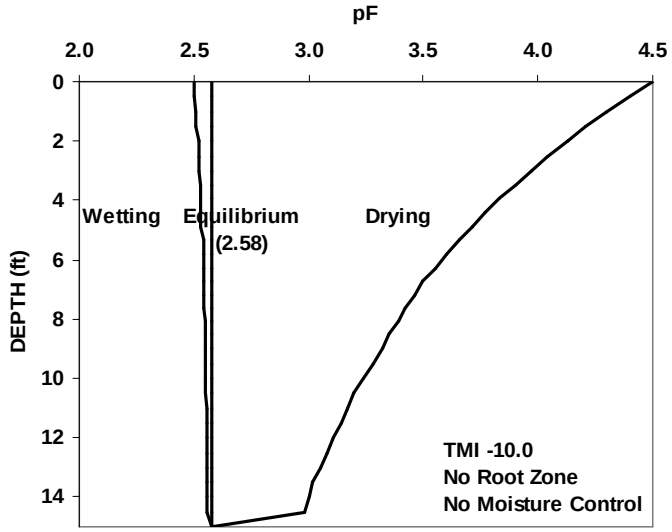

Fig. 8.1. Suction Profile versus Depth for the Case of No Moisture Control, Fort Worth North Loop IH 820, Section A

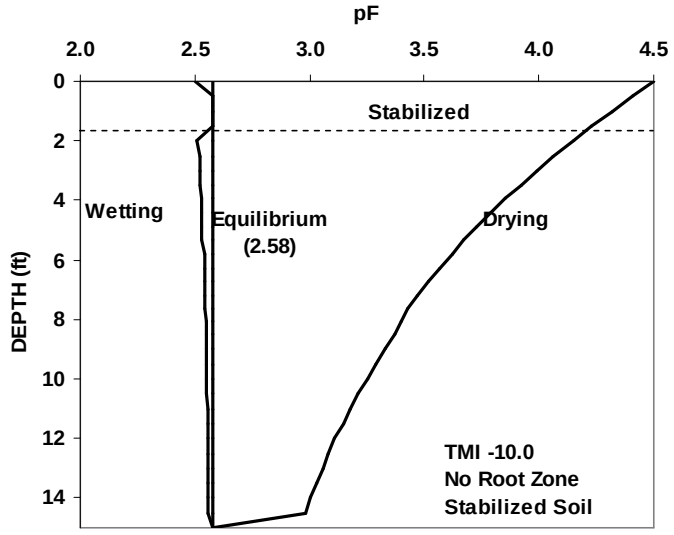

Fig. 8.2. Suction Profile versus Depth with Adding Stabilized Layer, Fort Worth North Loop IH 820, Section A

Table 8.3. Vertical Movement at the Edge of Pavement and at the Outer Wheel Path, Fort Worth North Loop IH 820, Section A

Systems of Pavement	At the Edge of the Pavement (inches)			At the Outer Wheel Path (inches)
	Swelling	Shrinkage	Total	
No moisture control	0.07	1.39	1.46	0.61
Stabilized soil (1.5 ft)	0.04	1.26	1.39	0.52

8.2.2 Performance of Various Pavement Systems

The input parameters for the structural properties of both flexible and rigid pavements and the traffic data are shown in Table 8.4. For flexible pavements with different treatments including a vertical moisture barrier and stabilized layers, the loss of serviceability and the increase of international roughness index versus time at a level of reliability of 50 percent are shown in Figs. 8.3 and 8.4, respectively. The results show that the serviceability index increases and the international roughness index decreases after 30 years, as the structural number increases. Both figures also show that for this site, a vertical barrier is less effective than stabilized layers in controlling roughness.

Table 8.4. Input Parameters for Structural Properties of Pavement and Traffic Data, Fort Worth North Loop IH 820

Flexible Pavement	Rigid Pavement
Reliability : 50% and 90% Falling Weight Deflectometer Modulus of Subgrade Soil : 10,000 psi Initial Serviceability Index : 4.2 Initial International Roughness Index : 75.2 in/mile	Reliability : 95% Modulus of Subgrade Soil : 515 pci (k =FWD/19.4) 28-day Compressive Strength of Concrete : 4,000 psi Mean Modulus of Rupture of Concrete : 650 psi Drainage Coefficient : 0.9 or 1.0 Load Transfer Coefficient : 3.2 Initial Serviceability Index : 4.5 Initial International Roughness Index : 65.4 in/mile
Distribution of Traffic for Five Lanes in One Direction (inner to outer): 0.16, 0.16, 0.16, 0.20, and 0.32 Average Daily Traffic of Outer Lane : 13,712 (T=0 yr), 21,744 (T=30 yr) Total W_{18} of Outer Lane (T=30 yr) : 8,415,520 Width of Pavement : 83.0 ft Distance from the Center of Pavement : 27.0 ft	

Figures 8.5 and 8.6 show the loss of SI and the development of IRI at a reliability of 90 percent for several different flexible pavement systems. The SI after 30 years is increased by 15 percent by adding an inert soil layer 1.5 ft thick beneath flexible pavements with the same SN of 5.06. The pavement system with a stabilized soil layer of 2.5 ft and an inert soil layer of 1.5 ft is expected to perform better than the same pavement without the stabilized layer.

In the design analysis of rigid pavements, the systems with a concrete thickness of 11.5 inches and a stabilized soil layer of 8.0 inches (=0.67 ft) have unacceptable performance as shown in Figs. 8.7 and 8.8. A stabilized soil layer in the pavement system with a concrete thickness of 12 inches has little effect.

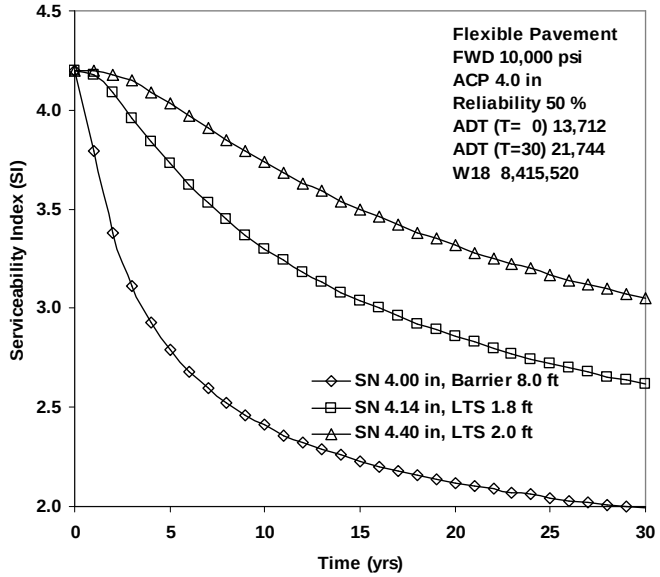

Fig. 8.3. Serviceability Index versus Time for Several Different Pavement Systems with Reliability 50% in the Flexible Pavement, Fort Worth North Loop IH 820, Section A

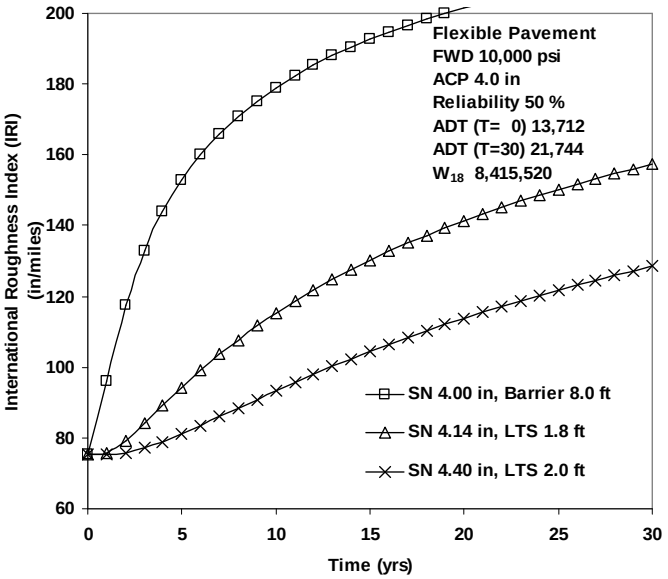

Fig. 8.4. International Roughness Index versus Time for Several Different Pavement Systems with Reliability 50% in the Flexible Pavement, Fort Worth North Loop IH 820, Section A

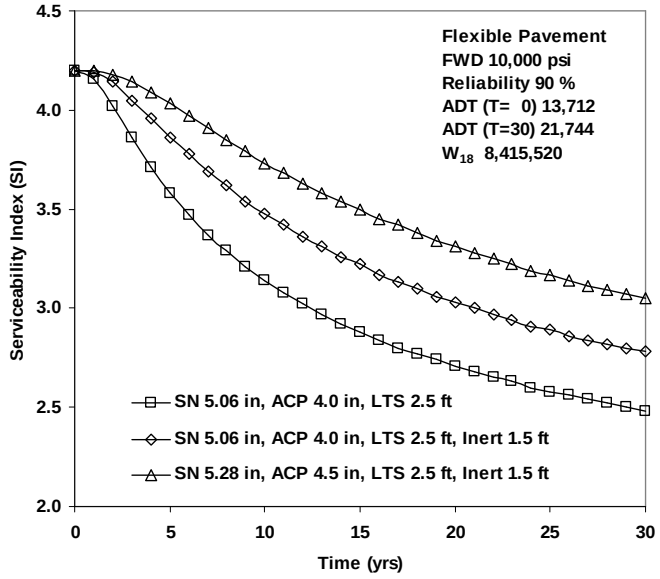

Fig. 8.5. Serviceability Index versus Time for Several Different Pavement Systems with Reliability 90% in the Flexible Pavement, Fort Worth North Loop IH 820, Section A

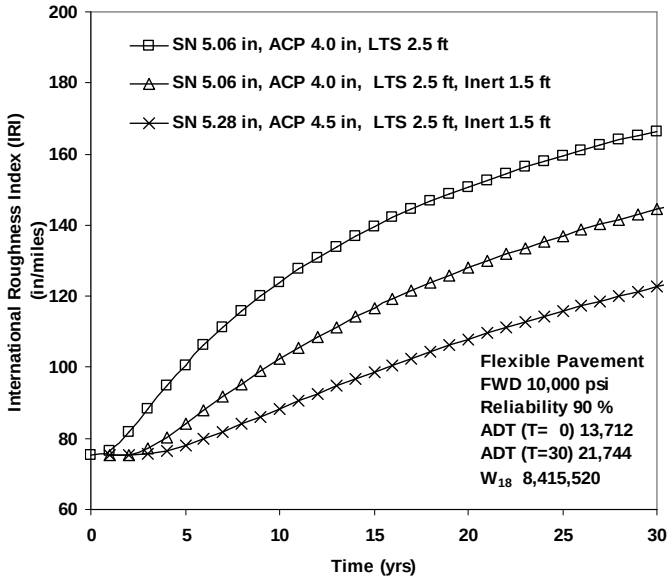

Fig. 8.6. International Roughness Index versus Time for Several Different Pavement Systems with Reliability 90% in the Flexible Pavement, Fort Worth North Loop IH 820, Section A.

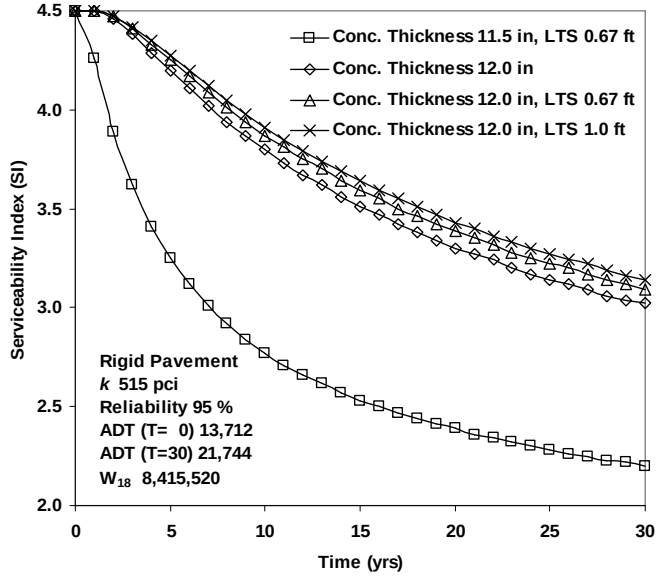

Fig. 8.7. Serviceability Index versus Time for Several Different Pavement Systems with Reliability 95% in the Rigid Pavement, Fort Worth North Loop IH 820, Section A

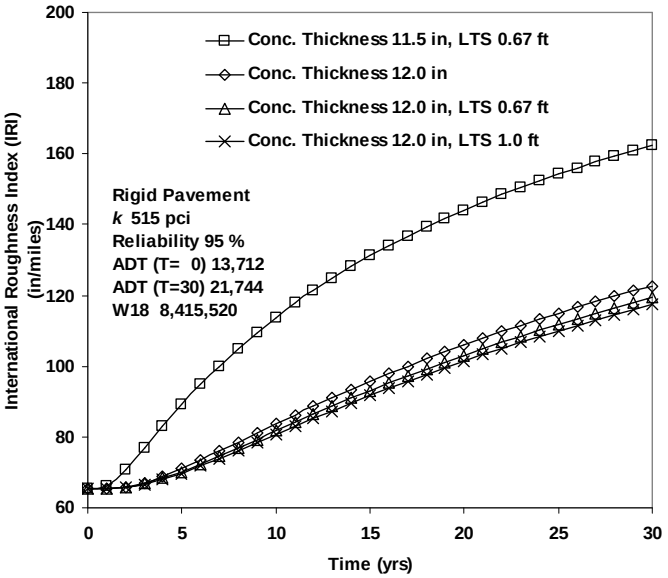

Fig. 8.8. International Roughness Index versus Time for Several Different Pavement Systems with Reliability 95% in the Rigid Pavement, Fort Worth North Loop IH 820, Section A

8.3 Fort Worth North Loop IH 820 Section B

8.3.1 One-Dimensional Model

The suction profile at this location is developed with the equilibrium suction of 3.45 pF; the limiting surface suction of 2.5 pF for wetting and 4.5 pF for drying is illustrated in Fig. 8.9. Figure 8.10 shows that the wet suction caused by the effect of the stabilized layer is controlled by the equilibrium suction. A total vertical movement of 4.68 inches is calculated in the natural soil with no moisture control and it may be reduced to 3.03 inches with a stabilized soil layer of 1.5 ft. The vertical movement in the outer wheel path can be reduced as much as 0.6 inch with a stabilized soil layer (Table 8.5).

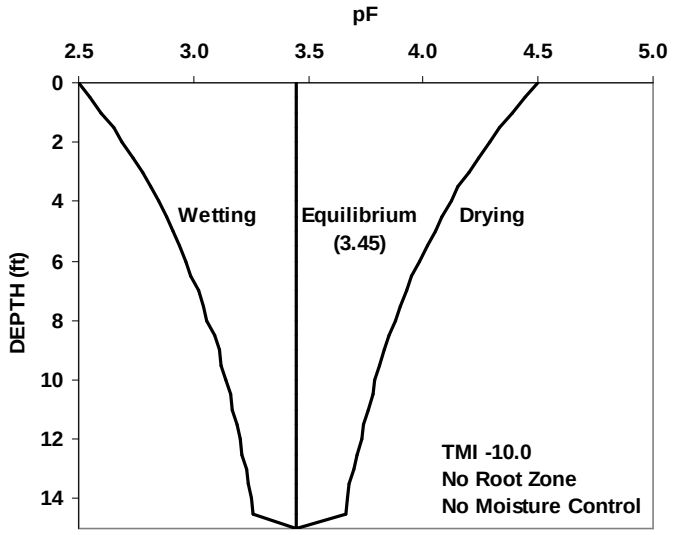

Fig. 8.9. Suction Profile versus Depth for the Case of No Moisture Control, Fort Worth North Loop IH 820, Section B

Table 8.5. Vertical Movement at the Edge of Pavement and at the Outer Wheel Path, Fort Worth North Loop IH 820, Section B

Systems of Pavement	At the Edge of the Pavement (inches)			At the Outer Wheel Path (inches)
	Swelling	Shrinkage	Total	
No moisture control	3.19	1.49	4.68	1.80
Stabilized soil (1.5 ft)	1.83	1.20	3.03	1.21

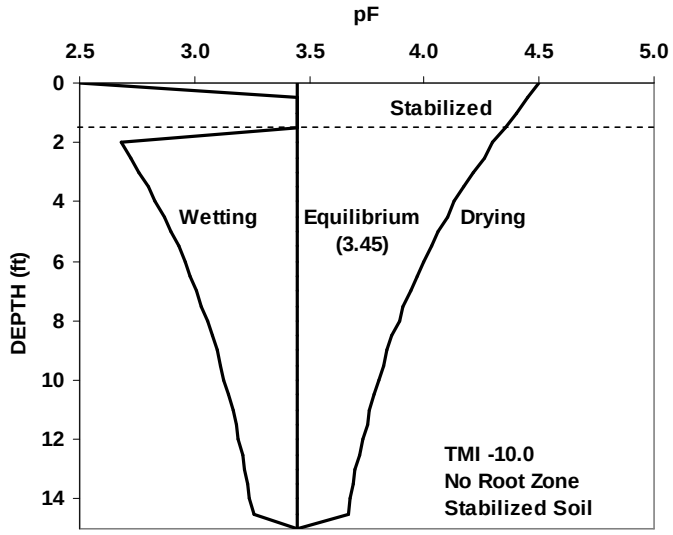

Fig. 8.10. Suction Profile versus Depth with Adding Stabilized Layer, Fort Worth North Loop IH 820, Section B

8.3.2 Performance of Various Pavement Systems

In the design analysis with a reliability of 50 percent, the structural number ranges between 4.40 and 5.06 inches (Figs. 8.11 and 8.12). The results show that the effect of a stabilized soil layer of 0.2 ft greater thickness is greater than that of an inert soil layer of 1.5 ft.

In the design analysis with a reliability of 90 percent, the flexible pavement system with a stabilized soil layer of 2.5 ft and an asphalt thickness of 4.5 inches will provide acceptable performance (Figs. 8.13 and 8.14). The results show that the depth of the stabilized soil layer that is required is over 2.5 ft to control the total vertical movement of 4.68 inches at the edge of the pavement.

For the rigid pavement, at a reliability of 95 percent, the pavement system with a slab thickness of 12.0 inches and a stabilized soil layer of 8.0 inches thick could produce acceptable performance when the minimum SI after 30 years is set at 2.5 (Figs. 8.15 and 8.16). The results show that the 30-year SI can be increased by 17 percent by adding a stabilized soil layer up to 1.0 ft.

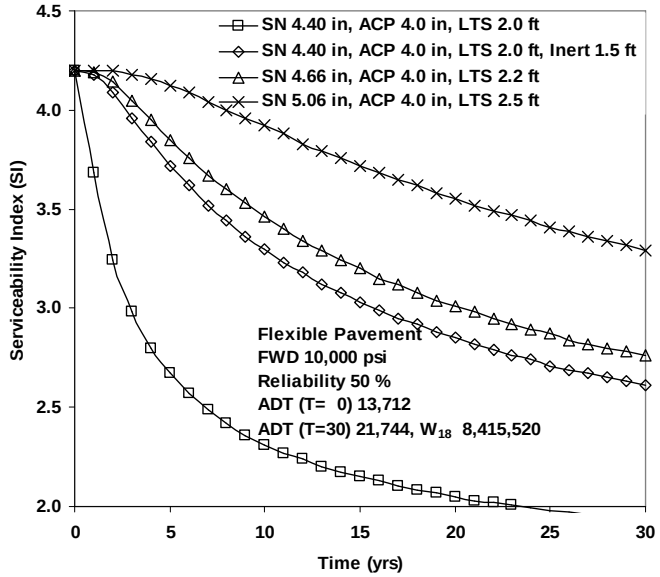

Fig. 8.11. Serviceability Index versus Time for Several Different Pavement Systems with Reliability 50% in the Flexible Pavement, Fort Worth North Loop IH 820, Section B

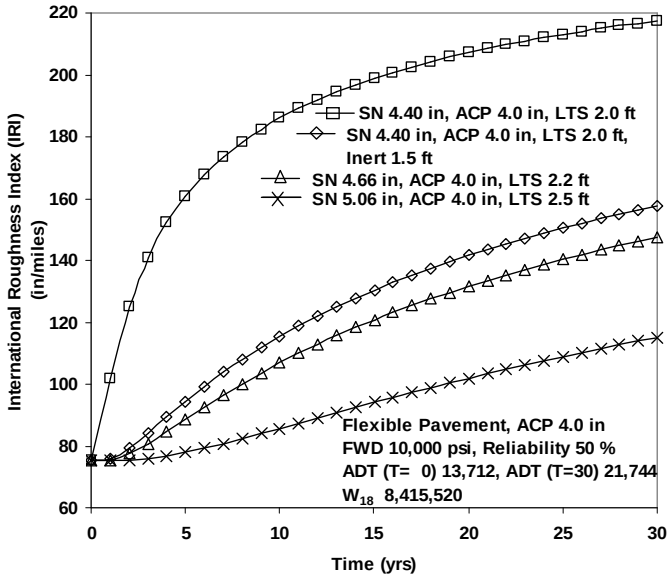

Fig. 8.12. International Roughness Index versus Time for Several Different Pavement Systems with Reliability 50% in the Flexible Pavement, Fort Worth North Loop IH 820, Section B

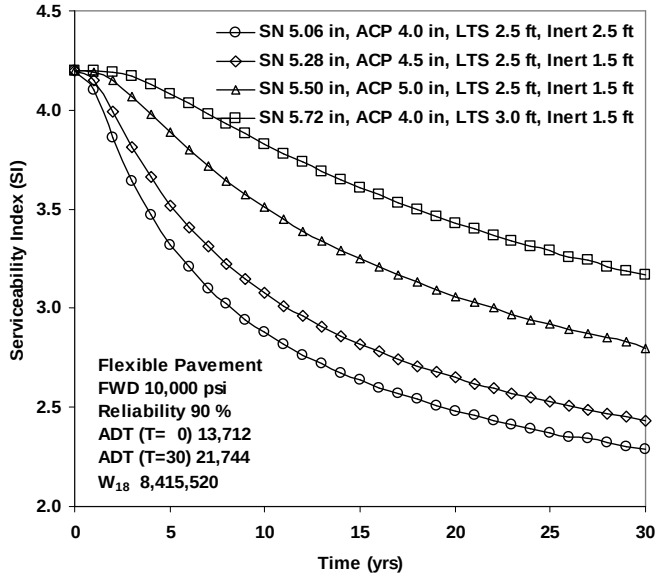

Fig. 8.13. Serviceability Index versus Time for Several Different Pavement Systems with Reliability 90% in the Flexible Pavement, Fort Worth North Loop IH 820, Section B

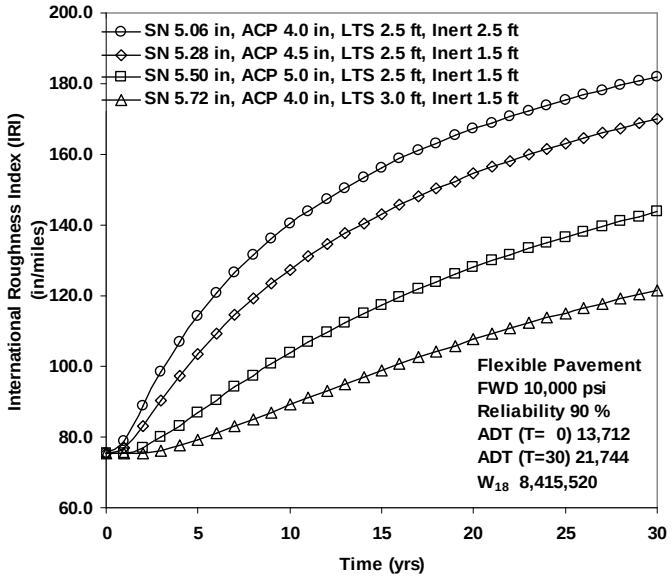

Fig. 8.14. International Roughness Index versus Time for Several Different Pavement Systems with Reliability 90% in the Flexible Pavement, Fort Worth North Loop IH 820, Section B

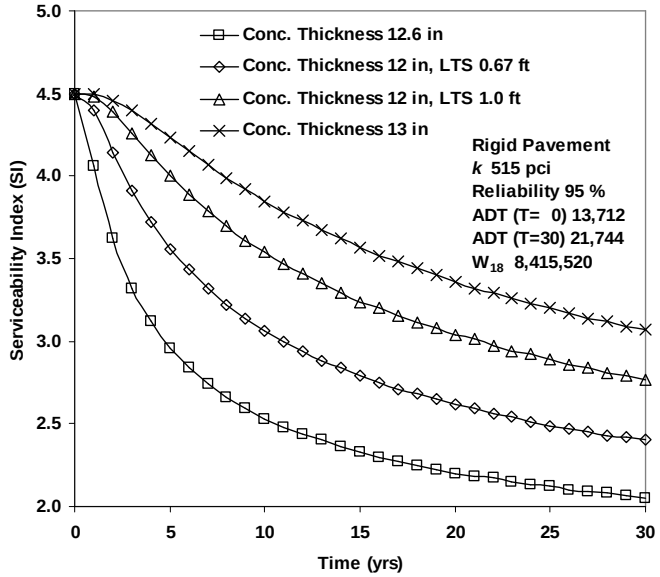

Fig. 8.15. Serviceability Index versus Time for Several Different Pavement Systems with Reliability 95% in the Rigid Pavement, Fort Worth North Loop IH 820, Section B

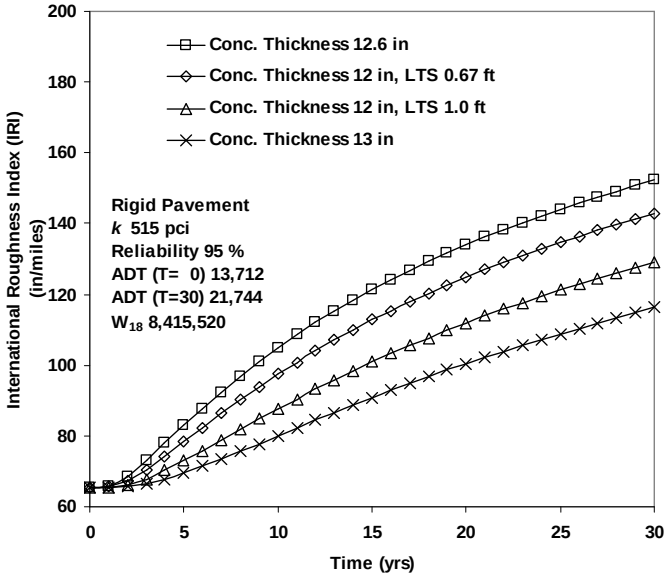

Fig. 8.16. International Roughness Index versus Time for Several Different Pavement Systems with Reliability 95% in the Rigid Pavement, Fort Worth North Loop IH 820, Section B

8.4 Fort Worth North Loop IH 820 Section C

8.4.1 One-Dimensional Model

The suction envelopes for the case of the natural soil with no moisture control and for the case with a stabilized soil layer 1.5 ft thick are shown in Figures 8.17 and 8.18, respectively. The vertical movements at the edge of the pavement and in the outermost wheel path are presented in Table 8.6. The results show that the vertical movement of 1.62 inches in the wheel path can be reduced to 1.13 inches by adding a stabilized soil layer 1.5 ft thick.

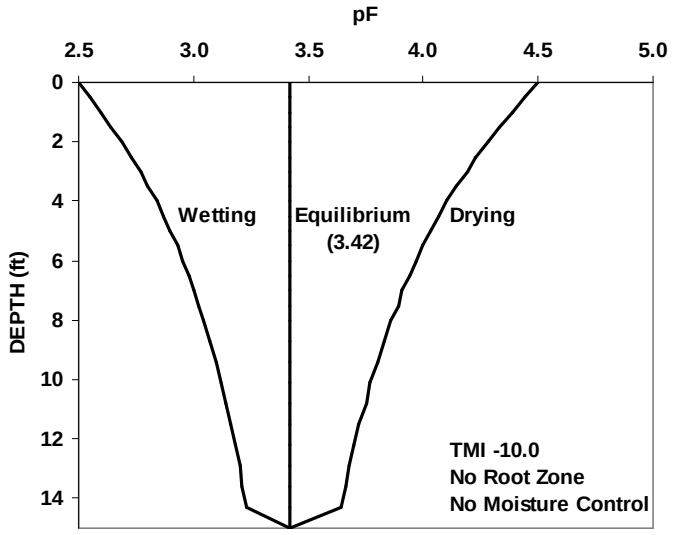

Fig. 8.17. Suction Profile versus Depth for the Case of No Moisture Control, Fort Worth North Loop IH 820, Section C

Table 8.6. Vertical Movement at the Edge of Pavement and at the Outer Wheel Path Fort Worth North Loop IH 820, Section C

Systems of Pavement	At the Edge of the Pavement (inches)			At the Outer Wheel Path (inches)
	Swelling	Shrinkage	Total	
No moisture control	2.58	1.33	3.91	1.62
Stabilized soil (1.5 ft)	1.62	1.11	2.73	1.13

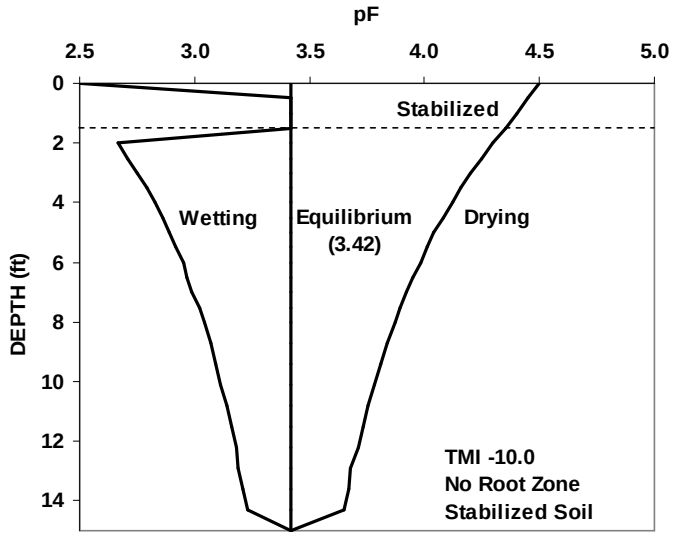

Fig. 8.18. Suction Profile versus Depth with Adding Stabilized Layer, Fort Worth North Loop IH 820, Section C

8.4.2 Performance of Various Pavement Systems

In the design analysis with a reliability of 50 percent for the flexible pavement, the effect of increasing the thickness of the stabilized soil layers is shown in Figures 8.19 and 8.20. The SI predicted at 30 years with stabilized soil layers of 2.0 ft, 2.2 ft, and 2.5 ft are 2.22, 2.88, and 3.35, respectively.

With a reliability of 90 percent, various structural numbers are used to estimate the serviceability and roughness (Figures 8.21 and 8.22). The results show that as the asphalt thickness increases from 4.0 inches to 4.5 inches, in the pavement systems with a stabilized soil layer of 2.5 ft and inert soil layer of 1.5 ft, the 30-year SI increases by 30 percent, from 2.22 to 2.88.

For the rigid pavement with a reliability level of 95 percent, the concrete pavement system with a slab thickness of 12.0 inches and a stabilized soil layer 1.0 ft thick will produce acceptable performance (Figures 8.23 and 8.24).

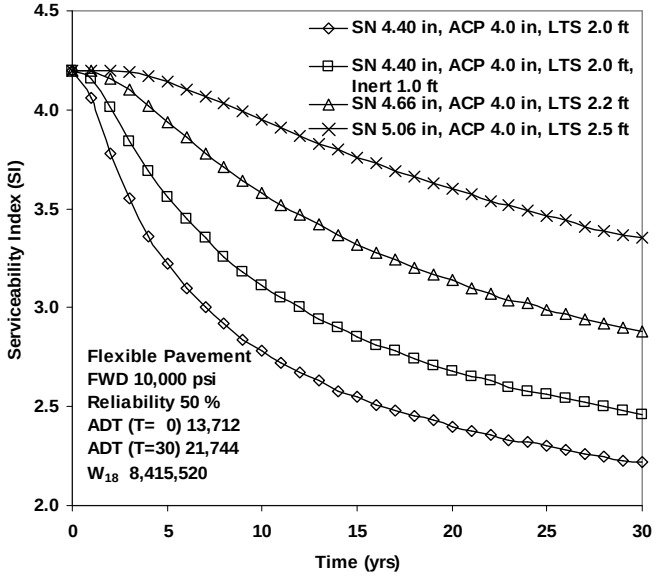

Fig. 8.19. Serviceability Index versus Time for Several Different Pavement Systems with Reliability 50% in the Flexible Pavement, Fort Worth North Loop IH 820, Section C

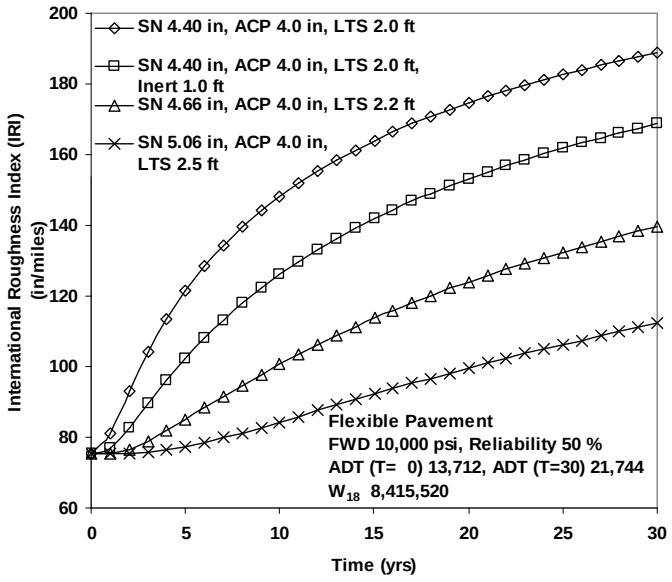

Fig. 8.20. International Roughness Index versus Time for Several Different Pavement Systems with Reliability 50% in the Flexible Pavement, Fort Worth North Loop IH 820, Section C

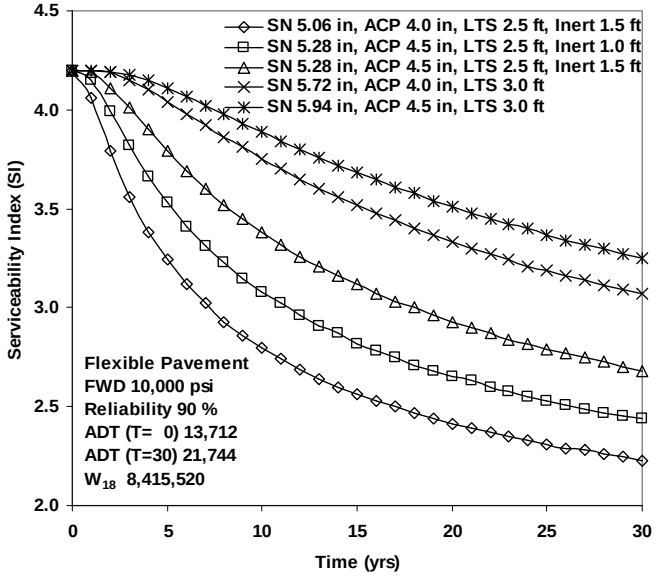

Fig. 8.21. Serviceability Index versus Time for Several Different Pavement Systems with Reliability 90% in the Flexible Pavement, Fort Worth North Loop IH 820, Section C

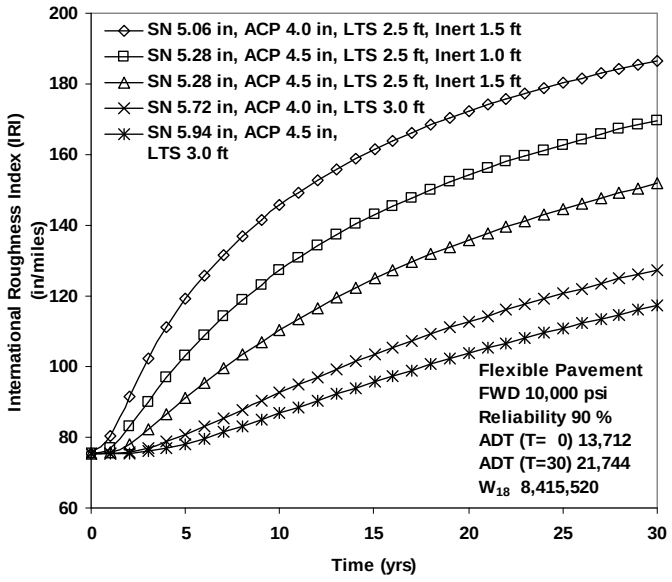

Fig. 8.22. International Roughness Index versus Time for Several Different Pavement Systems with Reliability 90% in the Flexible Pavement, Fort Worth North Loop IH 820, Section C

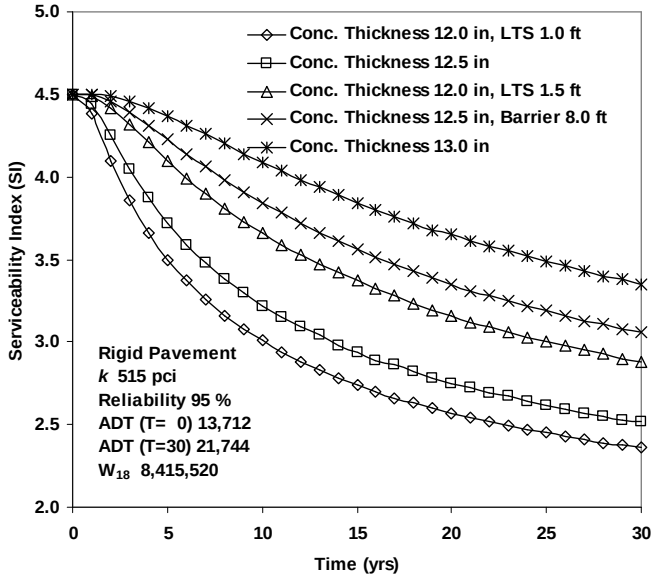

Fig. 8.23. Serviceability Index versus Time for Several Different Pavement Systems with Reliability 95% in the Rigid Pavement, Fort Worth North Loop IH 820, Section C

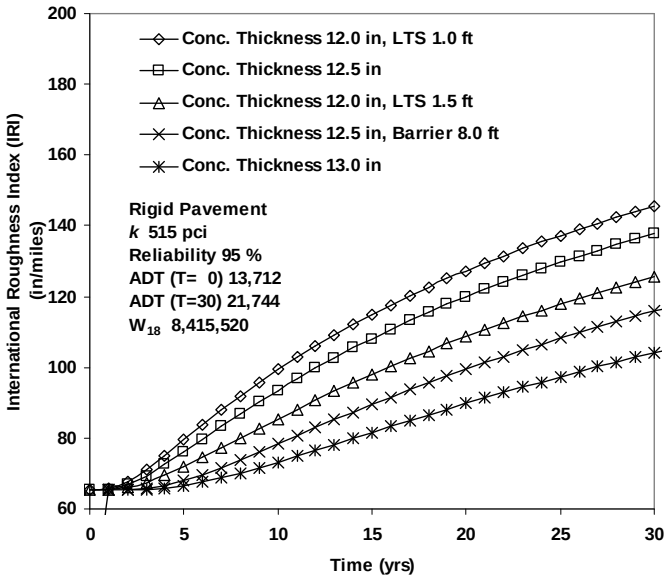

Fig. 8.24. International Roughness Index versus Time for Several Different Pavement Systems with Reliability 95% in the Rigid Pavement, Fort Worth North Loop IH 820, Section C

8.5 Atlanta District US 271

8.5.1 One-Dimensional Model

The suction profile at the edge of the pavement at the site in the Atlanta District along US 271 is generated with a root zone of 11.0 ft (Figures 8.25 and 8.26) based on the root fibers found in the boring log. The total vertical movement of 1.72 inches at the edge of the pavement is the sum of the heave of 0.68 inch and the shrinkage of 1.04 inches (Table 8.7). Generally, the swelling calculated is greater than the shrinkage because of consideration of the effect of lateral confinement within a possible upper crack zone. However, a large change between the equilibrium suction and the suction on the dry side provides more shrinkage movement than swelling movement.

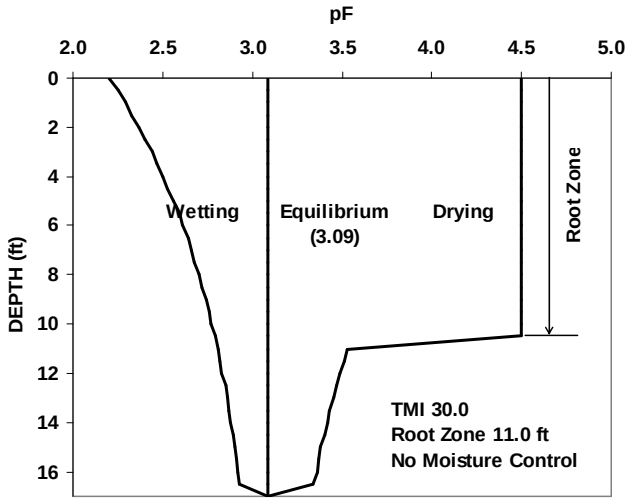

Fig. 8.25. Suction Profile versus Depth for the Case of No Moisture Control, Atlanta US 271

Table 8.7. Vertical Movement at the Edge of Pavement and at the Outer Wheel Path, Atlanta US 271

Systems of Pavement	At the Edge of the Pavement (inches)			At the Outer Wheel Path (inches)
	Swelling	Shrinkage	Total	
No moisture control	0.68	1.04	1.72	1.34
Stabilized soil (1.5 ft)	0.37	1.00	1.37	1.09

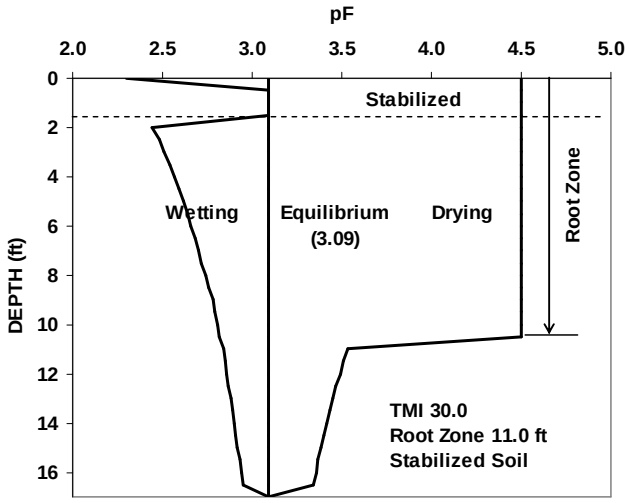

Fig. 8.26. Suction Profile versus Depth with Adding Stabilized Layer, Atlanta US 271

8.5.2 Performance of Various Pavement Systems

Input parameters for the structural properties of pavement and traffic data at the site in the Atlanta District along US 271 are assumed (Table 8.8). There is one lane in one direction with the width of pavement of 44.0 ft including the shoulder. The distance from the center of the pavement to the outer wheel path of interest is 9.0 ft. The average daily traffic and the total 18 kip ESALs in 30 years are assumed as 10,000, 20,000, and 2,500,000, respectively.

Table 8.8. Input Parameters for Structural Properties of Pavement and Traffic Data, Atlanta US 271

Flexible Pavement	Rigid Pavement
Reliability : 50% and 90% Falling Weight Deflectometer Modulus of Subgrade Soil : 10,000 psi Initial Serviceability Index : 4.2 Initial International Roughness Index : 75.2 in/mile	Reliability : 95% Modulus of Subgrade Soil : 515 pci (*k* =FWD/19.4) 28-day Compressive Strength of Concrete : 4,000 psi Mean Modulus of Rupture of Concrete : 650 psi Drainage Coefficient : 1.0 Load Transfer Coefficient : 3.2 Initial Serviceability Index : 4.5 Initial International Roughness Index : 65.4 in/mile
Average Daily Traffic (T= 0 yr) : 10,000 Total W_{18} (T= 30 yr) : 2,500,000 Width of Pavement : 44.0 ft	Average Daily Traffic (T=30 yr) : 20,000 Number of Lanes : 1 Distance from the Center of Pavement : 9.0 ft

In the design analysis with a reliability of 50 percent, the SI and IRI predicted after 30 years with a structural number of 3.72 inches are 2.42 and 173 inch/mile (Figs. 8.27 and 8.28). The results show that the SI after 30 years increases up to 2.84 from 2.42 if a moisture barrier 8.0 ft deep is installed.

Figures 8.29 and 8.30 show the effects of different asphalt layer thicknesses and thicknesses of stabilized soil layers in the design analysis with a reliability of 90 percent. A stabilized soil layer 2.2 ft thick is required in the pavement system with an ACP layer 4.0 inches thick when the SI after 30 years is required to be 2.5.

In the design analysis with a reliability of 95 percent, the various thicknesses of concrete slab, 10.5, 11.0, and 12.0 inches, are applied for the rigid pavement design (Figs. 8.31 and 8.32). Under design conditions with modulus of subgrade reaction of 515 pci, a 28-day compressive strength of 4000 psi, and a mean modulus of rupture of 650 psi, a concrete thickness of 10.5 inches is expected to produce acceptable performance.

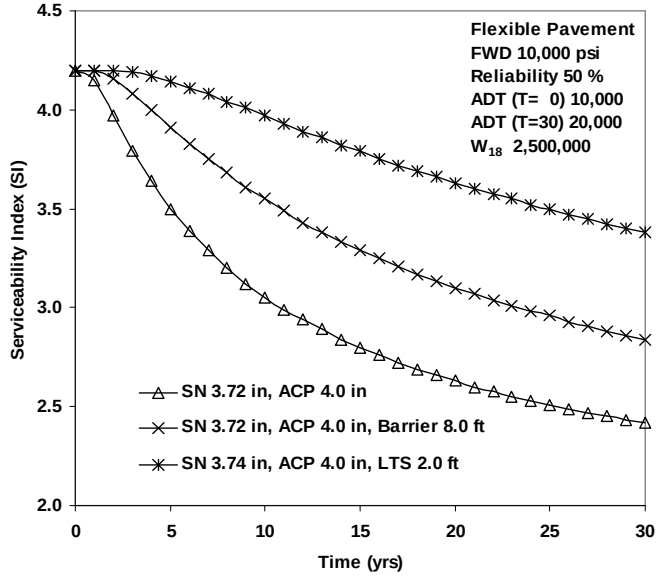

Fig. 8.27. Serviceability Index versus Time for Several Different Pavement Systems with Reliability 50% in the Flexible Pavement, Atlanta US 271

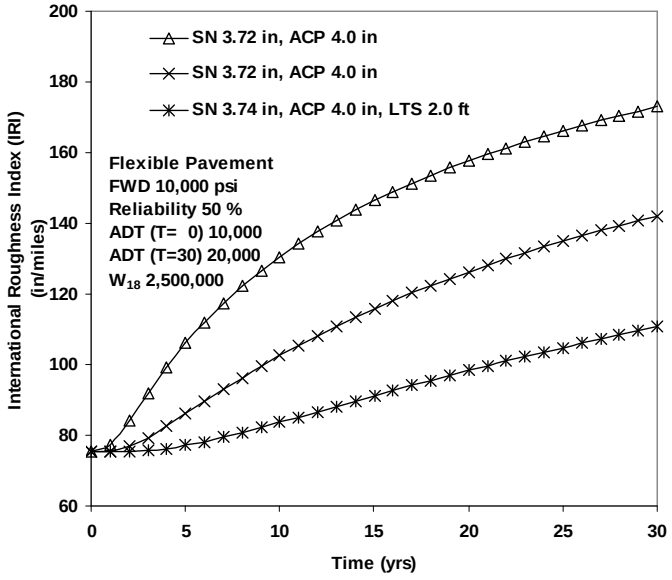

Fig. 8.28. International Roughness Index versus Time for Several Different Pavement Systems with Reliability 50% in the Flexible Pavement, Atlanta US 271

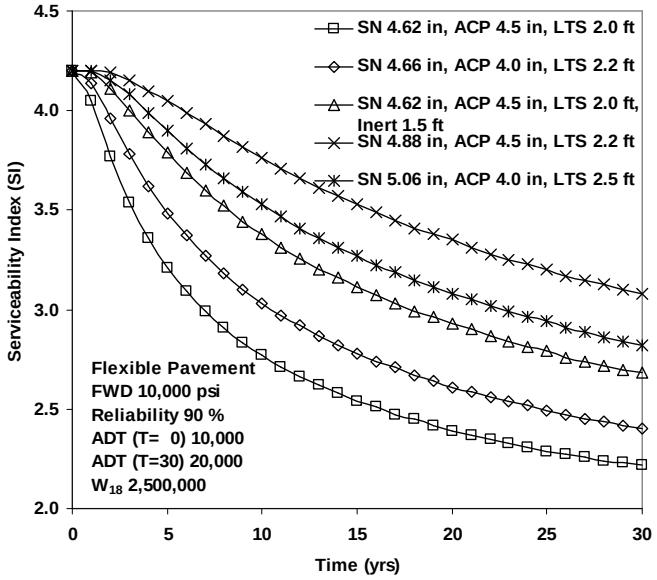

Fig. 8.29. Serviceability Index versus Time for Several Different Pavement Systems with Reliability 90% in the Flexible Pavement, Atlanta US 271

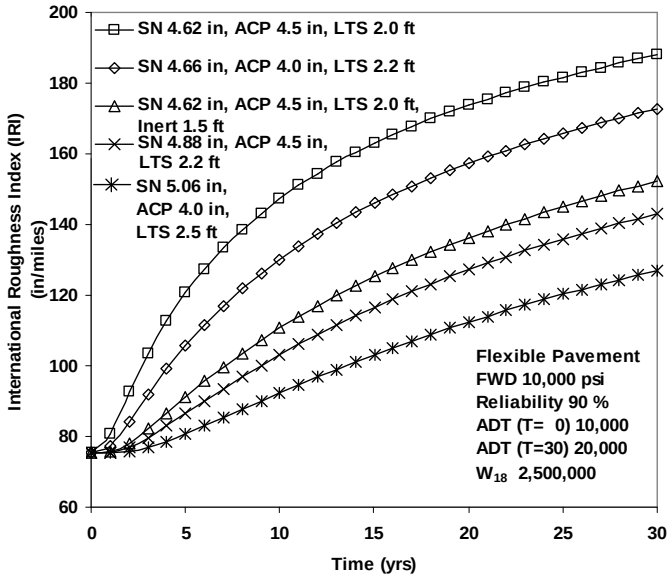

Fig. 8.30. International Roughness Index versus Time for Several Different Pavement Systems Conditions with Reliability 90% in the Flexible Pavement, Atlanta US 271

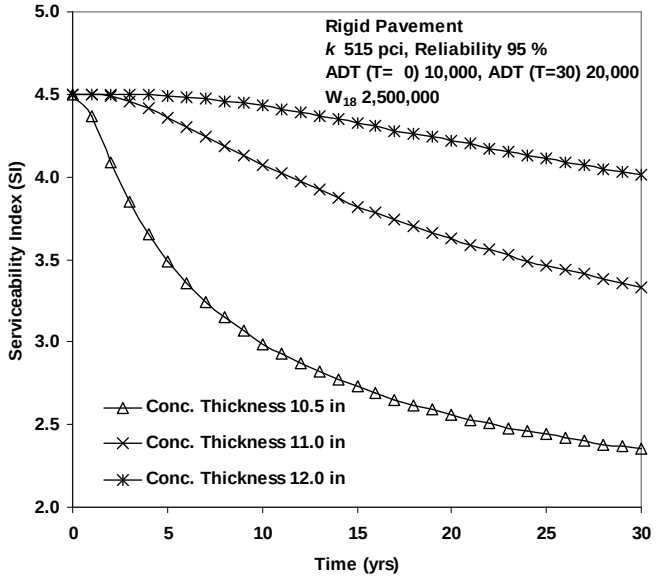

Fig. 8.31. Serviceability Index versus Time for Several Different Pavement Systems with Reliability 95% in the Rigid Pavement, Atlanta US 271

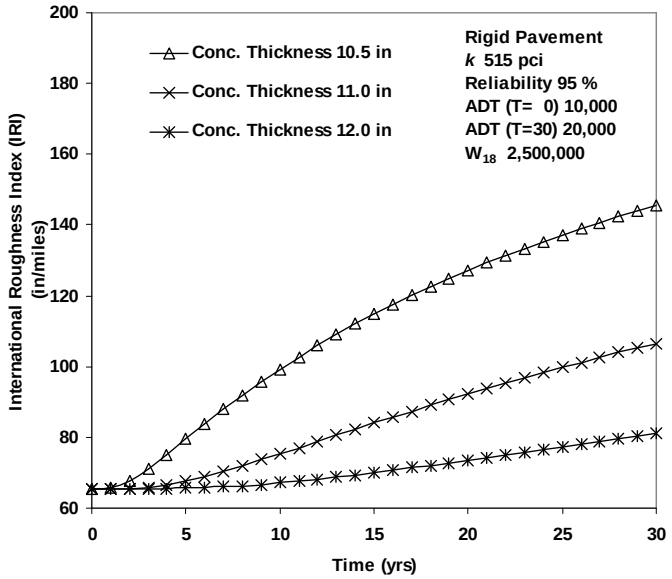

Fig. 8.32. International Roughness Index versus Time for Several Different Pavement Systems with Reliability 95% in the Rigid Pavement, Atlanta US 271

8.6 Austin Loop 1

8.6.1 One-Dimensional Model

The suction profiles with equilibrium suction of 3.45 pF in the natural soil with moisture control and in the stabilized soil layer 1.5 ft thick are illustrated in Figures 8.33 and 8.34, respectively. Based on the data obtained from laboratory tests and three boring logs located in the frontage road, the typical section for the design analysis is constructed (Appendix E). The soil profile for analysis at the main lane is assumed to be the same due to insufficient data. The total vertical movement at the edge of the pavement and the predicted movement in the outer wheel path, which is at a distance of 15.0 ft from the center of the pavement, are 2.46 inches and 1.21 inches (Table 8.9).

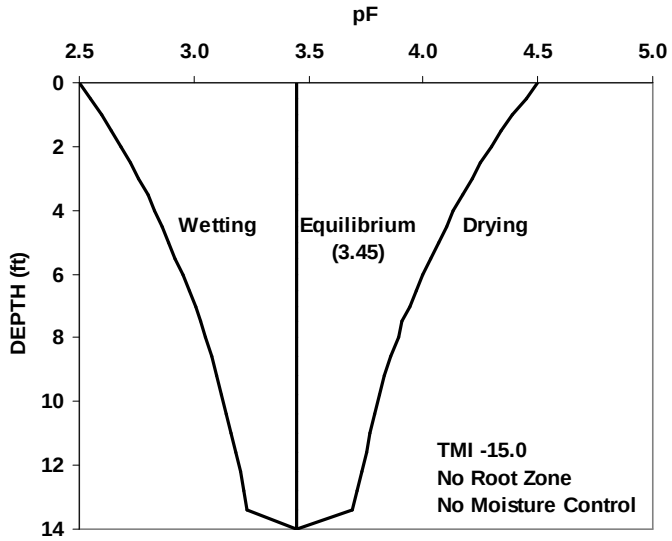

Fig. 8.33. Suction Profile versus Depth for the Case of No Moisture Control, Austin Loop 1

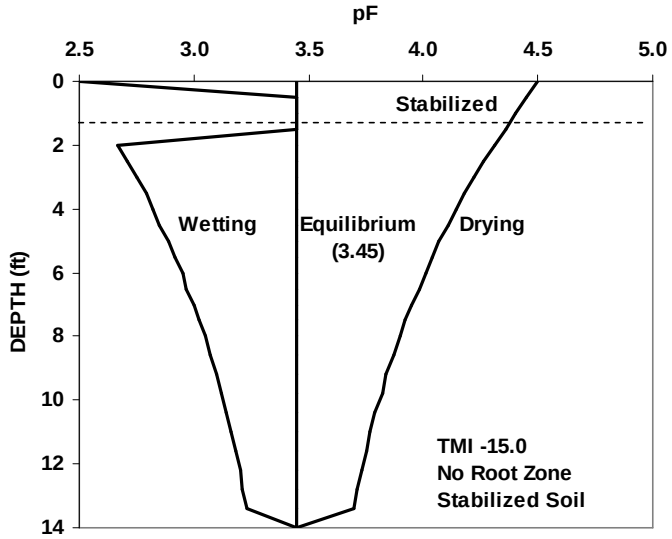

Fig. 8.34. Suction Profile versus Depth with Adding Stabilized Layer, Austin Loop 1

Table 8.9. Vertical Movement at the Edge of Pavement and at the Outer Wheel Path, Austin Loop 1

Systems of Pavement	At the Edge of the Pavement (inches)			At the Outer Wheel Path (inches)
	Swelling	Shrinkage	Total	
No moisture control	2.03	0.98	3.01	2.46
Stabilized soil (1.5 ft)	1.21	0.82	2.03	1.21

8.6.2 Performance of Various Pavement Systems

Table 8.10 shows the input parameters for the pavement and traffic data of the main lanes. The main roadway has four lanes in one direction, and the width of the pavement is 62.0 ft. The input ADT and the total 18-kip ESALs in 30 years are assumed to be the same as the Fort Worth North Loop IH 820 sections with 38 percent of the total traffic being applied to the outer lane.

Table 8.10. Input Parameters for Structural Properties of Pavement and Traffic Data, Austin Loop 1, Main Lane

Flexible Pavement	Rigid Pavement
Reliability : 50% and 90% Falling Weight Deflectometer Modulus of Subgrade Soil : 10,000 psi Initial Serviceability Index : 4.2 Initial International Roughness Index : 75.2 in/mile	Reliability : 95% Modulus of Subgrade Soil : 515 pci (*k* =FWD/19.4) 28-day Compressive Strength of Concrete : 4,000 psi Mean Modulus of Rupture of Concrete : 650 psi Drainage Coefficient : 1.0 Load Transfer Coefficient : 3.2 Initial Serviceability Index : 4.5 Initial International Roughness Index : 65.4 in/mile
Distribution of Traffic for Four Lanes in One Direction (inner to outer): 0.19, 0.19, 0.24, and 0.38 Average Daily Traffic of Outer Lane : 16,283 (T=0 yr), 25,821 (T=30 yr) Total W_{18} of Outer Lane (T=30 yr) : 9,993,430 Width of Pavement : 62.0 ft Distance from the Center of Pavement : 21.0 ft	

In the design analysis with a reliability of 50 percent, three different pavement systems with stabilized soil layers 2.2 to 2.5 ft thick and an inert soil layer 1.0 to 1.5 ft thick are analyzed and the SI and IRI are predicted (Figs. 8.35 to 8.36). The pavement systems with an ACP layer 4.0 inches thick, a stabilized soil layer 2.8 ft thick, and an inert soil layer 1.5 ft thick will produce acceptable performance with a reliability of 90 percent (Figs. 8.37 and 8.38). The results show that the SI after 30 years can be increased by 13 percent by adding an inert soil layer 1.5 ft thick.

For the rigid pavement design analysis with a reliability of 95 percent, we applied several different concrete thicknesses ranging between 12.0 and 13.2 inches, vertical moisture barrier of 10.0 to 13.0 ft, stabilized soil layer 2.0 ft thick, and inert soil layer 1.5 ft thick (Figs. 8.39 and 8.40). The results show that the loss of SI with time or the increase of international roughness index is practically the same in the pavement with concrete thickness of 12.0 inches and a vertical moisture barrier of 13.0 ft and the pavement with a stabilized soil layer of 2.0 ft thick. The SI after 30 years in these pavements is 2.4, which is nearly acceptable performance for that period of time.

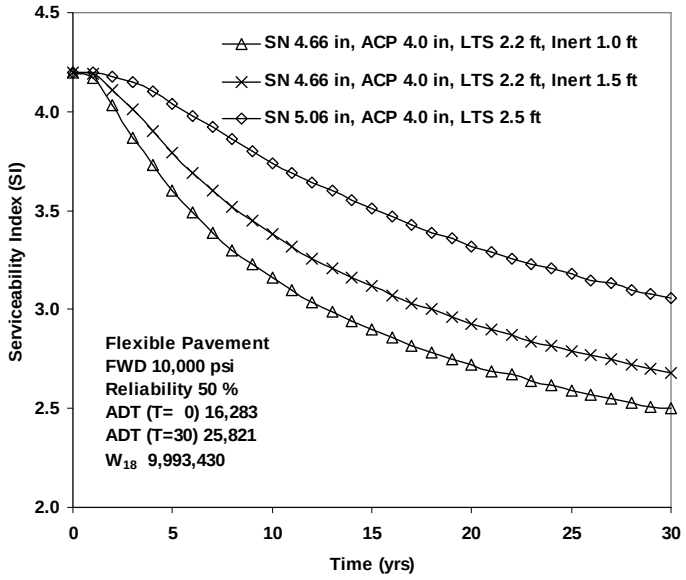

Fig. 8.35. Serviceability Index versus Time for Several Different Pavement Systems with Reliability 50% in the Flexible Pavement, Austin Loop 1, Main Lane

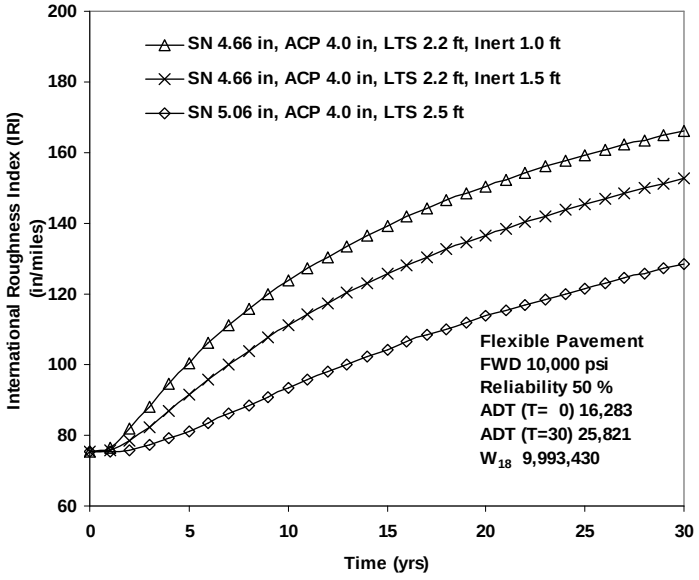

Fig. 8.36. International Roughness Index versus Time for Several Different Pavement Systems with Reliability 50% in the Flexible Pavement, Austin Loop 1, Main Lane

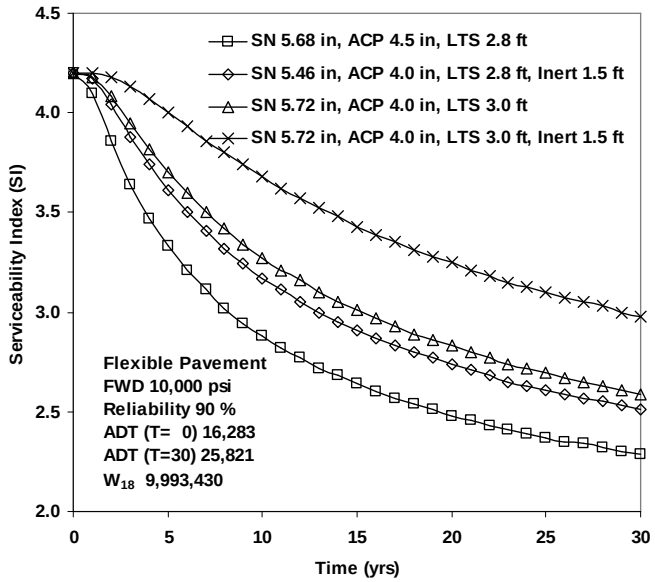

Fig. 8.37. Serviceability Index versus Time for Several Different Pavement Systems with Reliability 90% in the Flexible Pavement, Austin Loop 1, Main Lane

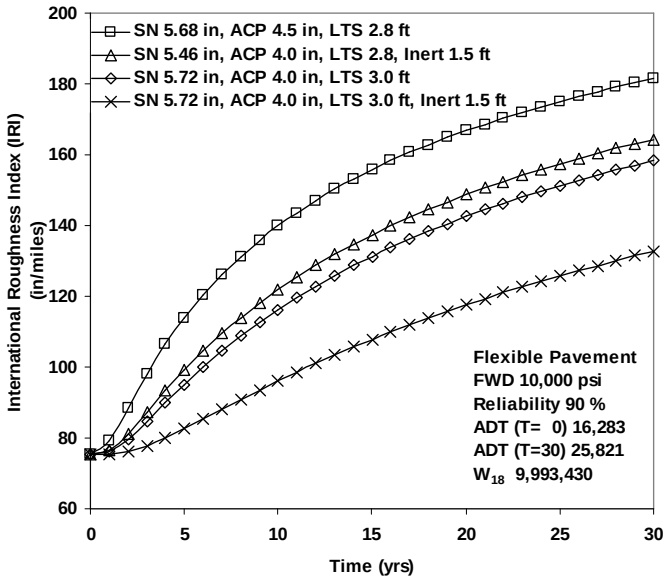

Fig. 8.38. International Roughness Index versus Time for Several Different Pavement Systems with Reliability 90% in the Flexible Pavement, Austin Loop 1, Main Lane

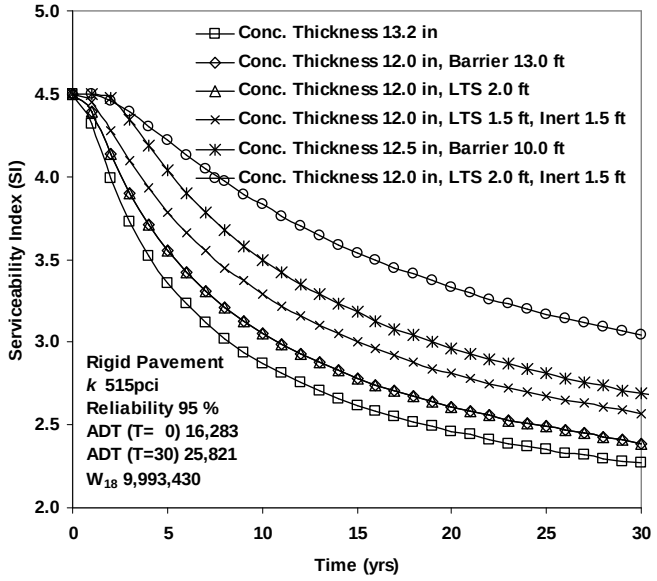

Fig. 8.39. Serviceability Index versus Time for Several Different Pavement Systems with Reliability 95% in the Rigid Pavement, Austin Loop 1, Main Lane

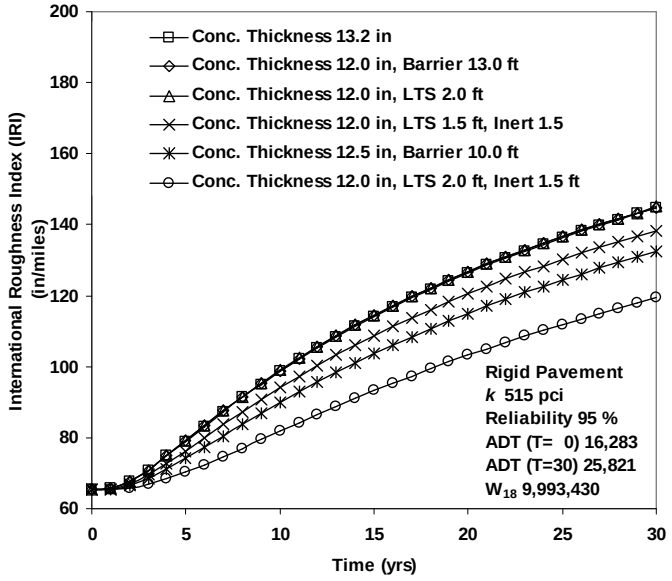

Fig. 8.40. International Roughness Index versus Time for Several Different Pavement Systems with Reliability 95% in the Rigid Pavement, Austin Loop 1, Main Lane

The volume of traffic in the frontage road is assumed to be 10 percent of the main lanes. The frontage road has three lanes in one direction and width of pavement of 50.0 ft. The distance from the center of the pavement to the outer wheel path is estimated as 15.0 ft. The input parameters for the frontage road are presented in Table 8.11.

Table 8.11. Input Parameters for Structural Properties of Pavement and Traffic Data, Austin Loop 1, Frontage Road

Flexible Pavement	Rigid Pavement
Reliability : 50% and 90% Falling Weight Deflectometer Modulus of Subgrade Soil : 10,000 psi Initial Serviceability Index : 4.2 Initial International Roughness Index : 75.2 in/mile	Reliability : 95% Modulus of Subgrade Soil : 515 pci (*k* =FWD/19.4) 28-day Compressive Strength of Concrete : 4,000 psi Mean Modulus of Rupture of Concrete : 650 psi Drainage Coefficient : 0.9 Load Transfer Coefficient : 3.2 Initial Serviceability Index : 4.5 Initial International Roughness Index : 65.4 in/mile
Distribution of Traffic for Three Lanes in One Direction (inner to outer): 0.20, 0.33, and 0.47 Average Daily Traffic of Outer Lane : 4,028 (T=0 yr), 6,837 (T=30 yr) Total W_{18} of Outer Lane (T=30 yr) : 2,472,059 Width of Pavement : 50.0 ft Distance from the Center of Pavement : 15.0 ft	

In order to predict the SI and IRI for the frontage road, several pavement systems are applied with a reliability of 50 percent (Figs 8.41 and 8.42). In the design analysis with a reliability of 90 percent for the frontage road, stabilized soil layers 2.0 to 2.5 ft thick and inert soil layers 1.5 to 2.5 ft thick are used to design the flexible pavement (Figs. 8.43 and 8.44). The pavement system with an asphalt thickness of 4.0 inches, a stabilized soil layer 2.0 ft thick, and an inert soil layer 2.5 ft thick will produce acceptable performance. Three different concrete thicknesses, 11.0, 11.5, and 12.0 inches, are used to estimate the loss of SI and the development of IRI with time (Figs. 8.45 and 8.46).

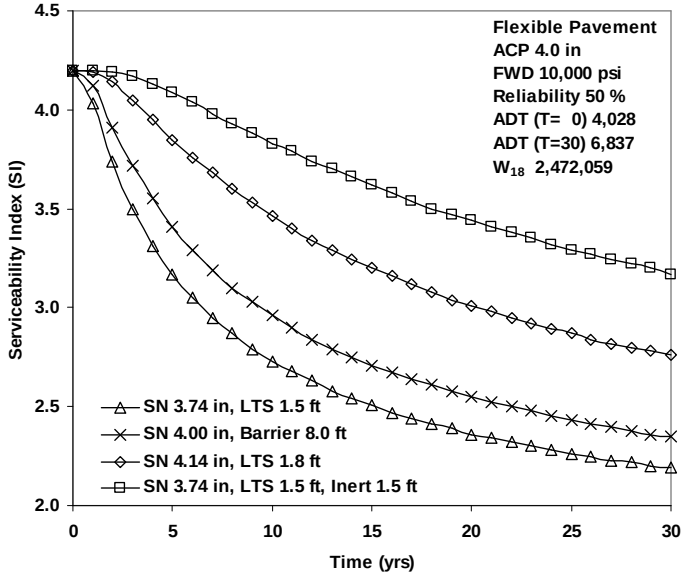

Fig. 8.41. Serviceability Index versus Time for Several Different Pavement Systems with Reliability 50% in the Flexible Pavement, Austin Loop 1, Frontage Road

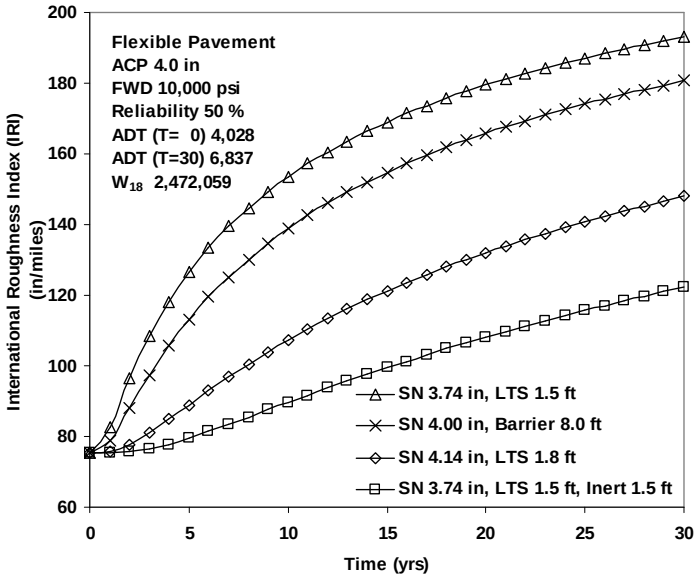

Fig. 8.42. International Roughness Index versus Time for Several Different Pavement Systems with Reliability 50% in the Flexible Pavement, Austin Loop 1, Frontage Road

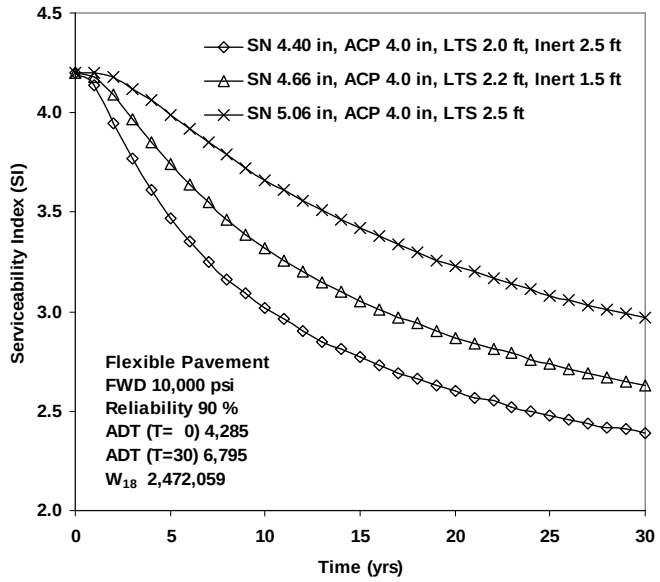

Fig. 8.43. Serviceability Index versus Time for Several Different Pavement Systems with Reliability 90% in the Flexible Pavement, Austin Loop 1, Frontage Road

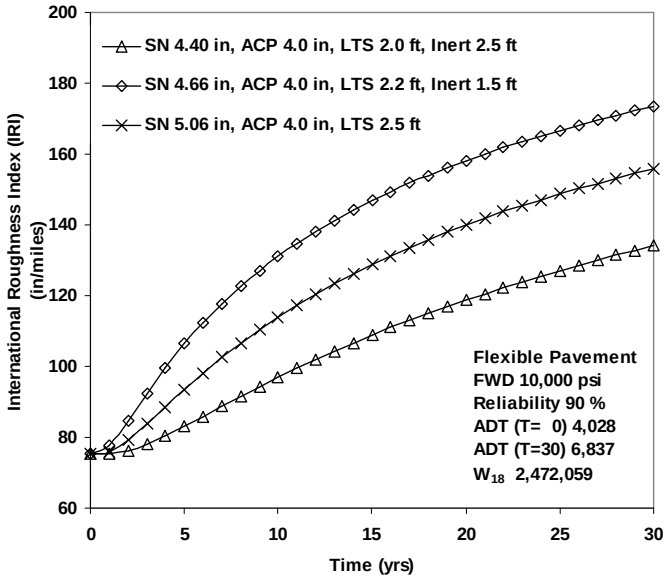

Fig. 8.44. International Roughness Index versus Time for Several Different Pavement Systems with Reliability 90% in the Flexible Pavement, Austin Loop 1, Frontage Road

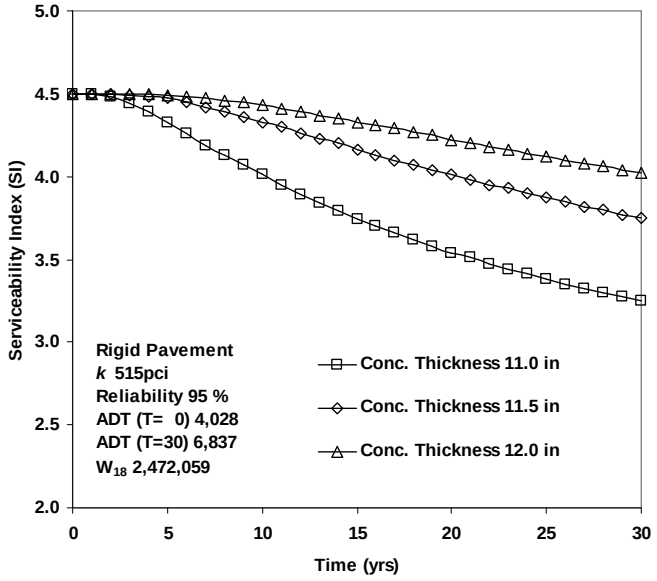

Fig. 8.45. Serviceability Index versus Time for Several Different Pavement Systems with Reliability 95% in the Rigid Pavement, Austin Loop 1, Frontage Road

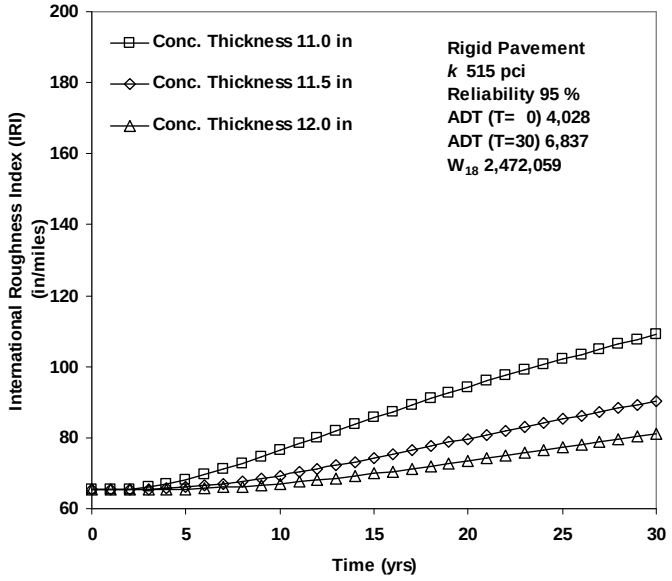

Fig. 8.46. International Roughness Index versus Time for Several Different Pavement Systems with Reliability 95% in the Rigid Pavement, Austin Loop 1, Frontage Road

8.7 Transverse Distribution of Vertical Movements

Fort Worth North Loop Interstate 820 case study results for extrapolating computed one-dimensional movements to two-dimensional roadway profiles are shown in Figure 8.47. Each of the three study sections has an upper (heave) and lower (shrink) bound of movements associated with wet and dry seasons, respectively. The three results correspond to Sections A through C on Fort Worth North Loop Interstate 820. Each pavement section has a width of 83 ft. Section A, comprising an embankment section, is unusually wet, which explains the low predicted heave profile. Section B, also an embankment, has what might be considered more normal moisture conditions for this region. Section C comprises an embankment on the north side of the roadway and is at grade on the South side. It too is at a higher moisture level than normally expected for the Fort Worth climatic zone.

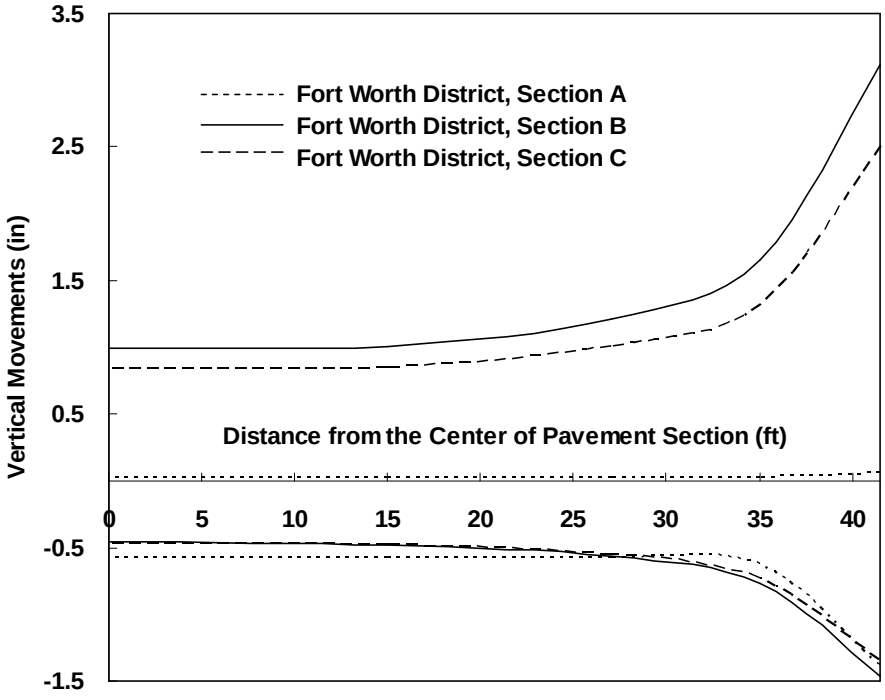

Fig. 8.47. Transverse Distributions of Vertical Movements

Figure 8.47 shows that both swelling and shrinking expected without treatments increase from the center of pavement to the edge of pavement. The swelling that is expected in Cross Section A is very small because of the moist condition of the embankment, but the expected shrinkage is very large. The swelling expected in the Cross Section B is a little larger than that in the Cross Section C and the shrinkage expected in the Cross Section A, B and C is similar. The average swelling and shrinking expected, in Cross Section A and B, beneath the outer wheel path which is located at the distance of 27 ft from the center of pavement are 1.1 inches and 0.56 inches, respectively.

CHAPTER IX
COMPARISON OF PVR DESIGN CRITERIA WITH CASE STUDY RESULTS

9.1 Introduction

This research evaluates the existing Texas Department of Transportation (TxDOT) procedure Tex-124-E, "Method for Determining the Potential Vertical Rise, PVR" (TxDOT 1999). The research also highlights the comprehensive framework developed at Texas A&M University (TAMU) for predicting the roughness that is developed in a pavement over a period of time due to swelling and shrinkage of expansive clays. Texas Transportation Institute (TTI) Research Report 0-1165-2F entitled "Effectiveness of Controlling Pavement Roughness Due to Expansive Clays with Vertical Moisture Barriers" (Jayatilaka et al. 1993) provides much of the groundwork for the TAMU approach. Using the methodology developed, this Chapter compares the predicted values of the vertical movements, which are calculated using both the existing TxDOT method and the method developed by the studies conducted at Texas A&M.

The Texas Department of Transportation has been a leader in the study and implementation of practical methods of anticipating the roughness that will develop in pavement surfaces due to the change of moisture in the expansive clay subgrade. In a landmark paper that was written by Chester McDowell and published in the Proceedings of the Highway Research Board (HRB) in 1956, a method was described by which the total swelling movement of expansive clay profile could be predicted. TxDOT took the results of this paper and built the standard specification Tex-124-E with it, adding several refinements along the way to the present version.

In the original report that was published in 1956, McDowell suggested that these movements could be reduced by moisture control, pre-wetting, or by removing and replacing some of the expansive soils near the surface of the subgrade. The paper and its discussions appeared on pages 754 to 772 of that year's HRB Proceedings. In putting together this method, McDowell made several assumptions, all of which were necessary

in order for the method to be implemented in the practical day-to-day operations of the Department. In the text of the paper, he acknowledged some of the limitations of his method. For example, he noted, “vertical volume change of soils in deep cuts and under certain types of structures will be greater than that shown,” and he later noted that “... cuts in marls and clays usually heave more than other sections because of their low moisture contents.” As a first attempt at putting some rational order into the process of engineered design of pavements on expansive clay, it was recognized by those who discussed the paper as being a very good synthesis of what was known at the time. Most practical engineers realize that McDowell intended that the Potential Vertical Rise (PVR) procedure should be used as an index of the potential activity of a pavement subgrade and they use it that way.

During the last two decades, significant advances have been made in the method for predicting the swelling and shrinkage of expansive soil. Lytton (1977) presented a method of estimating the volume change with depth based upon the initial and final suction values, the mean principal stress at all depths, and logarithmic compression coefficients of the soil for changes of both suction and mechanical pressure. Mitchell and Avalle (1984) used an approach that had originated in Australia, which used a logarithmic compression coefficient and the change of the logarithm of suction at all depths to estimate the surface movement of the expansive soil. This works only in shallow depths where the overburden pressures do not suppress much of the volume change due to the change of suction. Gay (1994) and Jayatilaka (1999) both used Lytton’s approach in predicting the roughness of pavements on expansive clay. Finally, Lytton et al. (2005) summarized all of the developments and presented a complete method of predicting heave and shrinkage.

9.2 Overview of Existing PVR Procedure

The current PVR method is based upon the work of McDowell (1956) in which he made five assumptions. A proper re-evaluation of the PVR method requires revisiting and reviewing each of the five assumptions.

A summary of these assumptions is listed below.

1. Soil at all depths has access to water in capillary moisture conditions (pp. 755, 756, 764).
2. Vertical swelling strain is one-third of the volume change at all depths (p. 755, Fig. 1).
3. Remolded and compacted soils adequately represent soils in the field (p. 757).
4. PVR of 0.5 inch produces unsatisfactory riding quality (p. 760).
5. Volume change can be predicted by use of the plasticity index alone (p. 763, Fig. 11).

Making use of these assumptions, McDowell worked out the Potential Vertical Rise of several hypothetical soil profiles with different amounts of volumetric swell. The results of these calculations are tabulated in Table 9.1 and illustrate the effect of the combination of the five assumptions listed above.

Table 9.1. PVR of Sites with 18-inch Thick Pavement

Page	Table	% Volumetric Swell	Depth of Swell (ft)	PVR (in)
758	2	35.0	82.1	24.09
759	3	25.0	58.6	11.77
759	4	22.5	52.8	9.67
760	5	15.0	33.9	3.71
760	6	7.5	16.7	0.77

(Figures in the above table were extracted from McDowell's 1956 HRB paper on the pages and tables cited.)

The above assumptions lead to the conclusion that by following this procedure, soil can be expected to swell to a depth greater than 82 ft, even allowing for the suppression of the swell by the effect of the overburden pressure and the weight of the

pavement. This is a direct result of Assumption 1, that soil at all depths has access to water under capillary moisture conditions. However, soil at all depths does not have access to moisture in the capillary condition. In a consulting report (Mitchell 1979) and a paper in the 4th International Conference on Expansive Clays (Mitchell 1980), Mitchell showed how the diffusion coefficient, alpha, can be measured using undisturbed shelby tube samples and how this value can be used to predict the transient changes of suction beneath a covered area like a pavement or a foundation. The determination of the alpha diffusion coefficient permits an estimate of the rate at which water will move into the soil both vertically and horizontally. It is also used to estimate the depth of the moisture active zone. The relations between the horizontal extent of the moisture zone and the alpha-value are given in the TTI Report 0-1165-2F (Jayatilaka, 1993) on page 58 and will not be repeated here.

In Assumption 2, vertical swelling strain is assumed to be one-third of the volume change at all depths. This assumption is unrealistic, especially at greater depths, due to high confining pressure. At these depths, the vertical swelling strain can be as high as the volumetric strain. If it were not for Assumption 2, the PVR figures would be three times higher than those in the table above. This leads to questions of the effects of Assumptions 3, 4, and 5.

Assumption 3 is that remolded and compacted soils adequately represent soils in the field. However, from actual observation it is found that the volume change characteristics of undisturbed soils are distinctively different than the remolded and compacted soils used by McDowell in developing his method. As mentioned in Chapter III, there is a very large database of such characteristics for over 100,000 soil samples from all over the United States that was developed over the last three decades by the U.S. Department of Agriculture's (USDA) Natural Resources Conservation Service. A set of volume change coefficient charts was developed from this database and published in a paper by Covar and Lytton in ASCE Geotechnical Special Publication No. 115 (Covar and Lytton 2001), which is a written record of the presentation that was made at the Houston National ASCE Convention in October 2001. The data are for undisturbed

clods of soil taken from the ground and tested in their natural state with all of the cracks, roots, and wormholes as occur in the field. It turns out that accurate estimates of the volume change coefficient requires measurements of the liquid limit (LL), the plasticity index (PI), the percent of soil particles passing the #200 sieve, and the percentage of soil particles finer than 2 microns. All of these are standard geotechnical tests. In the process of constructing these charts, the work of Covar and Lytton confirmed the earlier work of Professor Casagrande (1948), who located where the expansive minerals would fall on the plasticity chart. Some of these minerals have PI less than 15, namely chlorite and halloysite. This finding implies that Assumption 5 is inadequate.

Concerning Assumption 4, the multiple year study of the roughness of pavements on expansive clay subgrade that researchers conducted at the Texas Transportation Institute showed that the sum of the *shrinking* and *swelling* movements at a point beneath a pavement surface is related not to the pavement roughness, but to the *rate* at which roughness develops. Because this conclusion is based upon monitoring pavements all over Texas for periods ranging from 3 to 15 years, the result is not in doubt. These results were reported in TTI Research Report 0-1165-2F (Jayatilaka, Gay, Lytton, and Wray) titled “Effectiveness of Controlling Pavement Roughness Due to Expansive Clays with Vertical Moisture Barriers” (Jayatilaka 1999) as discussed in Chapter VII. In the process, the researchers developed a way to both measure and predict the maximum bump height on the pavement that was based on the thousands of pavement profile data points that were collected and analyzed in the monitoring process. Both the measured and predicted bump height for serviceability indexes between 2.5 and 4.0 were in the range between 0.5 and 1.0 inch (12 to 25 mm) for all pavements. A bump is not the total movement, such as PVR, but instead is a *differential* movement and it is this movement that causes pavement roughness.

In reviewing the assumptions that underlie the PVR method, it is seen that Assumptions 1 and 2, which form the core of the PVR method of Tex-124-E, are not realistic as they are not based on sound analytical principal. Furthermore, Assumptions 3, 4, and 5 cannot be supported by subsequent findings on actual Texas pavements and

on the soils of the United States. Therefore, it is suggested that Tex-124-E "Method for Determining the Potential Vertical Rise, PVR" (TxDOT 1999) be replaced by a more robust method based on sound rational principal such as the one developed at Texas A&M University.

9.3 Comparative Case Study

The potential vertical rise computed for a given site is currently used in pavement design to determine what depth of the natural soil must be removed and replaced with a more inert soil or modified in place in order to reduce the computed PVR to 1 inch, 1.5 inches, or 2 inches dependent upon the highway facility (1.0 inch for IH/US, 1.5 inches for SHs, and 2.0 inches for FMs). In this chapter, the amount of movement that is predicted both at the edge of the pavement and beneath the outer wheel path by the method described in Chapter VII is compared to the calculated PVR for the same cases. Contrary to the way the PVR is calculated, the predicted vertical movement is the sum of both shrinkage and swelling movements. The purpose of the comparison is to determine whether the previously used PVR criterion is conservative when compared to the movements that are calculated by the methods of this report. A secondary purpose is to illustrate with the case studies the design advantages that are provided by having an estimate of both shrinking and swelling movements.

The new method of predicting the vertical movement uses this information to predict the accumulation of pavement roughness with time and traffic. It was discovered in the course of the analysis of the field monitoring data that were collected for a period of over 20 years in some cases that the total movement in the subgrade beneath a given wheel path governs the *rate of increase* of roughness rather than the level of roughness itself. Roughness is predicted as a decrease of present serviceability index (PSI) as well as an increase of the international roughness index (IRI). The computed results are found in Tables 9.2 through 9.8. The calculation of PVR is summarized in Appendix. The case studies are discussed one cross section at a time for pavements with no treatment of the expansive subgrade soil (Tables 9.2 through 9.4). Then the reduced movements,

calculated both by the new method and by the PVR method, due to treatments applied to the subgrade are compared. The pavement treatments that are used for the comparisons were shown in Chapter VIII to provide a minimum acceptable predicted performance over 30 years with 90 percent reliability on flexible pavements and 95 percent reliability on rigid pavements (Tables 9.6 through 9.8).

9.3.1 Fort Worth North Loop IH 820 Case Study

Three cross sections were used as separate case studies along the IH 820 Loop north of Fort Worth. Cross Sections A and B were embankment sections with Cross Section A being unusually wet and Cross Section B being closer to the normally expected moisture level. Cross Section C had an embankment on the north side of the roadway and was at grade on the south side. It, too, was at a more normally expected moisture level for the Fort Worth climatic zone. Table 9.2 shows the calculated vertical movements for each of the cross sections as they were predicted by the new method and also by the PVR method. The predictions were made at two locations: at the edge of the pavement where the soil movement is not affected by the weight of the pavement and beneath the outer wheel path where the weight of the pavement will restrain the vertical movement to some extent. The new method predicts both a swelling and a shrinkage vertical movement and a total movement, which is the sum of the two. The swelling vertical movement is the figure to be compared to the PVR.

Table 9.2. Subgrade Movements Compared with PVR (Tex-124-E) for the Pavement with No Treatment, Fort Worth Distric, IH 820

Case Study Location	Pavement Location	Swelling (inches)	Shrinkage (inches)	Total (inches)	PVR (inches)
Cross Section A	Edge	0.07	1.39	1.46	2.22
	Outer Wheel Path	0.03	0.58	0.61	1.87
Cross Section B	Edge	3.19	1.49	4.68	3.07
	Outer Wheel Path	1.23	0.57	1.80	2.39
Cross Section C	Edge	2.58	1.33	3.91	2.38
	Outer Wheel Path	1.07	0.55	1.62	1.70

The swelling that is expected in Cross Section A is very small because of the moist condition of the embankment, but the expected shrinkage is very large. The new method shows that not much additional swelling is to be expected in Cross Section A, but a large amount of shrinkage is expected. The shrinkage figure is important because it is an indicator of future longitudinal shrinkage cracking along the edge of the pavement. The PVR for the same section is roughly in the same range as the total movement predicted by the new method, but it is considerably larger than the swelling that is predicted. The movement beneath the outer wheel path reflects the effect of the weight of the pavement in the case of the PVR calculation but also indicates the added effect of the diffusion of moisture from the edge of the pavement in the case of the new method predictions. The new method expects to have less movement beneath the outer wheel path than does the PVR method.

In Cross Section B, the swelling expected at the edge of the pavement using the new method is fairly close to the calculated PVR. However, the total movement is larger than the PVR because it includes the expected shrinkage. Once more, the movement beneath the outer wheel path predicted by the new method is less than is expected by the PVR method.

In Cross Section C, the new method predicts a swelling that is roughly equal to that of the PVR at the edge of the pavement. The addition of the shrinkage makes the total movement expected by the new method considerably larger than the PVR. The weight of the pavement makes the PVR about equal to the new method total movement beneath the outer wheel path.

In all three cross sections, the new method predicted about the same amount of vertical shrinkage movement beneath the outer wheel path, indicating that longitudinal shrinkage cracks can be expected along the edge of the pavement in all of the cross sections. This shrinkage can be reduced by controlling the moisture influx and efflux beneath the edge of the pavement with the use of a vertical moisture barrier or wide paved shoulder.

9.3.2 Atlanta District US 271 Case Study

The subgrade soil beneath the pavement at the Atlanta District case study site was not very expansive but there were trees growing within the right of way along the entire length of the case study site. The trees had extracted moisture from beneath the pavement and had caused a considerable amount of longitudinal shrinkage cracks. In the boring log taken beside the pavement in the roadside ditch, root fibers were logged at a depth of 13 ft. The predicted movements using the new method showed that more shrinkage should be expected at this site than at the Fort Worth site, which had even more expansive subgrade soil. So the longitudinal cracking that was observed at this case study site could have been expected using the new method. The calculated vertical movements by the new method and the PVR method are shown in Table 9.3.

Table 9.3. Subgrade Movements Compared with PVR (Tex-124-E) for the Pavement with No Treatment, Atlanta District, US 271

Case Study Location	Pavement Location	Swelling (inches)	Shrinkage (inches)	Total (inches)	PVR (inches)
US 271	Edge	0.68	1.04	1.72	1.62
	Outer Wheel Path	0.53	0.81	1.34	1.16

The table shows that the PVR predicts more swelling than is expected by the new method both at the edge of the pavement and beneath the outer wheel path. The total movement is close to the calculated PVR. The presence of a tree root zone to a depth of 13 ft in close proximity to the edge of the pavement is what accounts for the vertical shrinkage movement predicted by the new method being larger than the predicted swelling. Once more, as in the Fort Worth District case studies, the swelling predicted by the new method beneath the outer wheel path are smaller than the PVR, which accounts for the weight of the pavement.

9.3.3 Austin District Loop 1 Case Study

The case study site in the Austin District was a sloping site in which the main lanes of Loop 1 were at a higher elevation than the frontage road. The frontage road had been overlaid several times to correct for the expansive clay roughness that had developed over time. There was a deep, grass-covered median between the main lanes.

The calculated PVR is greater than the swelling vertical movement predicted by the new method, but the total movement, which includes the shrinkage movement, is nearly the same as the PVR. Because the same composite boring profile was used in computing the movements beside and beneath the main lanes and the frontage road, the movements predicted by both methods are the same for both cross sections. The calculated movements are shown in Table 9.4.

Table 9.4. Subgrade Movements Compared with PVR (Tex-124-E) for the Pavement with No Treatment, Austin District, Loop 1

Case Study Location	Pavement Location	Swelling (inches)	Shrinkage (inches)	Total (inches)	PVR (inches)
Main Lanes	Edge	2.03	0.98	3.01	2.97
	Outer Wheel Path	1.42	0.68	2.10	2.37
Frontage Road	Edge	2.03	0.98	3.01	2.97
	Outer Wheel Path	1.42	0.68	2.10	2.37

While the total movement predicted by the new method is nearly equal to the calculated PVR, the predicted swelling is only two-thirds of the total amount both at the edge of the pavement and beneath the outer wheel path for both the main lanes and the frontage road.

The computed results for analysis pavement sections without treatments in the expansive subgrade soil for three case study sites are summarized in Fig. 9.1.

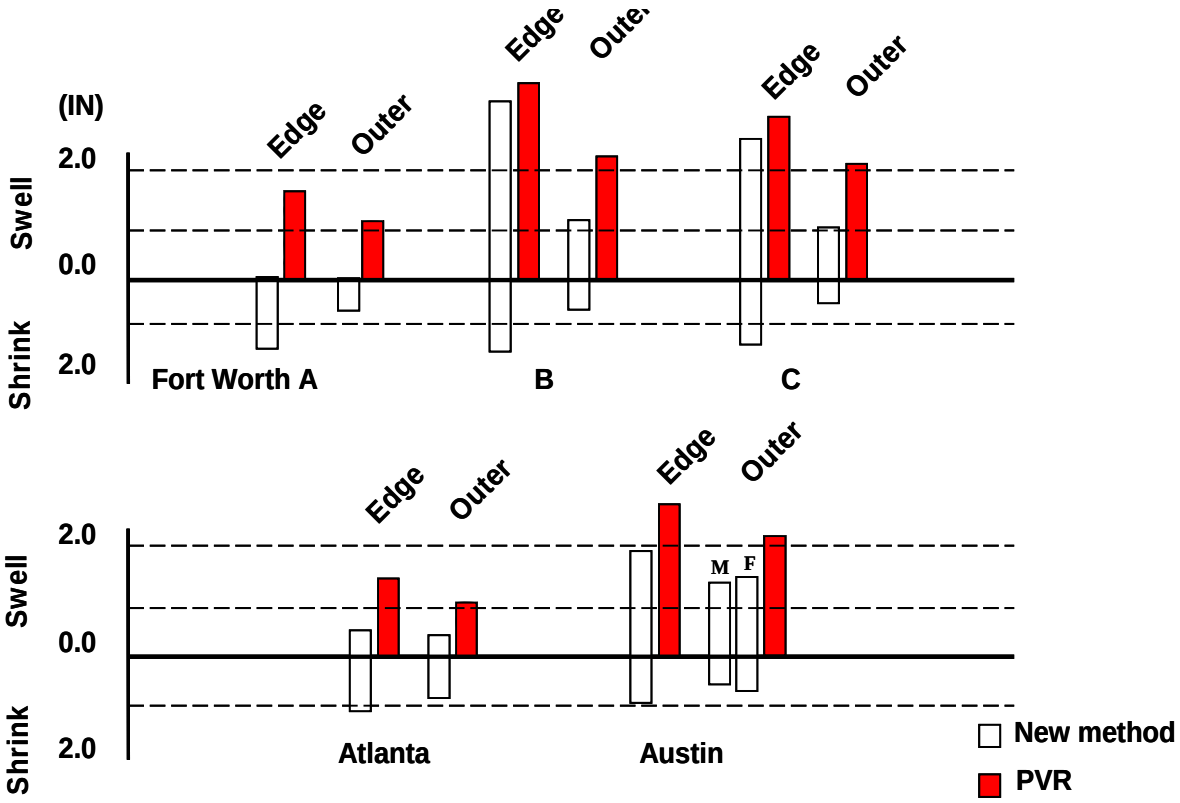

Fig. 9.1. Subgrade Movements Compared with PVR (Tex-124-E) for the Pavement without Treatments

Figure 9.1 shows the calculated vertical movements for each of the cross sections as they were predicted by the new method and also by the PVR method. The predictions were made at two locations: at the edge of the pavement where the soil movement is not affected by the weight of the pavement and beneath the outer wheel path where the weight of the pavement will restrain the vertical movement to some extent. The new method predicts both a swelling and a shrinkage vertical movement and a total movement, which is the sum of the two.

The swelling expected in Cross Section A is very small because of the moist condition of the embankment, but the expected shrinkage is very large. The new method shows that not much additional swelling is to be expected in Cross Section A, but a large amount of shrinkage is expected. The shrinkage figure is important because it is an indicator of future longitudinal shrinkage cracking along the edge of the pavement. The

PVR for the same section is roughly in the same range as the total movement predicted by the new method, but it is considerably larger than the swelling that is predicted. The movement beneath the outer wheel path reflects the effect of the weight of the pavement in the case of the PVR calculation but also indicates the added effect of the diffusion of moisture from the edge of the pavement in the case of the new method predictions. The new method expects to have less movement beneath the outer wheel path than does the PVR method. In Cross Section B, the swelling expected at the edge of the pavement using the new method is fairly close to the calculated PVR. However, the total movement is larger than the PVR because it includes the expected shrinkage. In Cross Section C, the new method predicts a swelling that is roughly close to that of the PVR at the edge of the pavement. The total movement expected by the new method is considerably larger than the PVR.

In all three cross sections, the new method predicted about the same amount of vertical shrinkage movement beneath the outer wheel path, indicating that longitudinal shrinkage cracks can be expected along the edge of the pavement in all of the cross sections. This shrinkage can be reduced by controlling the moisture influx and efflux beneath the edge of the pavement with the use of a vertical moisture barrier or wide paved shoulder.

In the Atlanta District U.S 271 case study, the PVR predicts more swelling than is expected by the new method both at the edge of the pavement and beneath the outer wheel path. The total movement is close to the calculated PVR.

9.4 Pavement Treatments with Acceptable Predicted Performance

Chapter VIII shows the results of the application of a number of alternative treatments to each of the six cross sections in the case studies. These alternatives included different pavement layer thickness, vertical moisture barriers, lime-treated subgrade layers, and removal and replacing of subgrade with a layer of a more inert soil. The design program WinPRES allows the designer to try a wide variety of alternative treatments to see which ones can provide acceptable performance at a reasonable cost and construction effort.

Some of these alternatives work better than others as can be seen in each of the figures in Chapter VIII. In this chapter, which compares the predicted results using the new method with the PVR method, it is important to compare the predicted movements at the edge of the pavement and beneath the outer wheel path for both the PVR method and the new method to determine whether and to what extent the PVR criterion of 1 inch is conservative. The pavement treatments in Table 9.5 do not represent current practice but instead were those found in Chapter VIII to provide minimally acceptable predicted performance for a period of 30 years. Both flexible and rigid pavements are shown in that table. The criterion that was used in selecting these minimally acceptable treatments was for the pavement riding quality to remain above a PSI of 2.5 for the entire 30-year period without requiring any rehabilitation such as overlaying. This performance was to be maintained at a reliability level of 90 percent for the flexible pavements and 95 percent for the rigid pavements.

The table shows the treatments that were found in the design case studies to provide minimally acceptable performance at the required level of reliability. A review of the relevant figures in Chapter VIII will reveal how these treatments were selected. The predicted movements by the new method and by the PVR both at the edge of the pavement and beneath the outer wheel path will be compared for the purpose of evaluating whether the PVR design criterion is too conservative.

Table 9.5. Pavement Treatments with Acceptable Predicted Performance

Case Study Site	Case Study Location	Type of Pavement	Design Reliability	Treatment for Acceptable Performance*
Fort Worth North Loop IH 820	Cross Section A	Flexible Rigid	90 % 95 %	ACP 4.0 in, LTS 2.5 ft CRCP 12.0 in
	Cross Section B	Flexible Rigid	90 % 95 %	ACP 5.0 in, LTS 2.5 ft, Inert 1.5 ft CRCP 12.0 in, LTS 8 in
	Cross Section C	Flexible Rigid	90 % 95 %	ACP 4.5 in, LTS 2.5 ft, Inert 1.0 ft CRCP 12.0 in, LTS 1.0 ft
Atlanta District US 271		Flexible Rigid	90 % 95 %	ACP 4.0 in, LTS 2.2 ft CRCP 10.5 in
Austin District Loop 1	Main Lanes	Flexible Rigid	90 % 95 %	ACP 4.0 in, LTS 2.8 ft CRCP 12.0 in, LTS 2.0 ft
	Frontage Road	Flexible Rigid	90 % 95 %	ACP 4.0 in, LTS 2.0 ft, Inert 2.0 ft CRCP 11.0 in

* LTS–Lime-Treated Subgrade; ACP–Asphalt Concrete Pavement; CRCP–Continuously Reinforced Concrete Pavement; Inert–Inert Soil Layer.

9.5 Subgrade Movements for Acceptable Performance

9.5.1 Fort Worth North Loop IH 820

Table 9.6 shows the results of the design calculations in the three case studies along the IH 820 route in the Fort Worth District. The table shows for each of the cross sections, A, B, and C, which of the treatments provided the minimally acceptable predicted performance for both flexible and rigid pavements. The next three columns show how much swelling and shrinkage and total movement were calculated at the edge of the pavement using the new method. The next column gives the amount of total movement that is expected beneath the outer wheel path using the new method. The amount of upward and downward movements that add up to this total are in the same proportion as with the movements at the edge of the pavement. The next two columns give the calculated values of the PVR both at the edge of the pavement and beneath the outer wheel path. Because the PVR is a calculated amount of swelling, the values in these columns should be compared only with the swelling movements that are calculated with the new method.

Table 9.6. Subgrade Movements Compared with PVR (Tex-124-E) for the Pavement Design with Acceptable Predicted Performance, Fort Worth District IH 820

Case Study Location	Type of Pavement	Acceptable Pavement Design*	Movements at the Edge of Pavement (in)			Movements in Outer Wheel Path (in)	PVR (in)	
			Swelling	Shrinkage	Total	Total	Edge	Outer +
Cross Section A	Flexible	ACP 4.0 in LTS 2.5 ft	0.02	1.16	1.19	0.46	1.77	1.62
	Rigid	CRCP 12.0 in	0.07	1.39	1.46	0.61	2.22	1.87
Cross Section B	Flexible	ACP 5.0 in LTS 2.5 ft Inert 1.5 ft	0.90	0.77	1.67	0.70	2.02	1.55
	Rigid	CRCP 12.0 in LTS 8.0 in	2.29	1.33	3.62	1.44	2.69	2.06
Cross Section C	Flexible	ACP 4.5 in LTS 2.5 ft Inert 1.0 ft	0.96	0.74	1.70	0.70	1.19	0.95
	Rigid	CRCP 12.0 in LTS 1.0 ft	1.90	1.21	3.11	1.29	1.99	1.64

* LTS–Lime-Treated Subgrade; ACP–Asphalt Concrete Pavement;
CRCP–Continuously Reinforced Concrete Pavement; Inert–Inert Soil Layer.
+ Outer Wheel Path.

Cross Section A was unusually wet and the calculated swelling using the new method was small, less than 0.1 inch, at the edge of the pavement. By way of contrast, the PVR values at the same location were 1.77 and 2.22 inches beneath the flexible and rigid pavements, respectively. In this case, the PVR greatly overpredicts the expected amount of swelling movement. A similar imbalance is seen between the expected swelling beneath the outer wheel path as calculated by the new method and by the PVR method. This imbalance would normally lead the designer to select an overly conservative treatment to restrain the development of roughness due to expansive clay. Instead, the new method alerts the designer that shrinkage, and not swelling, will be the major problem at this cross section. This will result in longitudinal cracking at the edge of the pavement and possibly in some transverse and random cracking in the pavement surface.

Cross Section B has a more typical moisture distribution in the embankment materials beneath the pavement. The new method shows that much larger movements, both swelling and shrinking, may be tolerated by the rigid pavement than by the flexible pavement that produces the minimally acceptable predicted performance. The expected total movements beneath the outer wheel paths are 0.70 and 1.44 inches in the flexible

and rigid pavements, respectively. The corresponding swelling movements calculated by the PVR method are 1.55 and 2.06 inches beneath the outer wheel path in the flexible and rigid pavements, respectively. Both of these are greater than the 1-inch criterion that is presently used for the design of interstate highway pavements on expansive clay. As with the previous section, the PVR method overpredicts the amount of swelling in the outer wheel path and would lead to an overly conservative treatment to restrain the development of roughness due to expansive clay.

Cross Section C is nearly at grade and has a moisture level that is similar to that of Cross Section B. The new method calculates expected movements at the edge of the pavement that are larger than the calculated value of the PVR. In this case, however, the values of the swelling movement calculated with the new method are close to the calculated values of the PVR at the edge of the pavement. The total movements of the subgrade beneath the outer wheel paths are 0.70 and 1.29 inches in the flexible and rigid pavements, respectively, while the amounts of swelling predicted by the PVR method are 0.95 and 1.64 inches beneath the same outer wheel paths. Although the flexible pavement treatment meets the 1-inch PVR criterion, the rigid pavement treatment does not and would require a more conservative treatment. In both cases, the PVR, a calculated amount of swelling movement, overpredicts the total movement that is calculated by the new method.

In each of the three cross sections, the PVR, which is a calculated vertical swelling movement, overpredicts the amount of total movement beneath the outer wheel path, which includes both swelling and shrinkage movements. A substantial amount of shrinkage movement, as is the case with all three cross sections, is a warning to the designer that some provision must be made to retain moisture beneath the pavement by use of a wider shoulder or a vertical moisture barrier in order to avoid longitudinal shrinkage cracking from reflecting through to the pavement surface. The treatments that are compared in this table are those that would work well on this site, providing an acceptable predicted performance with at least a 90 percent level of reliability. The use of the PVR method in choosing a treatment of these pavements to restrain the

development of roughness due to expansive clay will prove to be more conservative than these.

9.5.2 Atlanta District, US 271

Table 9.7 shows the movements at the edge of the pavement and beneath the outer wheel path as calculated by both the new method and the PVR method. The Atlanta case study site is in northeast Texas in a wet climate where trees are growing along the roadside within the right of way. Because of these site conditions, a certain amount of shrinkage is expected and is predicted by the new method. Root fibers were logged at a depth of 13 ft in the boring taken in the roadside ditch. The soil is not particularly expansive but the presence of the tree roots so close to the paved surface leads to the expectation that shrinkage cracking will be found in both the shoulder and the traveled lanes. Photographs of this site revealed longitudinal cracks along the edge of the pavement, as expected.

Table 9.7. Subgrade Movements Compared with PVR (Tex-124-E) for the Pavement Design with Acceptable Predicted Performance, Atlanta District, US 271

Case Study Location	Type of Pavement	Acceptable Pavement Design*	Movements at the Edge of Pavement (in)			Movements in Outer Wheel Path (in)	PVR (in)	
			Swelling	Shrinkage	Total	Total	Edge	Outer+
US 271	Flexible	ACP 4.0 in LTS 2.2 ft	0.30	0.97	1.27	1.02	1.21	0.91
	Rigid	CRCP 10.5 in	0.58	1.03	1.61	1.26	1.62	1.16

* LTS–Lime-Treated Subgrade; ACP–Asphalt Concrete Pavement; CRCP–Continuously Reinforced Concrete Pavement; Inert–Inert Soil Layer.
+ Outer Wheel Path.

The swelling movements calculated at the edge of the pavement by the new method were 0.30 and 0.58 inch for the flexible and rigid pavements, respectively. As a contrast, the swelling movements calculated by the PVR method were 1.21 and 1.62 inches, respectively, for the same pavements. The vertical shrinkage movements at the pavement edge were calculated to be 0.97 and 1.03 inches, respectively, indicating that much more shrinkage can be expected at this cross section than heaving. The total movements beneath the outer wheel paths were 1.02 and 1.26 inches beneath the flexible

and rigid pavements, respectively. These total movements compare well with the calculated swelling movement using the PVR method at the same location. However, these PVR movements are swelling, which are not expected to be the major problem at this location. The flexible pavement treatment meets the 1-inch PVR criterion beneath the outer wheel path but the rigid pavement treatment does not. The presence of the trees drawing moisture from beneath the pavement and shoulder makes the shrinkage much more than it would be if the trees were not present. In the absence of the trees, the total movements that would be predicted by the new method would be less than 1 inch. With this level of predicted shrinkage, the designer is alerted to the fact that the pavement surface must be protected from the reflection of shrinkage cracks in the subgrade due to the drying influences of the trees. The PVR criterion of 1 inch will require a more conservative treatment beneath the concrete pavement than the one that is predicted to provide acceptable performance at a level of reliability of 95 percent.

9.5.3 Austin District, Loop 1

Table 9.8 shows the movements that were calculated beneath the edge and outer wheel paths for both flexible and rigid pavements and for both the main lanes and the frontage road along the southbound Loop 1, the MoPac Freeway in Austin. This is a sloping site that is underlain by a sloping bed of limestone. A creek travels parallel to the frontage road and at about a 40 ft lower elevation. The main lanes are about 20 ft higher than the frontage road and there is a deep grass-covered median between the northbound and southbound main lanes. There has been a considerable amount of differential movement along the frontage road, which has been corrected periodically by a sequence of asphalt concrete overlays. The subgrade soil is a moderately active expansive clay. The table shows the amounts of movement that are expected in the future starting from its current condition, and the treatments that will provide for an acceptable predicted performance at a 90 percent level of reliability for the flexible pavement and at a 95 percent level of reliability for the rigid pavement.

The new method shows that somewhat more swelling is expected than is shrinkage movement at the edge of the pavement. The PVR method predicts more than twice as much swelling at this site than does the new method except for the rigid pavement on the frontage road. The PVR also predicts more swelling beneath the outer wheel path than the *total* movement predicted by the new method.

Table 9.8. Subgrade Movements Compared with PVR (Tex-124-E) for the Pavement Design with Minimum Acceptable Predicted Performance, Austin, Loop 1

Case Study Location	Type of Pavement	Acceptable Pavement Design*	Movements at the Edge of Pavement (in)			Movements in Outer Wheel Path (in)	PVR (in)	
			Swelling	Shrinkage	Total	Total	Edge	Outer+
Main Lanes	Flexible	ACP 4.0 in LTS 2.8 ft	0.78	0.66	1.44	0.93	2.40	1.93
	Rigid	CRCP 12.0 in LTS 2.0 ft	1.03	0.76	1.79	1.19	2.54	2.10
Frontage Road	Flexible	ACP 4.0 in LTS 2.0 ft Inert 2.0 ft	0.71	0.54	1.25	0.93	2.08	1.76
	Rigid	CRCP 11.0 in	2.03	1.00	3.03	2.28	2.97	2.37

* LTS–Lime-Treated Subgrade; ACP–Asphalt Concrete Pavement;
CRCP–Continuously Reinforced Concrete Pavement; Inert–Inert Soil Layer.
+ Outer Wheel Path.

Both of the total movements predicted by the new method beneath the outer wheel path of the flexible pavement are within the 1-inch criterion used with the PVR. However, none of the PVR values predicted for these acceptable treatments are within the 1-inch criterion. The PVR method would, in both the main lanes and the frontage road, require a more conservative treatment than the ones predicted by the new method to provide acceptable performance.

CHAPTER X
SUMMARY AND CONCLUSIONS

The work presented in this dissertation includes; refinement of previous version of one-dimensional swell-shrink model; refinement of previous pavement design model; evaluation of current pavement design method and comparative case study; development for prediction of horizontal earth pressure against a stationary wall; development of design model of drilled pier and retaining wall. This final chapter summarizes the methodology and features of above models and findings that have been drawn from the case studies.

10.1 Volume Change Model

The previous version of an one-dimensional swell-shrink model inserted in program PRES (Jayatilaka 1999) is refined to reinforce realistic characteristics of swelling and shrinkage behavior of expansive clay soils. Refinements include more realistic design soil suction versus depth profiles, and improved characterizations of the effects of soil cracking, overburden stress and lateral earth pressure. In the refined model, a critical parameter for predicting swell-shrink, the suction compression index, is estimated from standard test data such as Atterberg limits and soil particle size distributions. The refined model also has an algorithm of assigning suction- volumetric water content curves - a critical component of shrink-swell predictions - to various classes of soils including natural, inert, and stabilized soils.

The volume change model first predicts a so-called suction envelope, i.e., extremes of suction that occur in the soil profile due to seasonal variations in moisture, from which vertical shrink-swell movements are estimated. The suction envelope defines the depth of the moisture-active zone and the magnitude of seasonal suction variations that occur within this zone. Volume changes in the soil resulting from these seasonal suction variations are computed from a model that accounts for soil type and mechanical

overburden stress. Vertical deformations are calculated from volume change using a method that accounts for the effects of confinement.

10.2 Horizontal Earth Pressure in Expansive Soils

The concept of lateral earth pressure on a stationary wall due to suction change is presented. The lateral earth pressure increase with depth near the ground surface is limited by the maximum soil strength that can be supported by the overburden pressure. At greater depths, the lateral swelling pressure caused by small suction change is less than the classical at rest lateral earth pressure. Thus, the three zones for the typical distribution of lateral earth pressure are proposed.

The proposed stationary retaining wall-soil system condition in expansive soils includes an upper movement active zone and a lower anchor zone. Three typical stress state zones are proposed. Zone I is the upper zone where a passive failure state of stress exists to a depth z_{mp} at which the maximum lateral swelling pressure occurs. It is found that both the measured and predicted maximum lateral pressures occur within a depth between 2 and 4 ft. Zone II represents lateral passive pressure state due to large suction change. The lateral pressure decreases as the suction change decreases. It is considered that the zone III within the anchor zone is in the classical at rest condition.

Mohr's circles and failure envelopes are used to define the effective horizontal stress and shear failure in an unsaturated soil. The state of stress in a soil element in the movement active zone represents that the horizontal stress is greater than the vertical stress.

An agreement between the measured lateral pressures and predicted pressures is found in case study. It is found that the natural horizontal pressure in expansive clay soils can be equal the pressure required to cause passive failure. The high lateral pressure developed might be caused by the short width of test tank which does not allow the passive failure in a soil. The high lateral stresses predicted are of great significance in explaining some of the damage observed to structures founded in swelling clay soil

conditions. The importance is indicated of determining lateral pressures as a factor in design of structures exposed to forces from swelling soils.

10.3 Drilled Pier and Retaining Wall in Expansive Soils

A numerical model for use in design is presented for prediction of the stresses and axial and bending displacements in a drilled pier in expansive soils. With suction change around the pier, the prediction is based on the horizontal earth pressures caused by the expanding of the soil and shear stresses which act on the shaft of the drilled pier. The prediction of shear stress induced on the shaft of a drilled pier is supported by the load transfer curve which represents the relationship of the shear stress corresponding to the relative displacement between the soil and the pier shaft. In this study of the lateral behavior, the load-deflection curves are developed based upon the stress state around the pier and non-linear suction dependent elastic modulus of the unsaturated soils. It is appropriated that the curved surface forming the boundary of the wedge known as the horizontal active zone is parabolic. The proposed neutral, decrease and increase of lateral stress states are used to define the P-Y curve in the lateral behavior. A numerical model of the bending and stretching of a pier includes a beam column approach and linear distribution of shear stress around the circumference of the pier between the maximum and minimum shear stresses. Case studies of axial and bending of piers are presented with both uniform and non-uniform wetting.

A case study to determine the P-Y curves for the left and right sides of the pier is performed in the case of the non-uniform wetting around the pier in moderately expansive soils at a site NGES. Corresponding to the suction variation and soil profiles, the pier case study for axial behavior shows a good agreement with a heave at ground surface and uplift forces. Three case studies for bending behavior of the pier and retaining wall are used to describe the influence of suction change.

10.4 Pavement Design in Expansive Soils

The predicted behavior using pavement design model matched the observed differential movements in the field in all of the case studies. The differential movements were observed as the difference in the thickness of overlays that were placed to restore riding quality and the shrinkage cracking that was observed in those pavement sections in which a substantial amount of shrinkage movement was predicted. The close correspondence of the predicted and the observed behavior shows the importance to design of not only the expansive nature of the subgrade soil, but also the initial moisture condition, the presence of roadside vegetation including grass and trees, and slopes and drainage.

The pavement design model presented herein permits the designer to consider both flexible and rigid pavements, traffic expressed in 18-kip Equivalent Single Axle Loads, and multiple layers of subgrade soils characterized by their Atterberg limits, percentage fines, clay fraction, and unit weight. The designer can evaluate the effectiveness of various treatments for reducing roughness caused by expansive clay subgrades including lime- or cement-stabilized layers, removal and replacement with a more inert soil, and vertical and horizontal moisture barriers. The designer can specify the level of reliability associated with the various predictions made by the program and can designate several different wheel paths in which to evaluate the effectiveness of the treatment. Both the present serviceability index and the international roughness index are calculated in each selected wheel path for a period desired. The model also calculates the expected amount of vertical swelling and shrinkage movement beneath each selected wheel path that controls the predicted performance.

The pavement design model is user-friendly, flexible, and capable of a wide variety of design tasks. It allow the designer to consider a wide variety of treatment options (stabilized layers, inert layers, moisture barriers), drainage conditions, roadside vegetation, local climatic conditions, traffic conditions, and pavement type (asphalt and concrete).

While the design model provides a comprehensive analysis package for a broad spectrum of site conditions, certain limitations should be borne in mind. One is a caution that the effect of sulfate swelling is not included in the design method presented this paper. Designers in Texas are well aware of the problems that are caused by the growth of the expansive minerals that result from the combination of lime, soluble sulfates, and clay minerals in the subgrade. It is believed to be possible to represent the expansion that is a result of this crystalline growth in this program but that will require further development of testing procedures, theory, and program that is capable of representing the effects accurately. At present, it should be sufficient to use this design program as it is intended, and that is under the assumption that no sulfate swelling potential is present in the subgrade soil. A second caution is related to the treatment of the stabilized layers in this program. The prediction of the reduction in swelling and shrinking potential of both lime- and cement-stabilized soils is based upon a limited number of laboratory tests that were run on stabilized soils from previous projects. The assumptions in this model relating to shrink-swell characteristics of stabilized soils should be verified and perhaps modified in light of the results of further testing.

10.5 Comparative Case Studies of Pavement Performance

From evaluating the current PVR method, it is found that the assumptions on the method are not realistic and can not be supported by subsequent findings on actual Texas pavements and on the soils of the United States. Vertical movements calculated by the new method, including both the swelling and shrinking, were compared with the swelling movement predicted by the PVR method for each of the six case study cross sections. Pavement treatments had been selected to provide an acceptable predicted performance at high levels of reliability, and the vertical movements were calculated both at the edges of the pavements and beneath the outer wheel paths using both the new method and the PVR method. A major purpose of the comparisons of the movements was to evaluate the PVR method in light of the new method, which was based upon many years of monitoring of pavements in several locations across Texas and careful

modeling of the measured pavement roughness. A primary objective was to determine from these case studies whether the 1-inch PVR criterion, which has been used by the TxDOT in the past, required treatments to restrain the development of pavement roughness due to the expansive clay that were unnecessarily conservative.

The results of the case studies are that in every case, the PVR criterion of 1-inch proved to be unnecessarily conservative. The PVR overpredicts the swelling movement that can be expected using the new method both at the edge of the pavement and beneath the outer wheel path. Furthermore, the PVR does not provide a means of anticipating subgrade shrinkage that will result in longitudinal cracking along the edge of the pavement. In addition, both transverse and random cracks may reflect upward from shrinkage cracks in the subgrade.

The design criterion of lowering the PVR to 1-inch by removing and replacing the native soil with a more inert soil is conservative to differing degrees depending largely upon how wet the subgrade soil is at the time of construction. The wetter soils will not swell much but will shrink, and the pavement resting on them will get rougher than is estimated with the 1-inch PVR criterion. Also, if the soil is drier at the time of construction, it will swell substantially unless moisture control measures such as vertical and horizontal moisture barriers and stabilized and inert layers are used to control the moisture and the subsequent development of roughness. The new method shows that these control measures are more effective than is presently anticipated by the PVR method.

The design calculations with the new method have shown a total movement beneath the outer wheel path ranging between 0.42 to 1.08 inches for flexible pavements that had acceptable performance at a reliability level of 95 percent. On the same sites, rigid pavements were predicted to have acceptable performance when the total vertical movement beneath the outer wheel path ranged between 0.60 and 2.23 inches. This leads to the conclusion that neither the swelling movement, as in the PVR method, nor the total movement, as in the new method, is a reliable indicator of likely acceptable performance. Instead, all of these case studies show that it is important to use the

predicted history of the present serviceability index and the international roughness index as the proper design guideline for an acceptable treatment of the subgrade of an expansive soil.

REFERENCES

AASHTO (1993). *AASHTO Guide for Design of Pavement Structures*. American Association of State Highway and Transportation Officials, Washington, D.C.

Aitchison, G.D. and Woodburn, J.A. (1969). "Soil Suction in Foundation Design." *Proceedings of 7th ICSMFE*, Mexico City, Mexico, 2, 1-8.

Aurora, R.P., Peterson, E.H., and O'Neill, M.W. (1981). "Model Studies of Long Piles in Clays." *Proceedings 13th Offshore Technology Conference*, 331-338.

Bhandari, R.K., Balodhi, G.R., Chandra, Ramesh, and Prakash, Chandra. (1987). "Behaviour of Short Bored Piles in Expansive Soils during the Stage of Swelling." *Proceedings of the Sixth International Conference on Expansive Soils*, New Delhi, India, 295-300.

Blight, G.E. (1984). "Uplift Forces Measured in Piles in Expansive Clay." *Proceedings of the Fifth International Conference on Expansive Soils*. Adelaide, South Australia, 240-244.

Brackley, I.J.A. and Sanders, P.J. (1992). "In situ Measurement of Total Natural Horizontal Stresses in an Expansive Clay." *Geotechnique*. 42(2), 443-451.

Carey Jr., W.N., and Irick, P.E. (1960). "The Pavement Serviceability-Performance Concept." Bulletin 250, Highway Research Board, National Research Council, Washington, D.C., 40-58.

Casagrande, A., (1948). "Classification and Identification of Soils." *Transactions ASCE*, 113, 901-930.

Covar, A.P. and Lytton, R.L. (2001). "Estimating Soil Swelling Behavior Using Soil Classification Properties." *Geotechnical Special Publication No. 115*, ASCE, Houston, Texas, 44-63.

De Bruijn, C. M. A. (1973). "Moisture Distribution and Soil Movements at Vereeniging (Transvaal)" *Proc. 3rd Int. Conf. Exp. Soils*, Haifa, 279-288.

Dhowian, A., Erol, A.O., and Youssef, A. (1987). "Assessment of Oedometer Methods for Heave Prediction." *Proceedings, 6th International Conference of Expansive Soils*, New Delhi, India, 99-103.

Donaldson, G.W. (1967). "The Measurement of Stresses in Anchor Piles." *Proceedings of the Fourth Regional Conference on Soil Mechanics and Foundation Engineering*, Cape Town, South Africa, 253-256.

Fourie, A.B. (1989). "Laboratory Evaluation of Lateral Swelling Pressure." *Journal of Geotechnical Engineering, ASCE*, 115(10), 1481-1486.

Fredlund, D.G., Morgenstern, N.R., and Widger, R.A. (1978). "The Shear Strength of Unsaturated Soils." *Canadian Geotechnical Journal*, 15(3), 313-321.

Fredlund, D.G. and Rahardjo, H. (1993). *Soil Mechanics for Unsaturated Soils*, John Wiley and Sons, Inc., New York.

Gay, D.A. (1994). "Development of a Predictive Model for Pavement Roughness on Expansive Clay." Ph.D. Dissertation, Texas A&M University, College Station, Texas.

Holtz, R.D. and Kovacs, W.D. (1981). *An Introduction to Geotechnical Engineering*, Prentice Hall, Englewood Cliffs, NJ.

Hoyos, L.R. (1998). "Experimental and Computational Modeling of Unsaturated Soil Behavior Under True Triaxial Stress States." Ph.D. Dissertation, Georgia Institute of Technology, Atlanta, GA.

Huang, Y.H. (1993). *Pavement Analysis and Design*, Prentice Hall, Englewood Cliffs, NJ.

Jayatilaka, R. (1999). "A Model to Predict Expansive Clay Roughness in Pavements with Vertical Moisture Barriers." Ph.D. Dissertation, Texas A&M University, College Station, Texas.

Jayatilaka, R., Gay, D.A., Lytton, R.L., and Wray, W.K. (1993). "Effectiveness of Controlling Pavement Roughness Due to Expansive Clays with Vertical Moisture Barriers." Texas Transportation Institute Research Report 0-1165-2F, May.

Johnson, L.D. and Stroman, W.R. (1985). "Long-Term Behavior of a Drilled Shaft in Expansive Soil." *Transportation Research Record*, No. 1032, 53-59.

Joshi, R.P. and Katti, R.K. (1980). "Lateral Pressure Development under Surcharges." *Proceedings of the 4th International Conference on Expansive Soils*, Denver, CO, 227-241.

Juarez-Badillo, E. (1986). "General Theory of Consolidation for Clays." *Consolidation of Soils: Testing and Evaluation*, ASTM STP 892, R.N. Yong and F.C. Townsend, eds. American Society of Testing Materials, Philadelphia, 137-153.

Kassiff, G. and Zeitlen, J.G. (1962). "Behavior of Pipes Buried in Expansive Clays." *ASCE, Journal of the Soil Mechanics and Foundations Division*, 88(2), 133-148.

Kate, J.M., and Katti, R.K. (1980). "Effects of CNS Layer on the Behaviour of Underlying Expansive Soil-An Experimental Study." *Indian Geotechnical Journal*, 10(4), 281-305.

Kim, M.H. and O'Neill, M.W. (1998). "Side Shear Induced in Drilled Shaft by Suction Change." *Journal of Geotechnical and Geoenvironmental Engineering*, ASCE, 124(8), 771-780.

Komornik, A. (1962). "The Effect of Swelling Properties of Unsaturated Clay on Pile Foundations." D.Sc. Thesis, Israel Institute of Technology.

Komornik, A. and Zeitlen, J.G. (1973). "Effect of Swelling Clay on Piles." *Proceedings of the Eight International Conference on Soil Mechanics and Foundation Engineering*, Moscow, USSR, 123-128.

Kurzeme, M. and Richards, B. G. (1974). "Earth Pressure Observations on a Retaining Wall in Expansive Clay." Gouger Street Mail Exchange, Adelaide, Division of Applied Geomechanics Technical Report 17. Australia: CSIRO.

Lamborn, M.J. (1986). "A Micromechanics Approach to Modeling Partly Saturated Soils." M.S. thesis, Texas A&M University, College Station, TX.

Lytton, R.L. (1977). "The Characterization of Expansive Soils in Engineering." *Presentation at the Symposium on Water Movement and Equilibria in Swelling Soils*, American Geophysical Union, San Francisco, CA.

Lytton, R.L., (1994). "Prediction of Movement in Expansive Clay." *Geotechnical Special Publication* No. 40, ASCE, NY, 2, 1827-1845.

Lytton, R.L. (1995). "Foundations and Pavements on Unsaturated Soils." *Proceedings of the 1st International Conference on Unsaturated Soils*, Paris, France, 3, 1201-1220.

Lytton, R.L., Aubeny, C.P., and Bulut. R., (2005). "Design Procedures for Pavements on Expansive Soils." FHWA/TX-05/0-4518-1, Texas Transportation Institute. College Station.

Lytton, R.L., Boggess, R.L., and Spotts, J.W. (1976). "Characteristics of Expansive Clay Roughness of Pavements." *Transportation Research Record 568*, TRB, National Research Council, Washington, D.C., 9-23.

Mason, J.G., Ollayos, C.W., Guymo, G.L., and Berg, R.L. (1986). *User's Guide for the Mathematical Model of Frost Heave and Thaw Settlement in Pavements*, U.S. *Army Cold Region Research and Engineering Laboratory*, Hanover, NH.

Matlock, H., Bogard, D., and Lam, I. (1981). "BMCOL76: A Computer Program for the Analysis of Beam-Columns under Static Axial and Lateral Loading." Program developed at the University of Texas at Austin, under grant from Fugro, Inc., and documented at Ertec, Inc., Long Beach, CA.

McDowell, C. (1956). "Interrelationship of Load, Volume Change, and Layer Thickness of Soils to the Behavior of Engineering Structures." *Proceedings of the Highway Research Board*, No. 35, 754-772.

McKeen, R.G. (1981). "Design of Airport Pavements on Expansive Soils." Report No. DOT/FAA-RD-81-25, Federal Aviation Administration, Washington, D.C.

McKeen, R.G. (1985). "Validation of Procedures for Pavement Design on Expansive Soils." Report DOT/FAA/PM-85/15, U.S. Department of Transportation, Federal Aviation Administration, Washington, D.C.

McKenzie, D.W., Riddle, P., and Crandell, J. (1986). "VERTAC, a Vertical Acceleration Program for the Calculation of Serviceability Index, Version 6.0, Center for Transportation Research, The University of Texas at Austin, Texas.

Mitchell, P.W. (1979). "The Structural Analysis of Footings on Expansive Soil." Kenneth W. G. Smith and Associates Research Report No. 1, (1st Edition), Newton, South Australia.

Mitchell, P.W. (1980). "The Structural Analysis of Footings on Expansive Soils." *Proc. 4th International Conference on Expansive Soils*, ASCE, 1, 438-447.

Mitchell, P.W. and Avalle, D.L. (1984). "A Technique to Predict Expansive Soil Movements." *Proceedings, 5th International Conference on Expansive Soils*, Adelaide, South Australia, 124-130.

Mojeckwu, E.C. (1979). "A Simplified Method for Identifying the Predominant Clay Mineral," M.S. Thesis, Texas Tech University, Lubbock, Texas.

Osman, M.A. and Sharief, A.M.E. (1987). "Field and Laboratory Observations of Expansive Soil Heave." *Proceedings, 6th International Conference of Expansive Soils*, New Delhi, India, 105-110.

Rajendran, D. and Lytton, R.L. (1997). "Reduction of Sulfate Swell in Expansive Clay Subgrades in the Dallas District." Texas Transportation Institute Research Report 3929-1, September.

Richards, B.G. (1965). "Measurement of the Free Energy of Soil Moisture by the Psychrometric Technique Using Termistors." in *Moisture Equilibria and Moisture Changes in Soils Beneath Covered Areas*, A Symposium, Buttertworths, Australia, 39-46.

Sayers, M.W. (1995). "On the Calculation of International Roughness Index from Longitudinal Road Profile." *Transportation Research Record* 1501, TRB, National Research Council, Washington, D.C., 1-12.

Sayers, M.W., Gillespie, T.D., and Querioz, C.A.V. (1986). "The International Road Roughness Experiment: Establishing Correlation and a Calibration Standard for Measurements." Technical Paper 45, World Bank, Washington, D.C.

Sayers, M.W., and Karamihas, S.M. (1996). *The Little Book of Profiling*. Transportation Research Institute, University of Michigan, Ann Arbor, MI.

Symons, I.F., Clayton, C.R.I., and Darley, P., 1989. "Earth Pressures against of Experimental Retaining Wall Backfilled with Heavy Clays, Transport and Road Research Lab." Research Report No. 192, Crowthorne, Berkshine.

Terzaghi, K., Peck, R.B., and Mesri, G. (1996). *Soil Mechanics in Engineering Practice*. 3rd Edition, Wiley InterScience, New York.

Texas Department of Transportation (1999). "Method for Determining the Potential Vertical Rise, PVR." Manual of Testing Procedures, Chapter 1-Soils, Section 23, Tex-124-E, pp. 1-171 to 1-185.

Thomas, H. S. H. & Ward, W. H. (1969). "The Design, Construction and Performance of a Vibrating-wire Earth Pressure Cell." *Geotechnique*, 19(1), 39-51.

Vanapalli, S.K., Fredlund, D.E., and Pufahl, D.E., and Clifton, A.W. (1996). "Model for Prediction of Shear Strength with Respect to Soil Suction." *Canadian Geotechnical Journal*, 33(3), 379-392.

Velasco, M.O., and Lytton, R.L. (1981). "Pavement Roughness on Expansive Clays." Research Report 284-2, Texas Transportation Institute, Texas A&M University, College Station, Texas.

Williams, A. A. B. & Jennings, J. E. (1977). "The in-situ Shear Behavior of Fissured Soils." *Proc. 9th Int. Conf. Soil Mech.*, Tokyo 2, 169-176.

APPENDIX A

INPUT DATA FOR ANALYSIS OF CASE STUDY SECTIONS USING NEW METHOD

The input data required to use the pavement design program WinPRES for the six study sections are summarized in Tables A-1 through A-42. Figures A-1 through A-6 show the typical dimension of road for each study section.

Input Data for Section A, Fort Worth North Loop IH 820

Table A-1. Environmental and Geometry Conditions for Section A, Fort Worth North Loop IH 820.

TMI	-10.0
Lateral Slope	Fill
Longitudinal Drainage	Slope
Root Zone	0.0 (ft)
Depth of Moisture Active Zone, Zm	15.0 (ft)
Equilibrium Suction	2.58 (pF)
Note : water table is located at the depth of 17.0 ft (EL. 618)	

Table A-2. Soil Properties for Each Layer for Section A, Fort Worth North Loop IH 820.

Soil Type	Layer	Thickness (ft)	LL (%)	PI (%)	-#200 (%)	-2μm (%)	γ_d (pcf)	
Natural Soil	1	3.0	60.0	28.0	80.0	25.0	100.0	
	2	4.2	60.0	25.0	80.0	23.0	100.0	
	3	1.3	30.0	15.0	35.0	10.0	115.0	
	4	0.5	20.0	10.0	25.0	10.0	130.0	
	5	3.5	65.0	35.0	85.0	30.0	100.0	
	6	2.5	65.0	35.0	85.0	35.0	100.0	
Inert Soil		1.5	25.0	10.0	10.0	1.0	130	
								% Lime
Stabilized Soil		1.5	60.0	28.0	80.0	25.0	120	8

Table A-3. Vertical Moisture Barrier and Wheel Path for Section A, Fort Worth North Loop IH 820.

Depth of Vertical Moisture Barrier	0 and 8 (ft)
Width of Pavement (5 lanes)	83 (ft)
Number of Wheel Path	1
Distance from the Center of Pavement	27 (ft)

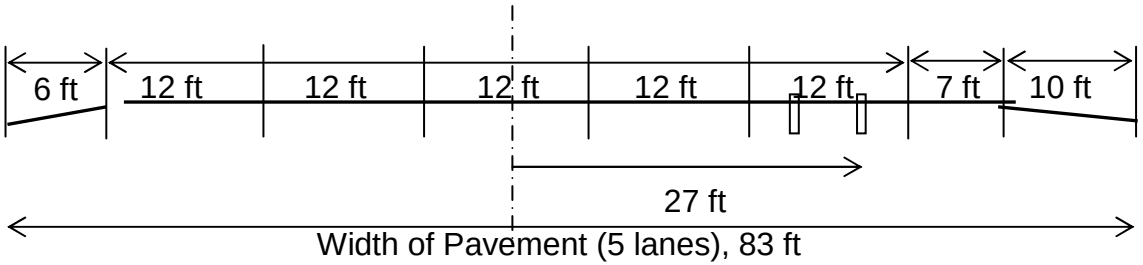

Figure A-1. Dimension of Cross Section of the Pavement for Section A, Fort Worth North Loop IH 820.

Table A-4. Structural Properties of the Flexible Pavement for Section A, Fort Worth North Loop IH 820.

SN	FWD	SN = Structural Number, in FWD = Falling Weight Deflectometer Modulus of Subgrade Soil (from drop weight closest to 9k load, psi)
(inches)	(psi)	
4.00-5.28	10,000	

Table A-5. Structural Properties of the Rigid Pavement for Section A, Fort Worth North Loop IH 820.

D (inches)	fc (psi)	Sc (psi)	Cd	J	FWD (psi)	P_t
11.5-12.0	4,000	650	0.90	3.2	10,000	3.0

D = Thickness of Concrete Layer, in
fc = 28-day Compressive Strength of concrete, psi, Ec = 57000 $(fc)^{0.5}$, psi
Sc = Mean Modulus of Rupture of concrete, psi
Cd = Drainage Coefficient
J = Load Transfer Coefficient
FWD=Falling Weight Deflectometer Modulus of Subgrade Soil (from drop weight closet to 9000lb load, psi, k (pci) = M_R / 19.4
Pt = Terminal Serviceability Index for the Concrete Pavement

Table A-6. Traffic and Reliability Data for Section A, Fort Worth North Loop IH 820.

Traffic Analysis Period, C	30 (yrs)
Average Daily Traffic of outer lane (T=0)	13,712
Average Daily Traffic of outer lane (T=C)	21,744
No of 18kip ESAL in the 30th years	8,415,520
Reliability for Traffic	50, 90, and 95 (%)
Reliability for Soil	50, 90, and 95 (%)

Table A-7. Initial and Terminal Serviceability Index and Roughness Data for Section A, Fort Worth North Loop IH 820.

	Flexible		Rigid	
	Initial	Terminal	Initial	Terminal
SI	4.2	2.5	4.5	3.0
IRI (in/miles)	75.2	166.2	65.4	131.7

IRI (inch/mile) = 63.36×8.4193×exp(-0.4664×SI)

Input Data for Section B, Fort Worth North Loop IH 820

Table A-8. Environmental and Geometry Conditions for Section B, Fort Worth North Loop, IH 820.

TMI	-10.0
Lateral Slope	Fill
Longitudinal Drainage	Slope
Root Zone	0.0 (ft)
Depth of Moisture Active Zone, Zm	15.0 (ft)
Equilibrium Suction	3.45 (pF)

Table A-9. Soil Properties for Each Layer for Section B, Fort Worth North Loop IH 820.

Soil Type	Layer	Thickness (ft)	LL (%)	PI (%)	-#200 (%)	-2μm (%)	γ_d (pcf)	
Natural Soil	1	3.5	60.0	36.0	85.0	30.0	100.0	
	2	1.5	55.0	30.0	80.0	25.0	105.0	
	3	4.0	65.0	38.0	85.0	30.0	100.0	
	4	0.5	30.0	15.0	35.0	10.0	115.0	
	5	1.5	53.0	32.0	80.0	25.0	100.0	
	6	4.0	45.0	15.0	99.4	37.0	100.0	
Inert Soil		1.5	25.0	10.0	10.0	1.0	130	
								% Lime
Stabilized Soil		1.5	60.0	28.0	80.0	25.0	120	8

Table A-10. Vertical Moisture Barrier and Wheel Path for Section B, Fort Worth North Loop IH 820.

Depth of Vertical Moisture Barrier	0 and 8 (ft)
Width of Pavement (5 lanes)	83 (ft)
Number of Wheel Path	1
Distance from the Center of Pavement	27 (ft)

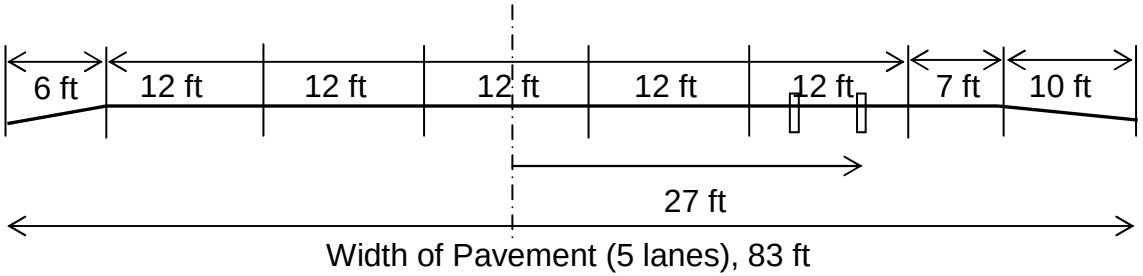

Figure A-2. Dimension of Cross Section of the Pavement for Section B, Fort Worth North Loop IH 820.

Table A-11. Structural Properties of the Flexible Pavement for Section B, Fort Worth North Loop IH 820.

SN	FWD	SN = Structural Number, in FWD = Falling Weight Deflectometer Modulus of Subgrade Soil (from drop weight closest to 9k load, psi)
(inches)	(psi)	
4.40-5.72	10,000	

Table A-12. Structural Properties of the Rigid Pavement for Section B, Fort Worth North Loop IH 820.

D (inches)	fc (psi)	Sc (psi)	Cd	J	FWD (psi)	P_t
12.0-13.0	4,000	650	1.0	3.2	10,000	3

D = Thickness of Concrete Layer, in
fc = 28-day Compressive Strength of concrete, psi, Ec = 57000 $(fc)^{0.5}$, psi
Sc = Mean Modulus of Rupture of concrete, psi
Cd = Drainage Coefficient
J = Load Transfer Coefficient
FWD=Falling Weight Deflectometer Modulus of Subgrade Soil (from drop weight closet to 9000lb load, psi, k (pci) = M_R / 19.4
Pt = Terminal Serviceability Index for the Concrete Pavement

Table A-13. Traffic and Reliability Data for Section B, Fort Worth North Loop IH 820.

Traffic Analysis Period, C	30 (yrs)
Average Daily Traffic of outer lane (T=0)	13,712
Average Daily Traffic of outer lane (T=C)	21,744
No of 18kip ESAL in the 30th years	8,415,520
Reliability for Traffic	50, 90, and 95 (%)
Reliability for Soil	50, 90, and 95 (%)

Table A-14. Initial and Terminal Serviceability Index and Roughness Data for Section B, Fort Worth North Loop IH 820.

	Flexible		Rigid	
	Initial	Terminal	Initial	Terminal
SI	4.2	2.5	4.5	3.0
IRI (in/miles)	75.2	166.2	65.4	131.7

Input Data for Section C, Fort Worth North Loop IH 820

Table A-15. Environmental and Geometry Conditions for Section C, Fort Worth North Loop IH 820.

TMI	-10.0
Lateral Slope	Fill
Longitudinal Drainage	Slope
Root Zone	0.0 (ft)
Depth of Moisture Active Zone, Zm	15.0 (ft)
Equilibrium Suction	3.42 (pF)

Table A-16. Soil Properties for Each Layer for Section C, Fort Worth North Loop IH 820.

Soil Type	Layer	Thickness (ft)	LL (%)	PI (%)	-#200 (%)	-2μm (%)	γ_d (pcf)	
Natural Soil	1	1.0	55.0	30.0	88.0	22.0	100.0	
	2	4.0	62.0	36.0	99.7	25.0	100.0	
	3	3.0	50.0	31.0	90.0	23.0	100.0	
	4	7.0	52.0	28.0	85.0	21.0	100.0	
Inert Soil		1.5	25.0	10.0	10.0	1.0	130	
								% Lime
Stabilized Soil		1.5	60.0	28.0	80.0	25.0	120	8

Table A-17. Vertical Moisture Barrier and Wheel Path for Section C, Fort Worth North Loop IH 820.

Depth of Vertical Moisture Barrier	0 and 8 (ft)
Width of Pavement (5 lanes)	83 (ft)
Number of Wheel Path	1
Distance from the Center of Pavement	27 (ft)

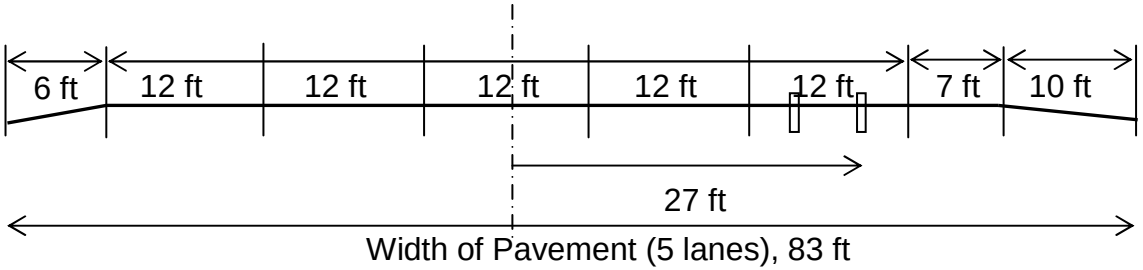

Figure A-3. Dimension of Cross Section of the Pavement for Section C, Fort Worth North Loop IH 820.

Table A-18. Structural Properties of the Flexible Pavement for Section C, Fort Worth North Loop IH 820.

SN	FWD	
(inches)	(psi)	SN = Structural Number, in FWD = Falling Weight Deflectometer Modulus of Subgrade Soil (from drop weight closest to 9k load, psi)
4.40-5.94	10,000	

Table A-19. Structural Properties of the Rigid Pavement for Section C, Fort Worth North Loop IH 820.

D (inches)	fc (psi)	Sc (psi)	Cd	J	FWD (psi)	P_t
12.0-13.0	4,000	650	1.0	3.2	10,000	3

D = Thickness of Concrete Layer, in
fc = 28-day Compressive Strength of concrete, psi, Ec = 57000 $(fc)^{0.5}$, psi
Sc = Mean Modulus of Rupture of concrete, psi
Cd = Drainage Coefficient
J = Load Transfer Coefficient
FWD=Falling Weight Deflectometer Modulus of Subgrade Soil (from drop weight closet to 9000lb load, psi, k (pci) = M_R / 19.4
Pt = Terminal Serviceability Index for the Concrete Pavement

Table A-20. Traffic and Reliability Data for Section C, Fort Worth North Loop IH 820.

Traffic Analysis Period, C	30 (yrs)
Average Daily Traffic of outer lane (T=0)	13,712
Average Daily Traffic of outer lane (T=C)	21,744
No of 18kip ESAL in the 30th years	8,415,520
Reliability for Traffic	50, 90, and 95 (%)
Reliability for Soil	50, 90, and 95 (%)

Table A-21. Initial and Terminal Serviceability Index and Roughness Data for Section C, Fort Worth North Loop IH 820.

	Flexible		Rigid	
	Initial	Terminal	Initial	Terminal
SI	4.2	2.5	4.5	3.0
IRI (in/miles)	75.2	166.2	65.4	131.7

IRI (inch/mile) = 63.36×8.4193×exp(-0.4664×SI)

Input Data for the Atlanta US 271 Site

Table A-22. Environmental and Geometry Conditions for the Atlanta US 271 Site.

TMI	30.0
Lateral Slope	Flat
Longitudinal Drainage	Slope
Root Zone	11.0 (ft)
Depth of Moisture Active Zone, Zm	17.0 (ft)
Equilibrium Suction	3.09 (pF)

Table A-23. Soil Properties for Each Layer for the Atlanta US 271 Site.

Soil Type	Layer	Thickness (ft)	LL (%)	PI (%)	-#200 (%)	-2μm (%)	γ_d (pcf)	
Natural Soil	1	5.0	48.0	26.0	90.0	14.0	100.0	
	2	3.0	37.0	17.0	92.0	8.7	100.0	
	3	4.0	40.0	25.0	93.4	8.6	100.0	
	4	5.0	37.0	15.0	93.3	7.7	100.0	
Inert Soil		1.5	25.0	10.0	10.0	1.0	130	
								% Lime
Stabilized Soil		1.5	60.0	28.0	80.0	25.0	120	8

Table A-24. Vertical Moisture Barrier and Wheel Path for the Atlanta US 271 Site.

Depth of Vertical Moisture Barrier	0 and 8 (ft)
Width of Pavement (5 lanes)	44 (ft)
Number of Wheel Path	1
Distance from the Center of Pavement	9.0 (ft)

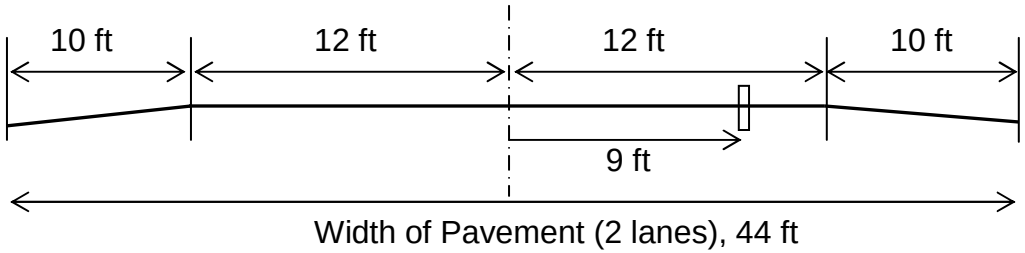

Figure A-4. Dimension of Cross Section of the Pavement for the Atlanta US 271 Site.

Table A-25. Structural Properties of the Flexible Pavement for the Atlanta US 271 Site.

SN	FWD	SN = Structural Number, in FWD = Falling Weight Deflectometer Modulus of Subgrade Soil (from drop weight closest to 9k load, psi)
(inches)	(psi)	
3.72-5.06	10,000	

Table A-26. Structural Properties of the Rigid Pavement for the Atlanta US 271 Site.

D (inches)	fc (psi)	Sc (psi)	Cd	J	FWD (psi)	P_t
10.5-12.0	4,000	650	1.0	3.2	10,000	3

D = Thickness of Concrete Layer, in
fc = 28-day Compressive Strength of concrete, psi, Ec = 57000 $(fc)^{0.5}$, psi
Sc = Mean Modulus of Rupture of concrete, psi
Cd = Drainage Coefficient
J = Load Transfer Coefficient
FWD=Falling Weight Deflectometer Modulus of Subgrade Soil (from drop weight closet to 9000lb load, psi, k (pci) = M_R / 19.4
Pt = Terminal Serviceability Index for the Concrete Pavement

Table A-27. Traffic and Reliability Data for the Atlanta US 271 Site.

Traffic Analysis Period, C	30 (yrs)
Average Daily Traffic in one Direction T=0	10,000
Average Daily Traffic in one Direction T=C	20,000
No of 18kip ESAL in the 30th years	2,500,000
Reliability for Traffic	50, 90, and 95 (%)
Reliability for Soil	50, 90, and 95 (%)

Table A-28. Initial and Terminal Serviceability Index and Roughness Data for the Atlanta US 271 Site.

	Flexible		Rigid	
	Initial	Terminal	Initial	Terminal
SI	4.2	2.5	4.5	3.0
IRI (in/miles)	75.2	166.2	65.4	131.7

IRI (inch/mile) = 63.36×8.4193×exp(-0.4664×SI)

Input Data for Austin Loop 1 Site (Main Lane)

Table A-29. Environmental and Geometry Conditions for the Austin Loop 1 Site (Main Lane).

TMI	-15.0
Lateral Slope	Fill
Longitudinal Drainage	Slope
Root Zone	0.0 (ft)
Depth of Moisture Active Zone, Zm	14.0 (ft)
Equilibrium Suction	3.45 (pF)

Table A-30. Soil Properties for Each Layer for the Austin Loop 1 Site (Main Lane).

Soil Type	Layer	Thickness (ft)	LL (%)	PI (%)	-#200 (%)	-2μm (%)	γ_d (pcf)	
Natural Soil	1	5.0	49.0	29.0	84.9	42.0	100.0	
	2	3.0	68.0	33.0	91.8	30.0	100.0	
	3	6.0	68.0	35.0	90.6	18.0	105.0	
Inert Soil		1.5	25.0	10.0	10.0	1.0	130	
								% Lime
Stabilized Soil		1.5	60.0	28.0	80.0	25.0	120	8

Table A-31. Vertical Moisture Barrier and Wheel Path for the Austin Loop 1 Site (Main Lane).

Depth of Vertical Moisture Barrier	0 and 8 (ft)
Width of Pavement (4 lanes)	62 (ft)
Number of Wheel Path	1
Distance from the Center of Pavement	21 (ft)

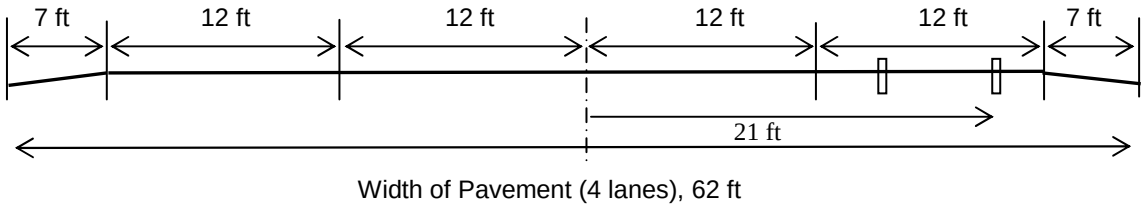

Figure a-5. Dimension of Cross Section of the Pavement for the Austin Loop 1 Site (Main Lane).

Table A-32. Structural Properties of the Flexible Pavement for the Austin Loop 1 Site (Main Lane).

SN	FWD	
(inches)	(psi)	SN = Structural Number, in FWD = Falling Weight Deflectometer Modulus of Subgrade Soil (from drop weight closest to 9k load, psi)
4.66-5.72	10,000	

Table A-33. Structural Properties of the Rigid Pavement for the Austin Loop 1 Site (Main Lane).

D (inches)	fc (psi)	Sc (psi)	Cd	J	FWD (psi)	P_t
12.0-13.2	4,000	650	1.0	3.2	10,000	3

D = Thickness of Concrete Layer, in
fc = 28-day Compressive Strength of concrete, psi, Ec = 57000 $(fc)^{0.5}$, psi
Sc = Mean Modulus of Rupture of concrete, psi
Cd = Drainage Coefficient
J = Load Transfer Coefficient
FWD=Falling Weight Deflectometer Modulus of Subgrade Soil (from drop weight closet to 9000lb load, psi, k (pci) = M_R / 19.4
Pt = Terminal Serviceability Index for the Concrete Pavement

Table A-34. Traffic and Reliability Data for the Austin Loop 1 Site (Main Lane).

Traffic Analysis Period, C	30 (yrs)
Average Daily Traffic of outer lane (T=0)	16,283
Average Daily Traffic of outer lane (T=C)	25,821
No of 18kip ESAL in the 30th years	9,993,430
Reliability for Traffic	50, 90, and 95 (%)
Reliability for Soil	50, 90, and 95 (%)

Table A-35. Initial and Terminal Serviceability Index and Roughness Data for the Austin Loop 1 Site (Main Lane).

	Flexible		Rigid	
	Initial	Terminal	Initial	Terminal
SI	4.2	2.5	4.5	3.0
IRI (in/miles)	75.2	166.2	65.4	131.7

Input Data for the Austin Loop 1 Site (Frontage Road)

Table A-36. Environmental and Geometry Conditions for the Austin Loop 1 Site (Frontage Road).

TMI	-15.0
Lateral Slope	Fill
Longitudinal Drainage	Slope
Root Zone	0.0 (ft)
Depth of Moisture Active Zone, Zm	14.0 (ft)
Equilibrium Suction	3.45 (pF)

Table A-37. Soil Properties for Each Layer for the Austin Loop 1 Site (Frontage Road).

Soil Type	Layer	Thickness (ft)	LL (%)	PI (%)	-#200 (%)	-2μm (%)	γ_d (pcf)	
Natural Soil	1	5.0	49.0	29.0	84.9	42.0	100.0	
	2	3.0	68.0	33.0	91.8	30.0	100.0	
	3	6.0	68.0	35.0	90.6	18.0	105.0	
Inert Soil		1.5	25.0	10.0	10.0	1.0	130	
								% Lime
Stabilized Soil		1.5	60.0	28.0	80.0	25.0	120	8

Table A-38. Vertical Moisture Barrier and Wheel Path for the Austin Loop 1 Site (Frontage Road).

Depth of Vertical Moisture Barrier	0 and 8 (ft)
Width of Pavement (3 lanes)	50 (ft)
Number of Wheel Path	1
Distance from the Center of Pavement	15 (ft)

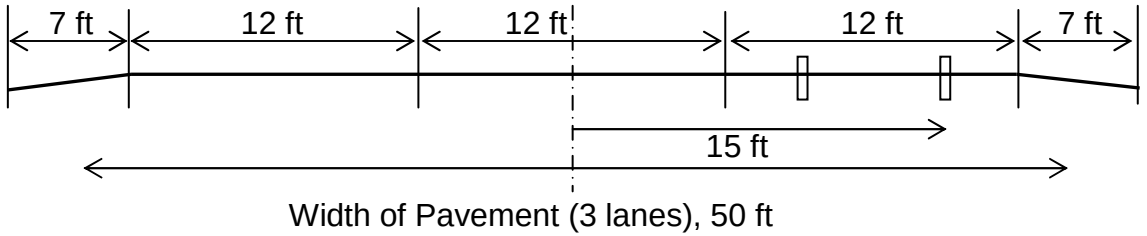

Figure A-6. Dimension of Cross Section of the Pavement for the Austin Loop 1 Site (Frontage Road).

Table A-39. Structural Properties of the Flexible Pavement for the Austin Loop 1 Site (Frontage Road).

SN	FWD	
(inches)	(psi)	SN = Structural Number, in FWD = Falling Weight Deflectometer Modulus of Subgrade Soil (from drop weight closest to 9k load, psi)
3.74-5.06	10,000	

Table A-40. Structural Properties of the Rigid Pavement for the Austin Loop 1 Site (Frontage Road).

D (inches)	fc (psi)	Sc (psi)	Cd	J	FWD (psi)	P_t
11.0-12.0	4,000	650	0.90	3.2	10,000	3

D = Thickness of Concrete Layer, in
fc = 28-day Compressive Strength of concrete, psi, Ec = 57000 $(fc)^{0.5}$, psi
Sc = Mean Modulus of Rupture of concrete, psi
Cd = Drainage Coefficient
J = Load Transfer Coefficient
FWD=Falling Weight Deflectometer Modulus of Subgrade Soil (from drop weight closet to 9000lb load, psi, k (pci) = M_R / 19.4
Pt = Terminal Serviceability Index for the Concrete Pavement

Table A-41. Traffic and Reliability Data for the Austin Loop 1 Site (Frontage Road).

Traffic Analysis Period, C	30 (yrs)
Average Daily Traffic of outer lane (T=0)	4,028
Average Daily Traffic of outer lane (T=C)	6,837
No of 18kip ESAL in the 30th years	2,472,059
Reliability for Traffic	50, 90, and 95 (%)
Reliability for Soil	50, 90, and 95 (%)

Table A-42. Initial and Terminal Serviceability Index and Roughness Data for the Austin Loop 1 Site (Frontage Road).

	Flexible		Rigid	
	Initial	Terminal	Initial	Terminal
SI	4.2	2.5	4.5	3.0
IRI (in/miles)	75.2	166.2	65.4	131.7

IRI (inch/mile) = 63.36×8.4193×exp(-0.4664×SI)

OUTPUT DATA FOR ANALYSIS OF SIX CASE STUDY SECTIONS USING NEW METHOD

The results of analysis of six study sections are presented in Table A-43 to A-60.

Output Data for Section A, Fort Worth North Loop IH 820

Table A-43. Results of Analysis of the Section A with Reliability of 50 % for the Flexible Pavement.

Case	Barrier (ft)	ACP (in)	Stab. Soil (ft)	Inert Soil (ft)	SN (in)	Movement(in) at the Edge			Movement (in) at the Outer Wheel Path	SI		IRI (in/mile)	
						Swelling	Shrinkage	Total		After 20yrs	After 30yrs	After 20yrs	After 30yrs
1	8.00	4.00	-	-	4.00	0.07	1.39	1.46	0.56	2.10	1.99	201	213
2	-	4.00	1.8	-	4.14	0.04	1.22	1.26	0.50	2.86	2.62	141	157
3	-	4.00	2.0	-	4.40	0.02	1.21	1.24	0.49	3.32	3.05	114	126

Table A-44. Results of Analysis of Section A with Reliability of 90 % for the Flexible Pavement.

Case	Barrier (ft)	ACP (in)	Stab. Soil (ft)	Inert Soil (ft)	SN (in)	Movement(in) at the Edge			Movement (in) at the Outer Wheel Path	SI		IRI (in/mile)	
						Swelling	Shrinkage	Total		After 20yrs	After 30yrs	After 20yrs	After 30yrs
1	-	4.00	2.5	-	5.06	0.02	1.16	1.19	0.45	2.91	2.67	137	153
2	-	4.00	2.5	1.5	5.06	0.01	1.04	1.07	0.40	3.03	2.78	130	146
3	-	4.50	2.5	1.5	5.28	0.01	1.04	1.07	0.40	3.30	3.03	114	129

Table A-45. Results of Analysis of Section A with Reliability of 95 % for the Rigid Pavement.

Case	Barrier (ft)	D (in)	Stab. Soil (ft)	Inert Soil (ft)		Movement(in) at the Edge			Movement (in) at the Outer Wheel Path	SI		IRI (in/miles)	
						Swelling	Shrinkage	Total		After 20yrs	After 30yrs	After 20yrs	After 30yrs
1	-	11.50	0.67	-		0.05	1.33	1.38	0.57	2.39	2.20	137	154
2	-	12.00	-	-		0.07	1.39	1.46	0.61	3.30	3.02	103	118
3	-	12.00	0.67	-		0.05	1.33	1.38	0.57	3.39	3.09	100	115
4		12.00	1.00	-		0.05	1.30	1.34	0.55	3.43	3.14	98	113

Output Data for the Section B, Fort Worth North Loop IH 820

Table a-46. Results of Analysis of Section B with Reliability of 50 % for the Flexible Pavement.

Case	Barrier (ft)	ACP (in)	Stab. Soil (ft)	Inert Soil (ft)	SN (in)	Movement(in) at the Edge			Movement (in) at the Outer Wheel Path	SI		IRI (in/mile)	
						Swelling	Shrinkage	Total		After 20yrs	After 30yrs	After 20yrs	After 30yrs
1	-	4.00	2.0	-	4.40	1.51	1.10	2.63	1.05	2.05	1.93	207	217
2	-	4.00	2.0	1.5	4.40	1.08	0.82	1.90	0.80	2.85	2.61	142	158
3	-	4.00	2.2	-	4.66	1.43	1.07	2.50	1.00	3.01	2.76	132	147
4	-	4.00	2.5	-	5.06	1.22	1.02	2.24	0.90	3.55	3.29	102	115

Table A-47. Results of Analysis of Section B with Reliability of 90 % for the Flexible Pavement.

Case	Barrier (ft)	ACP (in)	Stab. Soil (ft)	Inert Soil (ft)	SN (in)	Movement(in) at the Edge			Movement (in) at the Outer Wheel Path	SI		IRI (in/mile)	
						Swelling	Shrinkage	Total		After 20yrs	After 30yrs	After 20yrs	After 30yrs
1	-	4.00	2.5	2.5	5.06	0.72	0.66	1.37	0.59	2.48	2.29	167	182
2	-	4.50	2.5	1.5	5.28	0.90	0.77	1.67	0.70	2.65	2.43	154	170
3	-	5.00	2.5	1.5	5.50	0.90	0.77	1.67	0.70	3.06	2.80	128	144
4	-	4.00	3.0	1.5	5.72	0.61	0.67	1.28	0.53	3.52	3.26	103	117

Table A-48. Results of Analysis of Section B with Reliability of 95 % for the Rigid Pavement.

Case	Barrier (ft)	D (in)	Stab. Soil (ft)	Inert Soil (ft)		Movement(in) at the Edge			Movement (in) at the Outer Wheel Path	SI		IRI (in/miles)	
						Swelling	Shrinkage	Total		After 20yrs	After 30yrs	After 20yrs	After 30yrs
1	-	12.60	-	-		3.19	1.49	4.68	1.80	2.13	2.00	135	151
2	-	12.00	0.67	-		2.36	1.36	3.72	1.48	2.41	2.22	125	142
3	-	12.00	1.00	-		2.08	1.26	3.35	1.33	1.33	2.77	108	124
4		13.00	-	-		3.19	1.49	4.68	1.80	1.80	2.91	106	119

Output Data for the Section C, Fort Worth North Loop IH 820

Table A-49. Results of Analysis of Section C with Reliability of 50 % for the Flexible Pavement.

Case	Barrier (ft)	ACP (in)	Stab. Soil (ft)	Inert Soil (ft)	SN (in)	Movement(in) at the Edge			Movement (in) at the Outer Wheel Path	SI		IRI (in/mile)	
						Swelling	Shrinkage	Total		After 20yrs	After 30yrs	After 20yrs	After 30yrs
1	-	4.00	2.0	-	4.40	1.37	1.01	2.38	0.97	2.40	2.22	175	189
2	-	4.00	2.0	1.0	4.40	1.20	0.84	2.03	0.84	2.77	2.54	147	163
3	-	4.00	2.2	-	4.66	1.27	0.97	2.24	0.92	3.14	2.88	124	140
4	-	4.00	2.5	-	5.06	1.12	0.91	2.03	0.83	3.60	3.35	172	187

Table A-50. Results of Analysis of Section C with Reliability of 90 % for the Flexible Pavement.

Case	Barrier (ft)	ACP (in)	Stab. Soil (ft)	Inert Soil (ft)	SN (in)	Movement(in) at the Edge			Movement (in) at the Outer Wheel Path	SI		IRI (in/mile)	
						Swelling	Shrinkage	Total		After 20yrs	After 30yrs	After 20yrs	After 30yrs
1	-	4.00	2.5	1.5	5.06	0.78	0.66	1.44	0.60	2.41	2.23	172	187
2	-	4.50	2.5	1.0	5.28	0.96	0.74	1.70	0.70	2.65	2.44	154	170
3	-	4.50	2.5	1.5	5.28	0.78	0.66	1.44	0.60	2.93	2.68	136	152
4	-	4.00	3.0	-	5.72	0.89	0.82	1.70	0.69	3.33	3.07	113	127
5	-	4.50	3.0	-	5.94	0.89	0.82	1.70	0.69	3.51	3.51	104	117

Table A-51. Results of Analysis of Section C with Reliability of 95 % for the Rigid Pavement.

Case	Barrier (ft)	D (in)	Stab. Soil (ft)	Inert Soil (ft)		Movement(in) at the Edge			Movement (in) at the Outer Wheel Path	SI		IRI (in/miles)	
						Swelling	Shrinkage	Total		After 20yrs	After 30yrs	After 20yrs	After 30yrs
1	-	12.00	1.0	-		1.90	1.21	3.10	1.29	2.46	2.27	129	145
2	-	12.50	-	-		2.58	1.33	3.91	1.62	2.75	2.52	115	132
3	-	12.00	1.50	-		1.62	1.10	2.72	1.13	2.99	2.74	113	128
4	8.0	12.50	-	-		2.58	1.33	3.91	1.42	3.35	3.06	98	112
5		13.00	-	-		2.58	1.33	3.91	1.62	3.65	3.35	89	120

Output Data for the Atlanta US 271 Site

Table A-52. Results of Analysis of the Atlanta US 271 Site with Reliability of 50 % for the Flexible Pavement.

Case	Barrier (ft)	ACP (in)	Stab. Soil (ft)	Inert Soil (ft)	SN (in)	Movement(in) at the Edge			Movement (in) at the Outer Wheel Path	SI		IRI (in/mile)	
						Swelling	Shrinkage	Total		After 20yrs	After 30yrs	After 20yrs	After 30yrs
1	-	4.00	-	-	4.00	0.58	1.03	1.61	1.26	2.81	2.58	145	161
2	8.0	4.00	-	-	4.00	0.58	1.03	1.61	1.04	3.18	2.92	122	137
3	-	4.00	2.0	-	4.00	0.32	0.97	1.30	1.04	3.22	2.95	120	135

Table A-53. Results of Analysis of the Atlanta US 271 Site with Reliability of 90 % for the Flexible Pavement.

Case	Barrier (ft)	ACP (in)	Stab. Soil (ft)	Inert Soil (ft)	SN (in)	Movement(in) at the Edge			Movement (in) at the Outer Wheel Path	SI		IRI (in/mile)	
						Swelling	Shrinkage	Total		After 20yrs	After 30yrs	After 20yrs	After 30yrs
1	-	4.50	2.0	-	4.62	0.32	0.97	1.30	1.04	2.39	2.22	174	188
2	-	4.00	2.2	-	4.66	0.30	0.97	1.27	1.02	2.61	2.40	157	173
3	-	4.50	2.0	1.5	4.62	0.23	0.85	1.08	0.88	0.88	2.93	136	152
4	-	4.50	2.2	-	4.88	0.30	0.97	1.27	1.02	1.02	3.08	127	143
5	-	4.00	1.5	-	5.06	0.28	0.96	1.24	1.00	1.00	3.35	112	127

Table A-54. Results of Analysis of the Atlanta US 271 Site with Reliability of 95 % for the Rigid Pavement.

Case	Barrier (ft)	D (in)	Stab. Soil (ft)	Inert Soil (ft)		Movement(in) at the Edge			Movement (in) at the Outer Wheel Path	SI		IRI (in/miles)	
						Swelling	Shrinkage	Total		After 20yrs	After 30yrs	After 20yrs	After 30yrs
1	-	10.50	-	-		0.58	1.03	1.61	1.26	2.56	2.35	127	145
2	-	11.00	-	-		0.58	1.03	1.61	1.26	3.63	3.33	92	107
3	-	12.00	-	-		0.58	1.03	1.61	1.26	4.22	4.01	74	81

Output Data for the Austin Loop 1 Site (Main Lane)

Table A-55. Results of Analysis of the Austin Loop 1 Site (Main Lane) with Reliability of 50 % for the Flexible Pavement.

Case	Barrier (ft)	ACP (in)	Stab. Soil (ft)	Inert Soil (ft)	SN (in)	Movement(in) at the Edge			Movement (in) at the Outer Wheel Path	SI		IRI (in/mile)	
						Swelling	Shrinkage	Total		After 20yrs	After 30yrs	After 20yrs	After 30yrs
1	-	4.00	2.2	1.0	4.66	0.85	0.62	1.48	0.99	2.72	2.50	151	166
2	-	4.00	2.2	1.5	4.66	0.73	0.56	1.31	0.89	2.93	2.68	137	153
3	-	4.00	2.5	-	5.06	0.86	0.70	1.56	1.01	3.32	3.06	114	129

Table A-56. Results of Analysis of the Austin Loop 1 Site (Main Lane) with Reliability of 90 % for the Flexible Pavement.

Case	Barrier (ft)	ACP (in)	Stab. Soil (ft)	Inert Soil (ft)	SN (in)	Movement(in) at the Edge			Movement (in) at the Outer Wheel Path	SI		IRI (in/mile)	
						Swelling	Shrinkage	Total		After 20yrs	After 30yrs	After 20yrs	After 30yrs
1	-	4.50	2.8	-	5.68	0.78	0.66	1.44	0.93	2.48	2.29	167	182
2	-	4.00	2.8	1.5	5.46	0.55	0.50	1.06	0.70	2.74	2.51	149	164
3	-	4.00	3.0	-	5.72	0.70	0.64	1.33	0.85	2.83	2.59	143	158
4	-	4.00	3.0	1.5	5.72	0.50	0.48	0.98	0.65	3.25	2.98	118	133

Table A-57. Results of Analysis of the Austin Loop 1 Site (Main Lane) with Reliability of 95 % for the Rigid Pavement.

Case	Barrier (ft)	D (in)	Stab. Soil (ft)	Inert Soil (ft)		Movement(in) at the Edge			Movement (in) at the Outer Wheel Path	SI		IRI (in/mile)	
						Swelling	Shrinkage	Total		After 20yrs	After 30yrs	After 20yrs	After 30yrs
1	-	13.20	-	-		2.03	1.00	3.01	2.10	3.25	2.98	121	138
2	13.0	12.00	-	-		2.03	1.00	3.01	1.19	2.46	2.27	121	138
3	-	12.00	2.0	-		1.03	0.76	1.79	1.19	2.61	2.39	122	138
4	-	12.00	1.5	1.5		0.98	0.65	1.63	1.15	2.81	2.57	116	132
5	10.0	12.50	-	-		2.03	1.00	3.01	1.47	2.93	2.67	111	127
6	-	12.00	2.0	1.5		0.82	0.59	1.40	0.96	3.33	3.04	100	115

Output Data for the Austin Loop 1 Site (Frontage Road)

Table A-58. Results of Analysis of the Austin Loop 1 Site (Frontage Road) with Reliability of 50 % for the Flexible Pavement.

Case	Barrier (ft)	ACP (in)	Stab. Soil (ft)	Inert Soil (ft)	SN (in)	Movement(in) at the Edge			Movement (in) at the Outer Wheel Path	SI		IRI (in/mile)	
						Swelling	Shrinkage	Total		After 20yrs	After 30yrs	After 20yrs	After 30yrs
1	-	4.00	1.5	-	3.74	2.03	1.00	3.01	1.80	2.55	2.35	166	181
2	8.0	4.00	-	-	4.00	1.12	0.78	1.88	1.39	3.44	3.17	108	122
3	-	4.00	1.8	-	4.14	1.21	0.82	2.03	1.51	2.36	2.19	179	193
4	-	4.00	1.5	1.5	3.74	0.98	0.65	1.63	1.24	3.02	2.77	131	147

Table A-59. Results of Analysis of the Austin Loop 1 Site (Frontage Road) with Reliability of 90 % for the Flexible Pavement.

Case	Barrier (ft)	ACP (in)	Stab. Soil (ft)	Inert Soil (ft)	SN (in)	Movement(in) at the Edge			Movement (in) at the Outer Wheel Path	SI		IRI (in/mile)	
						Swelling	Shrinkage	Total		After 20yrs	After 30yrs	After 20yrs	After 30yrs
1	-	4.00	2.0	2.5	4.40	0.61	0.49	1.10	0.83	2.63	2.42	156	171
2	-	4.00	2.2	1.5	4.66	0.73	0.56	1.31	0.96	2.90	2.65	138	154
3	-	4.00	2.5	-	5.06	0.86	0.70	3.01	1.11	3.23	2.97	119	134

Table A-60. Results of Analysis of the Austin Loop 1 Site (Frontage Road) with Reliability of 95 % for the Rigid Pavement.

Case	Barrier (ft)	D (in)	Stab. Soil (ft)	Inert Soil (ft)		Movement(in) at the Edge			Movement (in) at the Outer Wheel Path	SI		IRI (in/mile)	
						Swelling	Shrinkage	Total		After 20yrs	After 30yrs	After 20yrs	After 30yrs
1	-	11.00	-	-		2.03	1.00	3.01	2.28	3.54	3.25	92	105
2	-	11.50	-	-		2.03	1.00	3.01	2.28	4.01	3.75	78	88
3	-	12.00	-	-		2.03	1.00	3.01	2.28	4.22	4.02	73	80

RESULTS OF ANALYSIS FOR SIX STUDY SECTIONS USING PVR METHOD (TEX-124-E)

The results of calculation using the Tex-124-E method for several cases on study six sections are presented in Table A-61 through A-94.

Analysis of the Case with No Surcharge and No Treatment

Table A-61. Calculations with No Surcharge and No Treatment for Section A, Fort Worth North Loop IH 820.

Depth (ft.)	Avg. Load (psi)	LL (%)	Dry 0.2LL+9 (%)	Wet 0.47LL+2 (%)	Moisture (%)	Dry/ Avg/Wet	No. 40 (%)	PI (%)	Volume Swell (%)	Free swell (%)	PVR, Top of Layer (in)	PVR, Bottom of Layer (in)	Diff. (in)	Mod.- No.40 factor	Mod. Density factor	PVR in Layer (in.)
0.0-2.0	1	60	22.2	30.2	25.4	dry	100	28	7.5	10.6	0.00	0.62	0.62	1	1	0.62
2.0-4.0	3	60	22.2	30.2	25.4	dry	100	28	7.5	10.6	0.62	1.15	0.53	1	1	0.53
4.0-6.0	5	60	22.2	30.2	25.4	dry	100	25	6.5	9.6	1.06	1.45	0.39	1	1	0.39
6.0-8.0	7	60	22.2	30.2	27.0	wet	100	25	6.5	9.6	1.45	1.55	0.1	1	1	0.10
8.0-10.0	9	60	22.2	30.2	23.8	dry	100	25	6.5	9.6	1.55	1.72	0.17	1	1	0.17
10.0-12.0	11	65	23.3	32.55	23.8	dry	100	35	10	13.3	2.90	3.00	0.1	1	1	0.10
12.0-14.0	13	65	23.3	32.55	24.8	dry	100	35	10	13.3	3.00	3.20	0.2	1	1	0.20
14.0-16.0	15	65	23.3	32.55	24.8	dry	100	35	10	13.3	3.20	3.31	0.11	1	1	0.11
NOTE : no surcharge and no treatment on sugrade soil														Total PVR (in) =		2.22

Table A-62. Calculations with No Surcharge and No Treatment for Section B, Fort Worth North Loop IH 820.

Depth (ft.)	Avg. Load (psi)	LL (%)	Dry 0.2LL+9 (%)	Wet 0.47LL+2 (%)	Moisture (%)	Dry/ Avg/Wet	No. 40 (%)	PI (%)	Volume Swell (%)	Free swell (%)	PVR, Top of Layer (in)	PVR, Bottom of Layer (in)	Diff. (in)	Mod.- No.40 factor	Mod. Density factor	PVR in Layer (in.)
0.0-2.0	1.00	60	22.2	30.2	12.8	dry	100	36	10.5	13.8	0.00	0.62	0.62	1	1	0.62
2.0-4.0	3.00	55	21.1	27.85	20.2	dry	100	30	8.4	11.6	0.60	1.28	0.68	1	1	0.68
4.0-6.0	5.00	55	21.1	27.85	11.35	dry	100	30	8.4	11.6	1.28	1.75	0.47	1	1	0.47
6.0-8.0	7.00	65	23.3	32.55	11.35	dry	100	38	11.1	14.5	2.22	2.70	0.48	1	1	0.48
8.0-10.0	9.00	65	23.3	32.55	18.41	dry	100	38	11.1	14.5	2.70	3.08	0.38	1	1	0.38
10.0-12.0	11.00	53	20.66	26.91	18.41	dry	100	32	9.0	12.2	2.38	2.69	0.31	1	1	0.31
12.0-14.0	13.00	45	18.9	23.15	18.41	dry	100	25	6.5	9.6	1.80	1.90	0.1	1	1	0.1
14.0-16.0	15.00	45	18.9	23.15	24.9	dry	100	15	3.0	5.8	0.58	0.61	0.03	1	1	0.03
NOTE : no surcharge and no treatment on sugrade soil														Total PVR (in) =		3.07

Table A-63. Calculations with No Surcharge and No Treatment for Section C, Fort Worth North Loop IH 820.

Depth (ft.)	Avg. Load (psi)	LL (%)	Dry 0.2LL+9 (%)	Wet 0.47LL+2 (%)	Moisture (%)	Dry/ Avg/Wet	No. 40 (%)	PI (%)	Volume Swell (%)	Free swell (%)	PVR, Top of Layer (in)	PVR, Bottom of Layer (in)	Diff. (in)	Mod.- No.40 factor	Mod. Density factor	PVR in Layer (in.)
0.0-2.0	1.00	55	21.1	27.85	22.8	dry	100	30	8.3	11.5	0.00	0.61	0.61	1	1	0.61
2.0-4.0	3.00	62	22.64	31.14	22.8	dry	100	36	10.5	13.8	0.60	1.41	0.81	1	1	0.81
4.0-6.0	5.00	62	22.64	31.14	25.0	dry	100	36	10.5	13.8	1.41	2.08	0.67	1	1	0.67
6.0-8.0	7.00	50	20	25.5	24.8	wet	100	31	4.0	6.9	0.72	0.82	0.1	1	1	0.1
8.0-10.0	9.00	50	20	25.5	25.2	wet	100	31	4	6.9	0.82	0.91	0.09	1	1	0.09
10.0-12.0	11.00	52	20.44	26.44	25.2	wet	100	28	3.5	6.3	0.72	0.78	0.06	1	1	0.06
12.0-14.0	13.00	52	20.44	26.44	25.2	wet	100	28	3.5	6.3	0.78	0.8	0.02	1	1	0.02
14.0-16.0	15.00	52	20.44	26.44	25.2	wet	100	28	3.5	6.3	0.8	0.8	0	1	1	0
NOTE : no surcharge and no treatment on sugrade soil														Total PVR (in) =		2.36

Table A-64. Calculations with No Surcharge and No Treatment for the Atlanta US 271 Site.

Depth (ft.)	Avg. Load (psi)	LL (%)	Dry 0.2LL+9 (%)	Wet 0.47LL+2 (%)	Moisture (%)	Dry/ Avg/Wet	No. 40 (%)	PI (%)	Volume Swell (%)	Free swell (%)	PVR, Top of Layer (in)	PVR, Bottom of Layer (in)	Diff. (in)	Mod.- No.40 factor	Mod. Density factor	PVR in Layer (in.)
0.0-2.0	1.00	48	19.56	24.56	16.1	dry	100	26	6.8	9.9	0.00	0.58	0.58	1	1	0.58
2.0-4.0	3.00	48	19.56	24.56	16.1	dry	100	26	6.8	9.9	0.58	1.10	0.52	1	1	0.52
4.0-6.0	5.00	37	17.14	19.39	17	dry	100	17	3.5	6.3	0.50	0.65	0.15	1	1	0.15
6.0-8.0	7.00	37	17.14	19.39	17	dry	100	17	3.5	6.3	0.65	0.72	0.07	1	1	0.07
8.0-10.0	9.00	40	17.8	20.8	16.7	dry	100	25	6.5	9.6	1.60	1.75	0.15	1	1	0.15
10.0-12.0	11.00	40	17.8	20.8	16.7	dry	100	25	6.5	9.6	1.75	1.82	0.07	1	1	0.07
12.0-14.0	13.00	37	17.14	19.39	15.8	dry	100	15	2.8	5.6	0.51	0.56	0.05	1	1	0.05
14.0-16.0	15.00	37	17.14	19.39	15.8	dry	100	15	2.8	5.6	0.56	0.58	0.02	1	1	0.02
16.0-18.0	17.00	37	17.14	19.39	15.8	dry	100	15	2.8	5.6	0.58	0.59	0.01	1	1	0.01
NOTE : no surcharge and no treatment on sugrade soil														Total PVR (in) =		1.62

Table A-65. Calculations with No Surcharge and No Treatment for the Austin Loop 1 Site.

Depth (ft.)	Avg. Load (psi)	LL (%)	Dry 0.2LL+9 (%)	Wet 0.47LL+2 (%)	Moisture (%)	Dry/ Avg/Wet	No. 40 (%)	PI (%)	Volume Swell (%)	Free swell (%)	PVR, Top of Layer (in)	PVR, Bottom of Layer (in)	Diff. (in)	Mod.- No.40 factor	Mod. Density factor	PVR in Layer (in.)
0.0-2.0	1.00	49	19.78	25.03	19.03	dry	100	29	8.0	11.2	0.00	0.60	0.6	1	1	0.6
2.0-4.0	3.00	49	19.78	25.03	19.03	dry	100	29	8.0	11.2	0.60	1.14	0.54	1	1	0.54
4.0-6.0	5.00	68	23.96	33.96	23.11	dry	100	33	9.4	12.7	1.35	1.94	0.59	1	1	0.59
6.0-8.0	7.00	68	23.96	33.96	23.11	dry	100	33	9.4	12.7	1.94	2.30	0.36	1	1	0.36
8.0-10.0	9.00	68	23.96	33.96	23.00	dry	100	33	9.4	12.7	2.30	2.58	0.28	1	1	0.28
10.0-12.0	11.00	68	23.96	33.96	23.00	dry	100	35	10.5	13.8	2.85	3.12	0.27	1	1	0.27
12.0-14.0	13.00	68	23.96	33.96	24.09	dry	100	35	10.5	13.8	3.12	3.30	0.18	1	1	0.18
14.0-16.0	15.00	68	23.96	33.96	24.09	dry	100	35	10.5	13.8	3.30	3.45	0.15	1	1	0.15
NOTE : no surcharge and no treatment on subgrade, assume the same soil profile for a Main Lanes and a Frontage Load														Total PVR (in) =		2.97

Analysis of the Case with the Surcharge of 1 psi and No Treatment

Table A-66. Calculations with the Surcharge of 1 psi and No Treatment for Section A, Fort Worth North Loop IH 820.

Depth (ft.)	Avg. Load (psi)	LL (%)	Dry 0.2LL+9 (%)	Wet 0.47LL+2 (%)	Moisture (%)	Dry/ Avg/Wet	No. 40 (%)	PI (%)	Volume Swell (%)	Free swell (%)	PVR, Top of Layer (in)	PVR, Bottom of Layer (in)	Diff. (in)	Mod.- No.40 factor	Mod. Density factor	PVR in Layer (in.)
0.0-2.0	2	60	22.2	30.2	25.4	dry	100	28	7.5	10.6	0.60	0.95	0.35	1	1	0.35
2.0-4.0	4	60	22.2	30.2	25.4	dry	100	28	7.5	10.6	0.95	1.40	0.45	1	1	0.45
4.0-6.0	6	60	22.2	30.2	25.4	dry	100	25	6.5	9.6	1.25	1.50	0.25	1	1	0.25
6.0-8.0	8	60	22.2	30.2	27	wet	100	25	6.5	9.6	1.50	1.68	0.18	1	1	0.18
8.0-10.0	10	60	22.2	30.2	23.8	dry	100	25	6.5	9.6	1.68	1.80	0.12	1	1	0.12
10.0-12.0	12	65	23.3	32.55	23.8	dry	100	35	10	13.3	2.90	3.12	0.22	1	1	0.22
12.0-14.0	14	65	23.3	32.55	24.8	dry	100	35	10	13.3	3.12	3.29	0.17	1	1	0.17
14.0-16.0	16	65	23.3	32.55	24.8	dry	100	35	10	13.3	3.29	3.42	0.13	1	1	0.13
NOTE : assume a surcharge load of 1 psi beneath pavement within a pavement, no treatment on sugrade soil														Total PVR (in) =		1.87

Table A-67. Calculations with the Surcharge of 1 psi and No Treatment for Section B, Fort Worth North Loop IH 820.

Depth (ft.)	Avg. Load (psi)	LL (%)	Dry 0.2LL+9 (%)	Wet 0.47LL+2 (%)	Moisture (%)	Dry/ Avg/Wet	No. 40 (%)	PI (%)	Volume Swell (%)	Free swell (%)	PVR, Top of Layer (in)	PVR, Bottom of Layer (in)	Diff. (in)	Mod.- No.40 factor	Mod. Density factor	PVR in Layer (in.)
0.0-2.0	2	60	22.2	30.2	12.8	dry	100	36	10.5	13.8	0.60	1.00	0.4	1	1	0.4
2.0-4.0	4	55	21.1	27.85	20.2	dry	100	30	8.4	11.6	0.98	1.55	0.57	1	1	0.57
4.0-6.0	6	55	21.1	27.85	11.35	dry	100	30	8.4	11.6	1.55	1.91	0.36	1	1	0.36
6.0-8.0	8	65	23.3	32.55	11.35	dry	100	38	11.1	14.5	2.45	2.90	0.45	1	1	0.45
8.0-10.0	10	65	23.3	32.55	18.41	dry	100	38	11.1	14.5	2.90	3.24	0.34	1	1	0.34
10.0-12.0	12	53	20.66	26.91	18.41	dry	100	32	9.0	12.2	2.61	2.80	0.19	1	1	0.19
12.0-14.0	14	45	18.9	23.15	18.41	dry	100	25	6.5	9.6	1.85	1.92	0.07	1	1	0.07
14.0-16.0	16	45	18.9	23.15	24.9	dry	100	15	3.0	5.8	0.61	0.62	0.01	1	1	0.01
NOTE : assume a surcharge load of 1 psi beneath pavement within a pavement, no treatment on sugrade soil														Total PVR (in) =		2.39

Table A-68. Calculations with the Surcharge of 1 psi and No Treatment for Section C, Fort Worth North Loop IH 820.

Depth (ft.)	Avg. Load (psi)	LL (%)	Dry 0.2LL+9 (%)	Wet 0.47LL+2 (%)	Moisture (%)	Dry/ Avg/Wet	No. 40 (%)	PI (%)	Volume Swell (%)	Free swell (%)	PVR, Top of Layer (in)	PVR, Bottom of Layer (in)	Diff. (in)	Mod.- No.40 factor	Mod. Density factor	PVR in Layer (in.)
0.0-2.0	2	55	21.1	27.85	22.8	dry	100	30	8.3	11.5	0.60	0.78	0.18	1	1	0.18
2.0-4.0	4	62	22.64	31.14	22.8	dry	100	36	10.5	13.8	1.02	1.79	0.77	1	1	0.77
4.0-6.0	6	62	22.64	31.14	25.0	dry	100	36	10.5	13.8	1.79	2.31	0.52	1	1	0.52
6.0-8.0	8	50	20	25.5	24.8	wet	100	31	4.0	6.9	1.05	1.17	0.12	1	1	0.12
8.0-10.0	10	50	20	25.5	25.2	wet	100	31	4.0	6.9	1.17	1.21	0.04	1	1	0.04
10.0-12.0	12	52	20.44	26.44	25.2	wet	100	28	3.5	6.3	1.03	1.08	0.05	1	1	0.05
12.0-14.0	14	52	20.44	26.44	25.2	wet	100	28	3.5	6.3	1.08	1.09	0.01	1	1	0.01
14.0-16.0	16	52	20.44	26.44	25.2	wet	100	28	3.5	6.3	1.09	1.1	0.01	1	1	0.01
NOTE : assume a surcharge load of 1 psi beneath pavement within a pavement, no treatment on sugrade soil														Total PVR (in) =		1.70

Table A-69. Calculations with the Surcharge of 1 psi and No Treatment for the Atlanta US 271 Site.

Depth (ft.)	Avg. Load (psi)	LL (%)	Dry 0.2LL+9 (%)	Wet 0.47LL+2 (%)	Moisture (%)	Dry/ Avg/Wet	No. 40 (%)	PI (%)	Volume Swell (%)	Free swell (%)	PVR, Top of Layer (in)	PVR, Bottom of Layer (in)	Diff. (in)	Mod.- No.40 factor	Mod. Density factor	PVR in Layer (in.)
0.0-2.0	2	48	19.56	24.56	16.1	dry	100	26	6.8	9.9	0.55	0.90	0.35	1	1	0.35
2.0-4.0	4	48	19.56	24.56	16.1	dry	100	26	6.8	9.9	0.90	1.30	0.4	1	1	0.4
4.0-6.0	6	37	17.14	19.39	17	dry	100	17	3.5	6.3	0.61	0.70	0.09	1	1	0.09
6.0-8.0	8	37	17.14	19.39	17	dry	100	17	3.5	6.3	0.70	0.72	0.02	1	1	0.02
8.0-10.0	10	40	17.8	20.8	16.7	dry	100	25	6.5	9.6	1.70	1.82	0.12	1	1	0.12
10.0-12.0	12	40	17.8	20.8	16.7	dry	100	25	6.5	9.6	1.82	1.93	0.11	1	1	0.11
12.0-14.0	14	37	17.14	19.39	15.8	dry	100	15	2.8	5.6	0.55	0.58	0.03	1	1	0.03
14.0-16.0	16	37	17.14	19.39	15.8	dry	100	15	2.8	5.6	0.58	0.60	0.02	1	1	0.02
16.0-18.0	18	37	17.14	19.39	15.8	dry	100	15	2.8	5.6	0.60	0.62	0.02	1	1	0.02
NOTE : assume a surcharge load of 1 psi beneath pavement within a pavement, no treatment on sugrade soil														Total PVR (in) =		1.16

Table A-70. Calculations with the Surcharge of 1 psi and No Treatment for the Austin Loop 1 Site.

Depth (ft.)	Avg. Load (psi)	LL (%)	Dry 0.2LL+9 (%)	Wet 0.47LL+2 (%)	Moisture (%)	Dry/ Avg/Wet	No. 40 (%)	PI (%)	Volume Swell (%)	Free swell (%)	PVR, Top of Layer (in)	PVR, Bottom of Layer (in)	Diff. (in)	Mod.- No.40 factor	Mod. Density factor	PVR in Layer (in.)
0.0-2.0	2	49	19.78	25.03	19.03	dry	100	29	8.0	11.2	0.61	0.98	0.37	1	1	0.37
2.0-4.0	4	49	19.78	25.03	19.03	dry	100	29	8.0	11.2	0.98	1.35	0.37	1	1	0.37
4.0-6.0	6	68	23.96	33.96	23.11	dry	100	33	9.4	12.7	1.65	2.12	0.47	1	1	0.47
6.0-8.0	8	68	23.96	33.96	23.11	dry	100	33	9.4	12.7	2.12	2.43	0.31	1	1	0.31
8.0-10.0	10	68	23.96	33.96	23.00	dry	100	33	9.4	12.7	2.43	2.72	0.29	1	1	0.29
10.0-12.0	12	68	23.96	33.96	23.00	dry	100	35	10.5	13.8	3.00	3.21	0.21	1	1	0.21
12.0-14.0	14	68	23.96	33.96	24.09	dry	100	35	10.5	13.8	3.21	3.43	0.22	1	1	0.22
14.0-16.0	16	68	23.96	33.96	24.09	dry	100	35	10.5	13.8	3.43	3.56	0.13	1	1	0.13
														Total PVR (in) =		2.37
NOTE : assume a surcharge load of 1 psi beneath pavement within a pavement, no treatment on sugrade soil, assume the same soil profile for a Main Lanes and a Frontage Load																

Analysis of the Case with No Surcharge and Treatment for the Pavement Acceptable Predicted Performance at the Edge.

Table A-71. Calculations with No Surcharge and Treatment for the Flexible Pavement for Section A, Fort Worth North Loop IH 820.

Depth (ft.)	Avg. Load (psi)	LL (%)	Dry 0.2LL+9 (%)	Wet 0.47LL+2 (%)	Moisture (%)	Dry/ Avg/Wet	No. 40 (%)	PI (%)	Volume Swell (%)	Free swell (%)	PVR, Top of Layer (in)	PVR, Bottom of Layer (in)	Diff. (in)	Mod.- No.40 factor	Mod. Density factor	PVR in Layer (in.)
0.0-2.0	1	30	15.6	16.1	15	dry	100	15	3.0	5.8	0.00	0.20	0.2	1	0.85	0.17
2.0-4.0	3	60	22.2	30.2	25.4	dry	100	28	7.5	10.6	0.62	1.15	0.53	1	1	0.53
4.0-6.0	5	60	22.2	30.2	25.4	dry	100	25	6.5	9.6	1.06	1.45	0.39	1	1	0.39
6.0-8.0	7	60	22.2	30.2	27.0	wet	100	25	6.5	9.6	1.45	1.55	0.1	1	1	0.1
8.0-10.0	9	60	22.2	30.2	23.8	dry	100	25	6.5	9.6	1.55	1.72	0.17	1	1	0.17
10.0-12.0	11	65	23.3	32.55	23.8	dry	100	35	10	13.3	2.90	3.00	0.1	1	1	0.1
12.0-14.0	13	65	23.3	32.55	24.8	dry	100	35	10	13.3	3.00	3.20	0.2	1	1	0.2
14.0-16.0	15	65	23.3	32.55	24.8	dry	100	35	10	13.3	3.20	3.31	0.11	1	1	0.11
NOTE :no surcharge, LTS 2.5 ft thick. (LL=30%, PI=15%, w=15%, Mod. Density factor =0.85)														Total PVR (in) =		1.77

Table A-72. Calculations with No Surcharge and Treatment for the Rigid Pavement for Section A, Fort Worth North Loop IH 820.

Depth (ft.)	Avg. Load (psi)	LL (%)	Dry 0.2LL+9 (%)	Wet 0.47LL+2 (%)	Moisture (%)	Dry/ Avg/Wet	No. 40 (%)	PI (%)	Volume Swell (%)	Free swell (%)	PVR, Top of Layer (in)	PVR, Bottom of Layer (in)	Diff. (in)	Mod.- No.40 factor	Mod. Density factor	PVR in Layer (in.)
0.0-2.0	1	60	22.2	30.2	25.4	dry	100	28	7.5	10.6	0.00	0.62	0.62	1	1	0.62
2.0-4.0	3	60	22.2	30.2	25.4	dry	100	28	7.5	10.6	0.62	1.15	0.53	1	1	0.53
4.0-6.0	5	60	22.2	30.2	25.4	dry	100	25	6.5	9.6	1.06	1.45	0.39	1	1	0.39
6.0-8.0	7	60	22.2	30.2	27	wet	100	25	6.5	9.6	1.45	1.55	0.1	1	1	0.1
8.0-10.0	9	60	22.2	30.2	23.8	dry	100	25	6.5	9.6	1.55	1.72	0.17	1	1	0.17
10.0-12.0	11	65	23.3	32.55	23.8	dry	100	35	10	13.3	2.90	3.00	0.1	1	1	0.1
12.0-14.0	13	65	23.3	32.55	24.8	dry	100	35	10	13.3	3.00	3.20	0.2	1	1	0.2
14.0-16.0	15	65	23.3	32.55	24.8	dry	100	35	10	13.3	3.20	3.31	0.11	1	1	0.11
NOTE: no surcharge, no treatment on subgrade soil														Total PVR (in) =		2.22

Table A-73. Calculations with No Surcharge and Treatment for the Flexible Pavement for Section B, Fort Worth North Loop IH 820.

Depth (ft.)	Avg. Load (psi)	LL (%)	Dry 0.2LL+9 (%)	Wet 0.47LL+2 (%)	Moisture (%)	Dry/ Avg/Wet	No. 40 (%)	PI (%)	Volume Swell (%)	Free swell (%)	PVR, Top of Layer (in)	PVR, Bottom of Layer (in)	Diff. (in)	Mod.- No.40 factor	Mod. Density factor	PVR in Layer (in.)
0.0-2.0	1	30	15.6	16.1	15	dry	100	15	3	5.8	0.00	0.20	0.2	1	0.85	0.17
2.0-4.0	3.00	20	13.4	11.4	20	dry	100	10	1.0	3.7	0.12	0.22	0.1	1	0.8	0.08
4.0-6.0	5.00	55	21.1	27.85	11.35	dry	100	30	8.4	11.6	1.28	1.75	0.47	1	1	0.47
6.0-8.0	7.00	65	23.3	32.55	11.35	dry	100	38	11.1	14.5	2.22	2.70	0.48	1	1	0.48
8.0-10.0	9.00	65	23.3	32.55	18.41	dry	100	38	11.1	14.5	2.70	3.08	0.38	1	1	0.38
10.0-12.0	11.00	53	20.66	26.91	18.41	dry	100	32	9.0	12.2	2.38	2.69	0.31	1	1	0.31
12.0-14.0	13.00	45	18.9	23.15	18.41	dry	100	25	6.5	9.6	1.80	1.90	0.1	1	1	0.1
14.0-16.0	15.00	45	18.9	23.15	24.9	dry	100	15	3.0	5.8	0.58	0.61	0.03	1	1	0.03
														Total PVR (in) =		2.02
NOTE :no surcharge, LTS 2.5 ft thick. (LL=30%, PI=15%, w=15%, Mod. Density factor =0.85), Inert 1.5 ft (LL=25%, PI=10%, w=20%, Mod. Density factor=0.8)																

Table A-74. Calculations with No Surcharge and Treatment for the Rigid Pavement for Section B, Fort Worth North Loop IH 820.

Depth (ft.)	Avg. Load (psi)	LL (%)	Dry 0.2LL+9 (%)	Wet 0.47LL+2 (%)	Moisture (%)	Dry/ Avg/Wet	No. 40 (%)	PI (%)	Volume Swell (%)	Free swell (%)	PVR, Top of Layer (in)	PVR, Bottom of Layer (in)	Diff. (in)	Mod.- No.40 factor	Mod. Density factor	PVR in Layer (in.)
0.0-2.0	1.00	40	17.8	20.8	20	dry	100	25	3	6.5	0.00	0.28	0.28	1	0.85	0.238
2.0-4.0	3.00	55	21.1	27.85	20.2	dry	100	30	8.4	11.6	0.60	1.28	0.68	1	1	0.68
4.0-6.0	5.00	55	21.1	27.85	11.35	dry	100	30	8.4	11.6	1.28	1.75	0.47	1	1	0.47
6.0-8.0	7.00	65	23.3	32.55	11.35	dry	100	38	11.1	14.5	2.22	2.70	0.48	1	1	0.48
8.0-10.0	9.00	65	23.3	32.55	18.41	dry	100	38	11.1	14.5	2.70	3.08	0.38	1	1	0.38
10.0-12.0	11.00	53	20.66	26.91	18.41	dry	100	32	9.0	12.2	2.38	2.69	0.31	1	1	0.31
12.0-14.0	13.00	45	18.9	23.15	18.41	dry	100	25	6.5	9.6	1.80	1.90	0.1	1	1	0.1
14.0-16.0	15.00	45	18.9	23.15	24.9	dry	100	15	3.0	5.8	0.58	0.61	0.03	1	1	0.03
NOTE :no surcharge, LTS 8.0 in thick. (LL=30%, PI=15%, w=15%, Mod. Density factor =0.85)														Total PVR (in) =		2.69

Table A-75. Calculations with No Surcharge and Treatment for the Flexible Pavement for Section C, Fort Worth North Loop IH 820.

Depth (ft.)	Avg. Load (psi)	LL (%)	Dry 0.2LL+9 (%)	Wet 0.47LL+2 (%)	Moisture (%)	Dry/ Avg/Wet	No. 40 (%)	PI (%)	Volume Swell (%)	Free swell (%)	PVR, Top of Layer (in)	PVR, Bottom of Layer (in)	Diff. (in)	Mod.- No.40 factor	Mod. Density factor	PVR in Layer (in.)
0.0-2.0	1	30	15.6	16.1	15	dry	100	15	3	5.8	0.00	0.20	0.2	1	0.85	0.17
2.0-4.0	3.00	20	13.4	11.4	20	dry	100	10	1.0	3.7	0.12	0.22	0.1	1	0.8	0.08
4.0-6.0	5.00	62	22.64	31.14	25.0	dry	100	36	10.5	13.8	1.41	2.08	0.67	1	1	0.67
6.0-8.0	7.00	50	20	25.5	24.8	wet	100	31	4.0	6.9	0.72	0.82	0.1	1	1	0.1
8.0-10.0	9.00	50	20	25.5	25.2	wet	100	31	4	6.9	0.82	0.91	0.09	1	1	0.09
10.0-12.0	11.00	52	20.44	26.44	25.2	wet	100	28	3.5	6.3	0.72	0.78	0.06	1	1	0.06
12.0-14.0	13.00	52	20.44	26.44	25.2	wet	100	28	3.5	6.3	0.78	0.8	0.02	1	1	0.02
14.0-16.0	15.00	52	20.44	26.44	25.2	wet	100	28	3.5	6.3	0.8	0.8	0	1	1	0
														Total PVR (in) =		1.19

NOTE :no surcharge, LTS 2.5 ft thick. (LL=30%, PI=15%, w=15%, Mod. Density factor =0.85), Inert 1.0 ft (LL=25%, PI=10%, w=20%, Mod. Density factor=0.8)

Table A-76. Calculations with No Surcharge and Treatment for the Rigid Pavement for Section C, Fort Worth North Loop IH 820.

Depth (ft.)	Avg. Load (psi)	LL (%)	Dry 0.2LL+9 (%)	Wet 0.47LL+2 (%)	Moisture (%)	Dry/ Avg/Wet	No. 40 (%)	PI (%)	Volume Swell (%)	Free swell (%)	PVR, Top of Layer (in)	PVR, Bottom of Layer (in)	Diff. (in)	Mod.- No.40 factor	Mod. Density factor	PVR in Layer (in.)
0.0-2.0	1	40	17.8	20.8	20	dry	100	25	3	6.5	0.00	0.28	0.28	1	0.85	0.238
2.0-4.0	3.00	62	22.64	31.14	22.8	dry	100	36	10.5	13.8	0.60	1.41	0.81	1	1	0.81
4.0-6.0	5.00	62	22.64	31.14	25.0	dry	100	36	10.5	13.8	1.41	2.08	0.67	1	1	0.67
6.0-8.0	7.00	50	20	25.5	24.8	wet	100	31	4.0	6.9	0.72	0.82	0.1	1	1	0.1
8.0-10.0	9.00	50	20	25.5	25.2	wet	100	31	4	6.9	0.82	0.91	0.09	1	1	0.09
10.0-12.0	11.00	52	20.44	26.44	25.2	wet	100	28	3.5	6.3	0.72	0.78	0.06	1	1	0.06
12.0-14.0	13.00	52	20.44	26.44	25.2	wet	100	28	3.5	6.3	0.78	0.8	0.02	1	1	0.02
14.0-16.0	15.00	52	20.44	26.44	25.2	wet	100	28	3.5	6.3	0.8	0.8	0	1	1	0
NOTE :no surcharge, LTS 1.0 ft thick. (LL=30%, PI=15%, w=15%, Mod. Density factor =0.85)														Total PVR (in) =		1.99

Table A-77. Calculations with No Surcharge and Treatment for the Flexible Pavement, Atlanta US 271.

Depth	Avg. Load	LL	Dry 0.2LL+9	Wet 0.47LL+2	Moisture	Dry/ Avg/Wet	No. 40	PI	Volume Swell	Free swell	PVR, Top of Layer	PVR, Bottom of Layer	Diff.	Mod.- No.40 factor	Mod. Density factor	PVR in Layer
(ft.)	(psi)	(%)	(%)	(%)	(%)		(%)	(%)	(%)	(%)	(in)	(in)	(in)			(in.)
0.0-2.0	1	30	15.6	16.1	15	dry	100	15	3	5.8	0.00	0.20	0.2	1	0.85	0.17
2.0-4.0	3.00	48	19.56	24.56	16.1	dry	100	26	6.8	9.9	0.58	1.10	0.52	1	1	0.52
4.0-6.0	5.00	37	17.14	19.39	17	dry	100	17	3.5	6.3	0.50	0.65	0.15	1	1	0.15
6.0-8.0	7.00	37	17.14	19.39	17	dry	100	17	3.5	6.3	0.65	0.72	0.07	1	1	0.07
8.0-10.0	9.00	40	17.8	20.8	16.7	dry	100	25	6.5	9.6	1.60	1.75	0.15	1	1	0.15
10.0-12.0	11.00	40	17.8	20.8	16.7	dry	100	25	6.5	9.6	1.75	1.82	0.07	1	1	0.07
12.0-14.0	13.00	37	17.14	19.39	15.8	dry	100	15	2.8	5.6	0.51	0.56	0.05	1	1	0.05
14.0-16.0	15.00	37	17.14	19.39	15.8	dry	100	15	2.8	5.6	0.56	0.58	0.02	1	1	0.02
16.0-18.0	17.00	37	17.14	19.39	15.8	dry	100	15	2.8	5.6	0.58	0.59	0.01	1	1	0.01
NOTE :no surcharge, LTS 2.2 ft thick. (LL=30%, PI=15%, w=15%, Mod. Density factor =0.85)														Total PVR (in) =		1.21

Table A-78. Calculations with No Surcharge and Treatment for the Rigid Pavement, Atlanta US 271.

Depth (ft.)	Avg. Load (psi)	LL (%)	Dry 0.2LL+9 (%)	Wet 0.47LL+2 (%)	Moisture (%)	Dry/ Avg/Wet	No. 40 (%)	PI (%)	Volume Swell (%)	Free swell (%)	PVR, Top of Layer (in)	PVR, Bottom of Layer (in)	Diff. (in)	Mod.- No.40 factor	Mod. Density factor	PVR in Layer (in.)
0.0-2.0	1.00	48	19.56	24.56	16.1	dry	100	26	6.8	9.9	0.00	0.58	0.58	1	1	0.58
2.0-4.0	3.00	48	19.56	24.56	16.1	dry	100	26	6.8	9.9	0.58	1.10	0.52	1	1	0.52
4.0-6.0	5.00	37	17.14	19.39	17	dry	100	17	3.5	6.3	0.50	0.65	0.15	1	1	0.15
6.0-8.0	7.00	37	17.14	19.39	17	dry	100	17	3.5	6.3	0.65	0.72	0.07	1	1	0.07
8.0-10.0	9.00	40	17.8	20.8	16.7	dry	100	25	6.5	9.6	1.60	1.75	0.15	1	1	0.15
10.0-12.0	11.00	40	17.8	20.8	16.7	dry	100	25	6.5	9.6	1.75	1.82	0.07	1	1	0.07
12.0-14.0	13.00	37	17.14	19.39	15.8	dry	100	15	2.8	5.6	0.51	0.56	0.05	1	1	0.05
14.0-16.0	15.00	37	17.14	19.39	15.8	dry	100	15	2.8	5.6	0.56	0.58	0.02	1	1	0.02
16.0-18.0	17.00	37	17.14	19.39	15.8	dry	100	15	2.8	5.6	0.58	0.59	0.01	1	1	0.01
NOTE : no surcharge, no treatment on sugrade soil														Total PVR (in) =		1.62

Table A-79. Calculations with No Surcharge and Treatment for the Flexible Pavement, Austin Loop 1, Main Lane.

Depth (ft.)	Avg. Load (psi)	LL (%)	Dry 0.2LL+9 (%)	Wet 0.47LL+2 (%)	Moisture (%)	Dry/ Avg/Wet	No. 40 (%)	PI (%)	Volume Swell (%)	Free swell (%)	PVR, Top of Layer (in)	PVR, Bottom of Layer (in)	Diff. (in)	Mod.- No.40 factor	Mod. Density factor	PVR in Layer (in.)
0.0-2.0	1	30	15.6	16.1	15	dry	100	15	3	5.8	0.00	0.20	0.2	1	0.85	0.17
2.0-4.0	3.00	40	17.8	20.8	18.00	dry	100	25	6.5	9.6	0.60	1.00	0.4	1	1	0.4
4.0-6.0	5.00	68	23.96	33.96	23.11	dry	100	33	9.4	12.7	1.35	1.94	0.59	1	1	0.59
6.0-8.0	7.00	68	23.96	33.96	23.11	dry	100	33	9.4	12.7	1.94	2.30	0.36	1	1	0.36
8.0-10.0	9.00	68	23.96	33.96	23.00	dry	100	33	9.4	12.7	2.30	2.58	0.28	1	1	0.28
10.0-12.0	11.00	68	23.96	33.96	23.00	dry	100	35	10.5	13.8	2.85	3.12	0.27	1	1	0.27
12.0-14.0	13.00	68	23.96	33.96	24.09	dry	100	35	10.5	13.8	3.12	3.30	0.18	1	1	0.18
14.0-16.0	15.00	68	23.96	33.96	24.09	dry	100	35	10.5	13.8	3.30	3.45	0.15	1	1	0.15
NOTE : no surcharge, LTS 2.8 ft (LL=30%, PI=15%, w=15%, Mod. Density factor =0.85)														Total PVR (in) =		2.40

Table A-80. Calculations with No Surcharge and Treatment for the Rigid Pavement, Austin Loop 1, Main Lane.

Depth (ft.)	Avg. Load (psi)	LL (%)	Dry 0.2LL+9 (%)	Wet 0.47LL+2 (%)	Moisture (%)	Dry/ Avg/Wet	No. 40 (%)	PI (%)	Volume Swell (%)	Free swell (%)	PVR, Top of Layer (in)	PVR, Bottom of Layer (in)	Diff. (in)	Mod.- No.40 factor	Mod. Density factor	PVR in Layer (in.)
0.0-2.0	1	30	15.6	16.1	15	dry	100	15	3	5.8	0.00	0.20	0.2	1	0.85	0.17
2.0-4.0	3.00	49	19.78	25.03	19.03	dry	100	29	8.0	11.2	0.60	1.14	0.54	1	1	0.54
4.0-6.0	5.00	68	23.96	33.96	23.11	dry	100	33	9.4	12.7	1.35	1.94	0.59	1	1	0.59
6.0-8.0	7.00	68	23.96	33.96	23.11	dry	100	33	9.4	12.7	1.94	2.30	0.36	1	1	0.36
8.0-10.0	9.00	68	23.96	33.96	23.00	dry	100	33	9.4	12.7	2.30	2.58	0.28	1	1	0.28
10.0-12.0	11.00	68	23.96	33.96	23.00	dry	100	35	10.5	13.8	2.85	3.12	0.27	1	1	0.27
12.0-14.0	13.00	68	23.96	33.96	24.09	dry	100	35	10.5	13.8	3.12	3.30	0.18	1	1	0.18
14.0-16.0	15.00	68	23.96	33.96	24.09	dry	100	35	10.5	13.8	3.30	3.45	0.15	1	1	0.15
NOTE : no surcharge, LTS 2.0 ft (LL=30%, PI=15%, w=15%, Mod. Density factor =0.85)														Total PVR (in) =		2.54

Table A-81. Calculations with No Surcharge and Treatment for the Flexible Pavement, Austin Loop 1, Frontage Road.

Depth (ft.)	Avg. Load (psi)	LL (%)	Dry 0.2LL+9 (%)	Wet 0.47LL+2 (%)	Moisture (%)	Dry/ Avg/Wet	No. 40 (%)	PI (%)	Volume Swell (%)	Free swell (%)	PVR, Top of Layer (in)	PVR, Bottom of Layer (in)	Diff. (in)	Mod.- No.40 factor	Mod. Density factor	PVR in Layer (in.)
0.0-2.0	1	30	15.6	16.1	15	dry	100	15	3	5.8	0.00	0.20	0.2	1	0.85	0.17
2.0-4.0	3.00	20	13.4	11.4	20	dry	100	10	1.0	3.7	0.12	0.22	0.1	1	0.8	0.08
4.0-6.0	5.00	68	23.96	33.96	23.11	dry	100	33	9.4	12.7	1.35	1.94	0.59	1	1	0.59
6.0-8.0	7.00	68	23.96	33.96	23.11	dry	100	33	9.4	12.7	1.94	2.30	0.36	1	1	0.36
8.0-10.0	9.00	68	23.96	33.96	23.00	dry	100	33	9.4	12.7	2.30	2.58	0.28	1	1	0.28
10.0-12.0	11.00	68	23.96	33.96	23.00	dry	100	35	10.5	13.8	2.85	3.12	0.27	1	1	0.27
12.0-14.0	13.00	68	23.96	33.96	24.09	dry	100	35	10.5	13.8	3.12	3.30	0.18	1	1	0.18
14.0-16.0	15.00	68	23.96	33.96	24.09	dry	100	35	10.5	13.8	3.30	3.45	0.15	1	1	0.15
														Total PVR (in) =		2.08
NOTE : no surcharge, LTS 2.0 ft (LL=30%, PI=15%, w=15%, Mod. Density factor =0.85), Inert 2.0 ft (LL=25%, PI=10%, w=20%, Mod. Density factor=0.8)																

Table A-82. Calculations with No Surcharge and Treatment for the Rigid Pavement, Austin Loop 1, Frontage Road.

Depth (ft.)	Avg. Load (psi)	LL (%)	Dry 0.2LL+9 (%)	Wet 0.47LL+2 (%)	Moisture (%)	Dry/ Avg/Wet	No. 40 (%)	PI (%)	Volume Swell (%)	Free swell (%)	PVR, Top of Layer (in)	PVR, Bottom of Layer (in)	Diff. (in)	Mod.- No.40 factor	Mod. Density factor	PVR in Layer (in.)
0.0-2.0	1.00	49	19.78	25.03	19.03	dry	100	29	8.0	11.2	0.00	0.60	0.6	1	1	0.6
2.0-4.0	3.00	49	19.78	25.03	19.03	dry	100	29	8.0	11.2	0.60	1.14	0.54	1	1	0.54
4.0-6.0	5.00	68	23.96	33.96	23.11	dry	100	33	9.4	12.7	1.35	1.94	0.59	1	1	0.59
6.0-8.0	7.00	68	23.96	33.96	23.11	dry	100	33	9.4	12.7	1.94	2.30	0.36	1	1	0.36
8.0-10.0	9.00	68	23.96	33.96	23.00	dry	100	33	9.4	12.7	2.30	2.58	0.28	1	1	0.28
10.0-12.0	11.00	68	23.96	33.96	23.00	dry	100	35	10.5	13.8	2.85	3.12	0.27	1	1	0.27
12.0-14.0	13.00	68	23.96	33.96	24.09	dry	100	35	10.5	13.8	3.12	3.30	0.18	1	1	0.18
14.0-16.0	15.00	68	23.96	33.96	24.09	dry	100	35	10.5	13.8	3.30	3.45	0.15	1	1	0.15
NOTE : no surcharge, no treatment on sugrade soil														Total PVR (in) =		2.97

Analysis of the Case with the Surcharge of 1 psi and Treatment for the Pavement Acceptable Predicted Performance at the Outer Wheel Path.

Table A-83. Calculations with the Surcharge of 1 psi and Treatment for the Flexible Pavement for Section A, Fort Worth North Loop IH 820.

Depth (ft.)	Avg. Load (psi)	LL (%)	Dry 0.2LL+9 (%)	Wet 0.47LL+2 (%)	Moisture (%)	Dry/ Avg/Wet	No. 40 (%)	PI (%)	Volume Swell (%)	Free swell (%)	PVR, Top of Layer (in)	PVR, Bottom of Layer (in)	Diff. (in)	Mod.- No.40 factor	Mod. Density factor	PVR in Layer (in.)
0.0-2.0	2	30	15.6	16.1	15	dry	100	15	3	5.8	0.20	0.32	0.12	1	0.85	0.102
2.0-4.0	4	60	22.2	30.2	25.4	dry	100	28	7.5	10.6	0.95	1.40	0.45	1	1	0.45
4.0-6.0	6	60	22.2	30.2	25.4	dry	100	25	6.5	9.6	1.25	1.50	0.25	1	1	0.25
6.0-8.0	8	60	22.2	30.2	27	wet	100	25	6.5	9.6	1.50	1.68	0.18	1	1	0.18
8.0-10.0	10	60	22.2	30.2	23.8	dry	100	25	6.5	9.6	1.68	1.80	0.12	1	1	0.12
10.0-12.0	12	65	23.3	32.55	23.8	dry	100	35	10	13.3	2.90	3.12	0.22	1	1	0.22
12.0-14.0	14	65	23.3	32.55	24.8	dry	100	35	10	13.3	3.12	3.29	0.17	1	1	0.17
14.0-16.0	16	65	23.3	32.55	24.8	dry	100	35	10	13.3	3.29	3.42	0.13	1	1	0.13
NOTE : surcharge load of 1 psi, LTS 2.5 ft thick. (LL=30%, PI=15%, w=15%, Mod. Density factor =0.85)														Total PVR (in) =		1.62

Table A-84. Calculations with the Surcharge of 1 psi and Treatment for the Rigid Pavement for Section A, Fort Worth North Loop IH 820.

Depth (ft.)	Avg. Load (psi)	LL (%)	Dry 0.2LL+9 (%)	Wet 0.47LL+2 (%)	Moisture (%)	Dry/ Avg/Wet	No. 40 (%)	PI (%)	Volume Swell (%)	Free swell (%)	PVR, Top of Layer (in)	PVR, Bottom of Layer (in)	Diff. (in)	Mod.- No.40 factor	Mod. Density factor	PVR in Layer (in.)
0.0-2.0	2	60	22.2	30.2	25.4	dry	100	28	7.5	10.6	0.60	0.95	0.35	1	1	0.35
2.0-4.0	4	60	22.2	30.2	25.4	dry	100	28	7.5	10.6	0.95	1.40	0.45	1	1	0.45
4.0-6.0	6	60	22.2	30.2	25.4	dry	100	25	6.5	9.6	1.25	1.50	0.25	1	1	0.25
6.0-8.0	8	60	22.2	30.2	27	wet	100	25	6.5	9.6	1.50	1.68	0.18	1	1	0.18
8.0-10.0	10	60	22.2	30.2	23.8	dry	100	25	6.5	9.6	1.68	1.80	0.12	1	1	0.12
10.0-12.0	12	65	23.3	32.55	23.8	dry	100	35	10	13.3	2.90	3.12	0.22	1	1	0.22
12.0-14.0	14	65	23.3	32.55	24.8	dry	100	35	10	13.3	3.12	3.29	0.17	1	1	0.17
14.0-16.0	16	65	23.3	32.55	24.8	dry	100	35	10	13.3	3.29	3.42	0.13	1	1	0.13
NOTE :surcharge load of 1 psi, no treatment on sugrade soil														Total PVR (in) =		1.87

Table A-85. Calculations with the Surcharge of 1 psi and Treatment for the Flexible Pavement for Section B, Fort Worth North Loop IH 820.

Depth (ft.)	Avg. Load (psi)	LL (%)	Dry 0.2LL+9 (%)	Wet 0.47LL+2 (%)	Moisture (%)	Dry/ Avg/Wet	No. 40 (%)	PI (%)	Volume Swell (%)	Free swell (%)	PVR, Top of Layer (in)	PVR, Bottom of Layer (in)	Diff. (in)	Mod.- No.40 factor	Mod. Density factor	PVR in Layer (in.)
0.0-2.0	2	30	15.6	16.1	15	dry	100	15	3	5.8	0.20	0.32	0.12	1	0.85	0.102
2.0-4.0	4	20	13.4	11.4	20	dry	100	10	1.0	3.7	0.18	0.22	0.04	1	0.8	0.032
4.0-6.0	6	55	21.1	27.85	11.35	dry	100	30	8.4	11.6	1.55	1.91	0.36	1	1	0.36
6.0-8.0	8	65	23.3	32.55	11.35	dry	100	38	11.1	14.5	2.45	2.90	0.45	1	1	0.45
8.0-10.0	10	65	23.3	32.55	18.41	dry	100	38	11.1	14.5	2.90	3.24	0.34	1	1	0.34
10.0-12.0	12	53	20.66	26.91	18.41	dry	100	32	9.0	12.2	2.61	2.80	0.19	1	1	0.19
12.0-14.0	14	45	18.9	23.15	18.41	dry	100	25	6.5	9.6	1.85	1.92	0.07	1	1	0.07
14.0-16.0	16	45	18.9	23.15	24.9	dry	100	15	3.0	5.8	0.61	0.62	0.01	1	1	0.01
														Total PVR (in) =		1.55
NOTE :surcharge load of 1 psi, LTS 2.5 ft thick. (LL=30%, PI=15%, w=15%, Mod. Density factor =0.85), Inert 1.5 ft (LL=25%, PI=10%, w=20%, Mod. Density factor=0.8)																

Table A-86. Calculations with the Surcharge of 1 psi and Treatment for the Rigid Pavement for Section B, Fort Worth North Loop IH 820.

Depth (ft.)	Avg. Load (psi)	LL (%)	Dry 0.2LL+9 (%)	Wet 0.47LL+2 (%)	Moisture (%)	Dry/ Avg/Wet	No. 40 (%)	PI (%)	Volume Swell (%)	Free swell (%)	PVR, Top of Layer (in)	PVR, Bottom of Layer (in)	Diff. (in)	Mod.- No.40 factor	Mod. Density factor	PVR in Layer (in.)
0.0-2.0	2	40	17.8	20.8	20	dry	100	25	3	6.5	0.27	0.35	0.08	1	0.85	0.068
2.0-4.0	4	55	21.1	27.85	20.2	dry	100	30	8.4	11.6	0.98	1.55	0.57	1	1	0.57
4.0-6.0	6	55	21.1	27.85	11.35	dry	100	30	8.4	11.6	1.55	1.91	0.36	1	1	0.36
6.0-8.0	8	65	23.3	32.55	11.35	dry	100	38	11.1	14.5	2.45	2.90	0.45	1	1	0.45
8.0-10.0	10	65	23.3	32.55	18.41	dry	100	38	11.1	14.5	2.90	3.24	0.34	1	1	0.34
10.0-12.0	12	53	20.66	26.91	18.41	dry	100	32	9.0	12.2	2.61	2.80	0.19	1	1	0.19
12.0-14.0	14	45	18.9	23.15	18.41	dry	100	25	6.5	9.6	1.85	1.92	0.07	1	1	0.07
14.0-16.0	16	45	18.9	23.15	24.9	dry	100	15	3.0	5.8	0.61	0.62	0.01	1	1	0.01
NOTE :surcharge load of 1 psi, LTS 8.0 in thick. (LL=30%, PI=15%, w=15%, Mod. Density factor =0.85)														Total PVR (in) =		2.06

Table A-87. Calculations with the Surcharge of 1 psi and Treatment for the Flexible Pavement for Section C, Fort Worth North Loop IH 820.

Depth (ft.)	Avg. Load (psi)	LL (%)	Dry 0.2LL+9 (%)	Wet 0.47LL+2 (%)	Moisture (%)	Dry/ Avg/Wet	No. 40 (%)	PI (%)	Volume Swell (%)	Free swell (%)	PVR, Top of Layer (in)	PVR, Bottom of Layer (in)	Diff. (in)	Mod.- No.40 factor	Mod. Density factor	PVR in Layer (in.)
0.0-2.0	2	30	15.6	16.1	15	dry	100	15	3	5.8	0.00	0.20	0.2	1	0.85	0.17
2.0-4.0	4	20	13.4	11.4	20	dry	100	10	1.0	3.7	0.18	0.22	0.04	1	0.8	0.032
4.0-6.0	6	62	22.64	31.14	25.0	dry	100	36	10.5	13.8	1.79	2.31	0.52	1	1	0.52
6.0-8.0	8	50	20	25.5	24.8	wet	100	31	4.0	6.9	1.05	1.17	0.12	1	1	0.12
8.0-10.0	10	50	20	25.5	25.2	wet	100	31	4	6.9	1.17	1.21	0.04	1	1	0.04
10.0-12.0	12	52	20.44	26.44	25.2	wet	100	28	3.5	6.3	1.03	1.08	0.05	1	1	0.05
12.0-14.0	14	52	20.44	26.44	25.2	wet	100	28	3.5	6.3	1.08	1.09	0.01	1	1	0.01
14.0-16.0	16	52	20.44	26.44	25.2	wet	100	28	3.5	6.3	1.09	1.1	0.01	1	1	0.01
NOTE :surcharge load of 1 psi, LTS 2.5 ft thick. (LL=30%, PI=15%, w=15%, Mod. Density factor =0.85), Inert 1.0 ft (LL=25%, PI=10%, w=20%, Mod. Density factor=0.8)														Total PVR (in) =		0.95

Table A-88. Calculations with the Surcharge of 1 psi and Treatment for the Rigid Pavement for Section C, Fort Worth North Loop IH 820.

Depth (ft.)	Avg. Load (psi)	LL (%)	Dry 0.2LL+9 (%)	Wet 0.47LL+2 (%)	Moisture (%)	Dry/ Avg/Wet	No. 40 (%)	PI (%)	Volume Swell (%)	Free swell (%)	PVR, Top of Layer (in)	PVR, Bottom of Layer (in)	Diff. (in)	Mod.- No.40 factor	Mod. Density factor	PVR in Layer (in.)
0.0-2.0	2	40	17.8	20.8	20	dry	100	25	3	6.5	0.28	0.42	0.14	1	0.85	0.119
2.0-4.0	4	62	22.64	31.14	22.8	dry	100	36	10.5	13.8	1.02	1.79	0.77	1	1	0.77
4.0-6.0	6	62	22.64	31.14	25.0	dry	100	36	10.5	13.8	1.79	2.31	0.52	1	1	0.52
6.0-8.0	8	50	20	25.5	24.8	wet	100	31	4.0	6.9	1.05	1.17	0.12	1	1	0.12
8.0-10.0	10	50	20	25.5	25.2	wet	100	31	4	6.9	1.17	1.21	0.04	1	1	0.04
10.0-12.0	12	52	20.44	26.44	25.2	wet	100	28	3.5	6.3	1.03	1.08	0.05	1	1	0.05
12.0-14.0	14	52	20.44	26.44	25.2	wet	100	28	3.5	6.3	1.08	1.09	0.01	1	1	0.01
14.0-16.0	16	52	20.44	26.44	25.2	wet	100	28	3.5	6.3	1.09	1.1	0.01	1	1	0.01
NOTE :surcharge load of 1 psi, LTS 1.0 ft thick. (LL=30%, PI=15%, w=15%, Mod. Density factor =0.85)														Total PVR (in) =		1.64

Table A-89. Calculations with the Surcharge of 1 psi and Treatment for the Flexible Pavement, Atlanta US 271.

Depth (ft.)	Avg. Load (psi)	LL (%)	Dry 0.2LL+9 (%)	Wet 0.47LL+2 (%)	Moisture (%)	Dry/ Avg/Wet	No. 40 (%)	PI (%)	Volume Swell (%)	Free swell (%)	PVR, Top of Layer (in)	PVR, Bottom of Layer (in)	Diff. (in)	Mod.- No.40 factor	Mod. Density factor	PVR in Layer (in.)
0.0-2.0	2	30	15.6	16.1	15	dry	100	15	3	5.8	0.20	0.32	0.12	1	0.85	0.102
2.0-4.0	4	48	19.56	24.56	16.1	dry	100	26	6.8	9.9	0.90	1.30	0.4	1	1	0.4
4.0-6.0	6	37	17.14	19.39	17	dry	100	17	3.5	6.3	0.61	0.70	0.09	1	1	0.09
6.0-8.0	8	37	17.14	19.39	17	dry	100	17	3.5	6.3	0.70	0.72	0.02	1	1	0.02
8.0-10.0	10	40	17.8	20.8	16.7	dry	100	25	6.5	9.6	1.70	1.82	0.12	1	1	0.12
10.0-12.0	12	40	17.8	20.8	16.7	dry	100	25	6.5	9.6	1.82	1.93	0.11	1	1	0.11
12.0-14.0	14	37	17.14	19.39	15.8	dry	100	15	2.8	5.6	0.55	0.58	0.03	1	1	0.03
14.0-16.0	16	37	17.14	19.39	15.8	dry	100	15	2.8	5.6	0.58	0.60	0.02	1	1	0.02
16.0-18.0	18	37	17.14	19.39	15.8	dry	100	15	2.8	5.6	0.60	0.62	0.02	1	1	0.02
NOTE :surcharge load of 1 psi, LTS 2.2 ft thick. (LL=30%, PI=15%, w=15%, Mod. Density factor =0.85)														Total PVR (in) =		0.91

Table A-90. Calculations with the Surcharge of 1 psi and Treatment for the Rigid Pavement, Atlanta US 271.

Depth (ft.)	Avg. Load (psi)	LL (%)	Dry 0.2LL+9 (%)	Wet 0.47LL+2 (%)	Moisture (%)	Dry/ AvgWet	No. 40 (%)	PI (%)	Volume Swell (%)	Free swell (%)	PVR, Top of Layer (in)	PVR, Bottom of Layer (in)	Diff. (in)	Mod.- No.40 factor	Mod. Density factor	PVR in Layer (in.)
0.0-2.0	2	48	19.56	24.56	16.1	dry	100	26	6.8	9.9	0.55	0.90	0.35	1	1	0.35
2.0-4.0	4	48	19.56	24.56	16.1	dry	100	26	6.8	9.9	0.90	1.30	0.4	1	1	0.4
4.0-6.0	6	37	17.14	19.39	17	dry	100	17	3.5	6.3	0.61	0.70	0.09	1	1	0.09
6.0-8.0	8	37	17.14	19.39	17	dry	100	17	3.5	6.3	0.70	0.72	0.02	1	1	0.02
8.0-10.0	10	40	17.8	20.8	16.7	dry	100	25	6.5	9.6	1.70	1.82	0.12	1	1	0.12
10.0-12.0	12	40	17.8	20.8	16.7	dry	100	25	6.5	9.6	1.82	1.93	0.11	1	1	0.11
12.0-14.0	14	37	17.14	19.39	15.8	dry	100	15	2.8	5.6	0.55	0.58	0.03	1	1	0.03
14.0-16.0	16	37	17.14	19.39	15.8	dry	100	15	2.8	5.6	0.58	0.60	0.02	1	1	0.02
16.0-18.0	18	37	17.14	19.39	15.8	dry	100	15	2.8	5.6	0.60	0.62	0.02	1	1	0.02
NOTE : surcharge load of 1 psi, no treatment on sugrade soil														Total PVR (in) =		1.16

Table A-91. Calculations with the Surcharge of 1 psi and Treatment for the Flexible Pavement, Austin Loop 1, Main Lane.

Depth (ft.)	Avg. Load (psi)	LL (%)	Dry 0.2LL+9 (%)	Wet 0.47LL+2 (%)	Moisture (%)	Dry/ Avg/Wet	No. 40 (%)	PI (%)	Volume Swell (%)	Free swell (%)	PVR, Top of Layer (in)	PVR, Bottom of Layer (in)	Diff. (in)	Mod.- No.40 factor	Mod. Density factor	PVR in Layer (in.)
0.0-2.0	2	30	15.6	16.1	15	dry	100	15	3	5.8	0.20	0.32	0.12	1	0.85	0.102
2.0-4.0	4	40	17.8	20.8	19.03	dry	100	20	4.7	7.6	0.60	0.80	0.2	1	1	0.2
4.0-6.0	6	68	23.96	33.96	23.11	dry	100	33	9.4	12.7	1.65	2.12	0.47	1	1	0.47
6.0-8.0	8	68	23.96	33.96	23.11	dry	100	33	9.4	12.7	2.12	2.43	0.31	1	1	0.31
8.0-10.0	10	68	23.96	33.96	23.00	dry	100	33	9.4	12.7	2.43	2.72	0.29	1	1	0.29
10.0-12.0	12	68	23.96	33.96	23.00	dry	100	35	10.5	13.8	3.00	3.21	0.21	1	1	0.21
12.0-14.0	14	68	23.96	33.96	24.09	dry	100	35	10.5	13.8	3.21	3.43	0.22	1	1	0.22
14.0-16.0	16	68	23.96	33.96	24.09	dry	100	35	10.5	13.8	3.43	3.56	0.13	1	1	0.13
NOTE : surcharge load of 1 psi, LTS 2.8 ft (LL=30%, PI=15%, w=15%, Mod. Density factor =0.85)														Total PVR (in) =		1.93

Table A-92. Calculations with the Surcharge of 1 psi and Treatment for the Rigid Pavement, Austin Loop 1, Main Lane.

Depth (ft.)	Avg. Load (psi)	LL (%)	Dry 0.2LL+9 (%)	Wet 0.47LL+2 (%)	Moisture (%)	Dry/ Avg/Wet	No. 40 (%)	PI (%)	Volume Swell (%)	Free swell (%)	PVR, Top of Layer (in)	PVR, Bottom of Layer (in)	Diff. (in)	Mod.- No.40 factor	Mod. Density factor	PVR in Layer (in.)
0.0-2.0	2	30	15.6	16.1	15	dry	100	15	3	5.8	0.20	0.32	0.12	1	0.85	0.102
2.0-4.0	4	49	19.78	25.03	19.03	dry	100	29	8.0	11.2	0.98	1.35	0.37	1	1	0.37
4.0-6.0	6	68	23.96	33.96	23.11	dry	100	33	9.4	12.7	1.65	2.12	0.47	1	1	0.47
6.0-8.0	8	68	23.96	33.96	23.11	dry	100	33	9.4	12.7	2.12	2.43	0.31	1	1	0.31
8.0-10.0	10	68	23.96	33.96	23.00	dry	100	33	9.4	12.7	2.43	2.72	0.29	1	1	0.29
10.0-12.0	12	68	23.96	33.96	23.00	dry	100	35	10.5	13.8	3.00	3.21	0.21	1	1	0.21
12.0-14.0	14	68	23.96	33.96	24.09	dry	100	35	10.5	13.8	3.21	3.43	0.22	1	1	0.22
14.0-16.0	16	68	23.96	33.96	24.09	dry	100	35	10.5	13.8	3.43	3.56	0.13	1	1	0.13
NOTE : surcharge load of 1 psi, LTS 2.0 ft (LL=30%, PI=15%, w=15%, Mod. Density factor =0.85)														Total PVR (in) =		2.10

Table A-93. Calculations with the Surcharge of 1 psi and Treatment for the Flexible Pavement, Austin Loop 1, Frontage Road.

Depth (ft.)	Avg. Load (psi)	LL (%)	Dry 0.2LL+9 (%)	Wet 0.47LL+2 (%)	Moisture (%)	Dry/ Avg/Wet	No. 40 (%)	PI (%)	Volume Swell (%)	Free swell (%)	PVR, Top of Layer (in)	PVR, Bottom of Layer (in)	Diff. (in)	Mod.- No.40 factor	Mod. Density factor	PVR in Layer (in.)
0.0-2.0	2	30	15.6	16.1	15	dry	100	15	3	5.8	0.20	0.32	0.12	1	0.85	0.102
2.0-4.0	4	20	13.4	11.4	20	dry	100	10	1.0	3.7	0.18	0.22	0.04	1	0.8	0.032
4.0-6.0	6	68	23.96	33.96	23.11	dry	100	33	9.4	12.7	1.65	2.12	0.47	1	1	0.47
6.0-8.0	8	68	23.96	33.96	23.11	dry	100	33	9.4	12.7	2.12	2.43	0.31	1	1	0.31
8.0-10.0	10	68	23.96	33.96	23.00	dry	100	33	9.4	12.7	2.43	2.72	0.29	1	1	0.29
10.0-12.0	12	68	23.96	33.96	23.00	dry	100	35	10.5	13.8	3.00	3.21	0.21	1	1	0.21
12.0-14.0	14	68	23.96	33.96	24.09	dry	100	35	10.5	13.8	3.21	3.43	0.22	1	1	0.22
14.0-16.0	16	68	23.96	33.96	24.09	dry	100	35	10.5	13.8	3.43	3.56	0.13	1	1	0.13
														Total PVR (in) =		1.76
NOTE : surcharge load of 1 psi, LTS 2.0 ft (LL=30%, PI=15%, w=15%, Mod. Density factor =0.85), Inert 2.0 ft (LL=25%, PI=10%, w=20%, Mod. Density factor=0.8)																

Table A-94. Calculations with the Surcharge of 1 psi and Treatment for the Rigid Pavement, Austin Loop 1, Frontage Road.

Depth (ft.)	Avg. Load (psi)	LL (%)	Dry 0.2LL+9 (%)	Wet 0.47LL+2 (%)	Moisture (%)	Dry/ AvgWet	No. 40 (%)	PI (%)	Volume Swell (%)	Free swell (%)	PVR, Top of Layer (in)	PVR, Bottom of Layer (in)	Diff. (in)	Mod.- No.40 factor	Mod. Density factor	PVR in Layer (in.)
0.0-2.0	2	49	19.78	25.03	19.03	dry	100	29	8.0	11.2	0.61	0.98	0.37	1	1	0.37
2.0-4.0	4	49	19.78	25.03	19.03	dry	100	29	8.0	11.2	0.98	1.35	0.37	1	1	0.37
4.0-6.0	6	68	23.96	33.96	23.11	dry	100	33	9.4	12.7	1.65	2.12	0.47	1	1	0.47
6.0-8.0	8	68	23.96	33.96	23.11	dry	100	33	9.4	12.7	2.12	2.43	0.31	1	1	0.31
8.0-10.0	10	68	23.96	33.96	23.00	dry	100	33	9.4	12.7	2.43	2.72	0.29	1	1	0.29
10.0-12.0	12	68	23.96	33.96	23.00	dry	100	35	10.5	13.8	3.00	3.21	0.21	1	1	0.21
12.0-14.0	14	68	23.96	33.96	24.09	dry	100	35	10.5	13.8	3.21	3.43	0.22	1	1	0.22
14.0-16.0	16	68	23.96	33.96	24.09	dry	100	35	10.5	13.8	3.43	3.56	0.13	1	1	0.13
NOTE : surcharge load of 1 psi, no treatment on sugrade soil														Total PVR (in) =		2.37

VITA

Name:	Gyeong Taek Hong
Address:	2856 Grasslands Drive #2212, Sacramento, CA 95833
Email Address:	gthong66@hotmail.com
Education:	B.Eng., Civil Engineering, Dongguk University, Seoul, Korea, 1997 M.Eng., Civil Engineering, Dongguk University,Seoul, Korea, 2000